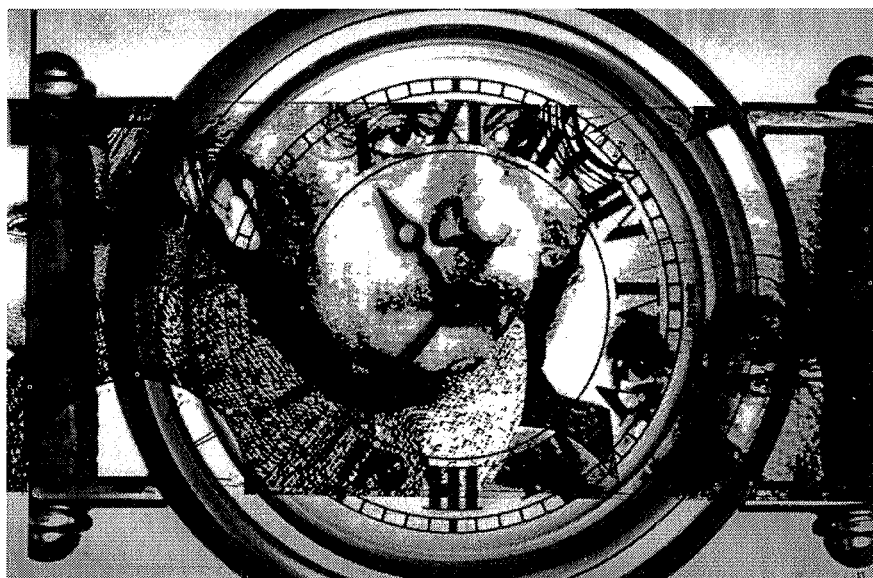


JPL Publication 97-15

Proceedings of the Workshop on the Scientific Applications of Clocks in Space November 7–8, 1996

Lute Maleki
Editor



August 1, 1997



National Aeronautics and
Space Administration

Jet Propulsion Laboratory
California Institute of Technology
Pasadena, California

JPL Publication 97-15

Proceedings of the Workshop on the Scientific Applications of Clocks in Space November 7–8, 1996

Lute Maleki
Editor



August 1, 1997



National Aeronautics and
Space Administration

Jet Propulsion Laboratory
California Institute of Technology
Pasadena, California

This publication was prepared by the Jet Propulsion Laboratory, California Institute of Technology, under a contract with the National Aeronautics and Space Administration.

PREFACE

The union of clocks and science experiments in space is a natural one. On the one hand, time and frequency are the most precisely determined of all physical parameters, and thus are the required tools for performing the most sensitive tests of physical theories. Yet on the other hand, space affords the opportunity to make measurements of parameters inaccessible on Earth, and enables some of the most unique and sensitive tests of fundamental theories. Additionally, in some cases space represents a highly benign environment which can enhance the performance of precision clocks.

The importance of clocks to science applications was recognized early on in the history of space science experiments. The Ultra-Stable Oscillator (USO) on board the Voyager spacecraft led to important measurements of parameters related to planetary atmospheres and rings, and opened the door for the search of long wavelength gravitational waves. Since that time many other such "radio science" experiments have been flown, and have produced a wealth of information in space science and planetary sciences. The advent of GPS has further advanced applications of space clocks for scientific investigations. GPS represents the first example of the orbital deployment of atomic clocks, the use of which has extended the opportunity for performing science experiments ranging from atmospheric occultation measurements to relativity physics.

Yet the most precise experiment with clocks in space is the celebrated Gravity Probe-A mission which entailed a hydrogen maser standard on board a Scout rocket in a sub-orbital flight. This flight tested the redshift prediction of Einstein's General Relativity, and produced the most precise value for this parameter, which still stands today, some twenty years after its completion. The significance of the Gravity Probe-A is that it directly tested the Equivalence Principle, which underpins all metric theories of gravity. Since that mission, the only other atomic clocks used for science experiments in space are the GPS clocks mentioned above.

In the past few years, new developments in clock technologies have pointed to the opportunity for flying ultrastable clocks in support of the science investigations of space missions. This development coincides with the new NASA paradigm for space flights, which relies on frequent, low-cost missions in place of the traditional infrequent and high-cost missions. The heightened interest in clocks in space is further advanced by new theoretical developments in various fields. For example, recent developments in certain Grand Unified Theory formalisms have vastly increased interest in fundamental tests of gravitation physics with clocks.

In view of these developments the notion of a workshop devoted to the subject of Scientific Applications of Clocks in Space appeared timely. This idea was supported by the JPL Earth and Space Science Directorate and ultimately led to a workshop on November 7-8, 1996, at the Ritz-Carlton Hotel in Pasadena. The workshop was organized with the purpose of bringing together scientists and technologists interested in applications of ultra-stable clocks for test of fundamental theories, and for other science investigations. Three specific objectives were adopted: 1) to identify areas of fundamental and applied science that can particularly benefit from ultra-stable clocks in space, 2) To promote scientific collaborations, both in the U.S. and internationally, toward the realization of "Space Clock" missions, and 3) to review the latest developments in promising clock technologies suitable for space applications. The workshop included sessions on all related science including relativity and gravitational physics, cosmology, orbital dynamics, radio science, geodynamics, and GPS and other science, as well as a session on advanced clock technology.

PREFACE (continued)

The two-day workshop brought together 57 participants from academia, government laboratories, and industry. There were 27 speakers from the United States, France, Germany, The Netherlands, Switzerland, and Australia in the four conference sessions. In the first session the presentations addressed the theoretical foundations for test of fundamental physics theories with clocks in space. The second session covered a discussion of previous seminal clock experiments on Earth, and GP-A, followed by the presentation of recent improvements in the performance of those clocks. The discussion of the emerging technologies of trapped ion clocks and clocks based on laser trapped and cooled atoms were covered in the third session. Finally, the fourth session included presentations on the role of clocks in various astrophysical and planetary experiments.

The single major result emerging from the workshop was the consensus that ultra-stable clocks in space offer an important opportunity to improve on previous tests, as well as to perform new tests, seeking a violation of the Equivalence Principle. Such tests will complement the findings of STEP, and will provide a unique approach for examining the validity of nonmetric theories of gravity as recently predicted by certain Grand Unified Theory formalisms. "Space Clock" missions will also provide a valuable opportunity for performing spacecraft search of gravitational waves with improved sensitivity compared with previous tests, and complement experiments planned with the Cassini mission. Depending on the configuration and the trajectory, the "Space Clock" mission can also support other investigations such as accurate timing of gamma ray bursts, the improvement of radio science experiments, and GPS and its related science.

I would like to acknowledge the support of Dr. Charles Elachi, Director of the Space and Earth Science Program Directorate (SESPD); Dr. Firouz Naderi, Manager of the Origins and Fundamental Physics Program, SESPD; and Dr. James Cutts, Manager of the Advanced Concepts Office, SESPD, who provided funds the Workshop. I would also like to thank Dr. Charles Edwards, Deputy Manager of the TMO Technology Program, for his support for the publication of this proceedings.

—Lute Maleki

TABLE OF CONTENTS

Session I: Theoretical Foundations	1
Physical Law and Precision Clocks.....	3
<i>K. Nordtvedt</i> Northwest Analysis, USA	
Gravity, Equivalence Principle and Clocks	13
<i>T. Damour</i> Institut des Hautes Etudes Scientifiques and DARC, CNRS–Observatoire de Paris, France	
Gravitation Physics and a Space Clock Mission	23
<i>M. P. Haugan</i> Purdue University, USA	
Spacecraft Tests of General Relativity	29
<i>J. D. Anderson</i> Jet Propulsion Laboratory, USA	
Gravitational Wave Search With the Clock Mission	33
<i>J. W. Armstrong</i> Jet Propulsion Laboratory, USA	
Clocks and General Relativity.....	41
<i>B. Mashhoon</i> University of New Mexico, USA	
The Nexus Between Cosmology and Elementary Particle Physics: Testing Theoretical Speculations Through Observations of the Cosmic Microwave Background Anisotropies	49
<i>Mairi Sakellariadou</i> Université de Genève, Switzerland	
Session II: Classic Tests and Their Clocks	57
The Superconducting Cavity Stabilized Oscillator.....	59
<i>J. P. Turneaure, S. Buchman, and J. Lipa</i> Stanford University, USA	
Space Experiments With High Stability Clocks	67
<i>R. F. C. Vessot</i> Smithsonian Astrophysical Observatory, USA	
Hydrogen Maser for Space.....	93
<i>E. M. Mattison, D. A. Boyd, J. F. Maddox, G. U. Nystrom, and R. F. C. Vessot</i> Smithsonian Astrophysical Observatory, USA	
Ultrastable and Ultralow Phase Noise Microwave Sapphire Oscillators.....	101
<i>D. G. Blair, S. Chang, E. N. Ivanov, A. N. Luiten, A. G. Mann, M. Tobar, and R. Woode</i> University of Western Australia, Australia	

TABLE OF CONTENTS (continued)

Cryo-Cooled Sapphire Oscillator for the Cassini Ka-band Experiment	127
<i>R. T. Wang and G. J. Dick</i> Jet Propulsion Laboratory, USA	
<u>Session III: New Directions in Atomic Clocks</u>	131
High-Accuracy Hg ⁺ Microwave and Optical Frequency Standards in Cryogenic Linear Ion Traps	133
<i>D. J. Berkeland, J. D. Miller, F. C. Cruz, J. C. Bergquist, W. M. Itano, and D. J. Wineland</i> National Institute of Standards and Technology, USA	
Progress on the CSIRO Trapped Ytterbium Ion Clocks.....	143
<i>P. T. H. Fisk, Malcolm A. Lawn, and C. Coles</i> CSIRO Division of Telecommunications and Industrial Physics, Australia	
Ion-Atom Cold Collisions and Atomic Clocks	153
<i>J. D. Prestage, L. Maleki, and R. L. Tjoelker</i> Jet Propulsion Laboratory, USA	
PHARAO: A Space Clock With Cold Cesium Atoms	163
<i>Ch. Salomon and P. Lemonde</i> Ecole Normale Supérieure, France <i>Ph. Laurent, E. Simon, G. Santarelli, and A. Clairon</i> BNM–Laboratoire Primaire du Temps et des Fréquences, France <i>P. Petit, N. Dimarcq, and C. Audoin</i> Université Paris–Sud, France <i>F. Gonzalez and F. J. Changeart</i> Centre National d’Etudes Spatiales, France	
Prospects for an Evaporatively Cooled Cesium Atomic Frequency Standard.....	171
<i>W. M. Klipstein, S. L. Rolston, and W. D. Phillips</i> National Institute of Standards and Technology, USA <i>C. R. Ekstrom</i> United States Naval Observatory, USA	
Future Laser-Cooled Microwave Clock Performance	179
<i>K. Gibble</i> Yale University, USA	
Rotation Sensing with an Atom Interferometer Gyroscope	185
<i>T. L. Gustavson and M. A. Kasevich</i> Stanford University, USA <i>P. Bouyer</i> Institut d’Optique, France	

TABLE OF CONTENTS (continued)

<p><u>Session IV: Planetary and Space Science Applications</u></p> <p>Trends In Performance and Characteristics of Ultra-Stable Oscillators for Deep Space Radio Science Experiments</p> <p style="padding-left: 2em;"><i>S. Asmar</i> Jet Propulsion Laboratory, USA</p> <p>A Xylophone Detector of Gravitational Radiation</p> <p style="padding-left: 2em;"><i>M. Tinto</i> Jet Propulsion Laboratory, USA</p> <p>Clock Requirements for Gamma-Ray Burst Localization Experiments</p> <p style="padding-left: 2em;"><i>D. Van Buren</i> California Institute of Technology, USA</p> <p>Rubidium Ultra-Stable Oscillators at Titan: the Huygens Doppler Wind Experiment</p> <p style="padding-left: 2em;"><i>M. K. Bird, R. Dutta-Roy, and M. Heyl</i> Universität Bonn, Germany</p> <p style="padding-left: 2em;"><i>M. Allison</i> NASA–Goddard Institute for Space Studies, USA</p> <p style="padding-left: 2em;"><i>D. H. Atkinson</i> University of Idaho, USA</p> <p style="padding-left: 2em;"><i>S. W. Asmar, W. M. Folkner, R. A. Preston, and R. Wohlmuth</i> Jet Propulsion Laboratory, USA</p> <p style="padding-left: 2em;"><i>P. Edenhofer and D. Plettmeier</i> Universität Bochum, Germany</p> <p style="padding-left: 2em;"><i>L. Iess</i> Università di Roma “La Sapienza,” Italy</p> <p style="padding-left: 2em;"><i>G. L. Tyler</i> Stanford University, USA</p> <p>Limits to the Stability of Phase Transfer from Ground to Space</p> <p style="padding-left: 2em;"><i>R. P. Linfield</i> Jet Propulsion Laboratory, USA</p> <p>DLR’s Research for Space-Maser Monitoring with Two-Way Microwave Links <i>J. Hahn</i> DLR Oberpfaffenhofen, Germany</p>	<p>193</p> <p>195</p> <p>201</p> <p>209</p> <p>211</p> <p>221</p> <p>225</p>
---	--

Session I

Theoretical

Foundations

PHYSICAL LAW AND PRECISION CLOCKS

Kenneth Nordtvedt
Northwest Analysis, 118 Sourdough Ridge, Bozeman MT 59715
kennordtvedt@mcn.net

ABSTRACT

The effects of proximate matter on the rates of clocks-as-physical-devices are discussed in terms of both underlying physical law and the Equivalence Principle. Three distinct types of clocks - oscillator, ruler and decay - are identified, though oscillator clocks are particularly discussed. Attention is given to the comparison between clock experiments and free-fall experiments as methods for searching for existence of new long range interactions. Clock experiments conducted close to the Sun would be competitive with today's free-fall experiments in probing physical law.

Generalizing from the apparent equivalence between local physics in an accelerating coordinate frame and in gravity, Einstein predicted that clocks at different altitudes in a gravitational acceleration field (universal to all bodies) would show a relative frequency shift:

$$\frac{v' - v}{v} \approx - \frac{\vec{g} \cdot (\vec{r}' - \vec{r})}{c^2} \quad (1)$$

More globally, this expression integrates to yield the frequency shifts between clocks at different gravitational potentials:

$$\frac{v' - v}{v} \approx U(\vec{R}) - U(\vec{R}') \quad U(\vec{R}) \equiv \frac{G}{c^2} \sum_n \frac{M(G)_n}{|\vec{R} - \vec{R}_n|} \quad (2)$$

gravitational mass of bodies indicated. This global version of the gravitational frequency shift of clocks was most precisely confirmed almost two decades ago by NASA's Gravitational Probe A mission in which a hydrogen maser clock in sub-orbital flight through the Earth's gravitational potential communicated via one and two-way radar links with another ground clock [Vessot et al, 1980]. Universality of gravitational free-fall rates have been

confirmed both in the Earth laboratory [Su et al, 1994], and to slightly higher fractional precision by using laser ranging between Earth and Moon as these bodies free-fall toward the Sun [Williams et al, 1996; Dickey et al, 1994]. The Earth's core material and the mantle-type material of the Moon and Earth shell are today found to accelerate equally to precision:

$$\frac{|a_{core} - a_{mantle}|}{g_{sun}} < 1.5 \cdot 10^{-12} \quad (3)$$

(My interpretation of the analyzed lunar laser ranging data concludes that this experiment actually confirms equality of free-fall by a factor of three or four higher precision than the conservative "realistic error" value given in (3)).

If other long range ($1/R^2$) forces act between matter, however, it is expected that both the universality of free-fall rates and the universality of clock frequency shifts will be violated. In this paper I focus on the comparison between these two types of experiments as to their relative quantitative abilities to test for the existence of other very weak, but long range, interactions.

A relationship between these two types of possible violations of Einstein's Equivalence Principle was developed some time ago for the case of "oscillator clocks" whose frequency is determined by the difference between two energy levels of a quantum system [Nordtvedt, 1975]:

$$\nu_{osc} = \frac{E_i - E_j}{\hbar} \quad (4)$$

A several step cyclic gedanken experiment was considered:

1. At height h above the floor a quantum system originally in state A makes a transition to a state B and in the process emits a quantum (such as a photon) which propagates down to the floor.

2. At the floor this quantum is absorbed and thereby excites an identical quantum system from state B up to a state A'.

3. The system at height h and in state B falls freely to the floor and acquires speed:

$$v_B^2 = 2g_B h \quad (5)$$

4. At the floor the two systems in states A' and B inelastically interact, ending up in states A and B with the system in state A traveling upward at just the speed necessary to reach the original height h:

$$v_A^2 = 2g_A h \quad (6)$$

Conservation of energy in the inelastic transition which took place at the floor required:

$$M_B \left(c^2 + \frac{1}{2} v_B^2 \right) + M_{A'} c^2 = M_B c^2 + M_A \left(c^2 + \frac{1}{2} v_A^2 \right) \quad (7)$$

Combining the several relationships (4-7) then yields a connection between the oscillator clock frequency shifts and the free-fall rates of the two quantum states:

$$\hbar(v(h) - v(0)) = (E_A - E_B) - (E_{A'} - E_B) = (M_B g_B - M_A g_A) h \quad (8a)$$

which can be reorganized to give:

$$\frac{v(h) - v(0)}{v(h)} = -\frac{gh}{c^2} \left(1 + \frac{M}{M_A - M_B} \frac{g_B - g_A}{g} \right) \quad (8b)$$

I will here reformulate this relationship to make it directly useful for testing an interesting class of possibilities in physical law --- that one or more of the dimensionless parameters of laboratory physics actually might vary in space-time by being related to some long range scalar field or entity. This possibility implies anomalous forces on any object:

$$\delta \vec{F}_a = \frac{\partial E_a}{\partial \alpha} \nabla \alpha \quad (9)$$

with α being some location-dependent dimensionless parameter in physical law. Two bodies then accelerate differently toward other bodies, the fractional difference of rates being:

$$\frac{|\vec{a}_k - \vec{a}_l|}{|\vec{g}|} \approx \left(\frac{\partial E_l}{E_l \partial \alpha} - \frac{\partial E_k}{E_k \partial \alpha} \right) \frac{|\nabla \alpha|}{|\nabla U|} \quad \text{with } \vec{g} = c^2 \nabla U \quad (10)$$

But this same positional dependence of the dimensionless parameter produces anomalous shifts of the oscillator clock rates (4):

$$\delta v' \approx \frac{1}{\hbar} \frac{\partial(E_i - E_j)}{\partial \alpha} \delta \alpha \quad (11)$$

Expressed as a fraction of the regular gravitational frequency shift, this anomalous clock effect is:

$$\frac{\delta v'}{\delta v} \approx - \frac{1}{E_i - E_j} \frac{\partial(E_i - E_j)}{\partial \alpha} \frac{\delta \alpha}{\delta U} \quad (12)$$

The ratio of gradients and changes for the dimensionless parameter and the gravitational potential which appear in (10) and (12) can be eliminated, leaving the desired connection between violations of the universality of free-fall rates and universality of clock frequency shifts which results if any dimensionless parameter of physical law varies in space-time:

$$\frac{\delta v'}{\delta v} \approx \frac{1}{E_i - E_j} \frac{\partial(E_i - E_j)}{\partial \alpha} \frac{\partial \alpha}{\partial \ln(E_k/E_l)} \frac{|\vec{a}_k - \vec{a}_l|}{|\vec{g}|} \quad (13)$$

Ruler and decay clocks are briefly defined in the later appendix to this paper.

Applications to Hyperfine Clocks.

The energy levels of clocks based on the hyperfine interaction have a specific dependence on the dimensionless parameters of physical law, determined in leading order by the products of the electron and nuclear magnetic moments and the inverse cube of electron orbit sizes:

$$v_{hf} \sim \frac{1}{\hbar} \frac{e\hbar}{m} \frac{e\hbar}{M} \left(\frac{\hbar^2}{me^2} \right)^{-3} \sim \left(\frac{e^2}{\hbar c} \right)^4 \left(\frac{m}{M} \right)^2 \frac{Mc^2}{\hbar} \quad (14)$$

On the other hand, different materials in free-fall experiments have fractional differences of their electromagnetic energy content of about a part in a thousand, this arising primarily from the coulomb energy between the nuclear protons. If the electromagnetic fine structure constant varies in space-time in proportion to inverse distance from other matter, and free-fall experiments are performed to the precision quoted previously (3), then the relationship (13) specifies the precision at which clock experiments must be performed to competitively test the varying fine structure constant hypothesis. Using (3), (13) and (14), I obtain:

$$\frac{\delta v'}{\delta v} \approx 4 \times 10^3 \times 1.5 \cdot 10^{-12} \approx 6 \cdot 10^{-9} \quad (15)$$

If a clock is brought to four solar radii from the Sun where that body's gravitational potential reaches the level:

$$U(\vec{R})_s \approx 5 \cdot 10^{-7} \quad \text{at 4 solar radii} \quad (16)$$

then measurement of the clock's gravitational frequency shift to precision of about three parts in 10^{15} is a competitive experiment with today's best free-fall experiments.

Such an experiment can be done two ways --- absolutely and differentially. In the absolute version of the experiment the strength coefficient for the inverse distance dependence of the clock's frequency shift is measured (by another clock on or near Earth) and compared with the Sun's Newtonian mass strength parameter Γ_s determined from solar system dynamics, i.e.:

$$\frac{d^2 \vec{R}}{dt^2} = -\frac{\Gamma_s}{R^3} \vec{R} + \dots \quad (17)$$

This parameter is sufficiently known to about a part in 10^{10} precision for the best-tracked planets such as Earth, Mars and Mercury. Such an absolute experiment also requires tracking the position of the spacecraft to better than 10 meters precision.

In the differential version of the experiment two precision clocks whose mechanisms depend differently on the fine structure constant are sent on a spacecraft which approaches the Sun. The shift in the frequency ratio of these two clocks on the spacecraft which varies as inverse distance from the Sun is measured. One needs neither a precision frequency link between spacecraft and Earth clocks, nor high precision knowledge of the position of the spacecraft. If one of these clocks is a hydrogen (hyperfine) maser clock, the other clock can not be a hyperfine clock based on a different atom, because all hyperfine clocks share at leading order the same dependence on the fourth power of the electromagnetic fine structure constant, though their individual frequencies are different multiples of this basic energy scale.

The weak interaction can also be tested for anomalous behavior. Although the electromagnetic and weak interactions have been beautifully unified into the "electro-weak" interaction, and we therefore should expect that the "weak fine structure constant" in (18) would probably mirror the behavior of the electromagnetic fine structure constant, one can hypothesize that the Z meson mass varies anomalously with space-time location. The weak interaction contributions to hyperfine levels, resulting from the parity-conserving part of the charge-neutral Z meson exchange between hadronic quarks and the atomic electrons, then scale as:

$$\delta v_{hf(w)} \sim \frac{1}{\hbar} \frac{\hbar^2 e_w^2}{M_z^2 c^2} \left(\frac{\hbar^2}{e^2 m} \right)^{-3} \sim \frac{e_w^2}{\hbar c} \left(\frac{e^2}{\hbar c} \right)^3 \left(\frac{m}{M} \right)^3 \left(\frac{M}{M_z} \right)^2 \frac{M c^2}{\hbar} \quad (18)$$

These energies are about 10^{-7} of the total hyperfine energy differences. On the other hand, the parity conserving weak interaction energy of the typical atomic nucleus is about 10^{-8} of the whole mass [Nordtvedt, 1972], while the fractional differences between nuclei only amounts to about a part in 10^{10} of the whole [Haugan and Will, 1976]. The basic relationship (13) for comparing free-fall and clock experiments then yields:

$$\frac{\delta v'}{\delta v} \approx 10^{-7} \times 10^{10} \times 1.5 \cdot 10^{-12} \approx 1.5 \cdot 10^{-9} \quad (19)$$

At four solar radii, hyperfine clock experiments precise to slightly better than a part in 10^{15} would therefore be competitive in testing anomalies in the weak interaction.

I have not considered possible space-time dependence of the strong interaction (quantum chromodynamics) dimensionless parameters. This dominant interaction of physics may also be coupled to long range scalar fields, however such coupling could probably be absorbed into the definition of the metric field, thereby showing none of the "non-metric" effects I have been discussing. For instance, if some strong interaction mass standard (such as a baryon mass) were space-time dependent, one may be able to define a new metric tensor field:

$$M(\vec{r}, t)^2 g(\vec{r}, t)_{\mu\nu} \rightarrow g(\vec{r}, t)'_{\mu\nu} \quad (20)$$

thereby revealing all gravitational effects to be those of alternative metric theories and quantified by the well known parameterized post-Newtonian (PPN) coefficients γ , β , etc.

Vector Interactions.

Another possible source of gravity-imitating but material-dependent acceleration rates of bodies results from a long range vector field (analogous to the electromagnetic field) which would couple to some other conserved current in matter. The associated "charge" of such a current could, for example, be a linear combination of a body's baryon number and electron number (we have yet to detect baryon-to-lepton conversions in physics):

$$B_{A,Z} = Q_A A + Q_Z Z \quad (21)$$

The total gravitational-like force between bodies is then:

$$F_{sk} = (GM_S M_k + B_S B_k) \frac{1}{R^2} \quad (22)$$

and the acceleration of a body "k" in the vicinity of the Sun is:

$$A_k = \frac{GM_s}{R^2} \left(1 + \frac{1}{G} \left(\frac{B}{M} \right)_s \left(\frac{B}{M} \right)_k \right) \quad (23)$$

Since the B/M ratio of different materials varies by about a part in a thousand, free-fall experiments constrain the absolute size of the material-dependent term in (23) to be less than about 10^{-9} . But this vector interaction does not affect oscillator clock rates because the conserved charge B of a clock quantum system is common to the two relevant states defining the clock:

$$\nu = \frac{(E_i + B_i/R) - (E_j + B_j/R)}{\hbar} = \frac{E_i - E_j}{\hbar} \quad \text{for } B_i = B_j \quad (24)$$

An absolute measurement of the $1/R$ dependent clock frequency shift will therefore measure solely the gravitational mass of the Sun - $GM(G)_s$ - while solar system dynamics measures the entire coupling strength Γ_{sk} in (17) for inner planets Earth, Mars, Mercury.

Appendix - Ruler and Decay Clocks.

Oscillator clocks were previously defined by (4). "Ruler clocks" such as the superconducting cavity stabilized oscillator (SCSO) have rates depending quite differently on the dimensionless parameters of physics - their frequencies scaling simply as the speed of light divided by the atomic length scale:

$$\nu_{\text{ruler}} \sim c \frac{me^2}{\hbar^2} \sim \left(\frac{e^2}{\hbar c} \right) \frac{mc^2}{\hbar} \quad (25)$$

"Decay clocks" are defined by the rate at which quantum systems make transitions from one state into another. Such rates can not be measured to anything like the precision with which oscillation frequencies are measured, nevertheless such decay clocks have interestingly different dependence on physical law. Many of them have rates determined by Fermi's "golden rule":

$$\Gamma = \frac{2\pi}{\hbar} |H_{if}|^2 \frac{dn}{dE_f} \quad (26)$$

If a decay clock is based on the weak interaction for its transition, for example, the rate is determined almost entirely by the weak interaction hamiltonian rather than the overwhelmingly stronger nuclear and electromagnetic interactions. Hence an anomalous coupling of the weak interaction to gravity could result in a relatively large anomaly in the gravitational frequency shift of such clocks.

There are other types of decay clocks. For instance, the rate of alpha decay of nuclei is governed by the tunneling integral for the alpha particle passing through the classically forbidden region of the combined nuclear-electrostatic potential:

$$\Gamma = \frac{V_{int}}{D} \exp -2 I \tag{27}$$

$$I = \frac{1}{\hbar} \int \left(2M_{\alpha} \left(E - \frac{2(Z-2)e^2}{r} - \frac{\hbar^2 l(l+1)}{2M_{\alpha} r^2} \right) \right)^{1/2} dr$$

This work supported in part by National Aeronautics and Space Administration NASW-4840.

References

- Dickey, J. O., Bender, P. L., Faller, J. E., Newhall, X X, Ricklefs, R. L., Ries, J. G., Shelus, P. J., Veillet, C., Whipple, A. L., Wiant, J. R., Williams, J. G. and Yoder, C. F. (1994). Lunar Laser Ranging: A Continuing Legacy of the Apollo Program. *Science* 265, 482.
- Haugan, M. P. and Will, C. Weak Interactions and Eotvos experiments. *Phys. Rev. Lett.* 37, 1.
- Nordtvedt, K. (1972). Gravitation Theory: Empirical Status from Solar System Experiments. *Science* 178, 1157.
- Nordtvedt, K. (1975). Quantitative Relationship Between Clock Gravitational "Red Shift" Violations and Nonuniversality of Free-Fall Rates in Nonmetric Theories of Gravity. *Phys. Rev. D* 11(2), 245.
- Su, Y., Heckel, B. R., Adelberger, E. G., Gundlach, J. H., Harris, M., Smith, G. L., Swanson, N. E. (1994). New Tests of the Universality of Free-Fall. *Phys. Rev. D* 50, 3614.
- Vessot, R. F. C., Levine, M. W., Mattison, E. M., Blomberg, E. L., Hoffman, T. E., Nystrom, G. U., Farrel, B. F., Decher, R., Eby, P. B., Baugher, C. R., Watts, J. W., Teuber, D. L., and Wills, F. O. (1980). Test of Relativistic Gravitation with a Space-Borne Hydrogen Maser. *Phys. Rev. Lett.* 45, 2081.
- Williams, J. G., Newhall, X X and Dickey, J. O. (1996). Relativity Parameters Determined from Lunar Laser Ranging. *Phys. Rev. D* 53, 6730.

Gravity, Equivalence Principle and Clocks

Thibault DAMOUR

Institut des Hautes Etudes Scientifiques, 91440 Bures-sur-Yvette, France
and DARC, CNRS - Observatoire de Paris, 92195 Meudon Cedex, France

Abstract

String theory suggests the existence of gravitational-strength scalar fields (“dilaton” and “moduli”) whose couplings to matter violate the equivalence principle. This provides a new motivation for high-precision clock experiments, as well as a generic theoretical framework for analyzing their significance.

1 Introduction

The basic question we wish to address is the following: given the existing experimental tests of gravity, and given the currently favored theoretical framework, can high-precision clock experiments probe interesting theoretical possibilities which remain yet unconstrained? In addressing this question we wish to assume, as theoretical framework, the class of effective field theories suggested by modern unification theories, and notably string theory.

To start, let us mention that the theoretical framework most studied in the phenomenology of gravitation, i.e. the class of “metric” theories of gravity [1], which includes most notably the “Brans-Dicke”-type tensor-scalar theories, appears as being rather artificial. This is good news because the

phenomenology of “non metric” theories is richer and offers new possibilities for clock experiments. Historically, the restricted class of “metric” theories was introduced in 1956 by Fierz [2] to prevent, in an *ad hoc* way, too violent a conflict between experimental tests of the equivalence principle and the existence of a scalar contribution to gravity as suggested by the theories of Kaluza-Klein [3] and Jordan [4]. Indeed, Fierz was the first one to notice that a Kaluza-Klein scalar would generically strongly violate the equivalence principle. He then proposed to restrict artificially the couplings of the scalar field to matter so as to satisfy the equivalence principle. The restricted class of equivalence-principle-preserving couplings introduced by Fierz is now called “metric” couplings. Under the aegis of Dicke, Nordtvedt, Thorne and Will a lot of attention has been given to “metric” theories of gravity¹, and notably to their quasi-stationary-weak-field phenomenology (“PPN framework”, see, e.g., [1]).

By contrast, we wish to stress that nearly all unification theories (from Kaluza-Klein to string theory) suggest that “gravitational interactions” are mediated not only by the tensor field ($g_{\mu\nu}$) postulated by Einstein, but also by one or more extra fields, having couplings which violate the equivalence principle. Among these extra fields the most universally present seem to be scalar fields, of the type of the “dilaton” of string theory.

Recently, a mechanism has been proposed [5] to reconcile in a natural manner the existence of a dilaton field as a fundamental partner of the graviton field $g_{\mu\nu}$ with the current level of precision ($\sim 10^{-12}$) of experimental tests of the equivalence principle. In the mechanism of [5] (see also [6] for metrically-coupled scalars) the very small couplings necessary to ensure a near universality of free fall, $\Delta a/a < 10^{-12}$, are dynamically generated by the expansion of the universe, and are compatible with couplings “of order unity” at a fundamental level.

The point of the present paper is to emphasize the rich phenomenological consequences of dilaton-like fields, and the fact that high-precision clock experiments might contribute to searching for, or constraining, their existence.

¹Note that Nordtvedt, Will, Haugan and others (for references see [1] and the contributions of Nordtvedt and Haugan to these proceedings) studied conceivable phenomenological consequences of generic “non metric” couplings, without, however, using, as we do here, a motivated field-theory framework describing such couplings.

2 Generic effective theory of a long-range dilaton

Motivated by string theory, we consider the generic class of theories containing a long-range dilaton-like scalar field φ . The effective Lagrangian describing these theories has the form:

$$L_{\text{eff}} = \frac{1}{4q} R(g_{\mu\nu}) - \frac{1}{2q} (\nabla\varphi)^2 - \frac{1}{4e^2(\varphi)} (\nabla_\mu A_\nu - \nabla_\nu A_\mu)^2 - \sum_A \left[\bar{\psi}_A \gamma^\mu (\nabla_\mu - iA_\mu) \psi_A + m_A(\varphi) \bar{\psi}_A \psi_A \right] + \dots \quad (1)$$

Here, $q \equiv 4\pi \bar{G}$ where \bar{G} denotes a bare Newton's constant, A_μ is the electromagnetic field, and ψ_A a Dirac field describing some fermionic matter. At the low-energy, effective level (after the breaking of $SU(2)$ and the confinement of colour), the coupling of the dilaton φ to matter is described by the φ -dependence of the fine-structure “constant” $e^2(\varphi)$ and of the various masses $m_A(\varphi)$. Here, A is a label to distinguish various particles. [A deeper description would include more coupling functions, e.g. describing the φ -dependences of the $U(1)_Y$, $SU(2)_L$ and $SU(3)_c$ gauge coupling “constants”.]

The strength of the coupling of the dilaton φ to the mass $m_A(\varphi)$ is given by the quantity

$$\alpha_A \equiv \frac{\partial \ln m_A(\varphi_0)}{\partial \varphi_0}, \quad (2)$$

where φ_0 denotes the ambient value of $\varphi(x)$ (vacuum expectation value of $\varphi(x)$ around the mass m_A , as generated by external masses and cosmological history). For instance, the usual PPN parameter $\gamma - 1$ measuring the existence of a (scalar) deviation from the pure tensor interaction of general relativity is given by [7], [5]

$$\gamma - 1 = -2 \frac{\alpha_{\text{had}}^2}{1 + \alpha_{\text{had}}^2}, \quad (3)$$

where α_{had} is the (approximately universal) coupling (2) when A denotes any (mainly) hadronic object.

The Lagrangian (1) also predicts (as discussed in [5]) a link between the coupling strength (2) and the violation of the universality of free fall:

$$\frac{\alpha_A - \alpha_B}{\frac{1}{2}(\alpha_A + \alpha_B)} \simeq (\alpha_A - \alpha_B) \alpha_E \sim -5 \times 10^{-5} \alpha_{\text{had}}^2. \quad (4)$$

Here, A and B denote two masses falling toward an external mass E (e.g. the Earth), and the numerical factor -5×10^{-5} corresponds to $A = \text{Be}$ and $B = \text{Cu}$. The experimental limit [8]

$$\left(\frac{\Delta a}{a}\right)_{\text{Be Cu}} = (-1.9 \pm 2.5) \times 10^{-12} \quad (5)$$

shows that the (mean hadronic) dilaton coupling strength is already known to be very small:

$$\alpha_{\text{had}}^2 \lesssim 10^{-7}. \quad (6)$$

Free fall experiments, such as Eq. (5) or the comparable Lunar Laser Ranging constraint [9], give the tightest constraints on any long-range dilaton-like coupling. Let us mention, for comparison, that solar-system measurements of the PPN parameters (as well as binary pulsar measurements) constrain the dilaton-hadron coupling to $\alpha_{\text{had}}^2 < 10^{-3}$, while the best current constraint on the time variation of the fine-structure “constant” (deduced from the Oklo phenomenon), namely [10]

$$-6.7 \times 10^{-17} \text{ yr}^{-1} < \frac{d}{dt} \ln e^2 < 5.0 \times 10^{-17} \text{ yr}^{-1}, \quad (7)$$

yields from Eq. (17) below, $\alpha_{\text{had}}^2 \lesssim 3 \times 10^{-4}$.

To discuss the probing power of clock experiments, we need also to introduce other coupling strengths, such as

$$\alpha_{\text{EM}} \equiv \frac{\partial \ln e^2(\varphi_0)}{\partial \varphi_0}, \quad (8)$$

measuring the φ -variation of the electromagnetic (EM) coupling constant², and

$$\alpha_A^{A^*} \equiv \frac{\partial \ln E_A^{A^*}(\varphi_0)}{\partial \varphi_0}, \quad (9)$$

where $E_A^{A^*}$ is the energy difference between two atomic energy levels.

²Note that we do not use the traditional notation α for the fine-structure constant $e^2/4\pi\hbar c$. We reserve the letter α for denoting various dilaton-matter coupling strengths. Actually, the latter coupling strengths are analogue to e (rather than to e^2), as witnessed by the fact that observable deviations from Einsteinian predictions are proportional to products of α 's, such as $\alpha_A \alpha_E$, α_{had}^2 , etc...

In principle, the quantity $\alpha_A^{A^*}$ can be expressed in terms of more fundamental quantities such as the ones defined in Eqs. (2) and (8). For instance, in an hyperfine transition

$$E_A^{A^*} \propto (m_e e^4) g_I \frac{m_e}{m_p} e^4 F_{\text{rel}}(Ze^2), \quad (10)$$

so that

$$\alpha_A^{A^*} \simeq 2\alpha_e - \alpha_p + \alpha_{\text{EM}} \left(4 + \frac{d \ln F_{\text{rel}}}{d \ln e^2} \right). \quad (11)$$

Here, the term $F_{\text{rel}}(Ze^2)$ denotes the relativistic (Casimir) correction factor [11]. Moreover, in any theory incorporating gauge unification one expects to have the approximate link [5]

$$\alpha_A \simeq \left(40.75 - \ln \frac{m_A}{1 \text{ GeV}} \right) \alpha_{\text{EM}}, \quad (12)$$

at least if m_A is mainly hadronic.

3 Clock experiments and dilaton couplings

The coupling parameters introduced above allow one to describe the deviations from general relativistic predictions in most clock experiments [12]. Let us only mention some simple cases.

First, it is useful to distinguish between “global” clock experiments where one compares spatially distant clocks, and “local” clock experiments where the clocks being compared are next to each other. The simplest global clock experiment is a static redshift experiment comparing (after transfer by electromagnetic links) the frequencies of the same transition $A^* \rightarrow A$ generated in two different locations \mathbf{r}_1 and \mathbf{r}_2 . The theory of Section 2 predicts a redshift of the form (we use units in which $c = 1$)

$$\frac{\nu_A^{A^*}(\mathbf{r}_1)}{\nu_A^{A^*}(\mathbf{r}_2)} \simeq 1 + (1 + \alpha_A^{A^*} \alpha_E) (\bar{U}_E(\mathbf{r}_2) - \bar{U}_E(\mathbf{r}_1)), \quad (13)$$

where

$$\bar{U}_E(\mathbf{r}) = \frac{\bar{G} m_E}{r} \quad (14)$$

is the *bare* Newtonian potential generated by the external mass m_E (say, the Earth). Such a result has the theoretical disadvantage of depending on other experiments for its interpretation. Indeed, the *bare* potential \bar{U}_E is not directly measurable. The measurement of the Earth potential by the motion of a certain mass m_B gives access to $(1 + \alpha_B \alpha_E) \bar{U}_E(\mathbf{r})$. The theoretical significance of a global clock experiment such as (13) is therefore fairly indirect, and involves other experiments and other dilaton couplings. One can generalize (13) to a more general, non static experiment in which different clocks in relative motion are compared. Many different “gravitational potentials” will enter the result, making the theoretical significance even more involved.

A conceptually simpler (and, probably, technologically less demanding) type of experiment is a differential, “local” clock experiment. Such “null” clock experiments have been proposed by Will [1] and first performed by Turneure et al. [13]. The theoretical significance of such experiments within the context of dilaton theories is much simpler than that of global experiments. For instance if (following the suggestion of [14]) one locally compares two clocks based on hyperfine transitions in alkali atoms with different atomic number Z , one expects to find a ratio of frequencies

$$\frac{\nu_A^{A^*}(\mathbf{r})}{\nu_B^{B^*}(\mathbf{r})} \simeq \frac{F_{\text{rel}}(Z_A e^2(\varphi_{\text{loc}}))}{F_{\text{rel}}(Z_B e^2(\varphi_{\text{loc}}))}, \quad (15)$$

where the local, ambient value of the dilaton field φ_{loc} might vary because of the (relative) motion of external masses with respect to the clocks (including the effect of the cosmological expansion). The directly observable fractional variation of the ratio (15) will consist of two factors:

$$\delta \ln \frac{\nu_A^{A^*}}{\nu_B^{B^*}} = \left[\frac{\partial \ln F_{\text{rel}}(Z_A e^2)}{\partial \ln e^2} - \frac{\partial \ln F_{\text{rel}}(Z_B e^2)}{\partial \ln e^2} \right] \times \delta \ln e^2. \quad (16)$$

The “sensitivity” factor in brackets due to the Z -dependence of the Casimir term can be made of order unity [14], while the fractional variation of the fine-structure constant is expected in dilaton theories to be of order [5], [12]

$$\begin{aligned} \delta \ln e^2(t) &= -2.5 \times 10^{-2} \alpha_{\text{had}}^2 U(t) \\ &- 4.7 \times 10^{-3} \kappa^{-1/2} (\tan \theta_0) \alpha_{\text{had}}^2 H_0(t - t_0). \end{aligned} \quad (17)$$

Here, $U(t)$ is the value of the externally generated gravitational potential at the location of the clocks, and $H_0 \simeq 0.5 \times 10^{-10} \text{ yr}^{-1}$ is the Hubble rate of expansion. [The factor $\kappa^{-1/2} \tan \theta_0$ is expected to be ~ 1 .]

The (rough) theoretical prediction (17) allows one to compare quantitatively the probing power of clock experiments to that of equivalence principle tests. Let us (optimistically) assume that clock stabilities of order $\delta\nu/\nu \sim 10^{-17}$ (for the relevant time scale) can be achieved. A differential *ground* experiment (using the variation of the Sun’s potential due to the Earth eccentricity) would probe the level $\alpha_{\text{had}}^2 \sim 3 \times 10^{-6}$. A geocentric satellite differential experiment could probe $\alpha_{\text{had}}^2 \sim 5 \times 10^{-7}$. These levels are impressive (compared to present solar-system tests of the PPN parameter γ giving the constraint $\alpha_{\text{had}}^2 \simeq (1 - \gamma)/2 < 10^{-3}$), but are not as good as the present equivalence-principle limit (6). To beat the level (6) one needs to envisage an heliocentric differential clock experiment (a few solar radii probe within which two hyper-stable clocks are compared). Such a futuristic experiment could, according to Eq. (17), reach the level $\alpha_{\text{had}}^2 \sim 10^{-9}$. [Let us also note that a gravitational time delay global experiment using clocks beyond the Sun as proposed by C. Veillet (SORT concept) might (optimistically) probe the level $\alpha_{\text{had}}^2 \sim 10^{-7}$.] It is, however, to be noted that a much refined test of the equivalence principle such as STEP (Satellite Test of the Equivalence Principle) aims at measuring $\Delta a/a \sim 10^{-18}$ which corresponds to the level $\alpha_{\text{had}}^2 \sim 10^{-14}$, i.e. five orders of magnitude better than any conceivable clock experiment.

4 Conclusions

In summary, the main points of the present contribution are:

- Independently of any theory, the result (7) of a recent reanalysis of the Oklo phenomenon [10] gives a motivation, and a target, for improving laboratory clock tests of the time variation of the fine-structure constant e^2 (which are at the $3.7 \times 10^{-14} \text{ yr}^{-1}$ level [14]).
- Modern unification theories, and especially string theory, suggest the existence of new gravitational-strength fields, notably scalar ones (“dilaton” or “moduli”), whose couplings to matter violate the equivalence principle. These fields would induce a spacetime variability of the coupling constants of physics (such as the fine-structure constant). High-precision clock experiments are excellent probes of such a possibility.

- The generic class of dilaton theories defined in Section 2 provides a well-defined theoretical framework in which one can discuss the phenomenological consequences of the existence of a dilaton-like field. Such a theoretical framework (together with some assumptions, e.g. about gauge unification and the origin of mass hierarchy) allows one to compare and contrast the probing power of clock experiments to that of other experiments.
- Local, differential clock experiments (of the “null” type of [13]) appear as conceptually cleaner, and technologically less demanding, probes of dilaton-motivated violations of the equivalence principle than global, absolute clock experiments (of the Gravity Probe A type).
- If we use the theoretical assumptions of Section 2 to compare clock experiments to free-fall experiments, one finds that one needs to send and intercompare two ultra-high-stability clocks in near-solar orbit in order to probe dilaton-like theories more deeply than *present* free-fall experiments. Currently proposed improved satellite tests of the equivalence principle would, however, beat any clock experiment in probing even more deeply such theories.
- At the qualitative level, it is, however, important to note that clock experiments (especially of the “global”, GPA type) probe different combinations of basic coupling parameters than free-fall experiments. This is visible in Eq. (11) which shows that $\alpha_A^{A^*}$ contains the leptonic quantity $\alpha_e = \partial \ln m_{\text{electron}}/\partial \varphi_0$ without any small factor³.

References

- [1] C.M. Will, *Theory and experiment in gravitational physics* (Cambridge University Press, 1981); second edition 1993.
- [2] M. Fierz, *Helv. Phys. Acta* **29** (1956) 128.

³Free-fall experiments couple predominantly to hadronic quantities such as $\alpha_p = \partial \ln m_{\text{proton}}/\partial \varphi_0$, and to Coulomb-energy effects proportional to α_{EM} . The effect of the leptonic quantity α_e is down by a small factor $\sim m_e/m_p \sim 1/1836$.

- [3] T. Kaluza, Sitz. der K. Preuss. Akad. der Wiss. (1921) 966;
O. Klein, Zeit. für Physik **37** (1926) 895.
- [4] P. Jordan, Nature **164** (1949) 637; *Schwerkraft und Weltall*
(Vieweg, Braunschweig, 1955).
- [5] T. Damour and A.M. Polyakov, Nucl. Phys. B **423** (1994) 532;
Gen. Rel. Grav. **26** (1994) 1171.
- [6] T. Damour and K. Nordtvedt, Phys. Rev. Lett. **70** (1993) 2217;
Phys. Rev. D **48** (1993) 3436.
- [7] T. Damour and G. Esposito-Farèse, Class. Quant. Grav. **9** (1992)
2093.
- [8] Y. Su et al., Phys. Rev. D **50** (1994) 3614.
- [9] J.O. Dickey et al., Science **265** (1994) 482;
J.G. Williams et al., Phys. Rev. D **53** (1996) 6730.
- [10] T. Damour and F. Dyson, Nucl. Phys. B **480** (1996) 37; hep-
ph/9606486.
- [11] H. Kopfermann, *Nuclear Moments* (Academic Press, New York,
1958), pp.123-138;
H.B.G. Casimir, *On the Interaction between Atomic Nuclei and
Electrons* (Freeman, San Francisco, 1963), p.54.
- [12] T. Damour, in preparation.
- [13] J.P. Turneaure et al., Phys. Rev. D **27** (1983) 1705.
- [14] J.D. Prestage, R.L. Tjoelker and L. Maleki, Phys. Rev. Lett. **74**
(1995) 3511.

Gravitation Physics and a Space Clock Mission

Mark P. Haugan

Department of Physics, Purdue University

West Lafayette, Indiana 47907

ABSTRACT

Inspired by developments in the technology of trapped-ion atomic frequency standards that promise to decrease the cost of a space clock mission significantly, we review some of the gravitation physics which motivates such a mission. The focus here is on physics that can be probed during a mission's initial phase, while the clock is in Earth orbit. John Armstrong discusses the significance of searches for low-frequency gravitational waves that can be conducted during a second mission phase later in these proceedings.

MAIN BODY OF PAPER

When considering the possibility of flying an atomic frequency standard in space discussions of gravitation physics that could be explored almost invariably focus on precision measurements of the gravitational redshift and on searches for low-frequency gravitational waves using the Doppler-ranging technique first suggested by Estabrook and Wahlquist¹. This is understandable. The former is a familiar test of the Einstein equivalence principle, the foundation upon which general relativity and all other metric gravitation theories rest, while detecting gravitational waves is a timely challenge to experimenters that will open a unique window on large scale mass motions in astronomical processes.

The purpose of this note is to reassess some of the motivation for a space clock mission stemming from gravitation physics. This review is inspired by the dramatic reduction in the cost of mounting a clock mission promised by advances in the technology of atomic frequency standards based on Hg^+ ions confined in linear ion traps². The combination of strong physics motivation and affordability suggest that the time for such a mission has come.

In this note we draw attention to two types of Einstein equivalence principle test that are independent of redshift measurements and can be conducted during a space clock mission. We argue that these tests add significantly to the already strong motivation for such a mission. Regarding that motivation, note particularly that observing gravitational waves with frequencies less than about 10 Hz must be done from space and that this low-frequency band carries information about the largest scale astronomical mass motions. A clock mission could be used to search for these low-frequency waves with unprecedented precision as John Armstrong shows later in these proceedings.

The notion of a space clock mission is not new. Indeed, rather detailed mission studies have already been performed. We base our remarks concerning gravitation physics that can be probed during a space clock mission on the Smarr *et al.* study³ published in 1983.

The Earth-orbit portion of the mission those authors considered features a clock with 10^{-15} stability on a satellite with commensurate ranging capabilities in an eccentric orbit with 24 hour period. That period makes it possible to monitor the clock's range and frequency continuously from a single ground station. The clock's range at perigee and at apogee are 1.5×10^4 and 5.7×10^4 kilometers. It follows that both the gravitational redshift and the second-order Doppler shift contribute at the 5×10^{-10} level to the perigee-apogee variation of the fractional difference between the frequencies of the ground station and orbiting clocks. Naively comparing this variation to the clock stability suggests that the redshift and

second-order Doppler shift could be measured to 2 parts in 10^6 . Smarr *et al.* estimate that this performance would be degraded by a factor of two or so by systematic errors in ranging and time transfer between the clocks. The dominant contribution to this error is noise introduced by the propagation of radio signals through the troposphere. Since the ability to compensate for such tropospheric noise has improved recently⁴ corresponding improvements in clock mission performance are likely.

To appreciate the motivation for experiments and observations like measurements of the gravitational redshift consider the interplay between experimental and theoretical gravitation physics. One way of characterizing this interplay is to say that experimental gravitation physics distinguishes unviable gravitation theories from viable ones. Alternatively, since potentially viable gravitation theories almost invariably admit a Lagrangian formulation via an action principle,

$$\delta \int \mathcal{L}(\psi_m, \psi_g) d^4x = 0, \quad (1)$$

where ψ_m and ψ_g denote matter and gravitational fields respectively, one may say that experimental gravitation physics aims to pin down the structure of the action (1). Indeed, one can begin with a general form of the scalar Lagrangian density \mathcal{L} constructed from matter and (possible) gravitational fields, make physical predictions and adjust \mathcal{L} 's form as necessary to keep the predictions consistent with experimental outcomes.

This approach to gravitation physics is analogous to effective field theory methods applied in particle physics. The form of an action (1) purporting to be that of a fundamental field theory would likely be constrained by technical demands like renormalizability or the validity of exotic symmetries, but effective field theories aspire only to account for low-energy physics and have more general structures. The focus on accessible energies is conservative in that it refuses to reject a possible form of the action (1) on such technical grounds. This conservatism seems wise since establishing the connection between a more fundamental theory's structure and the low-energy physics it predicts is a itself a challenging problem. As evidence of this we note that effective field theory continues to be an important tool in low-energy hadronic physics even though, in principle, this physics is derivable from QCD.

The significance of the Einstein equivalence principle is especially clear when one takes the view that experimental gravitation physics seeks to constrain empirically the form of the action (1). The principle's modern formulation⁵ states that the outcomes of nongravitational test experiments performed within a local, freely falling frame are independent of the frame's velocity through and location in an external gravitational field. This makes operational statements and is, therefore, directly testable. On the other hand, it can be argued convincingly that the validity of this principle implies that gravity is a metric phenomenon, that a single symmetric-tensor gravitational field couples universally to all matter. Consequently, experimental tests of the Einstein equivalence principle directly constrain the structure of that part of the action (1) responsible for coupling matter to the gravitational field. Current theoretical efforts to quantize gravity and to unify it with the other fundamental forces of Nature indicate a need to sharpen these constraints since almost all of these speculations suggest that the purely metric account of gravitation must eventually fail. We say little here about principles and experiments that constrain the structure of the rest of the action (1), despite their importance, because it is primarily the physics of the Einstein equivalence principle that can be probed in new ways during the orbital phase of a space clock mission.

To understand how the Einstein equivalence principle constrains (1) observe that this principle applies directly only to situations in which a local nongravitational system, like an atom whose transitions govern

the frequency of a space-borne clock, are immersed in an external gravitational field, $\psi_g^{(e)}$. Matter equations of motion that govern the behavior of the nongravitational system follow from the action principle,

$$\delta \int \mathcal{L}_{ng}(\psi_m, \psi_g^{(e)}) d^4x = 0, \quad (2)$$

where the matter fields, ψ_m , are varied but the external gravitational field, $\psi_g^{(e)}$ is not. The Lagrangian density \mathcal{L}_{ng} consists of those terms of \mathcal{L} that depend on matter fields. The outcome of an experimental test of the Einstein equivalence principle either forces \mathcal{L}_{ng} toward the metric form in which a single tensor field couples universally to all kinds of matter or reveals effects of nonmetric couplings between matter and the gravitational field that violate the Einstein equivalence principle.

Tests of this principle are often interpreted within a framework provided by a general model of \mathcal{L}_{ng} which uses phenomenological potentials to represent an external gravitational field of interest. The $TH\epsilon\mu$ and χg formalisms⁶ and their extensions⁷ provide such model actions. Given any particular gravitation theory one can determine how the components of its gravitational fields are related to the phenomenological potentials appearing in a model action. The advantage of working directly in terms of the potentials is that tests of the Einstein equivalence principle can be designed and interpreted in a theory-independent way. This approach also meshes nicely with heuristic discussions of familiar tests of the Einstein equivalence principle in terms of properties like the inertial and gravitational masses of test systems. For example, Eötvös-type experiments⁵ establish the equality of a system's inertial and passive gravitational masses to parts in 10^{11} regardless of the system's structure or composition. Haugan⁸ shows how to define a test system's inertial and gravitational masses in formalisms of the type considered above so that the impact of a constraint like this on the form of the action (1) can be determined.

As one thinks about a space clock mission it is important to realize that measurements of the gravitational redshift and second-order Doppler shift made with atomic clocks can also be related to inertial and gravitational masses, the masses of atoms in the two states involved in the transition that controls the clock frequency⁸ in this case. This implies that while such measurements are tests of the Einstein equivalence principle their outcomes are not independent of those of Eötvös-type tests. A clever cyclic argument due to Nordtvedt⁹ drives this point home by showing that one could build a perpetual motion machine if these tests were independent!

Gravitational redshift and second-order Doppler shift measurements made during a space clock mission would be significant because they improve by more than an order of magnitude on the precision of previous direct measurements. The GPA experiment¹⁰ achieved a precision of 7 parts in 10^5 , for example. On the other hand, GPA and a space clock mission directly measure a combination of the redshift and second-order Doppler shift that is sensitive to composition- and structure-dependence of inertial and gravitational masses in much the same way that Eötvös-type experiments are, and it turns out that testing the Einstein equivalence principle more stringently than those experiments do would require a space clock precision at least two orders of magnitude greater than that proposed. Consequently, space clock measurements of the gravitational redshift and second-order Doppler shift are important more as checks on the overall consistency of our conceptual framework for gravitation physics than as deep new tests of the Einstein equivalence principle.

A space clock mission does, however, offer other opportunities to test new aspects of the Einstein equiv-

alence principle. Will's recent analysis of an idealized space clock mission¹¹ reveals one. He shows that the expression for the second-order Doppler shift measured between the ground station and space clocks can include a term $2\alpha\vec{W} \cdot \vec{V}$, where \vec{V} is the velocity of the space clock relative to the ground station clock and where \vec{W} is the velocity of the Earth relative to the cosmic microwave background. In units of c , the magnitude of \vec{W} is 1.3×10^{-3} while that of \vec{V} at perigee is about 3.2×10^{-5} so the proposed clock mission could measure an α magnitude as small as 10^{-8} , nearly an order of magnitude smaller than the present limit set by a so-called Mössbauer rotor experiment¹². The significance of such a measurement lies in the relationship that can be established between the value of α and the inertial masses of atoms in the states involved in the transition that controls the clock frequency. Reference 8 derives this relationship for a rotor experiment analyzed within the $TH\epsilon\mu$ formalism, for example. Unlike Eötvös-type experiments and conventional space clock redshift-Doppler measurements, a measurement of α imposes a constraint directly on a system's inertial mass rather than on its gravitational to inertial mass ratio.

To see a second way in which a space clock mission can test a new aspect of the Einstein equivalence principle we must acknowledge a complication that we have ignored so far. The discussion above may leave the impression that a system's inertial and gravitational masses are scalar quantities, as they are in elementary physics. However, for systems that are not spherical they are generally tensors⁸ reflecting the fact that such a system's gravitational potential and kinetic energies can depend upon its orientation in space. Experiments of the Hughes-Drever type^{5,13} were developed to search for just such orientation dependence. It follows that they impose constraints directly on anisotropies of the inertial and gravitational masses of test systems. Performing a Hughes-Drever type experiment on a space clock mission would require that a $^{199}\text{Hg}+$ clock frequency be monitored relative to a $^{201}\text{Hg}+$ clock frequency on board the spacecraft. This would increase mission complexity marginally, but such an experiment would be the first sensitive to anisotropies of gravitational and inertial masses induced by the Earth's own gravitational field. An analogous Earth-bound experiment might conceivably be as sensitive to gravitational mass anisotropies, but the large magnitude of a space clock's orbital velocity at perigee ensures that a space-borne experiment would be at least two orders of magnitude more sensitive to inertial mass anisotropies. Recent research dealing with gravitational and other interactions having finite ranges makes the search for Einstein equivalence principle violations induced by the Earth's field alone particularly interesting.

References

1. F. Estabrook and H. Wahlquist, *GRG* **6**, 439 (1975).
2. see the contribution by J. Prestage in these proceedings and references therein.
3. L. Smarr, R. Vessot, C. Lundquist, R. Decher and Tsvi Piran, *GRG* **15**, 129 (1983).
4. see the contribution by J. Armstrong in these proceedings and references therein.
5. C. M. Will, *Theory and Experiment in Gravitation Physics, Revised Edition*, (Cambridge University Press, 1993).
6. A. Lightman and D. Lee, *Phys. Rev.* **D8**, 364 (1973) and W.-T. Ni, *Phys. Rev. Lett.* **38**, 301 (1977).
7. W.-T. Ni, *Phys. Lett. A* **120**, 174 (1987) and J. E. Horvath *et al.*, *Phys. Rev.* **38**, 1754 (1988).
8. M. P. Haugan *Ann. Phys. (NY)* **118**, 156 (1979).
9. K. Nordtvedt Jr., *Phys. Rev.* **11**, 245 (1975).
10. R. F. C. Vessot *et al.*, *Phys. Rev. Lett.* **45**, 2081 (1980).

11. C. M. Will, *Phys. Rev. D* **45**, 403 (1992).
12. G. R. Isaac, *Phys. Bull.* **21**, 255 (1970).
13. V. Hughes *et al.*, *Phys. Rev. Lett.* **4**, 342 (1960); R. W. P. Drever, *Phil. Mag.* **6**, 683 (1961); J. D. Prestage *et al.*, *Phys. Rev. Lett.* **54**, 2387 (1985); S. Lamoreaux *et al.*, *Phys. Rev. Lett.* **57**, 3125 (1986) and T. Chupp *et al.*, *Phys. Rev. Lett.* **63**, 1541 (1989).

Spacecraft Tests of General Relativity

John D. Anderson
Jet Propulsion Laboratory
California Institute of Technology
Pasadena, California 91109-8099

17 January 1997

Abstract

Current spacecraft tests of general relativity depend on coherent radio tracking referred to atomic frequency standards at the ground stations. This paper addresses the possibility of improved tests using essentially the current system, but with the added possibility of a space-borne atomic clock. Outside of the obvious measurement of the gravitational frequency shift of the spacecraft clock, a successor to the suborbital flight of a Scout D rocket in 1976 (GP-A Project), other metric tests would benefit most directly by a possible improved sensitivity for the reduced coherent data. For purposes of illustration, two possible missions are discussed. The first is a highly eccentric Earth orbiter, and the second a solar-conjunction experiment to measure the Shapiro time delay using coherent Doppler data instead of the conventional ranging modulation.

1 Introduction

The idea behind dynamical experiments with spacecraft is to fit a parameterized orbital model to radio Doppler data by weighted nonlinear least squares^{1,2,3}. Because of the large number of observations, formal error estimates from the least-squares covariance matrix are based on an assumption of independent measurements drawn from a Gaussian noise distribution. Reduced radio Doppler data are Gaussian, but if plasma noise dominates, their power spectral density follows an $f^{-2/3}$ law arising from propagation of the radio carrier wave through the plasma⁴, where f is the Fourier frequency. The variance of spectral estimates of a signal roughly follows the same power law dependence as the noise spectrum, so gravity signals are better determined at higher Fourier frequencies.

Data weighting is based on an assumed variance approximately equal to the variance of the Doppler residuals. This is about right for many gravity signals, where the peak Fourier components are around 2×10^{-3} Hz. However, for signals at lower Fourier frequencies, the formal errors from the covariance matrix are usually multiplied by a factor of three or more in order to obtain best estimates of realistic standard error.

With an atomic clock on the spacecraft, it becomes possible to obtain simultaneous one-way Doppler (spacecraft transmitting, ground receiving) and two-way Doppler (ground transmitting and receiving). Systematic errors from first-order Doppler or signal propagation can be canceled to a level appreciably below the inherent noise, as demonstrated in the 1976 SAO/NASA test of the gravitational redshift, Gravity Probe A (GP-A)⁵. By means of Doppler tracking at the NASA standard frequency in the X band (about 8.4×10^9 Hz or 3.6 cm wavelength), a similar three-link system could provide Doppler data with a fractional frequency error $\Delta\nu/\nu$ of 5×10^{-15} at a 1000 s sample interval.

2 Highly Eccentric Earth Orbiter

After encountering Venus, the Galileo spacecraft made two close approaches to Earth for purposes of gaining enough heliocentric orbital energy to reach Jupiter. These two Earth encounters have similar orbital characteristics to two orbits of a highly eccentric orbiter. The first Earth encounter on 8 December 1990 occurred at a perigee altitude of 960 km, while the second on 8 December 1992 occurred at a perigee altitude of 303 km. The first encounter, well above the region where atmospheric drag is important, experienced an anomalous apparent velocity increase of 4 mm/s at closest approach along the direction of motion. The second encounter was at a lower altitude where drag provided a velocity change contrary to the direction of motion of roughly 10 mm/s, but with a large uncertainty caused by unknown atmospheric density, hence it was not possible to determine whether or not an anomalous velocity increase occurred.⁶

The Tracking and Data Relay Satellite System (TDRSS) was used from high Earth orbit to provide continuous tracking of the 2.3 GHz Galileo carrier signal during perigee passage on the second encounter. Although it was impossible to check for a repeat of the anomalous velocity increase, because of atmospheric drag, there was an anomalous signal detected in the TDRSS tracking data prior to perigee. This signal could be significantly reduced by adjusting the Earth gravity model and by adding a single surface mass point just below the perigee location. However, these corrections to Earth gravity were inconsistent with the best gravity models provided by Earth satellites.

A spacecraft having a highly eccentric Earth orbit and containing an atomic clock could obtain much higher sensitivity to anomalous signals than the Galileo spacecraft with its space-borne crystal oscillator. Given the problems with the orbital fits to the Galileo data, it seems worthwhile to proceed with accurate orbit determination of an orbiter. Although a mission dedicated to this one objective is not justified, a dynamics experiment could be included in a mission with the primary objective of measuring the gravitational redshift. Because the orbit determination would most likely be important to the redshift measurement, a dynamics experiment could be done at a small incremental cost.

3 Solar Conjunction Experiment

General Relativity predicts that photons passing near the Sun are deflected by an amount⁷

$$\theta_{gr}(b) = \frac{2(1 + \gamma)M_{\odot}}{b} = 8 \times 10^{-6} \left(\frac{1 + \gamma}{2} \right) \left(\frac{R_{\odot}}{b} \right) \quad (1)$$

where b is the impact parameter of the ray, $M_{\odot} = 1.5 \text{ km}$ is the Sun's gravitational mass in length units (GM_{\odot}/c^2), $R_{\odot} = 6.96 \times 10^8 \text{ m}$ its radius, and γ is a free parameter restricted to exactly unity in General Relativity. Experimental data are used to determine an empirical value for γ . Its current value and standard error are⁷

$$\gamma = 1.000 \pm 0.001 \quad (2)$$

The current value of γ is consistent with General Relativity, and more accurate future determinations (by a factor of 100 or so) are expected to agree as well. However, this does not imply that more accurate tests are uninteresting. For example, a large class of alternative scalar-tensor gravitational theories contain a cosmological attractor mechanism that asymptotically approaches General Relativity over cosmological time^{8,9}. It is plausible that γ may differ from unity by an amount of order 10^{-7} to 10^{-5} . If such a discrepancy is confirmed, it could indicate the type of scalar-tensor theory governing cosmological evolution.

Future Doppler experiments utilizing three or more tracking links perhaps offer the best opportunity for significantly improving the empirical value of γ . The effect of solar ray bending on the fractional Doppler frequency shift $\Delta\nu/\nu$ is of order¹⁰

$$\frac{\Delta\nu}{\nu} = v\theta_{gr} = \frac{4M_{\odot}}{b}v \approx 8 \times 10^{-10} \left(\frac{R_{\odot}}{b}\right) \quad (3)$$

where $v \approx 10^{-4} c$ is a characteristic heliocentric orbital velocity for the spacecraft and tracking station. In principle, a Doppler accuracy of 5×10^{-15} over 1000 s for a three-link system, including a spacecraft atomic clock, could provide a signal to noise ratio for a measurement of γ of order 4 to 16×10^4 . A measurement of γ to an accuracy of 10^{-5} may be feasible. However, a detailed feasibility study, including the important noise sources, must be performed before the expected error in γ for any particular space mission is known with confidence.

Acknowledgement

I wish to thank J. W. Armstrong, B. Bertotti, G. Giampieri, M. Harwit, L. Maleki, K. Nordtvedt and R. F. C. Vessot for helpful discussions regarding the topics presented here. The research described in this paper was carried out by the Jet Propulsion Laboratory, California Institute of Technology, under contract with the National Aeronautics and Space Administration.

References

1. T. D. Moyer, *JPL Internal Technical Report No. TR 32-1527* (Jet Propulsion Laboratory, Pasadena, 1971).
2. J. D. Anderson, in *Experimental Gravitation*, B. Bertotti, Ed. (Academic Press, New York and London, 1974), pp. 163-199.

3. B. D. Tapley in *Recent Advances in Dynamical Astronomy*, B. D. Tapley and V. Szebehely, Eds. (D. Reidel, Dordrecht and Boston, MA, 1973), pp. 396–425.
4. R. Woo and J. W. Armstrong, *Jour. Geophys. Res.* **84**, 7288–7296 (1979).
5. R. F. C. Vessot, M. W. Levine, E. M. Mattison, E. L. Blomberg, T. E. Hoffmann, G. U. Nystrom, B. F. Farrell, R. Decher, P. B. Eby, C. R. Baugher, J. W. Watts, D. L. Teuber, and F. D. Wills, *Phys. Rev. Lett.* **45**, 2081–2084 (1980).
6. C. Edwards, J. Anderson, P. Beyer, S. Bhaskaran, J. Border, S. DiNardo, W. Folkner, R. Haw, S. Nandi, F. Nicholson, C. Ottenhoff, and S. Stephens, *Astrodynamics 1993* **85**, A. K. Misra, Ed. (Univelt, San Diego, 1994), pp. 1609–1620.
7. C. M. Will, *Theory and Experiment in Gravitational Physics*, (Cambridge University Press, New York and Cambridge, 1993).
8. T. Damour and K. Nordtvedt, *Phys. Rev. Lett.* **70**, 2217 (1993).
9. T. Damour and K. Nordtvedt, *Phys. Rev.* **D48**, 3436 (1993).
10. B. Bertotti and G. Giampieri, *Class. Quantum Grav.* **9**, 777 (1992).

GRAVITATIONAL WAVE SEARCH WITH THE CLOCK MISSION

J. W. Armstrong

Jet Propulsion Laboratory, California Institute of Technology

Doppler tracking of distant spacecraft is the only method currently available to search for gravitational waves in the low-frequency (~ 0.0001 – 0.1 Hz) band. In this technique the Doppler system measures the relative dimensionless velocity $2\Delta v/c = \Delta f/f_0$ between the earth and the spacecraft as a function of time, where Δf is the frequency perturbation and f_0 is the nominal frequency of the radio link. A gravitational wave of amplitude h incident on this system causes small frequency perturbations, of order h in $\Delta f/f_0$, replicated three times in the observed record (Estabrook and Wahlquist 1975). All experiments to date and those planned for the near future involve only “two-way” Doppler—i.e., uplink signal coherently transponded by the spacecraft with Doppler measured using a frequency standard common to the transmit and receive chains of the ground station. If, as on the proposed Clock Mission, there is an additional frequency standard on the spacecraft and a suitable earth-spacecraft radio system, some noise sources can be isolated and removed from the data (Vessot and Levine 1978). Supposing that the Clock Mission spacecraft is transferred into a suitable interplanetary orbit, I discuss here how the on-board frequency standard could be employed with an all-Ka-band radio system using the very high stability Deep Space Network station DSS 25 being instrumented for Cassini. With this configuration, the Clock Mission could search for gravitational waves at a sensitivity limited by the frequency standards, rather than plasma or tropospheric scintillation effects, whenever the sun-earth-spacecraft angle is greater than 90 degrees.

I. Introduction

The general idea of combining a mission to measure gravitational redshift with one to search for low-frequency gravitational radiation is due to R. F. C. Vessot and colleagues (Vessot and Levine 1978; Smarr et al. 1983) and is at least 18 years old. Anticipating that phase scintillation due to wave propagation through the troposphere, ionosphere, and the solar wind would be a leading noise source, Vessot and Levine (1978) proposed an elegant symmetrical radio system to cancel or drastically reduce these noises. Here I propose gravity wave observations based on an alternate radio system involving 3 links, all at Ka-band (~ 32 GHz): an uplink driven by a high quality frequency standard on the ground, a downlink coherent with this uplink, and a second downlink referenced to a high-quality frequency standard on the spacecraft. One thus gets one “two-way” Doppler observable and one “one-way” Doppler observable, each associated with a very stable frequency standard. The use of Ka-band reduces the charged particle scintillation noise (ionosphere and solar wind) to below the residual uncalibrated tropospheric noise for observations in the anti-solar hemisphere. The discussion below shows how the one-way link can be used

either to correct the two-way data for tropospheric scintillation or to contribute to the pattern-recognition for gravitational signals.

II. Doppler Technique and Low-Frequency Gravitational Waves

For a very thorough review of gravitational radiation, including detection techniques and expected wave strengths, see Thorne (1987). Briefly, in General Relativity gravitational waves (GWs) are propagating, polarized gravitational fields which change the distance between separated test masses and shift the rates at which separated clocks keep time. They are characterized by a dimensionless strain amplitude, $h = \Delta \ell / \ell \sim \Delta v / c$ where ℓ is the fiducial distance between the masses and Δv is the change in relative speed of the test masses associated with the GW. Like electromagnetism, GWs are transverse, have two independent polarization states and propagate at the speed of light. Unlike electromagnetism, GWs are *extremely* weak. This extreme weakness has two consequences. First, GWs are only generated at potentially detectable levels by extremely massive objects undergoing extremely violent dynamics, i.e. by astrophysical sources. Second, because of the extreme weakness there is negligible scattering or absorption by intervening matter. GWs thus preserve information about the *generation* of the waves in the deep interiors of astrophysical sources, not about the last scattering surface.

Detection methods depend on the time scale of the radiation (Thorne 1987). At high frequencies ($f > 10$ Hz), resonant bars and laser interferometers are used. In resonant bars the GW excites an acoustic wave which is read out with a transducer. In laser interferometers the test masses at the ends of the interferometer arms are perturbed as the GW passes, giving rise to a change in relative arm length and thus a fringe shift. For frequencies lower than about 10 Hz, it becomes prohibitively difficult to isolate any ground-based apparatus from seismic noise and time-variable environmental gravity gradient noise. To search for this longer wavelength radiation all the test masses must be put into space.

Currently the only method sensitive to low-frequency GWs is Doppler tracking of distant spacecraft (Estabrook and Wahlquist, 1975), although there are proposals to place very sensitive laser interferometers in space in the future. In the Doppler tracking method, the earth and spacecraft act as free test masses and the (two-way) Doppler tracking system measures the relative dimensionless velocity $2\Delta v / c = \Delta f / f_0$. A gravitational wave of amplitude h incident on the system causes Doppler perturbations of order $h \approx \Delta v / c$. The waveform is replicated three times in the two-way tracking record (Estabrook and Wahlquist, 1975). The sum of these three perturbations in the Doppler record is zero; thus the low-frequency band edge is set by pulse cancellation to be $\sim 1/T_2$ where T_2 is the two-way light time. (The low frequency band “edge” is soft, however; the Doppler response to a signal of duration $\tau > T_2$ is proportional to T_2/τ , giving degraded but non-negligible sensitivity even to very low frequency waves.) The high frequency band limit is set mainly by the stability of the frequency standard driving the link and by finite signal-to-noise ratio on the downlink. Thus to perform a low-frequency experiment, one needs a “reasonable” earth-spacecraft distance (for good response to the lowest frequencies), the spacecraft in cruise and as operationally quiet as possible (far from perturbing masses and with minimal unmodeled motion of the spacecraft), high radio frequency (or multiple links for tropospheric and charged particle calibration), and of course a highly stable ground system driven by a high-stability frequency standard.

III. Principal Noise Sources

Attempts to detect GWs must deal with other variations in the Doppler record. After all “deterministic effects” (such as orbital signature) have been removed, the principal sources of variability in the Doppler record are: frequency and timing system (FTS) noise; propagation noise (an extended medium—the solar wind—and media that are localized very close to the antenna—ionosphere and solar wind); thermal noise; spacecraft antenna unmodeled motion; ground antenna unmodeled motion; ground electronics and FTS distribution; spacecraft transponder noise; spacecraft buffeting; gravitational radiation; and systematic errors. These noises enter the observable via transfer functions (Estabrook and Wahlquist, 1975; Armstrong 1989) which are in general different from the three-pulse response function of the system to gravitation radiation. If “*” indicates convolution, the time series can be modeled as:

$$\begin{aligned}
 y(t) = \Delta f(t)/f_0 = & \text{solar wind plasma}(t) * [\delta(t) + \delta(t - T_2 + 2x/c)] + \\
 & \text{ionospheric plasma}(t) * [\delta(t) + \delta(t - T_2)] + \\
 & \text{troposphere}(t) * [\delta(t) + \delta(t - T_2)] + \\
 & \text{ground station buffeting}(t) * [\delta(t) + \delta(t - T_2)] + \\
 & \text{FTS}(t) * [\delta(t) - \delta(t - T_2)] + \\
 & 2 \times \text{spacecraft antenna residuals}(t) * \delta(t - T_1) + \\
 & \text{ground electronics}(t) + \text{FTS distribution}(t) + \\
 & \text{thermal}(t) + \\
 & \text{spacecraft transponder}(t) * \delta(t - T_1) + \\
 & \text{spacecraft buffeting}(t) * \delta(t - T_1) + \\
 & \text{gravity waves}(t) * [(\mu - 1)/2] \delta(t) - \mu \delta[t - (1/2)(1 + \mu)T_2] + [(1 + \mu)/2] \delta(t - T_2) + \\
 & \text{systematic errors}(t)
 \end{aligned}$$

where T_1 and T_2 are the one- and two-way light times to the spacecraft, x is the distance of a solar wind plasma cloud from the earth, and μ is the cosine of the angle between the GW wavevector and a vector with its foot at the earth and its arrow at the spacecraft. A treatment of the noise sources and their spectra for a Ka-band observation is given by Riley et al. (1990); refinements of that model, based on the X-band Mars Observer observations in 1993, are given by Armstrong (1996) and Armstrong et al. (1997). For a properly-designed experiment at Ka-band, the leading noise sources will be the FTS and the residual troposphere after calibration.

Figure 1 shows the spectra of the principal noises for observations at S-, X-, and Ka-band. The power spectrum of $y = \Delta f/f_0$, $S_y(f)$, is plotted versus Fourier frequency on log-log scales. In some cases, measurements expressed as Allan deviation versus integration time have been converted to S_y under the assumption that S_y has a smooth powerlaw spectrum. References for the data are: Vessot and Levine (1978) for the GP-A raw S-band data; Armstrong, Woo, and Estabrook (1979) for the charged particles at elongations of 90 and 180 degrees, Keihm (1995) for the uncalibrated Goldstone winter troposphere, Armstrong and Sramek (1982) for the VLA troposphere; Cassini Project, Document PD 699-501 (1995) for the stability of ground station plus residual uncalibrated troposphere for the gravity wave experiment. The Mars Observer X-band spectrum is unpublished, and the line marked 'frequency standard' is for a frequency standard with

stability of 7×10^{-16} at 10^4 seconds and degrading as $\tau^{-1/2}$ for shorter integration times. It is clear that the tropospheric calibration is crucial for Ka-band observations.

IV. A Specific Configuration Using Ka-Band Tracking Links

Any low-frequency gravity wave experiment added to a mission principally intended for redshift observations will necessarily increase the cost, if only because of the necessity to transfer the spacecraft to interplanetary orbit. Thus it is essential that the incremental cost be both low and credible (especially if the Clock Mission were to be proposed to a SMEX announcement of opportunity). Is there a way to get most or all of the sensitivity of a symmetrical multi-link system by building on a capability already in place?

In the Cassini-era (> April 2001), DSS 25 at Goldstone will be instrumented for high sensitivity two-way Ka-band tracking in support of Cassini radio science investigations, including an elaborate tropospheric calibration system. What would the sensitivity be if we were able to take advantage of the investment that the Cassini Project and DSN will have already made? In particular, suppose the Clock Mission had a simplified-version of the Cassini-heritage radio system: Ka-band two-way, plus a one-way downlink Doppler referenced to the high-quality on-board frequency standard required for the redshift experiment.

It is clear from Figure 1 that the two way link would be limited by frequency standard or residual troposphere noise for observations made in the antisolar direction, since the high radio frequency has drastically reduced charged particle effects compared to these other noises. Figure 2 shows how one might employ the extra information from the one-way link. The top diagram in Figure 2 is a space-time plot showing the earth and the spacecraft with some of the microwave photon paths illustrated. The gravity wave signature for a wavevector 60 degrees from the earth-spacecraft line is shown for the two-way and one-way links. If the tropospheric calibration is as good as expected, then this "5-pulse" response could be used in the GW pattern recognition algorithm. Alternatively, one could use the one-way data themselves to correct for the troposphere. Illustrated in Figure 2 are the tropospheric response functions for the two- and one-way links. One can cancel the troposphere to the level of the clocks by forming the observable $D_2(t) - (D_1(t) + D_1(t + T_2))$, shown in the bottom panel. This might be operationally preferable to the tropospheric calibration scheme and might be the most effective use of the one-way link. With this tropospheric cancellation or with calibration using water vapor radiometers, GW sensitivity at the Cassini-level would be possible for observations with elongation > 150 degrees; slightly degraded sensitivity would be possible to elongation ≈ 90 degrees (i.e., an observing duty cycle of $\sim 1/2$ year per year can be contemplated).

As a variation on this theme, one can also consider a configuration where one-way Doppler is additionally read out at the spacecraft and telemetered to the ground. This would require additional spacecraft instrumentation (the Doppler readout system). This provides the two-way and one-way signals described above, and another one-way signal received on the spacecraft. As before, this configuration gives the opportunity to use the data themselves to correct for the troposphere, and now there is the potential for a "7-pulse response" to gravitational waves: three pulses on the two-way link and two pulses on each of the one-way links. This offers a very powerful signature for rejection of false alarms.

V. Some practical considerations

Adding a low-frequency GW experiment to a predominately earth-orbiting redshift experiment, although highly-desirable from a science viewpoint, does require additional cost and complexity to transfer the spacecraft to an interplanetary orbit. Also there is a possible power consideration: the maximum two-way light time might be set by the distance over which solar power is practical, thus limiting Fourier bandpass to $f > 0.001$ Hz (or so). (This is not as bad as it might seem—as noted above, the transfer function for waves of duration $\tau >$ two-way light time is geometry-dependent and only falls off as (two-way light time)/ τ , asymptotically, so sensitivity degrades gracefully at the low-frequency band “edge”.) Finally, there is probably additional complexity in the attitude control system—the spacecraft would have to point a Ka-band high-gain antenna accurately enough for these observations.

VI. Conclusions

Low-frequency gravity wave observations are a natural science addition to a redshift experiment. A Clock Mission with Ka-band radio links could reach gravitational wave sensitivity set by clock stability, not charged particles, at sun-earth-probe angles greater than 150 degrees. With minimally degraded sensitivity, observations could be made for solar elongations as small as 90 degrees (i.e., with a duty cycle of $\sim 1/2$ year of observations/year.) The use of a Ka-band radio system builds on ground-system investment for Cassini (station stability and tropospheric calibration); one would then get a Cassini-sensitivity experiment (at least for high-frequencies: $f > 0.001$ Hz) for a small incremental cost. As proposed here, “5- or 7-pulse response” allows tropospheric calibration plus some sensitivity improvement in signal processing (the efficacy of which will depend on waveform). The real utility of a 5- or 7-pulse-response, however, is tropospheric calibration and removal of systematic effects and false alarms, not SNR improvement. Finally, adding a gravity wave search to the Clock Mission fits in with the Zeitgeist—testing fundamental effects at the “right price”.

Acknowledgment

The precision Doppler tracking capability described here is the result of work by hundreds of people in the NASA Deep Space Network and the Flight Projects; the contributions of these individuals are gratefully acknowledged. I thank S. Asmar, B. Bertotti, F. Estabrook, L. Iess, M. Tinto, and H. Wahlquist for discussions. The research described here was carried out at the Jet Propulsion Laboratory, California Institute of Technology, under a contract with the National Aeronautics and Space Administration.

References

- Armstrong, J. W., Woo, R. and Estabrook, F. B. *Ap. J.*, **230** 570 (1979).
- Armstrong, J. W. and Sramek, R. A. *Radio Science*, **17**, 1579 (1982).
- Armstrong, J. W. "Spacecraft Gravitational Wave Experiments" in *Gravitational Wave Data Analysis*, B. Schutz ed. (Kluwer: Dordrecht), 1989.
- Armstrong, J. W. "Radiowave Scintillation in the Neutral Atmosphere as Noise in Precision Spacecraft Tracking Observations", presented at 188-th AAS meeting, Madison WI (1996).
- Armstrong, J. W., Bertotti, B., Estabrook, F., Iess, L., and Wahlquist, H. "Low-Frequency Gravitational Wave Experiments", in *Proceedings of the 12-th Italian Conference on General Relativity and Gravitational Physics*, M. Bassan, V. Ferrari, M. Francaviglia, F. Fucito, and I. Modena eds. (World Scientific: Singapore), 1997.
- Cassini Project, "Detailed Mission Requirements on the Deep Space Network", Document PD 699-501 (internal document), page 39, Jet Propulsion Laboratory, Pasadena, CA. (January 9, 1995).
- Estabrook, F. B. and Wahlquist, H. D. *GRG* **6** 439 (1975).
- Keihm, S. J. *TDA Progress Report*, Jet Propulsion Laboratory, Pasadena, CA, **42-122**, 1 (1995).
- Riley, A. L. et al. "Cassini Ka-Band Precision Doppler and Enhanced Telecommunications System Study," JPL/NASA/ASI internal report (1990).
- Smarr, L. L., Vessot, R. F. C., Lundquist, C. A., Decher, R., and Piran, T. *GRG* **15** 129 (1983).
- Thorne, K. S. "Gravitational Radiation," in *300 Years of Gravitation*, S. Hawking and W. Israel eds. (Cambridge University Press: Cambridge), 1987.
- Vessot, R. F. C. and Levine, M. W. "A Time-Correlated Four-Link Doppler Tracking System," in *A Close-Up of the Sun* (JPL Publication 78-70, M. Neugebauer and R. W. Davies, eds.), pages 457-497 (1978).

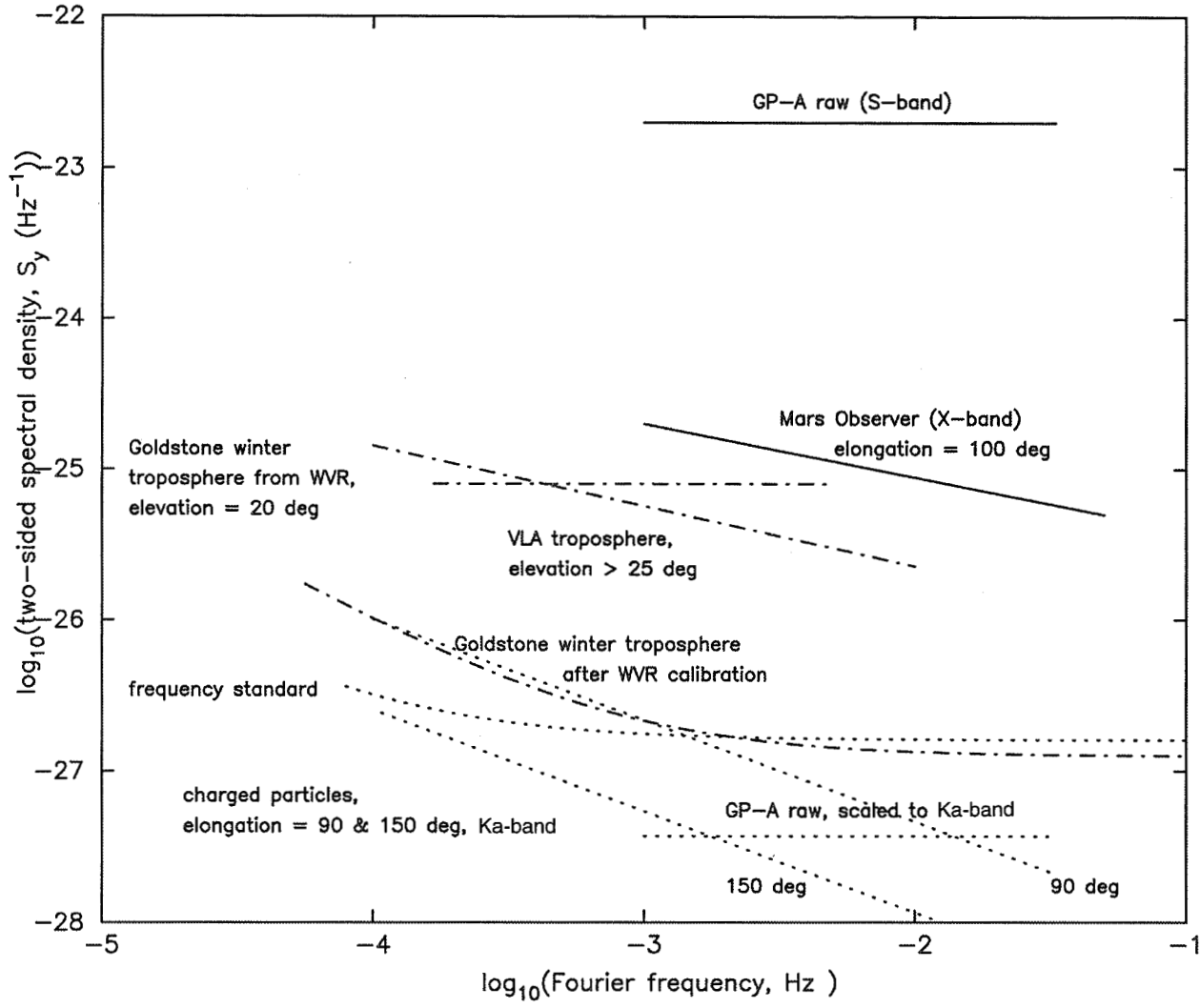


Figure 1. Power spectrum of $y = \Delta f/f_0$, $S_y(f)$, versus Fourier frequency, for major noise sources. In some cases measurements expressed as Allan deviation versus integration time have been converted to S_y under the assumption that S_y is a smooth powerlaw. See text for references to the observations.

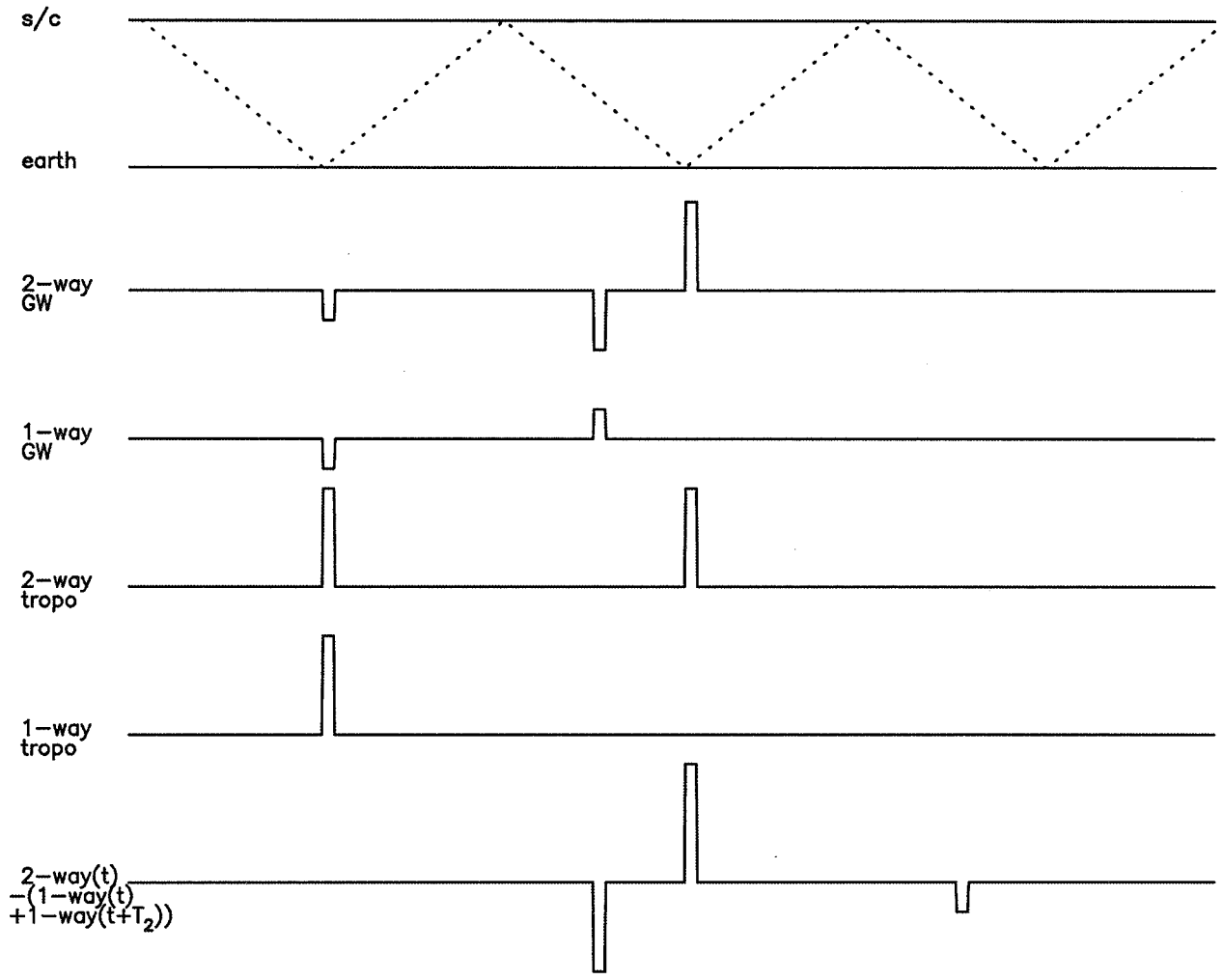


Figure 2. Impulse responses in two- and one-way Doppler links, illustrating how the one-way Doppler link might be used to correct the two-way link for tropospheric scintillation to the level of the clock noise. See text for discussion.

Clocks and General Relativity

Bahram Mashhoon*

Center for Advanced Studies

University of New Mexico

Albuquerque, NM 87131

January 21, 1997

Abstract

The basic role of the hypothesis of locality in the theory of relativity is discussed. A consequence of this assumption is the accelerated clock hypothesis (ACH). The limitations of ACH are investigated and compared with experimental data. The possibility of using highly accurate clocks to test various aspects of general relativity is emphasized.

*Permanent address: Department of Physics and Astronomy, University of Missouri-Columbia, Columbia, MO 65211

1 Introduction

General relativity (GR) is the most successful relativistic theory of the gravitational field inasmuch as it is in agreement with all available observational data. The basic elements of this theory may be summarized as follows.

Lorentz Invariance connects the measurements of ideal inertial observers in Minkowski spacetime. All actual observers are accelerated. It is therefore necessary to extend physical laws to accelerated observers; this is done in relativity theory via the hypothesis of locality.

The Hypothesis of Locality states that an accelerated observer in Minkowski spacetime is at each instant equivalent to a momentarily comoving inertial observer. *Standard* measuring devices are defined to conform with this assumption; thus a standard clock measures proper time. The laws of physics can be pointwise extended to all observers in Minkowski spacetime via the hypothesis of locality. To extend these laws further to observers in gravitational fields, Einstein's principle of equivalence is indispensable.

Einstein's Principle of Equivalence postulates a pointwise equivalence between an accelerated observer in Minkowski spacetime and an observer in a gravitational field. This cornerstone of GR is based on the equivalence of inertial and gravitational masses. Einstein's principle of equivalence *together with the hypothesis of locality* implies that an observer in a gravitational field is pointwise inertial. The simplest way to connect such local inertial frames

is to assume a curved spacetime manifold whose Riemannian curvature is the gravitational field.

The Gravitational Field Equations must connect the spacetime curvature with the energy-momentum tensor of matter and fields, thereby generating a natural generalization of Newtonian gravitation. The simplest possibility is provided by the Einstein field equations of GR [1].

The purpose of this brief description of the foundations of GR has been to place the hypothesis of locality in its proper context in the hierarchy of notions that underlie GR.

2 Accelerated Clock Hypothesis

The hypothesis of locality has its origin in Newtonian mechanics: the two observers in this hypothesis have the same *state* (i.e., position and velocity). The ACH thus refers to this local immateriality of acceleration for standard clocks. However, a realistic accelerated measuring device (“clock”) is affected by inertial effects that can be neglected if they do not integrate to any measurable influence over the length and time scales characteristic of the measurement.

It is permissible to replace the curved worldline of an accelerated observer at each instant by its tangent if the intrinsic length scale of the phenomenon under observation (λ) is negligible compared to the acceleration length (L).

Here λ could be the wavelength of electromagnetic radiation or the Compton wavelength of a particle, and L is the natural length that can be formed from the acceleration and the speed of light in vacuum c ; thus, $L = c^2/g$ for translational acceleration g , while $L = c/\Omega$ for rotation of frequency Ω . The ACH is exactly valid if $\lambda/L = 0$, i.e. either $\lambda = 0$, so that the phenomena could be expressed in terms of pointlike *coincidences*, or $L = \infty$, so that $g = 0$ and $\Omega = 0$ and hence the observer is inertial. The deviation from the ACH is thus expected to be proportional to λ/L . In practice, such effects are very small; for the Earth, $c^2/g \approx 1$ yr and $c/\Omega \approx 28$ AU. A detailed analysis reveals that the deviations under consideration here have been negligibly small in all experiments performed thus far that have searched for a direct dependence of clock rate upon acceleration [2].

To illustrate these ideas, let us imagine an observer rotating uniformly with frequency Ω about an axis and a plane monochromatic electromagnetic wave of frequency ω and definite helicity propagating along the axis of rotation. If the observer is assumed to be instantaneously inertial according to the hypothesis of locality, then $\omega' = \gamma\omega$ by the transverse Doppler effect. However, the electromagnetic field appears to rotate with frequency $\omega - \Omega$ or $\omega + \Omega$ about the direction of propagation depending on whether the wave has positive or negative helicity, respectively. A detailed treatment reveals that $\omega' = \gamma(\omega \mp \Omega) = \gamma\omega(1 \mp \Omega/\omega)$, where $\Omega/\omega = \lambda/(2\pi L)$ with $L = c/\Omega$. A peculiar aspect of this phenomenon is that the wave can stand completely still

with respect to the rotating observer (i.e., $\omega' = 0$ for positive helicity waves with $\omega = \Omega$). In terms of energy $E' = \gamma(E \mp \hbar\Omega)$, where the “interaction” term is due to the coupling of helicity with rotation. This electromagnetic effect has yet to be observed; however, a similar spin-rotation coupling for spin $\frac{1}{2}$ particles with $H = -\sigma \cdot \Omega$ has been verified experimentally [3]. Such spin-dependent interactions were investigated by Wineland and Ramsey in 1972 [4]. The effect due to Earth’s rotation is very small, $\hbar\Omega \sim 10^{-19}$ eV; nevertheless, the coupling of intrinsic spin to the rotation of the Earth has been detected recently via the experiments of Wineland *et al.* [5] and Venema *et al.* [6].

The natural way to think about such effects is to assume that matter waves propagate with respect to an underlying Minkowski spacetime and hence spin keeps its aspect with respect to the inertial frame. From the viewpoint of the rotating observer, the spin would then be precessing in the opposite sense and this apparent motion is expressed in quantum mechanics by the spin-rotation Hamiltonian. In a similar way, one expects that intrinsic spin should precess in the gravitomagnetic field of the Earth just like a GP-B gyroscope, and this spin-rotation-gravity coupling is expressed by $H = -\sigma \cdot \Omega + \sigma \cdot \Omega_D$, where Ω_D is the dragging frequency of the local inertial frames and $\hbar\Omega_D \sim 10^{-29}$ eV for the Earth. The dragging frequency is position-dependent; therefore, the spinning particle is subject to a force. This gravitomagnetic Stern-Gerlach force violates the principle

of equivalence, since the weight of a particle with spin up would in general be different from its weight with spin down [3]. The violation is proportional to the ratio of the Compton wavelength of the particle and $L = c/\Omega$; for a laboratory test with neutrons or protons, this ratio is extremely small ($\sim 10^{-28}$). One can only hope that such a basic relativistic quantum gravity effect may become measurable in future via improvements in spin-rotation experiments [5, 6] or atom interferometry [7].

3 Standard Clocks and Gravitomagnetism

The spacetime interval contains many aspects of the gravitational field that could be studied using standard clocks; in this connection, a gravitomagnetic effect [8] that is briefly described below is of particular interest.

Imagine a clock in a circular equatorial orbit about a rotating mass. Let τ_+ (τ_-) be the period of this geodesic motion in the same (opposite) sense as the rotation of the mass. If the orbital radius r is much larger than the gravitational radius of the body, $r \gg 2GM/c^2$, then it can be shown that

$$\tau_+ - \tau_- \approx 4\pi \frac{J}{Mc^2} \quad , \quad (1)$$

where the quadrupole and higher moments of the central body (of mass M and angular momentum J) have been neglected. The gravitational effect under consideration becomes independent of the coupling constant G in this approximation; this situation can come about as a result of integrating a

small quantity over a long interval. Absence of G in equation(1) indicates that the effect might be “large”. Moreover, the effect is independent of orbital radius r in this approximation; in fact, this gravitomagnetic effect is reminiscent of the topological Aharonov-Bohm effect. For Earth orbits, $\tau_+ - \tau_- \approx 2 \times 10^{-7}$ sec. The effect comes about as a result of a coupling of the *azimuthal* orbital motion with the rotation of the central body; thus, the effect vanishes for a polar orbit.

The influence of the gravitomagnetic potential on clock synchronization via light signals has been the subject of investigations by Cohen, Rosenblum, and coworkers [9]. They considered the “synchronization gap”, which turns out to be essentially equivalent to the difference in the time that it would take for the rays of light to traverse a path all around a rotating mass in opposite directions [8]. Such experiments in the solar system have been discussed by Davies and Lass [10]. The effect is smaller than in equation (1) by a factor that is proportional to the gravitoelectric potential $\Phi = GM/(c^2r)$, which is $< 10^{-9}$ for the Earth.

References

- [1] A. Einstein, *The Meaning of Relativity* (Princeton University Press, 1955).
- [2] D. Newman *et al.*, Phys. Rev. Lett. **40**, 1355 (1978).

- [3] B. Mashhoon, Phys. Lett. A **198**, 9 (1995); Phys. Rev. A **47**, 4498 (1993); Phys. Rev. Lett. **61**, 2639 (1988).
- [4] D. J. Wineland and N. F. Ramsey, Phys. Rev. A **5**, 821 (1972).
- [5] D. J. Wineland *et al.*, Phys. Rev. Lett. **67**, 1735 (1991).
- [6] B. J. Venema *et al.*, Phys. Rev. Lett. **68**, 135 (1992).
- [7] M. Kasevich and S. Chu, Appl. Phys. B **54**, 321 (1992).
- [8] J. M. Cohen and B. Mashhoon, Phys. Lett. A **181**, 353 (1993).
- [9] J. M. Cohen, A. Rosenblum and Y. Clifton, Phys. Lett. A **131**, 163 (1988); J. M. Cohen, H. E. Moses and A. Rosenblum, Class. Quantum Grav. **1**, L57 (1984).
- [10] R. W. Davies, in: *Experimental Gravitation*, ed. B. Bertotti (Academic Press, 1974) p. 405; R. W. Davies and H. Lass, JPL Technical Memorandum no. 58 (1970).

The Nexus between Cosmology and Elementary Particle Physics:
Testing Theoretical Speculations through Observations of the
Cosmic Microwave Background Anisotropies

Mairi Sakellariadou

Département de Physique Théorique, Université de Genève
24 quai Ernest-Ansermet, CH-1211 Genève 4, Switzerland

Abstract

The origin of the large scale structure in the universe — galaxies, quasars, clusters, voids, sheets — is one of the most important questions in cosmology. One can show that some non-thermal energy density fluctuations must have been present in the early universe. These fluctuations grew by gravitational instability to form the observed structures. There are at present two families of models to explain the origin of these initial fluctuations: inflationary models and topological defect scenarios. Current observational developments provide a link with theoretical predictions, allowing us to test our theoretical models. In this contribution, I present a sketch of the current status of the origin of cosmological structure formation.

1 Introduction

At present, our understanding of the evolution of the observed universe rests on the hot big bang model, which, being particularly successful, is considered as the standard cosmology. In favor of this model, there is direct evidence which extends back to about 10^{-2} sec after the explosion, at the onset of primordial nucleosynthesis. Combining theories of fundamental physics at ultra-high energies, with the notion that standard cosmology is very robust, allows us to speculate about the history of our universe at times as early as 10^{-43} sec after the bang.

The standard cosmology, described by the Friedmann-Robertson-Walker metric, lies upon three theoretical pillars: (i) the Einstein's general theory of relativity, which determines the dynamics of the universe; (ii) the cosmological principle, which states that the universe is homogeneous and isotropic on large scales; and (iii) a perfect fluid description of the matter content. On the other hand, its main observational pillars consist of: (i) the Hubble's redshift-distance relation, showing that the universe is expanding; (ii) the existence of a blackbody cosmic microwave background, discovered in 1965 by Penzias and Wilson [1]; and (iii) the agreement between observed and theoretically determined, according to nucleosynthesis, abundances of light elements.

Despite its successes, the standard big bang model faces a number of unanswered questions, like the requirement up to a high degree of accuracy of an initially homogeneous and flat universe, the origin of the observed large scale structure, the small value of the cosmological constant, the nature of the dark matter; as well as the problem of the age of the universe, a possible conflict between theory and observations.

An appealing solution to the homogeneity and flatness problems is to introduce, during the very early stages of the universe, a period of exponential expansion known as inflation [2]. According to the inflationary paradigm, the expansion of the universe was driven, at an early stage of its history, by a scalar field. During that period the expansion was quite dramatic, and the quantum fluctuations of the scalar field [3] were enormously amplified when that phase ended. Thus, inflation provides a mechanism [4] for the causal generation of the primordial density perturbations required for the observed large scale structures.

Inflationary models are not entirely free from problems and therefore it is important to address the issue of the origin of structure formation according to some other theory. The main alternative approach lies on the topological defect scenarios, based on the idea that a number of cosmological phase transitions took place, as the universe cooled down, associated with spontaneous symmetry breakings of the previous phase. Therefore, topological defects — a well-studied phenomenon in condensed matter physics — could have appeared in our universe [5] and played the role of seeds for structure formation. Topological defect models have the advantage of depending on very few parameters and therefore are, in a sense, more appealing than the inflationary ones. Depending on the nature of the broken symmetry, topological defects can either be local or global, while their classification depends on the number of components of an order parameter which breaks the symmetry group. Among the various topological defects, global monopoles, global textures and both global or local cosmic strings, are viable candidates. Since the initial density fluctuations have tiny amplitudes, their evolution at early times can be studied using linear cosmological perturbation theory.

2 Cosmic Microwave Background Radiation

The Cosmic Microwave Background (CMB) radiation is the extraterrestrial electromagnetic radiation that uniformly fills the space at wavelengths in the range of millimeters to centimeters. At present, the spectrum of CMB radiation is, to a high degree of accuracy, a thermal Planck blackbody spectrum at a temperature [6] $T_0 = 2.728 \pm 0.002K$, as measured by the FIRAS (Far Infrared Absolute Spectrophotometer) on the COBE (Cosmic Background Explorer) satellite developed by NASA. Since now the universe is optically thin to radio radiation, the sea of CMB radiation, having almost completely relaxed to thermodynamic equilibrium, must be the remnant heat from the early hot and dense phase of the expanding universe.

The existence of the CMB radiation with an almost thermal nature consists the main evidence that the universe did indeed expand from a dense and hot state. In addition, the CMB radiation is extremely close to isotropic; this uniformity cannot be explained within the context of standard cosmology. The CMB radiation offers an essential probe of the origin of structure formation, through the effects of cosmological structure on the spectrum and isotropy of the relic CMB radiation.

In 1992, the COBE-DMR (Differential Microwave Radiometer) experiment detected anisotropies (temperature irregularities) in the CMB radiation [7]. These anisotropies, imprinted on the CMB radiation by primordial perturbations generated within 10^{-35} sec after the big bang, were found to be at the level $\Delta T/T \approx 1. \times 10^{-5}$ on all angular scales larger than 10° and compatible with a scale invariant (spec-

tral index of $n_s = 1.2 \pm 0.3$ [8]) Harrison-Zel'dovich spectrum. While confirming the idea that indeed large structures grew from small initial fluctuations through gravitational instability, the COBE-DMR observations could not discriminate between inflationary models and topological defect scenarios. The planned MAP (Microwave Anisotropy Probe) and COBRAS/SAMBA (COsmic Background Radiation Anisotropy Satellite / SATellite for Measurement of Background Anisotropies) satellite experiments, as well as balloons and ground based experiments, will probe anisotropies on smaller angular scales, which may allow us to distinguish between these two classes of models for structure formation. Such experiments show how the early universe offers an ideal laboratory to test high energy physics models, on energy scales far beyond those of any conceivable terrestrial accelerator. Moreover, from the point of view of a cosmologist, the CMB radiation offers the unique way of determining basic cosmological parameters — like $\Omega_0, H_0, \Omega_b, \Lambda$ — to within a few percent, through measurements of the CMB anisotropy spectrum. The justification for this belief is mainly that CMB anisotropies can be determined almost fully within linear cosmological perturbation theory and are not particularly affected by nonlinear physics.

The CMB fluctuation spectrum is usually parametrized in terms of multiple moments C_ℓ , defined as the coefficients in the expansion of the temperature auto-correlation function

$$\left\langle \frac{\delta T}{T}(\mathbf{n}) \frac{\delta T}{T}(\mathbf{n}') \right\rangle_{(\mathbf{n} \cdot \mathbf{n}' = \cos \vartheta)} = \frac{1}{4\pi} \sum_{\ell} (2\ell + 1) C_{\ell} P_{\ell}(\cos \vartheta), \quad (1)$$

which compares points in the sky separated by an angle ϑ . The value of C_{ℓ} is determined by fluctuations on angular scales of order π/ℓ . One usually plots $\ell(\ell + 1)C_{\ell}$ versus ℓ — known as the power spectrum — which is the power per logarithmic interval in ℓ , giving the spectrum of anisotropies observed today.

For scalar perturbations, I will describe the main physical mechanisms which contribute to the redshift of photons propagating in a perturbed Friedmann geometry.

(i) On large angular scales, the main contribution to CMB anisotropies comes from inhomogeneities in the spacetime geometry. These inhomogeneities determine the change in the photon energy, due to the difference of the gravitational potential at the position of emitter and observer, and account for red-shifting or blue-shifting, caused by the time dependence of the gravitational field along the path of the photon. They are known as “ordinary” Sachs-Wolfe and Integrated Sachs-Wolfe (ISW) effects respectively.

(ii) On angular scales $0.1^{\circ} \lesssim \theta \lesssim 2^{\circ}$, the main contribution comes from the intrinsic inhomogeneities on the surface of the last scattering, due to acoustic oscillations in the coupled baryon-radiation fluid prior to decoupling. On the same angular scales as this acoustic term, there is a Doppler contribution to the CMB anisotropies, due to the relative motions of emitter and observer. The sum of these two contributions is denoted by the term “acoustic peaks”.

(iii) On scales smaller than about 0.1° , the anisotropies are damped due to the finite thickness of the recombination shell, as well as by photon diffusion during recombination (Silk damping).

Both, generic inflationary models and topological defect scenarios, predict an approximately scale-invariant spectrum of density perturbations on large angular scales ($\ell \lesssim 50$), thus the COBE-DMR data provide mainly a normalization for the different models. Cosmic microwave background anisotropies on intermediate and small angular scales are very important. If the two classes of theories predict different characteristics for the acoustic peaks (e.g., amplitude and position of primary peak, existence or absence of secondary peaks) we can discriminate among them. In the

nearby future, a number of sophisticated experiments will scrutinize various regions of the sky trying to reveal the characteristics of the relic CMB radiation.

3 Families of Models for Structure Formation

Within the framework of gravitational instability theory, there are two currently investigated families of models to explain the origin of the observed structure in the universe.

(i) Initial density perturbations can be due to freezing in of quantum fluctuations of a scalar field during an inflationary era [9]. Such fluctuations were produced at a very early time in the history of the universe, and were driven far beyond the Hubble radius by the enormous (inflationary) expansion. As a result, inflationary fluctuations are not altered anymore and evolve freely according to homogeneous linear perturbation equations until basically the time of galaxy formation. Moreover, as a result of the nature of quantum fluctuations, the distribution of amplitudes of these initial perturbations is usually Gaussian.

(ii) Initial density perturbations can be seeded by an inhomogeneously distributed form of energy, called “seed”, which contributes only a small fraction to the total energy density of the universe and which interacts with the cosmic fluid only gravitationally. A familiar example is the case of topological defects, which could have appeared naturally during a symmetry breaking phase transition in the early universe [5]. According to these models, cosmological structure was formed as a result of a symmetry breaking phase transition and a phase ordering. Such initial fluctuations are generated continuously and evolve according to non-homogeneous linear perturbation equations. Perturbations from defect models are generally non-Gaussian.

On large angular scales, both families of models predict an approximately scale-invariant Harrison-Zel’dovich spectrum [10, 11], the Sachs-Wolfe plateau. The acoustic peaks on intermediate scales in the CMB power spectrum, might represent a mean to support or rule out one of these two families of models.

In the case of inflationary models, there has been a large number of studies and a lot of excitement, in particular since CMB anisotropies might lead to a determination of fundamental cosmological parameters, such as the spatial curvature of the universe Ω_0 , the baryon density Ω_b , the Hubble constant H_0 and the cosmological constant Λ . At multipoles $\ell \geq 200$, the CMB anisotropies become sensitive to fluctuations inside the Hubble horizon at recombination. Since these fluctuations had enough time to evolve prior to last scattering, they are sensitive to evolutionary effects that depend on a number of cosmological parameters. The new generation of satellites (MAP and especially COBRAS/SAMBA) having high sensitivity, angular resolution and large sky coverage, are expected to provide a mean to determine these fundamental cosmological parameters to a precision of a few percent.

The power spectrum predicted for a generic inflationary model reveal the existence of a primary peak at $\ell \sim 200$ with an amplitude $\sim (4-6)$ times the Sachs-Wolfe plateau, and the existence of secondary oscillations [9].

On the other hand, seed models (like topological defect models), generally predict a quite different power spectrum than inflation, due to the behaviour of perturbations on super-horizon scales. Causality and scale invariance have quite different implementations in this class of models. While in inflationary models randomness appears only when initial conditions are set up and the time evolution is linear and deterministic, in seed models randomness also appears during the time evolution, as a result of a complex non-linear process. Seed models are more complicated to be solved than inflationary ones, due to the fact that the linear perturbation equations are non-homogeneous with a source term due to the seed. Since the seed evolution

is, in general, a non-linear and complicated process, much less precise predictions have been made so far, and there is a limited number of studies on the family of seed models.

Recent studies [12, 13, 14] on generic topological defect models show that the primary acoustic peak is located to the right of the adiabatic position, at which the peak arises in a generic inflationary model. The value of this shift to smaller angular scales is determined by the coherence length of the defect. Also the structure of secondary peaks may be quite different for generic defects as compared to inflation. Depending on whether the defect is effectively coherent or not, which is a direct implication of the constraints imposed by causality on defect formation and evolution, secondary peaks will or will not appear in the power spectrum [14]. Considering density perturbations seeded by global textures, π_3 defects [15], in a universe dominated by cold dark matter, the position of the primary acoustic peak was found to be displaced by $\Delta\ell \sim 150$ towards smaller angular scales than in standard inflationary models [12, 13], while its amplitude was only a factor of $\sim 1.5 - 3.3$ times higher than the Sachs-Wolfe plateau [13]. In an attempt to reveal the robust features of the power spectrum in a seed model, it was found [16, 17] that there are defect models leading to a primary acoustic peak located at the adiabatic position, however its amplitude may be substantially smaller than the one in generic inflationary models [17].

The satellites MAP and, in particular, COBRAS/SAMBA with planned launch years around 2000 and 2005 are designed to image anisotropies of the CMB radiation to an uncertainty better than $\Delta T/T \sim 2 \times 10^{-6}$ at all angular scales larger than ~ 10 arcmin over the whole sky. We therefore expect to have a full power spectrum against which we could test our theoretical models.

4 Conclusions

The nexus between cosmology and elementary particle physics has become an especially active area of research in recent years. Current frontiers of particle physics involve energy scales far beyond those available now or in the near future terrestrial particle accelerators. An obvious place to look is to the very early universe, where conditions of extreme energy and density are realized. At the same time, the standard big bang model provides a reliable framework for describing the evolution of our universe as early as 10^{-2} sec after the explosion, when the temperature was about 10 MeV. Extending our understanding to earlier times and higher temperatures, requires knowledge about the fundamental particles and their interactions at very high energies; progress in cosmology has become linked to progress in particle physics.

Among the main, still open problems in modern cosmology, remains the origin of the observed structure in the universe. Based on all present indications, we believe that the large-scale structure was produced by gravitational instability from small primordial fluctuations in the energy density, generated during the early stages of the universe. Within this framework, the two families of models to explain the origin of primordial density perturbations are inflationary models and topological defect scenarios. Either of these two families of models predicts precise fingerprints in the cosmic microwave background anisotropies, which can be used to differentiate among these models using a purely linear analysis. Both families lead to approximately scale-invariant Harrison-Zel'dovich spectrum of density fluctuations on large angular scales. However, the power spectrum predicted from each of these families, has different properties on smaller angular scales. The next satellite experiments (MAP and COBRAS/SAMBA), as well as ground-based (e.g., Jodrell Bank, CAT, SASKATOON, VSA) and balloons experiments (e.g., BOOMER, FIRS, MAX, MAX-

IMA, MSAM, UCSB) will provide a detailed power spectrum, against which we will be able to test our theoretical models. In addition, we expect to be able to determine a number of fundamental cosmological parameters up to a high degree of accuracy. It is therefore believed that these coming years will be particularly fruitful for cosmology and one may conclude that as cosmologists we are currently living through what can be considered a scientific revolution.

Acknowledgements

It is a pleasure to thank the members of the Jet Propulsion Laboratory, who organized this workshop and, in particular, Lute Maleki, for inviting me to deliver this talk.

References

- [1] A. Penzias and R. Wilson, *Ap. J.* **142** (1965) 419.
- [2] A.H. Guth, *Phys. Rev. D* **23** (1981) 347.
- [3] T. Bunch and P.C.W. Davies, *Proc. Roy. Soc. London A* **360** (1978) 117; S.W. Hawking, *Phys. Lett. B* **115** (1982) 295; A.A. Starobinsky, *Phys. Lett. B* **117** (1982) 175; A.H. Guth and S.-Y. Pi, *Phys. Rev. Lett.* **49** (1982) 1110.
- [4] A. Albrecht and P.J. Steinhardt, *Phys. Rev. Lett.* **48** (1982) 1220; A.D. Linde, *Phys. Lett. B* **108** (1982) 389; A.D. Linde, *Phys. Lett. B* **129** (1983) 177; D. La and P.J. Steinhardt, *Phys. Rev. Lett.* **62** (1989) 376; D. La and P.J. Steinhardt, *Phys. Lett. B* **220** (1989) 375.
- [5] T.W.B. Kibble, *Phys. Rep.* **67** (1980) 183.
- [6] J.C. Mather, *et al.*, *Ap. J.* **354** (1990) L37.
- [7] G. Smoot, *et al.*, *Ap. J.* **396** (1992) L1.
- [8] K.M. Gorski, *et al.*, "Power Spectrum of Primordial Inhomogeneity Determined from the 4-Year COBE DMR Sky Maps", *astro-ph/9601063* (1996).
- [9] P.J. Steinhard, "Cosmology at the Crossroads", to appear in the *Proceedings of the Snowmass Workshop on Particle Astrophysics and Cosmology*, E. Kolb and R. Peccei, eds. (1995), *astro-ph/9502024*.
- [10] H.R. Harrison, *Phys. Rev. D* **1**, 2726 (1970).
- [11] Y.B. Zel'dovich, *Mon. Not. Roy. Ast. Soc.* **160**, 1 (1972).
- [12] Crittenden R.G., and Turok N., *Phys. Rev. Lett.* **75** 2642 (1995).
- [13] R. Durrer, A. Gangui and M. Sakellariadou, *Phys. Rev. Lett.*, **76**, 579 (1996).
- [14] J. Magueijo, A. Albrecht, P. Ferreira and D. Coulson, "The structure of Doppler peaks induced by active perturbations", *astro-ph/9605047* (1996).
- [15] N. Turok, *Phys. Rev. Lett.* **63** 2625 (1989).

[16] N. Turok, *Phys. Rev. D* **54** 3686 (1996).

[17] R. Durrer and M. Sakellariadou, "Microwave Background Anisotropies from Scaling Seed Perturbations" (1996) (in preparation).

Session II

Classic Tests

and Their Clocks

THE SUPERCONDUCTING CAVITY STABILIZED OSCILLATOR

J. P. Turneure, Saps Buchman, and John Lipa
W. W. Hansen Experimental Physics Laboratory, Stanford University, Stanford, U.S.A.

ABSTRACT

Superconducting Cavity Stabilized Oscillators (SCSOs) have produced the most stable clocks to date for integration times between 10^2 and 10^3 seconds, achieving a fractional frequency stability of 2×10^{-16} for a sampling time of 100 s. The principal contributors to cavity frequency variations are: (a) acceleration effects due to gravity and vibrations (b) temperature variations, (c) variations in the energy stored in the cavity, and (d) noise introduced by the frequency stabilization circuit. We discuss the prospects for improvements in all these areas for both ground-based and space-based SCSOs, which may lead to SCSOs with fractional frequency stabilities below 10^{-17} . SCSOs of this frequency stability will be useful for testing fundamental physical principles.

I. INTRODUCTION

High stability clocks or oscillators, as discussed in independent papers by Nordtvedt, Damour, and Haugen in these proceedings, are useful for testing fundamental physical principles. For example, an H-maser in a sub-orbital flight verified the Einstein weak equivalence principle to about 0.01% by measuring the gravitational redshift of a rocket borne H-maser relative to a ground-based H-maser¹.

Superconducting Cavity Stabilized Oscillators (SCSOs) utilizing 8.6 GHz TM_{010} Nb cavities with unloaded quality factors (unloaded Qs) of up to 1×10^{11} have achieved fractional frequency stabilities² of a few parts in 10^{16} for sampling times of about 100 s, making them the most precise clocks in this range of sampling times. An SCSO can be classified as a “ruler” clock since its frequency is proportional to the velocity of light divided by a length, the cavity radius (see Eqn 1). An ensemble of three SCSOs has been used to make a null gravitational redshift measurement relative to an H-maser with a 2% accuracy³ and to set a limit on the secular drift of the fine structure constant⁴. This paper discusses the possibility of improving both the short-term and the

long-term fractional frequency stability of both ground-based and space-based SCSOs to below 10^{-17} allowing them to make more precise measurements of fundamental physical principles.

II. THE DESCRIPTION OF THE SCSO

This section describes the SCSO, which was developed^{5,6} from 1971 until 1978. The SCSO utilizes a superconducting Nb microwave cavity operating at 1.2 K in the TM_{010} mode, at 8.6 GHz, with its interior under ultrahigh vacuum. To insure mechanical stability the walls of the cavity are of about the same thickness as its 1.3 cm radius. At 1.2 K, these cavities have achieved unloaded Qs of up to 1×10^{11} after undergoing ultrahigh vacuum firing and chemical polishing⁷.

Figure 1 is a schematic of the cavity and its mounting in a vacuum can that is immersed in pumped liquid helium. The cavity is supported from its top, and it is connected with indium sealed vacuum flanges to the pump-out port and to the microwave waveguide. High vacuum conditions for the cavity are maintained by means of a permanent internal vacuum accomplished with a copper pinch-off and by the exterior vacuum can. The cavity temperature is controlled to $1 \mu\text{K}$ short term (over times up to 1000 s) and to $10 \mu\text{K}$ long term (for a fraction of a day and longer) with an active temperature control system, which uses a Ge resistance thermometer (GRT) and a heater. To limit trapped magnetic flux in the superconducting cavity and to reduce the magnetic stress on the cavity, magnetic shields reduce the magnetic field at the cavity to less than 10 mG. Both the dewar and the microwave electronics are tilt controlled to reduce the effect of angular variations with respect to the local gravity. The entire apparatus consisting of three SCSO systems is cooled in a top loading liquid helium dewar.

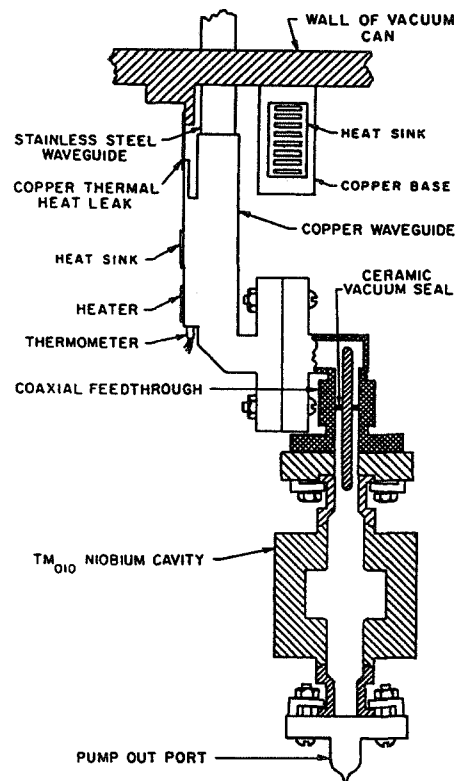


Figure 1. Schematic of SCSO cavity and its mounting.

A simplified schematic of the SCSO circuit is shown in Fig. 2. The circuit utilizes the high Q cavity resonance to frequency stabilize a voltage controlled oscillator, a Gunn oscillator. A small portion of the Gunn oscillator power is phase modulated at 1 MHz. The Gunn oscillator is tuned so the carrier of the phase modulated signal is near the cavity resonance. An AM modulated signal is reflected by the cavity and then detected with a square law detector. The sign and

amplitude of the detected AM signal represent the deviation of the Gunn oscillator frequency from the cavity frequency. The AM signal, after demodulation, is used to servo the frequency of the Gunn oscillator. The connection of the resonator to the room temperature electronics is made using stainless steel waveguide with copper baffles in order to minimize thermal losses.

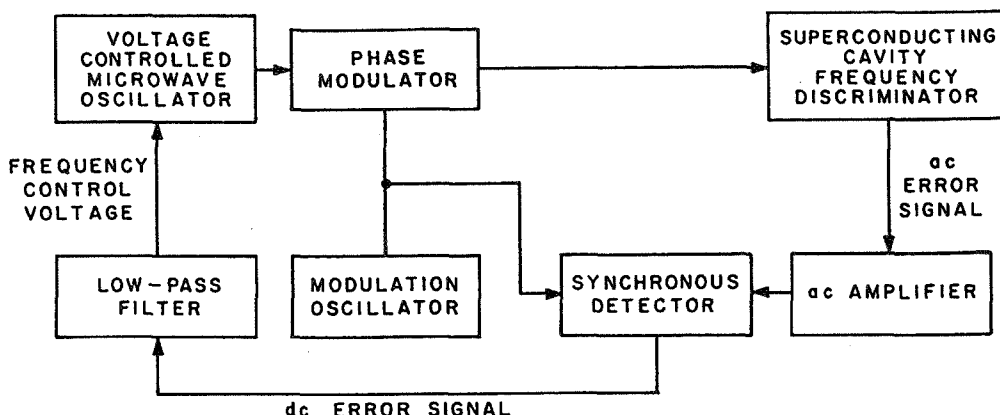


Figure 2. Simplified block diagram of SCSO

Figure 3 is a graph of the square root of the Allan variance, σ_y , as a function of sampling time, τ . The figure contains data from three sources. The circles are data² from the ensemble of three SCSOs and the square is a data point at 100 s for SCSO #3 which has the highest unloaded Q (1×10^{11}) in the ensemble. This data was taken with a measurement noise bandwidth of 10 Hz. For $\tau < 100$ s, σ_y is approximated by $10^{-14}/\tau$. The noise floor of $\sigma_y = 1.3 \times 10^{-16}$ for SCSO #3 is reached at 100 s. For longer sampling times, σ_y increases due to long-term frequency drift. The triangles are data derived from the comparison of SCSO #3 with an H-maser³. The Allan variance is calculated after the effects of ambient conditions (barometric pressure, earth tides, temperatures) are removed. For sampling times less than 100 s, σ_y is limited by the H-maser. The combination of the H-maser and SCSO #3 gives σ_y of 1.2×10^{-15} for sampling times out to about 10^5 s. These data indicate that an SCSO with an

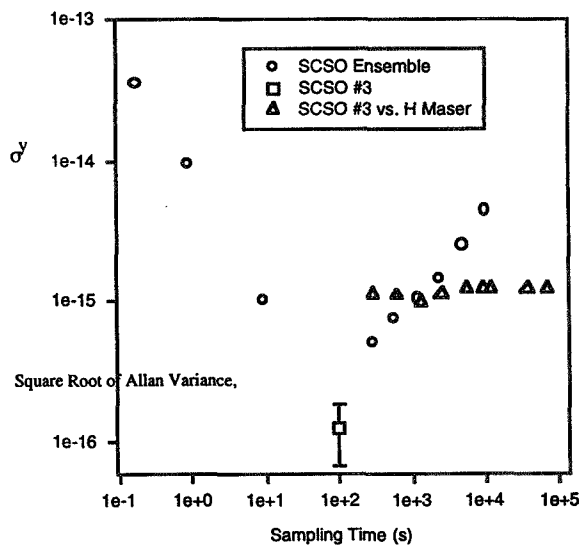


Figure 3. Allan variance vs. sampling time for an 8.6 GHz SCSO.

unloaded Q of 1×10^{11} has a fractional frequency drift of $\leq 10^{-15}$ per day demonstrating that stress relaxation and creep are not yet evident in the SCSO frequency drift.

III. PERFORMANCE OF IMPROVED SCSO

We consider the strategies for improving both the noise floor and the long-term frequency stability of the SCSOs. The discussion is divided into two sections: stability of the superconducting cavity frequency, and frequency noise introduced by the frequency stabilization circuit. A number of smaller disturbance effects including quantum fluctuations, thermally induced phonons, external pressure variations, motion of flux quanta, particle radiation effects, and low temperature structural changes (creep and stress relaxation) are estimated to cause frequency instabilities below the 10^{-18} level, and thus they are not discussed.

B. STABILITY OF CAVITY FREQUENCY

The superconducting cavity serves as the frequency determining element of the SCSO. Thus, the cavity frequency and its stability must be well understood and controlled. The cavity is approximately a right circularly cylindrical cavity of radius R and length L, and it is operated in the TM_{010} mode. The frequency, ν_0 , of an ideal TM_{010} mode cavity is independent of its length.

$$\nu_0 \cong \frac{2.405}{2\pi} \frac{c}{R} \quad (1)$$

The numerical factor is the argument of the zeroth order Bessel function at its first root, and c is the velocity of light. This expression for frequency is only approximately correct since the actual cavity has holes in its end plates to assist in manufacture and to provide a means of coupling to a waveguide. The practical factors that limit the stability of the cavity frequency are discussed below.

Acceleration. Vibrations and variations in local gravity will affect the frequency by changing the cavity dimensions. For the vertically mounted TM_{010} mode cavity, the frequency is dependent to first order only on the average cavity radius and by symmetry is only sensitive to second order in the tilt angle from vertical. The frequency sensitivity to changes in gravitational acceleration Δg is estimated by assuming that the length of the cavity is stretched by its self weight, and the cavity radius is reduced due to the effect of Poisson's ratio.

$$\frac{\Delta \nu}{\nu_0} \cong -\frac{\Delta R}{R} \cong \frac{1}{3} \cdot \frac{\Delta l}{l} \cong \frac{1}{3} \cdot \frac{l \rho (\Delta g)}{Y} \Rightarrow \frac{\Delta \nu}{\nu_0} \cong 4 \times 10^{-9} \cdot \frac{\Delta g}{g} \quad (2)$$

where R, l, ρ , and Y are the radius, length, density and Young's modulus of the cavity.

The sensitivity to acceleration variations can be significantly reduced by supporting the cavity from its center, thus through symmetry compensating any contribution to frequency change in the top half with an opposite change in the bottom half. The connection to the waveguide can be made via a choke flange joint, thus leaving the center support as the only mechanical connection to the cavity. The expected improvement from the center support should decrease the frequency sensitivity to acceleration by at least a factor of 10^2 , yielding a sensitivity of 4×10^{-11} $\Delta g/g$. For a ground-based SCSO, the principal contribution to Δg is due to earth tides, which typically give a peak-to-peak Δg of 200 μGal . This yields a fractional frequency variation of 8×10^{-18} , and a contribution to σ_y much less than this value for sampling times much shorter or longer than 6 hours (1/2 of the tidal period). For a space-based SCSO, the principal contribution to Δg is drag on the space vehicle. For space vehicle accelerations at the 10^{-7} g level, the fractional frequency variations are about 4×10^{-18} . If the space vehicle were drag compensated, the frequency variations from this source would be much smaller.

Temperature. Fluctuations in temperature affect the frequency stability via two main effects on the cavity: thermal expansion and the variation with temperature of the skin depth. The thermal expansion has phonon and electron (superconducting) contributions. The skin depth temperature dependence is described by the BCS theory⁸. One of the authors (Turneaure) has measured the temperature dependence of the 8.6 GHz, TM010 mode Nb cavities, and it can be represented by

$$\frac{\partial(\Delta \nu/\nu_0)}{\partial T} = \frac{1.58 \times 10^{-4}}{T^2} \cdot \exp\left(\frac{-17.12}{T}\right) + 4.32 \times 10^{-11} \cdot T^3 \quad (3a)$$

$$\left. \frac{\partial(\Delta \nu/\nu_0)}{\partial T} \right|_{T=1.2 \text{ K}} \cong 1.45 \times 10^{-10} \text{ K}^{-1} \quad (3b)$$

where the first term of Eqn 3a represents the skin depth temperature dependence and the electron thermal expansion, and the second term represents the lattice thermal expansion. In the configuration described in Section II, the short-term temperature stability was 1 μK , and the long-term stability was about 10 μK . Chui and Lipa⁹ have used paramagnetic salt thermometers in a four stage thermal isolation system to demonstrate temperature stability better than 1 nK. Their system has also been flown in space as part of the Shuttle Lambda Point Experiment program. We propose to use a simplified version of this system to achieve temperature control to 10 nK or better, therefore reducing the temperature induced frequency fluctuations to approximately the 10^{-18} level.

Stored energy. Fluctuations in the energy U stored in the cavity will change the electromagnetic radiation pressure on the cavity walls and will vary the non-linear superconducting surface reactance. This variation has been measured by one of the authors (Turneure), and it can be represented by:

$$\frac{\Delta v}{v_0} = -(k_{EM} + k_x)U \Rightarrow \frac{\partial (\Delta v/v_0)}{\partial U} \cong -1.7 \times 10^{-6} \text{ J}^{-1} \quad (4)$$

where the k coefficients quantify the electromagnetic radiation pressure and the non-linear surface reactance. In the configuration described in Section II, the stored energy in the cavity was 6×10^{-8} J with a short-term stability on the order of 10^{-3} , yielding a contribution to σ_y of less than 1.0×10^{-16} . Improved electronics will allow better power control, therefore reducing the frequency instabilities caused by this effect to the 10^{-18} level.

B. STABILIZATION CIRCUIT

Conceptually the scheme for the SCSO electronics will be quite similar to the original design. However, some major changes to the circuit design will be incorporated based on the following principles: (a) use of improved microwave technology, which was not available for the original circuit, (b) a lower modulation frequency of about 10 kHz, (c) a stabilizing power servo, and (d) use of cryogenic components. The Gunn oscillator will be replaced with a varactor-tuned dielectric resonator oscillator (DRO) selected for very low close-in phase noise. A lower modulation frequency will reduce the spurious AM due to frequency dependence of the transmission line wave velocity, attenuation, and spurious reflections. Power stability of better than 0.1% should be easily achievable. We will also investigate the use of a lower noise AM detector, which currently limits σ_y to about $10^{-15}/\sqrt{\tau}$ for a cavity stored energy of 6×10^{-8} J. We expect to be able to reduce the noise floor of σ_y to below 10^{-17} .

IV. CONCLUSIONS

SCSO clocks have demonstrated a σ_y noise floor of 2×10^{-16} for a sampling time of 100 s and σ_y of 1.2×10^{-15} for sampling times out to $\sim 10^5$ s. The main disturbance effects are due to noise in the electronics and long-term drift caused by fluctuations in the temperature, the local gravity, and the electromagnetic energy stored in the resonator. Proposed improvements show the promise of achieving fractional frequency stabilities below 10^{-17} for ground-based and space-based experiments.

ACKNOWLEDGMENTS

This work was supported by NASA contract No. NAS8-39225.

REFERENCES

-
- ¹ R. F. C. Vessot and M. W. Levine, *Phys. Rev. Lett.* **45**, 2081 (1980).
 - ² S. R. Stein and J. P. Turneaure, in *AIP Conference Proc. No. 44*, Hugh C. Wolfe, Series ed. (AIP, N.Y., 1978) pp. 192-213.
 - ³ J. P. Turneaure, C. M. Will, B. F. Farrel, E. M. Mattison, and R. F. C. Vessot, *Phys. Rev. D* **27**, 1705 (1983)
 - ⁴ J. P. Turneaure and S. R. Stein, in *Atomic Masses and Fundamental Constants 5*, J. H. Sanders and A. H. Wapstra, eds. (Plenum, N.Y., 1976) pp. 636-42.
 - ⁵ S. R. Stein and J. P. Turneaure, *Electronic Letters* **8**, 321 (1972).
 - ⁶ S.R. Stein and J.P. Turneaure, *Proc. IEEE* **63**, 1249 (1975)
 - ⁷ J. P. Turneaure and N. T. Viet, *Appl. Phys. Letters* **16**, 333 (1970).
 - ⁸ J. P. Turneaure, J. Halbritter, and H. A. Schwettman, *J. Superconductivity* **4**, 341 (1991).
 - ⁹ J. A. Lipa, D. R. Swanson, J. A. Nissen, and T. C. P. Chui, *Cryogenics* **34**, 341 (1994).

SPACE EXPERIMENTS WITH HIGH STABILITY CLOCKS

ROBERT F. C. VESSOT

*Smithsonian Astrophysical Observatory
Cambridge Massachusetts 02138*

1 Introduction

One of the most significant scientific improvements in our era is the unparalleled precision of measurement made possible by atomic clocks. The meter, the SI unit of length, is now defined in terms of the velocity of light, a pivotal quantity in our present Relativistic concepts of space and time.

This discussion is meant to provide a picture of where we stand in the present state of clocks, of techniques for clock-related space experiments, and of some now technically feasible space experiments.

2 Present State of Clock Technology and Systems for Space Experiments

Progress of clock development is shown in Figure 1, which shows that the frequency stability of highly stable oscillators has improved by a factor of about 7 every decade since the 1960 era, when atomic clocks were first introduced.

The most commonly used definition of frequency stability is the Allan deviation, $\sigma_y(\tau)$. This is the one-sigma expectation of the fractional frequency difference $\Delta f/f$ (designated by the subscript y), between time-adjacent frequency measurements, each made over time intervals of duration, τ . The functional relationship of $\sigma_y(\tau)$ versus (τ) depends on the Fourier spectrum of of the phase variations.¹

An estimate of the time dispersion of a clock or oscillator for a future time interval, τ , can be obtained from the relation

$$\sigma_{\Delta\tau}(\tau) \sim \tau \sigma_y(\tau) \quad (1)$$

The representation of oscillator performance given by $\sigma_y(\tau)$ can provide statistical estimates of the limits imposed by clock performance on measurements made with electromagnetic signals.

Figure 2 shows $\sigma(\tau)$ versus τ plots for recently developed stored ion devices², atomic hydrogen masers³, and for the binary pulsar⁴. This figure also includes the Allan deviation of disturbances caused by the earth's troposphere and ionosphere on signals traversing vertically.

In the following discussions of experimental techniques, the H maser performance data in Figure 2 will be used as a basis for numerical examples.

2.1 Measurements using Electromagnetic Signals

2.1.1 The effects of oscillator instability on measurements of distance and of range-rate using Doppler data.

In the case of distance measurements made from the one-way propagation of light we can obtain an estimate of range dispersion from time dispersion given in Equation 1, by writing

$$\sigma_{\Delta r}(\tau) = c\tau \sigma_y(\tau) \quad (2)$$

where c is the velocity of light.

The one-way Doppler frequency shift of signals from an oscillator transmitting at a frequency, f , moving with velocity v_r toward the receiver is

$$\frac{\Delta f}{f} = \frac{v_r}{c}$$

The contribution of the oscillator to the imprecision of determining range rate, v_r , during measurement intervals, τ , is given by

$$\sigma_{v_r}(\tau) = c \sigma_y(\tau) \quad (3)$$

Figure 3 is a nomograph of range-rate error and range distance error based on the H-maser data in Figure 2. On the left hand axes are scales for $\sigma_y(\tau)$ and the corresponding one-way Doppler frequency range-rate measurement error, $\sigma_{v_r}(\tau)$. On the right hand axes are the scales for time dispersion, $\sigma_{\Delta t}(\tau)$, and the corresponding one-way range measurement error.

2.1.2 A Systems or Cancelling First-Order Doppler and Signal Propagation

The concept of one-way and two-way Doppler measurements leads naturally to the three-link Doppler-cancelling system used in the 1976 SAO/NASA Gravity Probe A test of the gravitational redshift.^{5 6} This "Doppler cancellation" scheme was pivotal to the success of the experiment. By measuring the Doppler effects in a *separate* two-way system and subtracting one-half the number of the two-way cycles from the phase of the received signal from the phase of the one-way microwave link connecting the space vehicle clock to the earth station, the propagation effects were *systematically* removed.

Figure 4 schematically describes the phase-coherent analog system that was used in the 1976 SAO-NASA test of the gravitational redshift.

With this system, the fractional output frequency variations obtained by subtracting one-half of the two-way Doppler cycles from the one-way cycles received by the earth station is given in the expression:

$$\frac{f_s - f_e}{f_0} = \frac{(\phi_s - \phi_e)}{c^2} - \frac{|\vec{v}_e - \vec{v}_s|^2}{2c^2} - \frac{\vec{r}_{se} \cdot \vec{a}_e}{c^2} \quad (4)$$

Here the total frequency shift is $f_s - f_e$, and f_0 is the clock downlink frequency. The term $(\phi_s - \phi_e)$ is the Newtonian potential difference between the spacecraft and earth station, \vec{v}_e and \vec{v}_s are the velocities of the earth station and the spacecraft, \vec{r}_{se} is the vector distance between the spacecraft and earth station, and \vec{a}_e is the acceleration of the earth station in an inertial frame. For the 1976 test, an earth-centered frame with axes aimed at the fixed stars was sufficiently "inertial" to satisfy the requirements of the two-hour experiment.

The first term is the gravitational redshift resulting from the difference in the Newtonian gravitational potential between the two clocks, the second term is the second-order Doppler effect of special relativity, and the third term is the result of the acceleration of the earth station during the light time, r/c , owing to the earth's rotation. During the two-hour near-vertical flight, the first-order Doppler shifts were as large as $\pm 2 \times 10^{-5}$ and the noise from ionospheric and tropospheric propagation effects was about 1×10^{-12} at $\tau \sim 100$ sec, as shown in the top left curve of Figure 2. After the frequency variations predicted in Equation 4 were fitted to the data, the error in the fit of the data was within $(+2.5 \pm 70) \times 10^{-6}$ of Einstein's prediction.⁷ The residuals were analyzed after subtracting the predicted frequency variation over the time of the mission. The resulting Allan standard deviation of the frequency residuals is shown in Figure 5. Here we see that the stability of the frequency comparison made through the three-link system over signal paths of 10,000 km, in the presence of Doppler shifts of magnitude ± 44 kHz, plus the ionospheric and tropospheric noise shown in Figure 2, is comparable to the frequency comparison made between the two reference masers in the same room, reaching 6×10^{-15} stability at about 10^3 sec.

Figure 6 shows how phase coherence throughout the system was provided by ratio frequency synthesizers. We see that there was a considerable difference in the S-band (2 GHz) frequencies, owing to the transponder's turn-around frequency ratio, 240/221. Because of ionospheric electron content in the signal path, there could have been serious problems from phase delay owing to the frequency differences in the three microwave links⁸ This error was removed by choosing the frequency ratios so that the ionospheric effects in the three signal paths were cancelled at the output of mixer M3 in Figure 6.^{9,10}

2.1.3 A Symmetrical Four-Link System to Provide Time-Correlated Doppler Data

The three-link system can be made symmetrical by providing a transponded signal back to the spacecraft as shown in Figure 7. Here one-way, two-way, and Doppler-cancelled data are recorded at both stations of the system in terms of the proper time scale kept by the station's clock. In the case where the light time between stations is long compared, for example, to the intervals required for measurements, a dominant, spatially localized noise process can be cancelled *systematically* by time correlation of the data from the two stations. For example, Figure 8 shows the continuum of space-time paths of the four signals in Figure 7. Here the dots signify the clocks, and the arrows, $E_1(t)$ and $E_2(t)$, signify signal outputs representing earth-based one- and two-way data at a particular epoch in the continuum. $S_1(t)$ and $S_2(t)$ represent one- and two-way data recorded in space. By time-correlating the Doppler responses we can systematically cancel a strong localized noise source such as the earth's troposphere and ionosphere.^{11,12}

For example, let us consider the frequency variations in Doppler outputs $E_1(t)$, $E_2(t)$, $S_1(t)$, and $S_2(t)$ shown in Figure 7. We see that the ionotrope noise pattern received from the the spacecraft transmitted at time t_i and received at earth at time t_i+R/c is the same as the noise received at the spacecraft at time (t_i+2R/c) . By advancing $E_1(t)$ by time R/c with respect to $S_1(t)$ and subtracting the two data sets we can systematically remove the noise in the $S_1(t_i+2R/c) - E_1(t_i+R/c)$ combined data set at the small expense of increasing the random noise in the data by $\sqrt{2}$. In situations where the localized dominant noise is substantially larger than the nonlocalized random noise, this process can be highly effective.

2.1.3.1 Relativistic Doppler Shifts and Redshifts with the 4Four-Link System

The Doppler-cancelled signal outputs $S_o(t)$ and $E_o(t)$ in Figure 7 contain relativistic and gravitational information that can be time correlated. Equation 4 is repeated below as $E_o(t)$, along with its counterpart expression at the spacecraft, $S_o(t)$:

$$E_o(t) = \frac{\phi_s - \phi_e}{c^2} - \frac{|\vec{v}_s - \vec{v}_e|^2}{2c^2} - \frac{\vec{r}_{se} \cdot \vec{a}_e}{c^2} \quad (5)$$

$$S_o(t) = \frac{\phi_e - \phi_s}{c^2} - \frac{|\vec{v}_e - \vec{v}_s|^2}{2c^2} - \frac{\vec{r}_{es} \cdot \vec{a}_s}{c^2} \quad (6)$$

By adding these two time-ordered data sets we cancel the first term and double the magnitude of the second term representing the second-order shift. Conversely, if we subtract the data sets, we double the first-term representing

the gravitational red (blue) shift and cancel the second term. In both instances we must account for the components of acceleration of the earth and space stations along the line of sight in a suitable inertial frame.

3 Tests of Relativistic Gravitation with Clocks

3.1 *A Proposed Test of Relativistic Gravitation with a Clock in a 24-Hour Eccentric Earth Orbit*

The original concept for testing the Gravitational Redshift called for operating a spaceborne clock in a spacecraft placed in a highly eccentric 24-hour earth orbit.¹¹¹³ Low-inclination orbits with eccentricities as high as 0.6 can produce apogee-to-perigee redshifts of about 4.8×10^{-10} , and still keep the spacecraft in view of an earth station with a minimum elevation angle greater than 15 degrees. Accompanying the redshift there is a second-order Doppler shift of comparable magnitude, which produces a combined frequency variation of 9.6×10^{-10} in the Doppler cancelled data described in Equation 9.

Table 1 shows an error analysis of the combined gravitational redshift and second-order Doppler test made in 1976 using a near-vertical trajectory. The improvement from 70 parts per million to 2 parts per million in the proposed test results partly from improved clocks, but mostly from the longer averaging intervals and estimates of the smaller systematic bias errors made possible by having time for adjusting and tuning the space maser before taking data.

3.2 *A Proposed Extension of the GP-A Experiment to Test General Relativity with a Solar Probe*

A series of studies of tests of relativistic gravitation has been conducted for a clock in a space probe approaching within 4 solar radii of the sun's center in a polar orbit.¹⁴ This test is intended to measure directly the second-order behavior of the redshift, $[\Delta\phi/c^2]^2$.

During the 10 hours before and after perihelion, the value of Φ/c^2 varies from 5.3×10^{-7} at perihelion to 2.0×10^{-7} at times ± 10 hours from perihelion. Over the same time interval, the second-order redshift $[\Phi/c^2]^2$, varies from 2.81×10^{-13} to 4×10^{-14} , as shown in Figure 9. Taking the Allan standard deviation of today's H-masers over 10 hours averaging time as 6×10^{-16} , the inaccuracy of measurement imposed by the maser instability for the first-order measurement is 1.8×10^{-9} , the corresponding inaccuracy for the second-order measurement is 2.5×10^{-3} .

The sun's gravitational potential is complicated by having a number of multipole components. The largest of these is the solar quadrupole moment,

J_2 , which must be accounted for in the measurement of the second-order term in the redshift. Estimates of J_2 have been made from solar oscillations,¹⁵ and we can estimate the effect of the uncertainty in these measurements from the behavior of the J_2 signature in the data. At order c^{-2} the first-order redshift has the following behavior:

$$\frac{\phi}{c^2} = \frac{\mu}{r} + \frac{\mu}{r^3} J_2 R_{\text{sun}}^2 \frac{3\cos^2\vartheta - 1}{2} = \frac{\Phi_1}{c^2} + \frac{\Phi_2}{c^2} \quad (11)$$

where $\mu = GM_{\text{sun}}/c^2$. Assuming $J_2 = 1.7 \times 10^{-7} \pm 0.17 \times 10^{-7}$, then at perihelion, $r = 4R_{\text{sun}}$, $\vartheta = \pi/2$, and $\Phi_2/c^2 = -2.8 \times 10^{-15}$.

At about ± 7 hours from perihelion,

$$\begin{aligned} \vartheta=0, r = 8R_{\text{sun}}, \text{ and} \\ \Phi_2/c^2 = +7.0 \times 10^{-16} \end{aligned} \quad (12)$$

The frequency variation caused by the J_2 contribution to the sun's redshift is shown in Figure 9 before and after perihelion. Its peak-to-peak magnitude is 3.5×10^{-15} . If we have an error of 10% in the estimate of J_2 , the uncertainty in its contribution to the redshift over this interval is about 3.5×10^{-16} , comparable to the instability of the clock. The error contribution will have a distinctive $(3\cos^2\vartheta - 1)/r^3$ signature in contrast to the very smooth $1/r$ dependence of the first-order redshift and the $1/r^2$ dependence of the second-order redshift.

An crucial feature is the ability to take Doppler-cancelled data at the probe. In Figure 8, we have shown how the localized noise near earth can be cancelled by correlation. While the spacecraft Doppler cancellation system can systematically remove the effect of the tropo-iono noise when it produces the $S_o(t_i + 2R/c)$ data, this is not the case for the earth station Doppler-cancelled output E_o . In the earth station cancelled Doppler there would be about 1000 sec of time delay between the uplink transmission and reception from the transponder. During this interval the combined atmospheric and ionospheric delay could have varied considerably.

A joint SAO/NASA Jet Propulsion Lab study has been made to evaluate the feasibility of this experiment.¹⁶

3.3 Detection of Pulsed Gravitational Radiation using Doppler Techniques

During the long travel time to the sun there will be an opportunity to search for gravitational radiation using Doppler techniques.^{17 18} In Einstein's General Theory of Relativity (GRT), gravitational radiation results whenever a massive body is accelerated. Rotating binary stars radiate energy and will

eventually collapse together. While evidence for such radiation has not been observed directly, the orbital decay of a binary pulsar has been observed since 1975 and its rate continues to follow closely the predicted behavior for loss of energy by gravitational radiation.¹⁹

According to GRT, gravitational radiation is a wavelike distortion of space-time travelling at the speed of light. When a gravitational wave intercepts bodies connected by electromagnetic signals, it distorts the frequency by $h = \Delta f/f$. It should be possible to detect gravitational waves by observing Doppler shifts of a signals from a highly stable microwave (or laser) transmitter and detected by a receiver located at a distance greater than about one-half the wavelength of the gravitational wave.

Figure 10 shows an example of Doppler detection²⁰ of a pulsed gravitational wave using the four-link Doppler measurement system. Here the wavefront of the gravitational pulse is assumed to intercept the earth-probe line at an angle, $\theta = 60$ degrees. The effect of the pulse would be observed three times in the Earth 2-way Doppler trace as follows:

$$\frac{df}{f} = \frac{(1-\mu)\psi(t_R)}{2} - \mu\psi\left[t_R - L\frac{(1+\mu)}{c}\right] + (1+\mu)\psi\left(t_R - 2\frac{L}{c}\right) \quad (13)$$

- by a Doppler shift of the gravitational wave disturbing the earth station at $t=t_1$, while it is receiving a signal transmitted earlier by the spacecraft.
- by its "echo" when the earth station receives a transponded signal at $t = t_1 + 2R/c$.
- when the gravitational wave arrives at the spacecraft at time t_2 and is reported at earth at $t = t_2 + R/c$.

The spacing of the pulses, their time signature designated by the parameter $\psi(t)$, and the relative magnitude and sign of the signature are described by a single parameter, $\mu = \cos\theta$ ^{21,22}. Here t_R signifies arrival time at the first station.

The one-way transmission from the spacecraft would show the pulses at t_1 and at $t_2 + R/c$.

A similar set of five observations of the same gravitational pulse is available at the spacecraft. In this case $\mu = \cos(\pi+\theta)$ and another set of five manifestations of the pulse appears in the spacecraft data. While only four of the ten pulses, i.e., those from the two one-way Doppler signals, are unique, the other six are obtained from other paths through the electronics system and provide redundancy to help prevent interpreting noise as gravitational wave signals. If one of the stations is on earth, noise from the earth's troposphere and ionosphere would be the main limitation to the sensitivity of detection. Reduction of ionospheric noise is possible by operating at higher frequencies than the currently used S-band (2 GHz) and X-band (10 GHz) systems.

However, tropospheric noise cannot be reduced by such techniques and will substantially degrade the stability of a signal. Studies show that the Allan deviation of the tropospheric noise for signals passing vertically has a $\tau^{-2.5}$ behavior for intervals between 20 and 200 sec, with $\sigma_y(100 \text{ sec}) = 8 \times 10^{-14}$, as shown in Figure 2²³. While it is possible to model the tropospheric frequency shifts using other data, such as the columnar water vapor content and the local barometric pressure, tropospheric propagation variations will nevertheless severely limit the detection of gravitational radiation with transponded two-way Doppler signals. Estimates have been made that the sensitivity with ideal tropospheric conditions at night in the desert will be at a level of $h = \Delta f/f \sim 3 \times 10^{-15}$ for gravitational waves in the millihertz region, which is one to two orders of magnitude above the levels estimated by astrophysicists^{18,21}.

Tropospheric noise can be removed systematically by simultaneously recording Doppler data from a clock in a spacecraft and at the earth station and combining these data. Simulations of this process¹² show nearly complete rejection of such spatially localized sources as near-earth tropospheric and ionospheric variations and earth station antenna motion noises. With both clock systems operating in space and at frequencies where the noise from the solar corona ionization is not significant, the principal nongravitational noise sources will likely be from the buffeting of the space vehicles by nongravitational forces such as light pressure, particle collisions, and sporadic outgassing of the spacecraft. Here, again, since these disturbances are localized at the ends of the system, the time signatures of the noises are separated by R/c , and can be distinguished from the patterns expected from pulsed gravitational waves, which have signatures that depend only on the parameter μ of equation 13.

4 High Resolution Very Long Baseline Interferometry (VLBI) Astronomy in Space

4.1 *The Effect of Oscillator Instability on the Measurement of Angles*

High precision measurement of the angle between the propagation vector of a signal and the direction of a baseline, defined as the line between the phase centers of two widely separated radio telescope antennas, can be made with VLBI techniques²⁴ shown in Figure 11. Here, two radio telescopes, separated by a distance, L , each detect the arrival of radio noise signals from a distant radio star. After heterodyning to a lower frequency the noise signals are recorded as a function of time and the two sets of noise data are subsequently time-correlated. The observable quantities from the correlation process are the correlated amplitude and the relative phase of the signals detected at the widely separated points on the wavefront. VLBI

measurements have been used in light deflection tests of relativistic gravitation.²⁵

The stability limit on the successive measurements of angle imposed by the oscillator instability on successive measurements of angle taken τ seconds apart is

$$\sigma_{\Delta\theta}(\tau) \sim \frac{c \tau \sigma_y(\tau)}{L \sin\theta} \quad (14)$$

where θ is the angle between the propagation vector and the baseline. The result of correlating the noise data obtained from a common source by the two stations is the production of fringes analogous to those observed from two-slit optical diffraction. The spacing between the fringes is $\lambda/L \sin\theta$, where λ is the average wavelength of the signals arriving at the antennas. The visibility of the fringes depends on the extent to which the signals arriving at the antennas are correlated.

The angular resolution of the interferometer is given by the change of fringe phase, ϕ , with θ

$$\frac{d\phi}{d\theta} = \frac{2\pi L}{\lambda} \quad (15)$$

The error in successive angular measurements owing to the instability of the clocks in a terrestrial system with $L = 6000$ km, assuming $\sigma_y(10^3 \text{ sec}) = 1 \times 10^{-15}$, and $\theta = \pi/2$, is given by

$$\sigma_{\Delta\theta}(10^3 \text{ sec}) = 5 \times 10^{-11} \text{ rad or } 2 \mu \text{ arcsec.}$$

This is far smaller than the present actual limit of 100μ arcsec level from terrestrial stations with an 8000-km baseline operating at 7 mm wavelength.²⁶ The effects of tropospheric and ionospheric fluctuations impose limits that are far more serious than clock instability.

By operating VLBI stations in space, limits in angular resolution owing to tropospheric and ionospheric propagation and baseline distance, imposed by the size of the earth, can be overcome.

A successful demonstration of a spaceborne radio telescope operating as a VLBI terminal was made in 1986²⁷ using NASA's orbital Tracking and Data Relay Satellite System (TDRSS) system as a spaceborne radio telescope in conjunction with a number of radio telescopes on earth.

As an example of the limits that a spaceborne two station system could achieve, let us consider a spaceborne system where $L = 5 \times 10^6$ km, $\sigma_y(10^4 \text{ sec}) = 4 \times 10^{-16}$, and $\theta = \pi/2$. In this case,

$$\sigma_{\Delta\theta} (10^4) = 2 \times 10^{-13} \text{ rad or } 0.05 \text{ } \mu\text{arcsec} .$$

For $\lambda = 1 \text{ mm}$ we have $\lambda/L = 2 \times 10^{-13} \text{ rad}$ and we see that the limit imposed by clock stability with 10^4 sec integration time is capable of resolving fringes at 1-mm wavelengths in a spaceborne system with baseline distances of $5 \times 10^6 \text{ km}$. The numbers in this example are chosen to be close to present estimates of the limits for having reasonably well correlated flux at the two stations ²⁸ at the distances chosen.

Terrestrial VLBI systems are now used to record polar motion and rotation of the earth and to monitor the movements of the earth's tectonic plates. While *relative* positions of radio stars, and features of their brightness distribution, can be made with a precision of a few tenths of a milliarcsecond, the *absolute* directions in space of the baselines between VLBI stations depend on the choice of a frame of reference. This reference is usually taken from the position of very distant radio sources.

4.2 A Spaceborne Four Terminal (VLBI) Array that Establishes an Inertial Reference Frame, a "Gedanken" System to Exercise our Imaginations.

Let us assume an array of four stations, separated by about 5×10^6 kilometers and in the form of a tetrahedron defining a three-dimensional figure in space. Figure 12 shows such an array. Each station contains a clock and is connected to its three neighbors by the four link system shown in Figure 7. ²⁹ The six baseline distances can be precisely measured, using one-way and two-way Doppler techniques discussed earlier, and thus precisely define the *configuration* of the array as a function of time.

Defining the *orientation* of the array of six baselines poses an interesting problem. The distant radio stars define the conventionally used inertial frame. By invoking the Sagnac effect,³⁰ we can define an inertial frame based on the velocity of light, and it should be possible to determine *changes* in the orientation of the array in terms this frame.

To describe the Sagnac process, we visualize the arrival times of light signals sent in opposite senses about a closed path on a surface rotating at Ω rad/second. If the projected area, perpendicular to the rotation axis, on that surface is A , then the difference in the arrival times of light signals going around the path in opposite senses is $\Delta\tau = 4\Omega A/c^2$. By measuring the difference in arrival times of signals going in opposite senses about a triangle defining one face of the tetrahedron, we can obtain the component of rotation normal to that face. From the four triangles that define the tetrahedron we have an overdetermination of the rotation and can make an estimate of the accuracy of its measurement.

For the array shown in Figure 12, the limitation due to the accuracy of the detection of changes in rotation rate, $\Delta\Omega$, is $1.2 \times 10^{-15} \text{ rad/sec}$. If the array

is located at 1 AU from the sun, such a rotation measurement would include the Einstein–deSitter precession of 2×10^{-2} arcsec/yr (3×10^{-15} rad/sec) owing to the bending of space-time by the sun's gravity.

This array could compare, with very high precision, the frame of reference defined by the most distant radio sources with an inertial frame defined by the local isotropy and constancy of the velocity of light. Could it provide a way to observe some aspect of the behavior of the missing matter in the universe? Perhaps theorists could be tempted to speculate about scenarios that could be revealed with this system.

5 Conclusion

Since the mid 1960s the frequency stability of atomic clocks (or oscillators) has been improving by a factor of about ten every decade, so far with no end in sight. The units of time and frequency, and the now redefined unit of distance through the velocity of light, are solidly based on atomic frequency standards. This metrology has been made consistent with present concepts of gravitation and relativity. We now make measurements of astronomical and astrophysical objects near the edge of our universe with clocks that operate using quantum processes whose dimensions encompass staggeringly smaller distance scales. As the performance of atomic clocks improves and their uses are extended in astrophysical measurements, perhaps we will see some surprises about the nature of our universe.

References

-
- 1 J. Ruttman and F.L. Walls, "Characterization of frequency stability in precision frequency sources," *Proc. IEEE*, vol. 79, 1991.
 - 2 D. J. Wineland, J.C. Bergquist, J.J. Bollinger, W.M. Itano, D.J. Heinzen, S. L. Gilbert, C.H. Manney, and M.G. Raizen, "Progress at NIST toward absolute frequency standards using stored ions," *IEEE Trans. on Ultrasonics, Ferroelectrics and Frequency Control*, vol. 37, no. 6, Nov. 1990.
 - 3 R.F.C.Vessot, E.M. Mattison, W.J. Klepczynski, G.M.R. Winkler, I.F. Silvera, H.P. Godfried, and R.L. Walsworth, "Present clock stability and realistic prospects for the future," in *Proc. Fourth Marcel Grossman Meeting on General Relativity* (R. Ruffini, Ed.) Rome, Italy, June 17-21, 1985
 - 4 L.A. Rawley, J.H. Taylor, M.M. Davis, and D.W. Allan, "Millisecond pulsar PSR 1937 + 21: A highly stable clock," *Science*, vol. 238.

-
- 5 R.S. Badessa, R.S. Kent, R.L. Nowell, and C. L. Searle, "A Doppler-cancellation technique for determining the altitude dependence of gravitational redshift in an earth satellite," *Proc. IRE*, vol. 48, p. 758, 1960.
- 6 D. Kleppner, R.F.C. Vessot, and N.F. Ramsey, "An orbiting clock experiment to determine the gravitational redshift," *Astrophys. Space Sci.*, vol. 6, pp. 13-32, 1970.
- 7 R.F.C. Vessot, M.W. Levine, E.M. Mattison, E.L. Blomberg, T. E. Hoffmann, G.U. Nystrom, B.F. Farrell, R. Decher, P.B. Eby, C.R. Baugher, J.W. Watts, D.L. Teuber, and F.D. Wills, "Tests of relativistic gravitation with a space-borne hydrogen maser," *Phys. Rev. Lett.*, vol. 45, pp. 2081-2084, Dec. 1980.
- 8 A.J. Tucker and B.M. Fannin, "Analysis of ionospheric contributions to the Doppler shift of C.W. signals from artificial earth satellites," *J. Geophys. Res., Space Physics*, vol. 73, no. 13, pp. 4325-4334, 1968.
- 9 R.F.C. Vessot and M.W. Levine, "Performance data of space and ground hydrogen masers and ionospheric studies for high-accuracy frequency comparison between space and ground clocks," in *Proc. Twenty-eighth Annual Symp. Frequency Control*, U.S. Army Electronics Command, Ft. Monmouth, NJ, 1974, pp. 408-414.
- 10 R.F.C. Vessot and M.W. Levine, NASA Experimental Final Redshift Report, GPA Project Report, Contract NAS8-27969.
- 11 R.F.C. Vessot and M.W. Levine, "A time-correlated four-link Doppler tracking system," in *A Closeup of the Sun* (M. Neugebauer, and R.W. Davies, Eds.) JPL Publication 78-70, NASA, 1978.
- 12 T. Piran, E. Reiter, W.G. Unruh, and R.F.C. Vessot, "Filtering of spacecraft Doppler tracking data and detection of gravitational radiation," *Phys. Rev. Lett.*, D, 34, no. 4, p. 984, 1986.
- 13 L.L. Smarr, R.F.C. Vessot, C.A. Lundquist, R. Decher, and T. Piran, "Gravitational waves and redshifts: A space experiment for testing relativistic gravity using multiple time-correlated radio signals," *Gen. Rel. and Grav.* vol. 15, no. 2, pp. 129-163, 1983.
- 14 M. Neugebauer and R.W. Davies, *A Closeup of the Sun*, JPL Publications 78-70, NASA, 1978.
- 15 T. M. Brown, J. Christensen-Dalsgaard, W.A. Dziembowski, R. Goode, D.O. Gough, and C.A. Morrow, "Inferring the sun's internal angular velocity from observed P-mode frequency splitting," *Astrophys. J.*, vol. 343, p. 526, 1989.
- 16 NASA contract number NAS-918 by J.D. Anderson of JPL and E.M. Mattison and R.F.C. Vessot of SAO.
- 17 F. B. Estabrook, "Gravitational wave searches with ground tracking networks," *ACTA Astronautica*, vol. 17, no. 5, pp. 585-587, 1988.

-
- 18 J. W. Armstrong, J.D. Anderson, and E.L. Lau, "Application of hydrogen maser technology to the search for gravitational radiation," in *Proc. of Twenty-first Annual Precise Time and Time Interval (PTTI) Applications and Planning Meeting*, Redondo Beach, CA. Nov. 28-30, 1989, pp. 259-263.
- 19 J. H. Taylor and J.M. Weisberg, "Further experimental tests of relativistic gravity using the binary pulsar PSR 1913 + 16," *Astrophys. J.*, vol. 345, pp. 434-450, Oct, 1989.
- 20 A. J. Anderson, "Probability of long period (VLF) gravitational radiation," *Nature*, vol. 229, pp. 547-548, 1971.
- 21 F. B. Estabrook and H.D. Wahlquist, "Response of Doppler spacecraft tracking to gravity waves," *Gen. Rel. Grav.*, vol. 6, pp. 439-447, 1975.
- 22 K. S. Thorne and V.B. Braginsky, "Gravitational-wave bursts from the nuclei of distant galaxies and quasars: proposal for detection using Doppler tracking of interplanetary spacecraft," *Astrophys. J. Lett.*, vol. 204, L1, 1976.
- 23 A.E.E. Rogers, A.T. Moffet, D.C. Backer, and J.M. Moran, "Coherence limits in VLBI observations at 3-millimeter wavelength," *Radio Sci.*, vol. 19, no. 6, pp. 1552-1560, 1984.
- 24 A.E.E. Rogers and J.M. Moran, Chapter 5, "Interferometers and Arrays," Chapter 5 in *Methods of Experimental Physics*, Astrophysics, M.L. Meeks, Ed., vol. 12. New York: Academic Press, 1976.
- 25 E. B. Formalont and R.A. Sramek, "Measurement of the solar gravitational deflection of radiowaves in agreement with general relativity," *Phys. Rev. Lett.*, vol. 36, p. 1475, 1976.
- 26 N. Bartel, V. Dhawan, T. Krichbaum, D.A. Graham, I.I.K. Pauliny-Toth, A.E.E. Rogers, B.O. Rönnäng, J.H. Spencer, H. Hirabayashi, M. Inoue, C.R. Lawrence, I.I. Shapiro, B.F. Burke, J.M. Marcaide, K.J. Johnston, R.S. Booth, A. Witzel, M. Morimoto, and A.C.S. Readhead, "VLBI imaging with an angular resolution of 100 microarcseconds," *Nature*, vol. 334, no. 6178, pp. 131-135, 1988.
- 27 G.S. Levy, C.S. Christensen, J. F. Jordan, R.A. Preston, C.D. Edwards, R.P. Linfield, S.J. DiNardo, L. Skjerve, J.S. Ulvestad, T. Hayashi, T. Nishimura, T. Taskano, T. Yamada, T. Shiomi, H. Kunimori, N. Kawaguchi, M. Inoue, M. Morimoto, H. Hirabayashi, B.F. Burke, A. Whitney, D.L. Jauncey, C.H. Ottenhoff, K. Blaney, and W. Peters, "Results and communications considerations of the very long baseline interferometry demonstration using the tracking and data relay satellite system," *Acta Astron.*, vol. 15, no. 6/7, pp. 481-487, 1986.
- 28 V.V. Andrejanov *et al.* "Quasat, A VLBI Observatory in Space," in *Proc. Workshop*, Gross Enzersdorf, Austria, June 18-22, 1984, ESA Publication SP-213.

-
- 29 R.F.C. Vessot, "Clocks and spaceborne tests of relativistic gravitation," in *Advances in Space Research*, Eds. (R.D. Reasenber and R.F.C. Vessot Eds.) Pergammon Press, vol.9, No. 9, 1989.
- 30 E.J. Post, "Sagnac Effect," *Rev. Mod. Phys.* , vol. 39, p. 475, 1967.

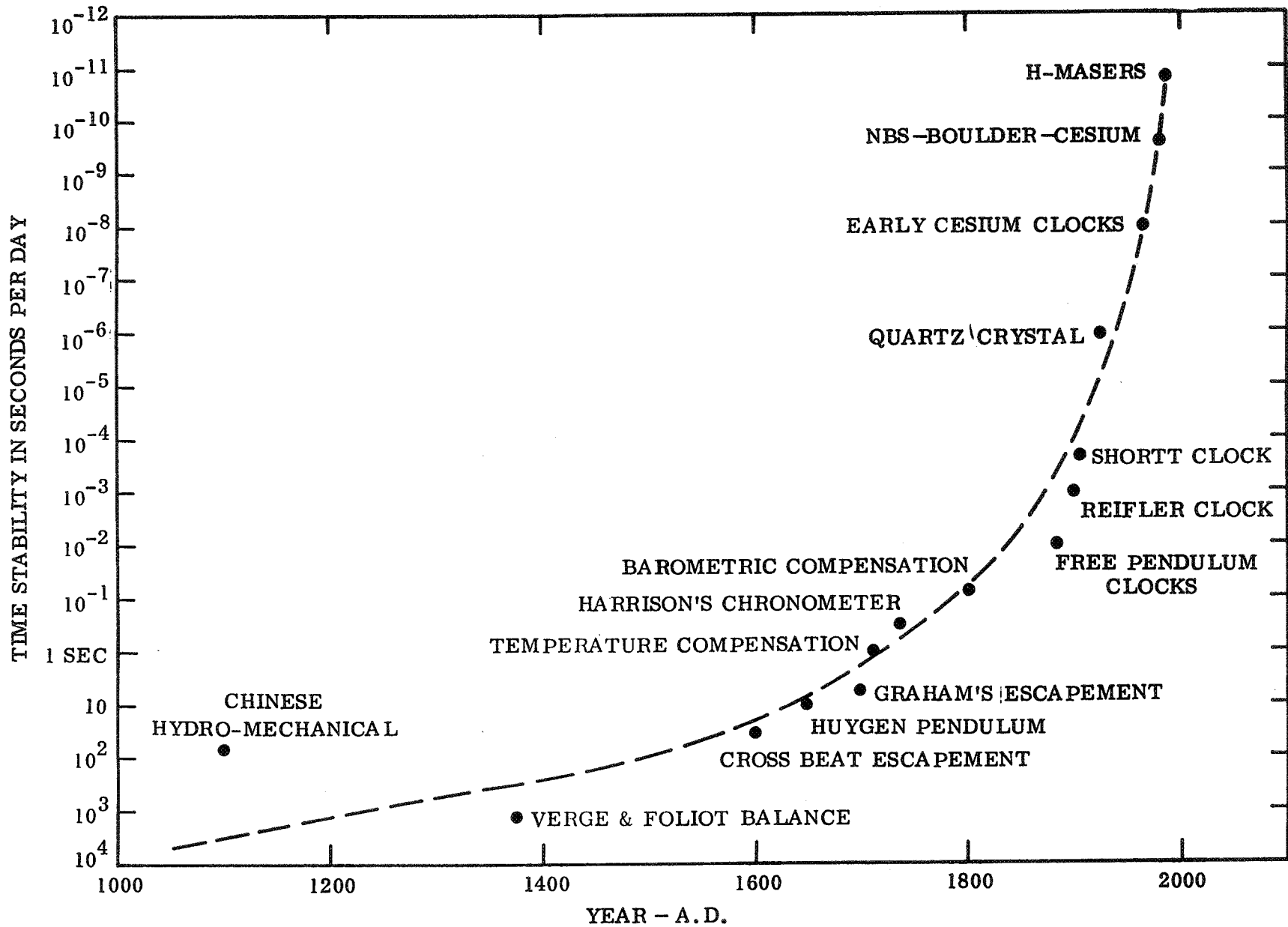


Figure 1
Progress in Timekeeping during This Millenium

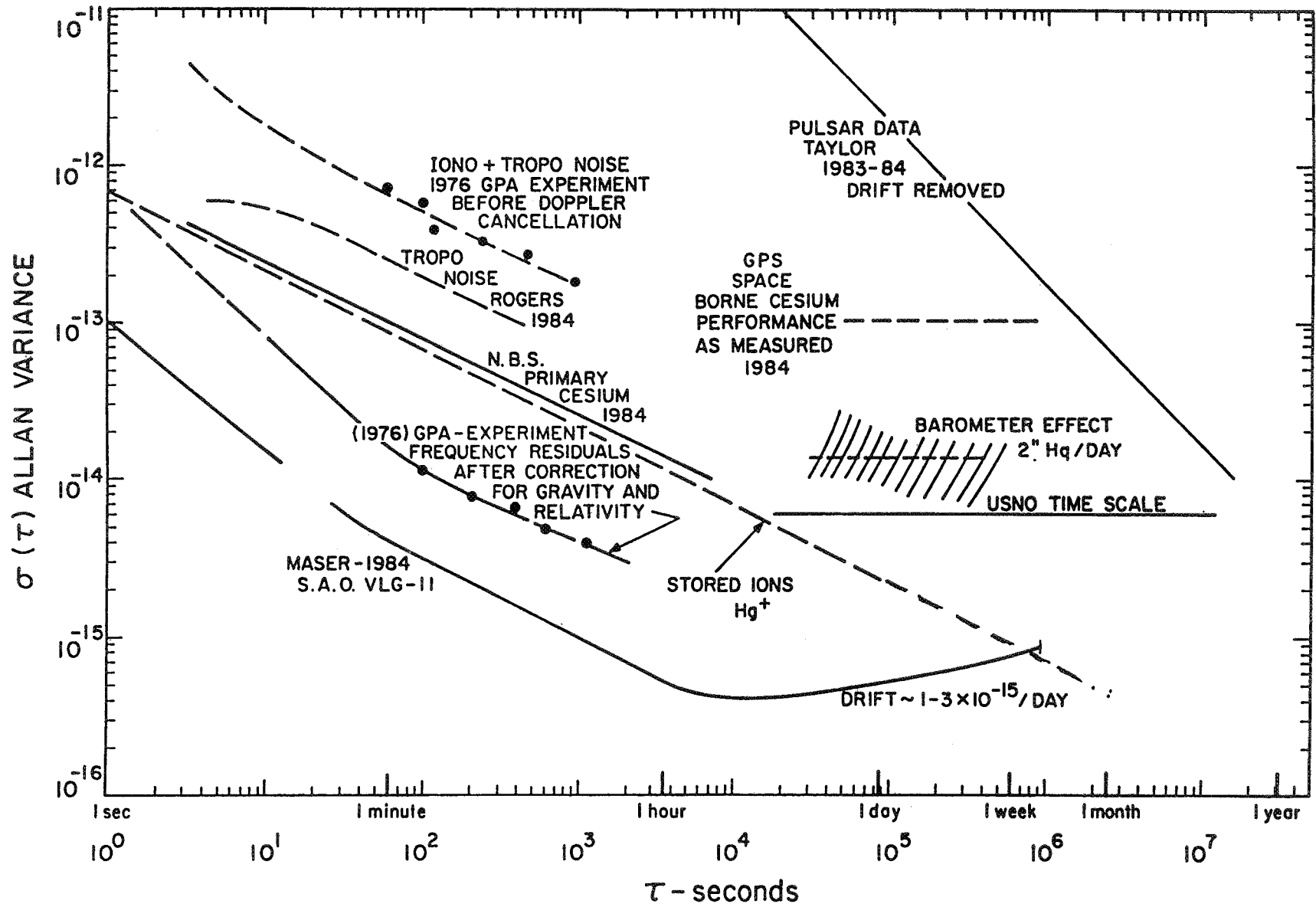


Figure 2
Allan Standard Deviation of Frequency Stability and Signal Propagation effects

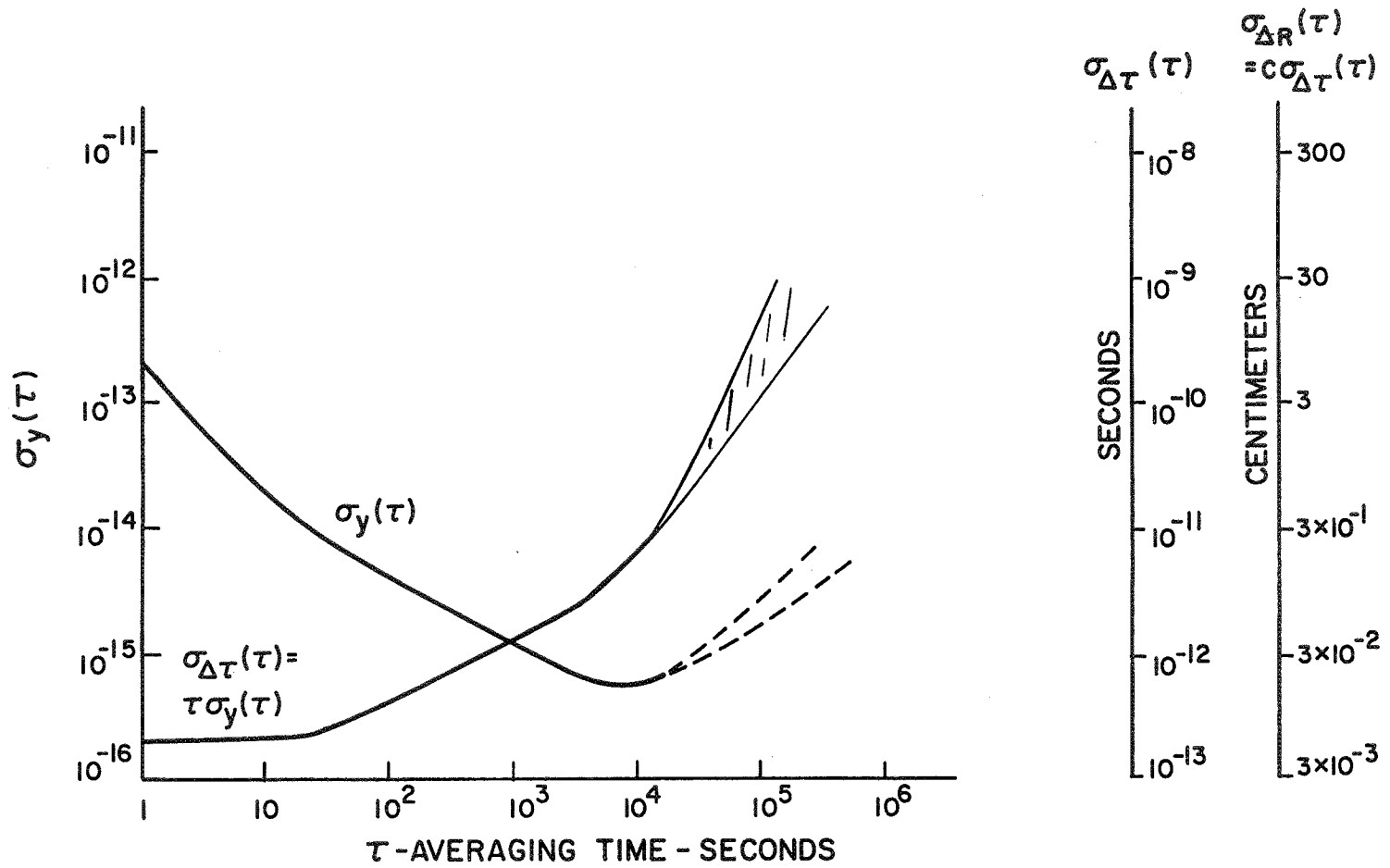


Figure 3

Time and Range Distance Dispersion from the Allan Standard Deviation of Maser Data in Figure 2

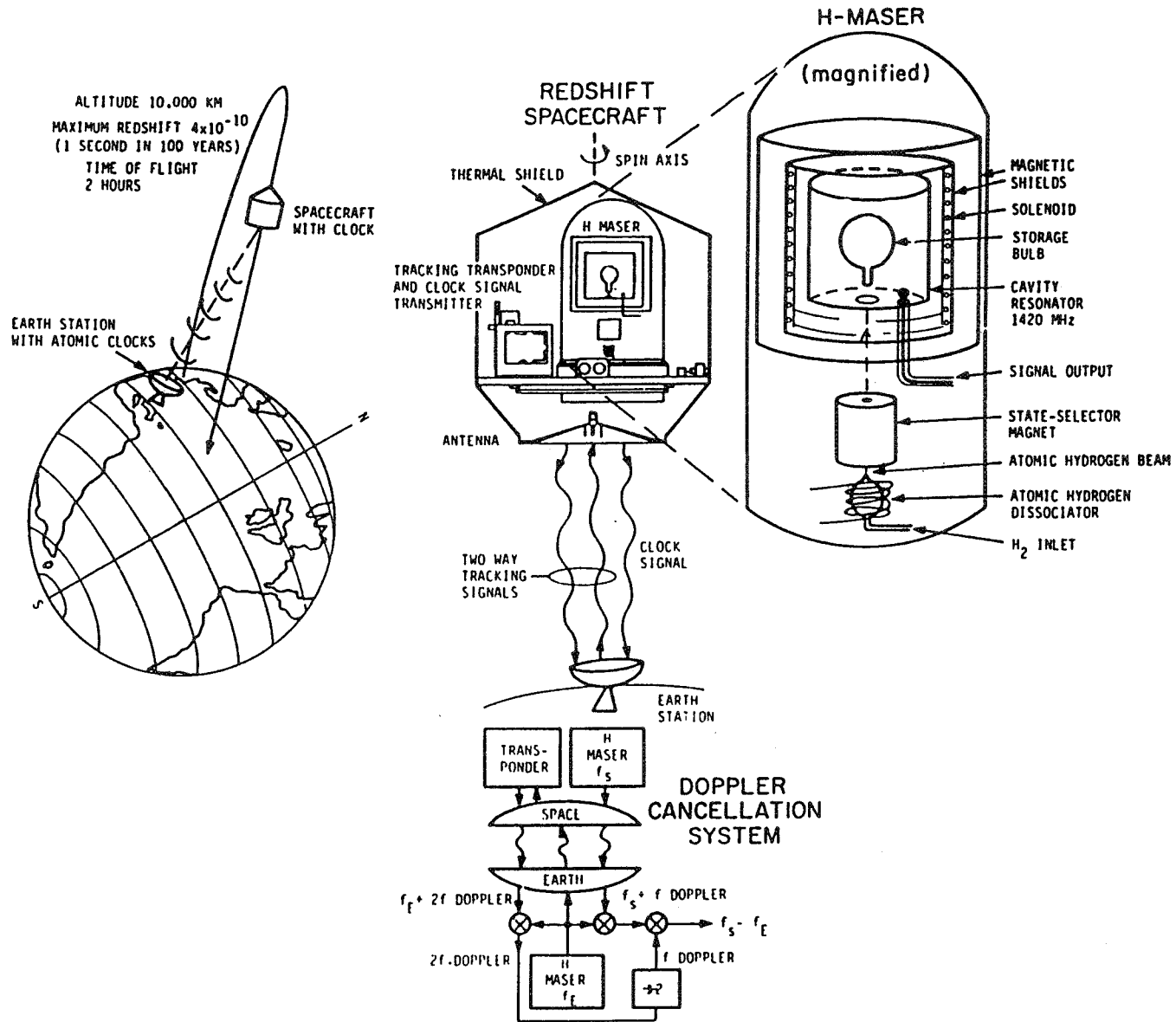


Figure 4
 Schematic Description of the 1976 SAO-NASA Test of the Gravitational Redshift (GP-A)

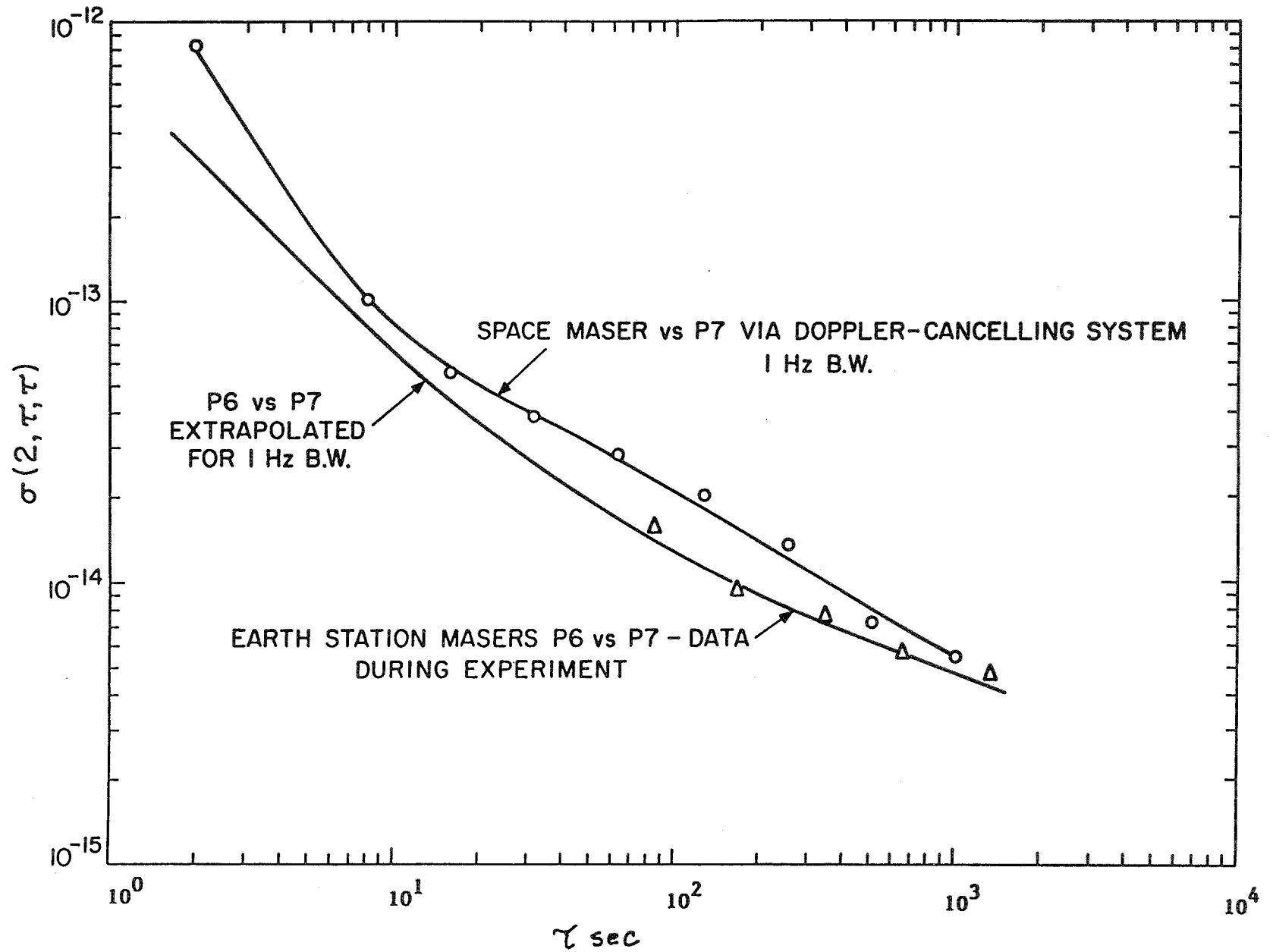


Figure 5
Residuals From Doppler Cancelled Signals after Removal of Relativistic Effects

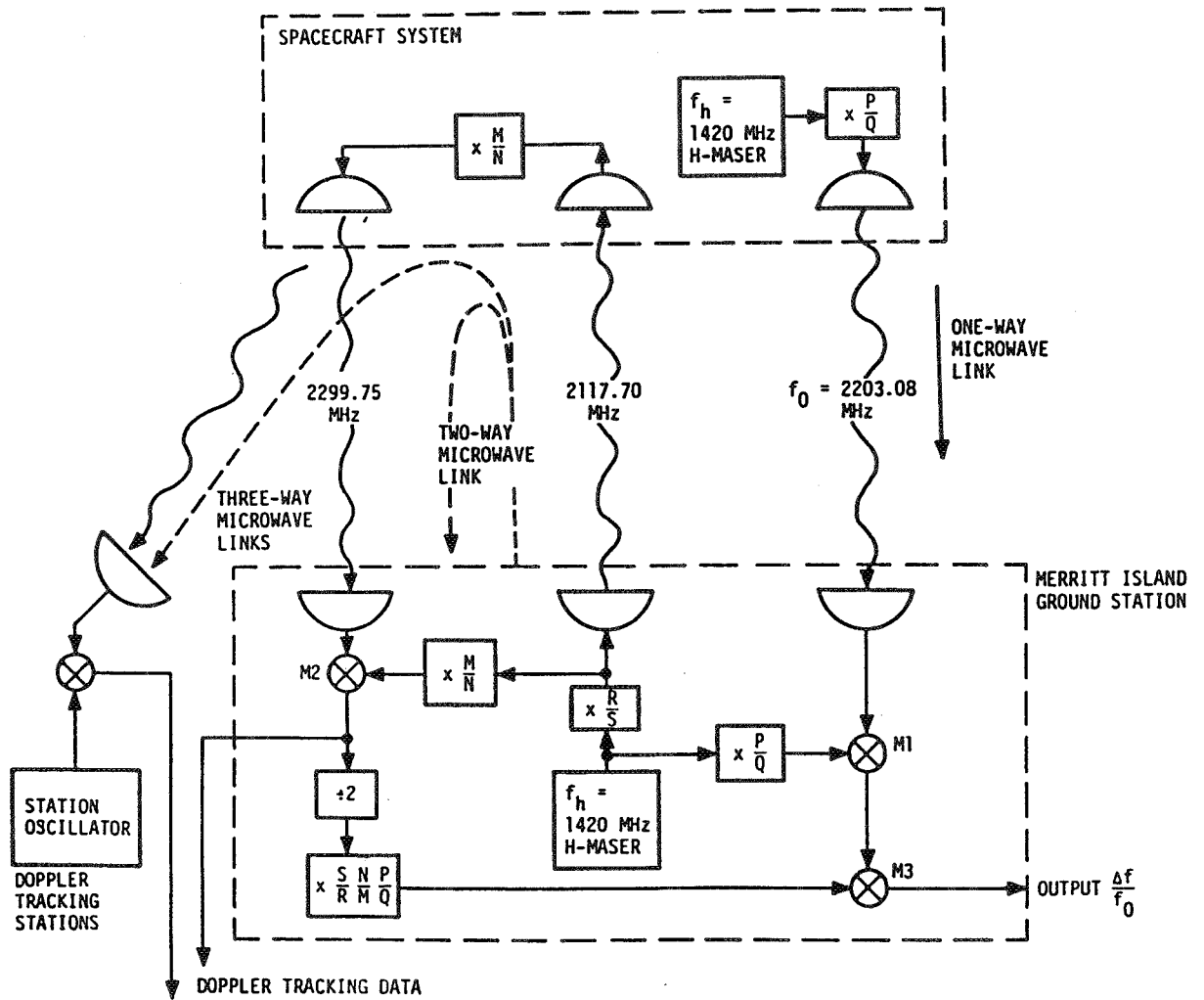


Figure 6
Tracking Station Schematic Configuration
Showing Ratio Synthesizers

$M/N = 240 / 221$ (Standard U.S.B Transponder Ratio)

$R/S = 82/55$ and $P/Q = 76/49$

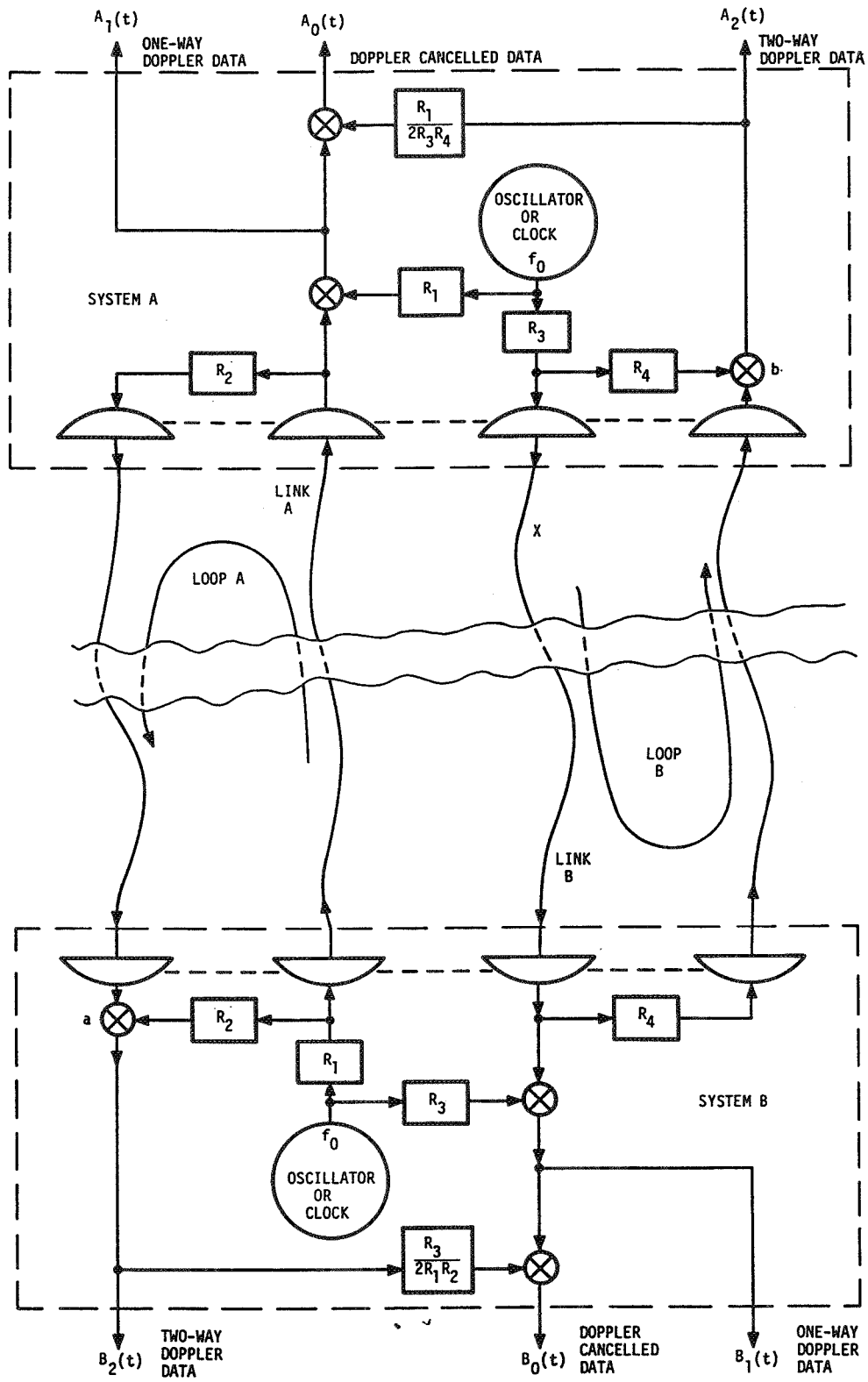


Figure 7

Concept of the Four-Link Time-Correlated Doppler System

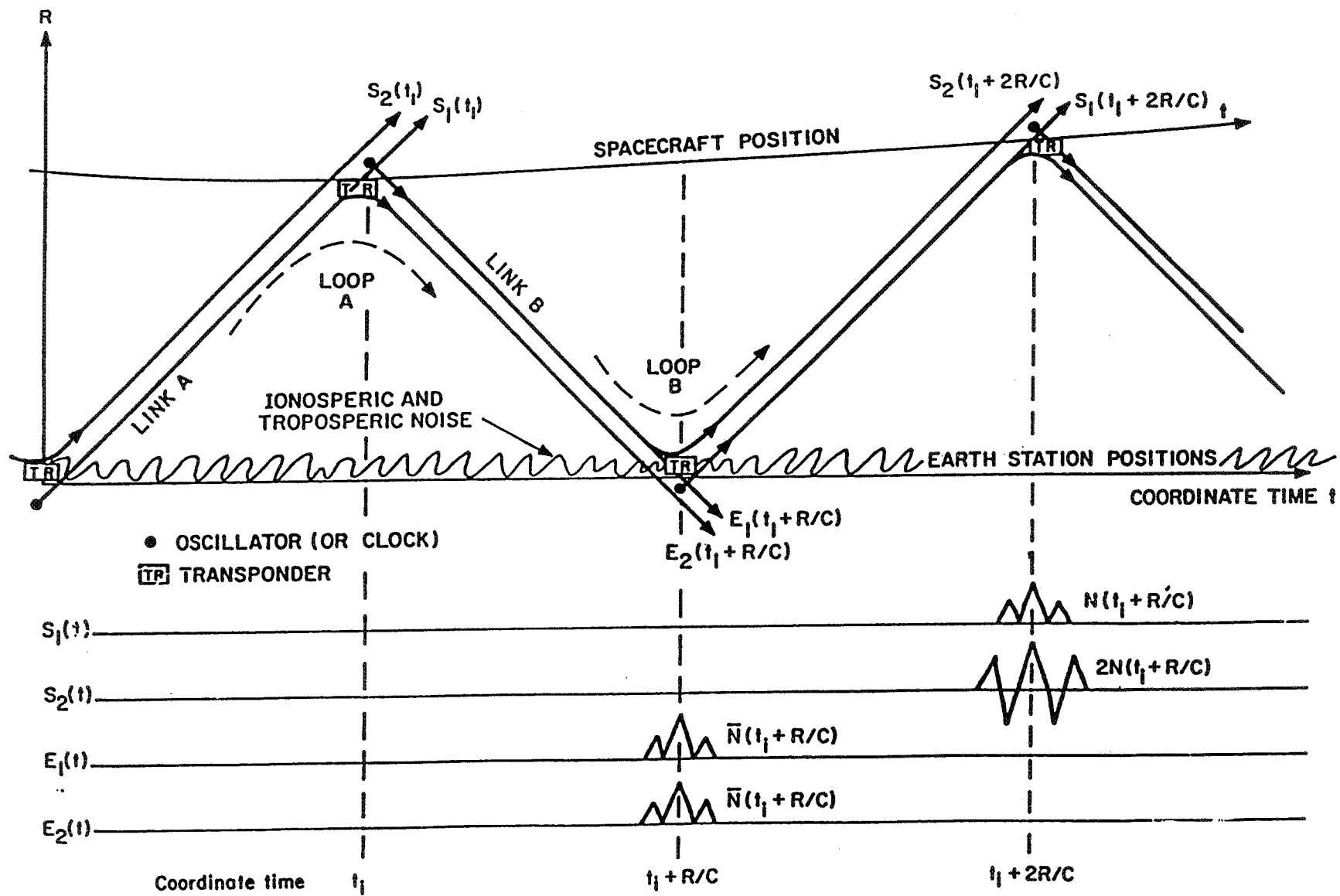


Figure 8
Space-Time Diagram of Signals the 4 Link System Showing Cancellation of Near Earth Disturbances

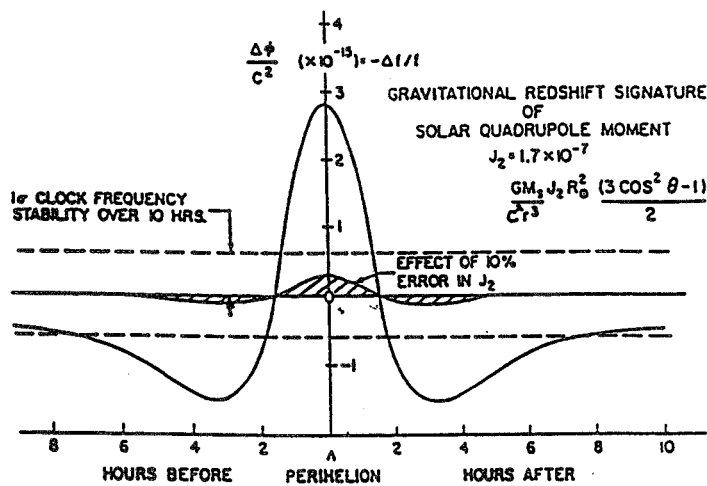
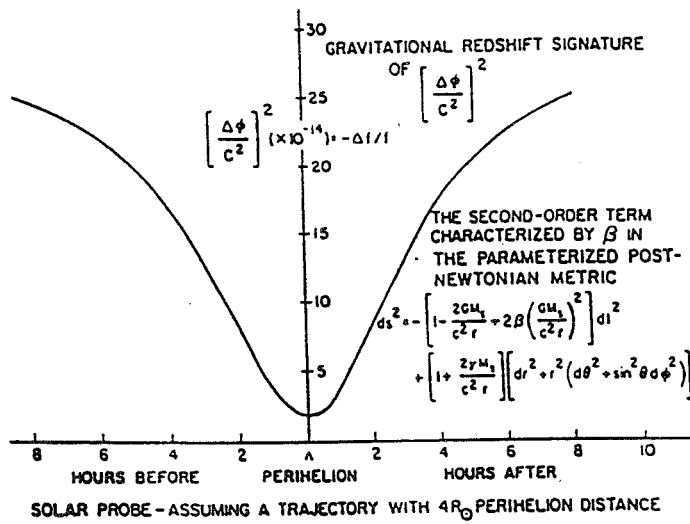
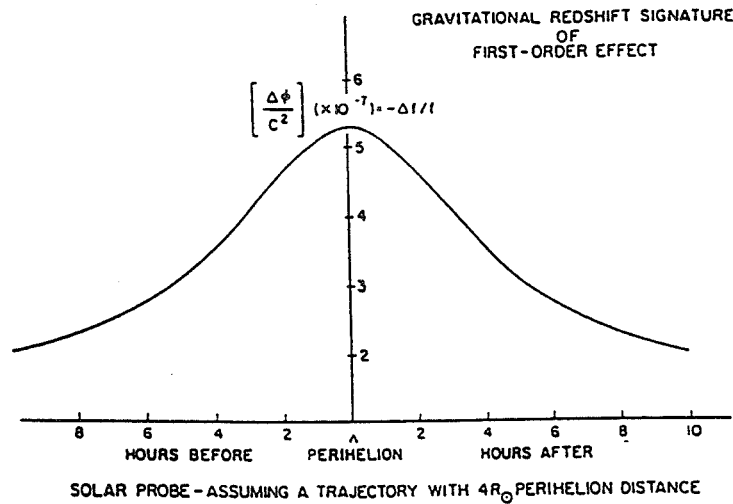


Figure 9

Gravitational Frequency Signatures in Solar Probe Data

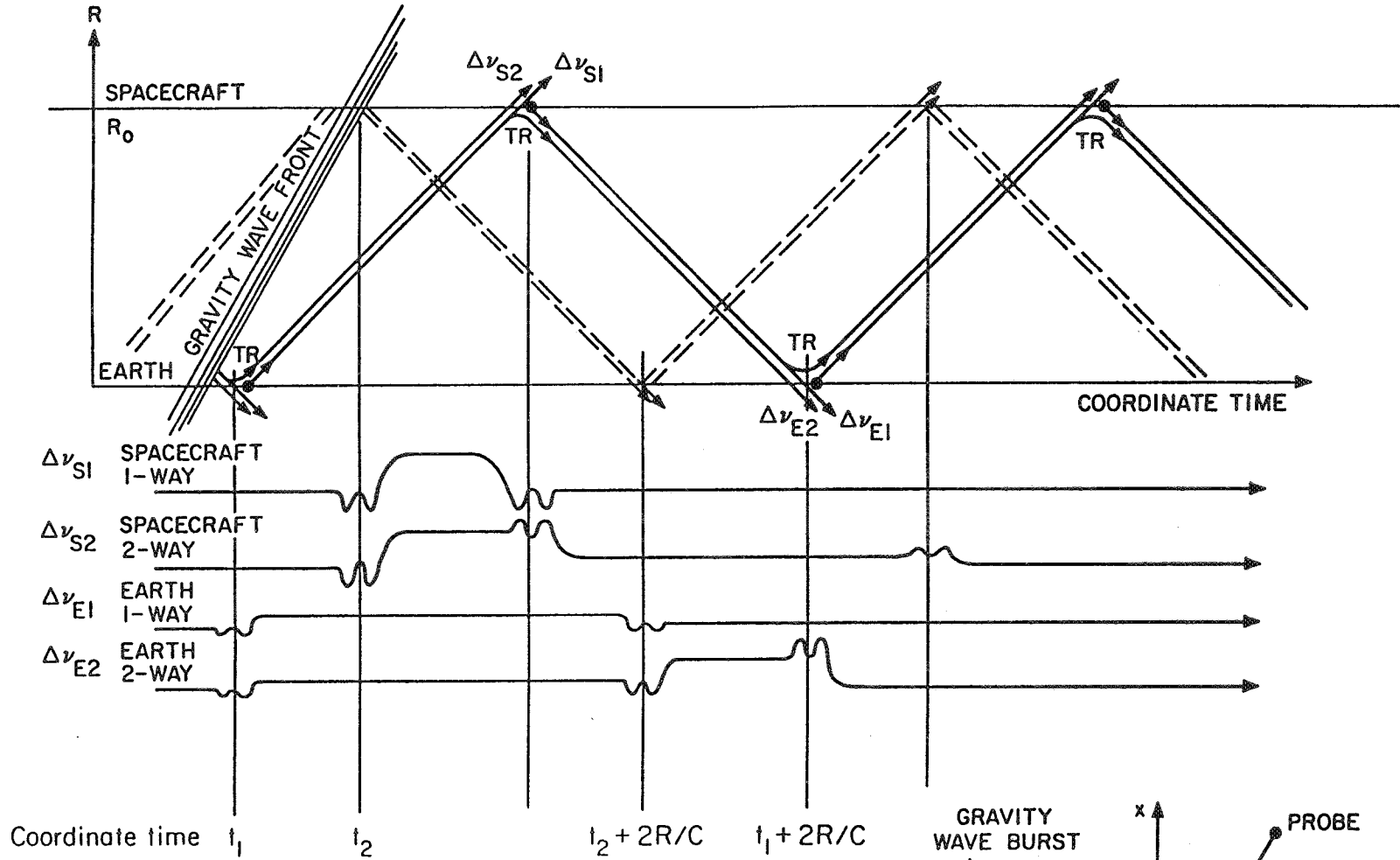


ILLUSTRATION OF GRAVITY-WAVE SIGNATURE FOR A 4-LINK CORRELATED SYSTEM $\theta = 60^\circ$

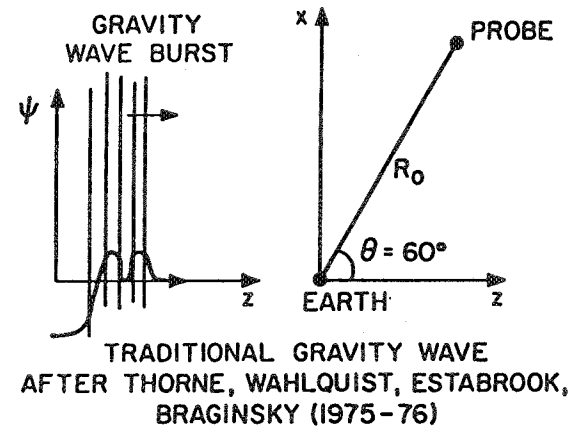
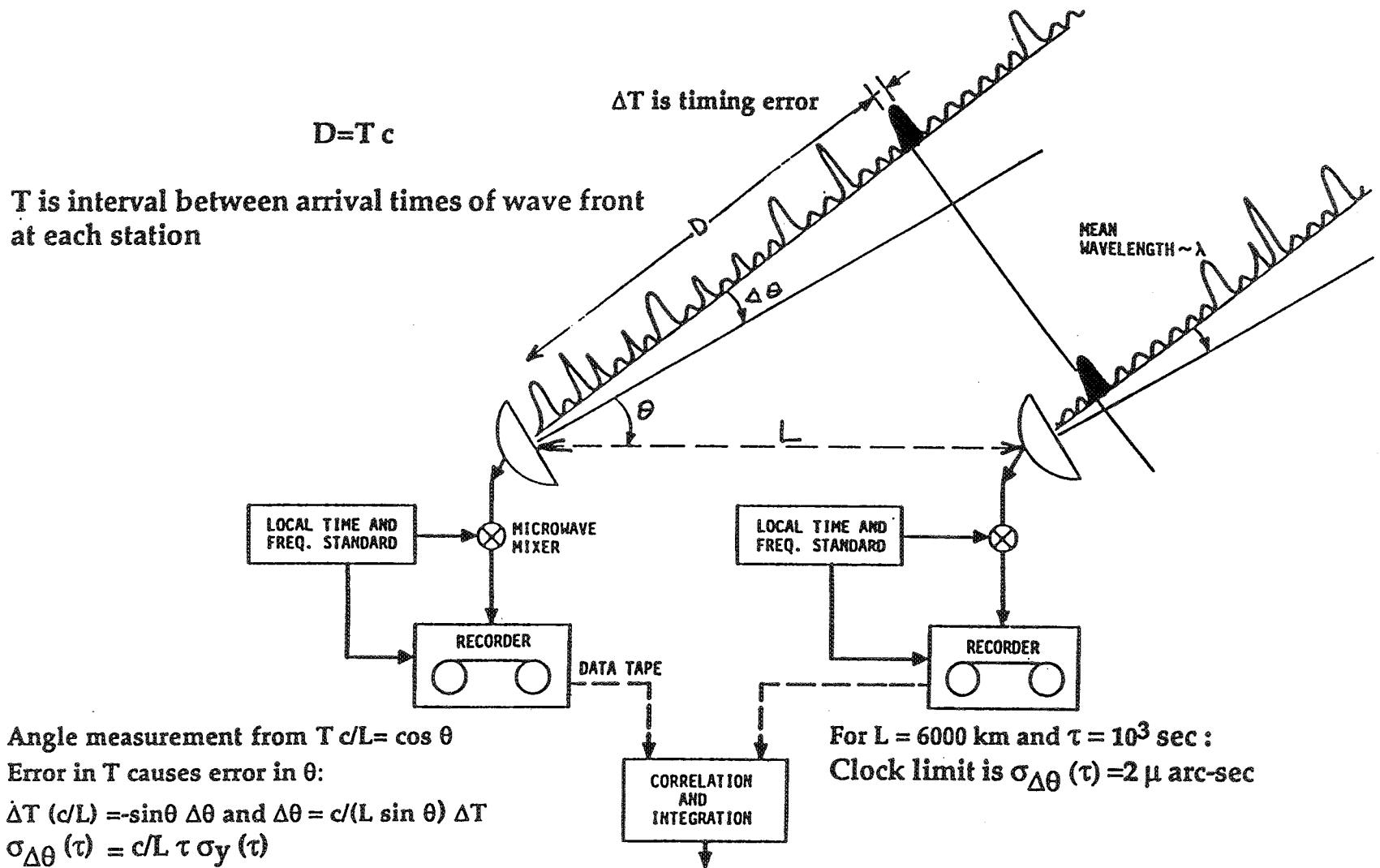


Figure 10



**VLBI enables the highest angular resolution of any astronomical technique (100 μ arc-sec)
Operation in space removes limitations imposed by atmospheric disturbances and finite baseline length**

Figure 11

Measurement of Angle by Very Long baseline Interferometry

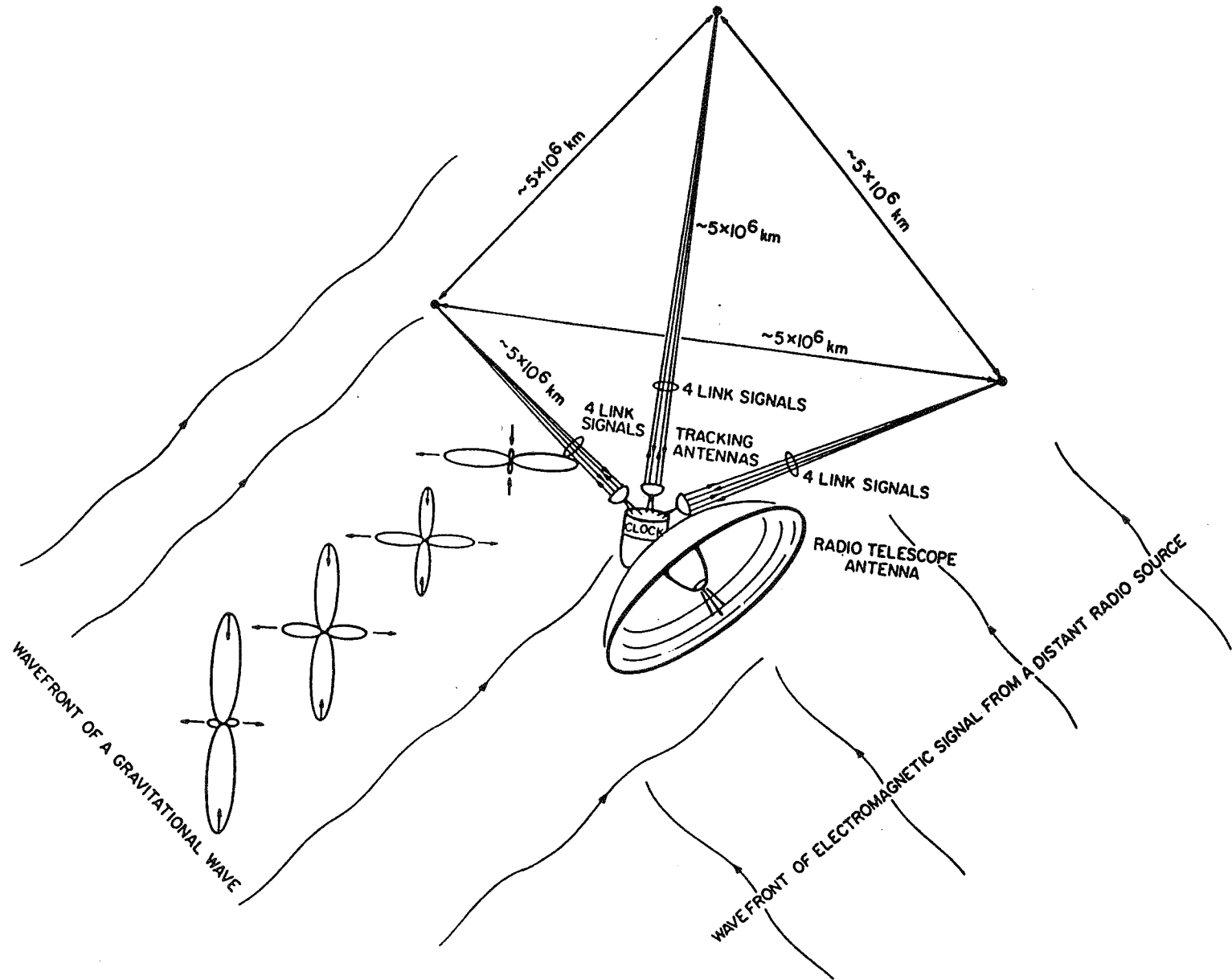


Figure 12

A Spaceborne Array of Radiotelescopes Interconnected by 4 Link Systems

Hydrogen Maser for Space
E.M. Mattison, D.A. Boyd, J.F. Maddox, G.U. Nystrom and R.F.C. Vessot
Smithsonian Astrophysical Observatory
Cambridge, Massachusetts

Clocks in Space; the Hydrogen Maser Clock Program

Frequency references – high stability clocks – increasingly find applications in space missions. Atomic clocks of ever increasing stability have present and potential uses as frequency references for the GLONASS and Global Positioning System navigation systems, local oscillators for space-based Very Long Baseline Interferometry, “proper” clocks for tests of general relativity, frequency references for detection of gravitational radiation, and “traveling clocks” for worldwide time transfer.

Clocks for use in space must satisfy several restrictions and requirements, many of which are also requirements or desirable features of earth-based clocks. These requirements include:

- Limitations on mass, size and power
- Requirements for reliable long-term unattended operation
- Ability to withstand vibrational loads during launch
- Ability to tolerate varying magnetic fields
- Ability to cope with a varying thermal environment

An active atomic hydrogen maser for long-term use in space has been designed and built as part of the Smithsonian Astrophysical Observatory’s Hydrogen Maser Clock (HMC) project. HMC is a NASA-sponsored program with the goal of producing and demonstrating a space-qualified hydrogen maser with drift-removed fractional frequency stability of 10^{-15} or better in one day. The HMC maser is an evolutionary outgrowth of a two-decade long SAO program of research and development of hydrogen masers for earth and space use.^{1,2,3} The maser and its control electronics have been designed as an integrated system to cope with the requirements of space flight. We discuss below characteristics of its mechanical, magnetic and thermal design that are particularly relevant to use in space.

The HMC maser is designed for use with a variety of spacecraft, requiring only an appropriate mechanical connection and electrical interface. It was originally to be tested aboard the European Space Agency’s Eureka spacecraft, and then, following cancellation of the planned Eureka reflight, on the Russian Mir space station⁴. At present the flight portion of the HMC program has been terminated, and the flight model maser and its electronics are undergoing laboratory testing at SAO.

Mechanical and Structural Characteristics

The HMC maser’s physics unit, shown in in cross-section in figures 1 and 2, takes the general form of a cylinder 84 cm long and 43 cm in diameter. The maser’s main components are its quartz storage bulb and low-expansion resonant cavity; the titanium vacuum tank that contains the cavity; a stainless steel vacuum manifold that includes

two sorption pumps for scavenging hydrogen and two small ion pumps for removing other gases; a LiAlH_4 hydrogen source and a glass dissociator chamber for producing a beam of hydrogen atoms; electrical heaters, insulation and thermistors for temperature control; and magnetic shields and solenoids for magnetic field control. In addition, the physics unit contains electronic components that amplify the 1420 MHz maser signal from the cavity and electrically isolate the cavity from external perturbations. Separate units contain analog and digital control and monitoring electronics, the R.F. receiver that phase-locks a 100 MHz crystal oscillator to the maser signal, and a microprocessor that controls the maser's electronics and acts as an interface with the spacecraft's data and telecommand system. The masses of the major instrument elements are given in Table 1. Additional elements, whose masses depend upon the specific spacecraft used, are the bracket that mounts the maser to the spacecraft, and any additional spacecraft-specific electronics.

Element	Mass (kg)
Maser physics unit	70.7
Control and RF electronics	27.9

Structurally, the maser is supported from a circular aluminum midplane plate, which supports the maser's resonant cavity and vacuum tank on one side, and its vacuum manifold and hydrogen source on the other. The midplane plate is the main structure for mounting the maser to the spacecraft. A titanium "aft neck" tube connects one end of the vacuum tank to the midplane plate and the vacuum manifold, while a similar "forward neck" connects the other end of the vacuum tank to the maser's cylindrical outer aluminum housing. The housing, in turn, transfers the forward neck's load to the midplane plate. By means of an ANSYS finite element model with approximately 2800 nodes, the HMC maser has been designed to cope with the vibrational and accelerational loads of a Space Shuttle launch. It can withstand at least 15 g's r.m.s., in all axes acting simultaneously, in a spectrum from 20 Hz to 2 kHz. The maser's lowest mechanical resonant frequency is 46 Hz. The flight cavity and vacuum tank, which are the most critical components, have been tested to flight input vibrational levels.

Magnetic Field Control

A spacecraft in low earth orbit experiences the earth's magnetic field, with a magnitude of about 0.5 gauss and a variation over an orbit of up to ± 0.5 gauss, depending upon the spacecraft's attitude in orbit. In addition, some spacecraft create variable magnetic fields themselves, for example by magnetic torquers used for attitude control. The magnetic field within the maser's storage bulb must be maintained at a level on the order of 0.3 milligauss. To achieve frequency stability of better than $\Delta f/f < 1 \times 10^{-15}$, the temporal variation of the internal magnetic field must be less than $\Delta H < 0.8 \times 10^{-6}$ gauss. To achieve these conditions the HMC maser utilizes passive magnetic shields, internal solenoids and an active magnetic compensation system.

As shown in figure 1, the maser's resonant cavity and titanium vacuum tank are surrounded by a three-section, two-layer cylindrical printed circuit solenoid that creates the internal magnetic field of approximately 0.3 milligauss, and by four layers of concentric magnetic shields that attenuate external fields. The outermost shield extends to enclose the vacuum pump manifold and atomic hydrogen dissociator, reducing external fields that could perturb the state-selected atomic hydrogen beam. The measured shielding factor of these Hypernom shields is

$$S_{\text{passive}} = \frac{\Delta H_{\text{ext}}}{\Delta H_{\text{int}}} \approx 3.4 \times 10^5$$

The passive shields are augmented by an active magnetic compensation system. A single-axis fluxgate magnetometer sensor is mounted inside the outer shield to sense the axial field near the end of the maser. A compensation coil is wound on the outside cylindrical surface of the next shield, and a feedback circuit drives the coil to keep the field sensed by the magnetometer constant. The shielding factor for the total magnetic control system, determined by measuring the transverse ("Zeeman") resonance frequency in the oscillating maser' storage bulb, is

$$S_{\text{total}} \approx 2.8 \times 10^6$$

With this shielding factor, the expected maximum fractional frequency variation due to movement through the earth's field is on the order of $\Delta f/f \sim 2 \times 10^{-16}$.

Thermal Control System Design Features

Temperature changes of the maser's resonant cavity and storage bulb affect the maser's output frequency. To keep frequency variations below the level of 1 part in 10^{15} , the cavity temperature must be maintained constant to approximately 10^{-4} °C. The HMC maser employs several strategies to achieve this level of temperature control. To control heat flow from the vacuum tank, the maser's structure is divided into three concentric isothermal control regions. Thermal gradients are controlled by subdividing each isothermal region into multiple independently controlled zones, by mounting controlled guard heaters on heat leakage paths, by separating heaters from the primary controlled structure (the vacuum tank) and by carefully calibrating and matching thermistors and setpoint resistors to ensure that all zones of an isothermal region control at the same temperature. Radiative heat flow is reduced by means of multilayer insulation in the spaces between the regions, which are evacuated by being open to the space environment, while conductive heat flow is controlled by design of the segmented nylon rings that support the magnetic shields.

As shown in Figure 2, the innermost isothermal region, which is the titanium vacuum tank that surrounds the resonant cavity, is maintained at 50°C. The resolution of the tank control system is 1×10^{-4} degrees. To reduce thermal gradients in the tank, the three tank heaters are separate from the tank itself, one being located on the outside surface of the inner magnetic shield that is directly outside the tank and the others on the titanium neck tubes where they connect to either end of the tank.

The tank, in turn, is surrounded by an aluminum oven that is located directly over the third magnetic shield and whose temperature is maintained at 41°C. The oven region acts as a guard to control heat that flows from the tank region both radiatively from the tank surface and conductively along the magnetic shield supports and the titanium support necks. The oven region consists of three control zones located on the cylinder and end surfaces of the oven, and two zones mounted on the outer ends of the support necks.

The third isothermal region consists of the midplane plate and an outer aluminum support shell that directly surrounds the fourth magnetic shield. This zone is maintained at approximately 27°C by a control thermistor and set of heaters mounted on the midplane plate.

In addition to the thermal control zones that are integral with the maser, the system includes a controlled temperature guard station on the structure that mounts the maser to the spacecraft, to act as a first stage of isolation from the conductive environment. The entire instrument is surrounded with multilayer insulation to isolate it from the radiative environment.

The thermal control system incorporates several electronic and hardware features to achieve the high degree of thermal stability required. The digital electronic control system is based upon four 68HC11 microcontrollers, each of which can control up to five thermal zones. Each 68HC11 includes a microprocessor, an 8-bit analog-to-digital converter with eight-channel multiplexer, and timer registers that are used as pulse-width modulators (PWM) for high-efficiency switched heater power control. The vacuum tank heaters, which are closest to the maser's resonant cavity, are powered by high-frequency (~8 kHz) PWMs to avoid perturbation of the maser oscillation; the other heaters are switched at a 30 Hz rate. The thermal control program incorporates a three-mode PID (proportional, integral and differential) algorithm to eliminate proportional offset. (Differential control is included in the algorithm, but has not been found to be useful in this application.)

Components of the thermal control system have been chosen for thermal stability and low magnetic field production. Thermistors are glass-encapsulated, high stability units that have been burned in. Monitor and control thermistors for each zone are chosen to be matched. Temperature setpoint resistors are chosen to have low temperature coefficients, and are physically mounted on a temperature controlled zone within the maser for minimum temperature perturbation. Heaters are flexible printed circuits with Kapton film insulation. For each heater identical etched foil elements are overlaid with opposite current flow, to minimize magnetic field production.

The ability of the thermal control system to stabilize the tank zone temperatures in the face of external temperature changes is shown by the data of Table 2. For these measurements, which were made on the engineering model of the maser, the temperatures of the maser support structure and the forward neck guard zone were separately lowered by 2°C.

Table 2. Response of tank control zones to external temperature change

	$\Delta T(\text{Support}) = -2\text{ }^{\circ}\text{C}$	$\Delta T(\text{Fwd neck}) = -2\text{ }^{\circ}\text{C}$
$\Delta T(\text{Tank forward}):$	$-0.1 \times 10^{-4}\text{ }^{\circ}\text{C}$	$+0.2 \times 10^{-4}\text{ }^{\circ}\text{C}$
$\Delta T(\text{Tank cylinder}):$	$+1 \times 10^{-4}\text{ }^{\circ}\text{C}$	$-1 \times 10^{-4}\text{ }^{\circ}\text{C}$
$\Delta T(\text{Tank aft}):$	$+3 \times 10^{-4}\text{ }^{\circ}\text{C}$	$-2 \times 10^{-4}\text{ }^{\circ}\text{C}$

References

1. "A hydrogen maser design for ground applications." M.W. Levine, R.F.C. Vessot, E.M. Mattison, E. Blomberg, T.E. Hoffman, G. Nystrom, D.F. Graveline, R.L. Nicoll, C. Dovidio and W. Brymer, *Proc. Eighth Annual Precise Time and Time Interval Applications and Planning Meeting*, Naval Research Laboratory, Washington, D.C., pp. 249–276 (1976).
"A new generation of SAO hydrogen masers." M.W. Levine, R.F.C. Vessot, E.M. Mattison, G. Nystrom, T.E. Hoffman, and E. Blomberg, *Proc. 31st Annual Frequency Control Symposium*, USAERADCOM, Ft. Monmouth, N.J. 07703, pp. 525–534 (1977).
2. "Test of relativistic gravitation with a space-borne hydrogen maser." R.F.C. Vessot, M.W. Levine, E.M. Mattison, E.L. Blomberg, T.E. Hoffman, G.U. Nystrom, B.F. Farrell, R. Decher, P.B. Eby, C.R. Baugher, J.W. Watts, D.L. Teubr, and F.D. Wills, *Phys. Rev. Lett.* **45**, 2081 (1980).
3. "Ultra-stable clocks for use in space." E.M. Mattison, *Advances in Space Research* **9**, pp. (9)13–(9)19 (1989)
4. "High precision time transfer to test a hydrogen maser on Mir." E.M. Mattison and R.F.C. Vessot, *Proc. 27th Annual Precise Time and Time Interval Applications and Planning Meeting* (San Diego, CA, 25 Nov-1 Dec 1995) (NASA Conference Publication 3334), pp. 181-192 (1995).

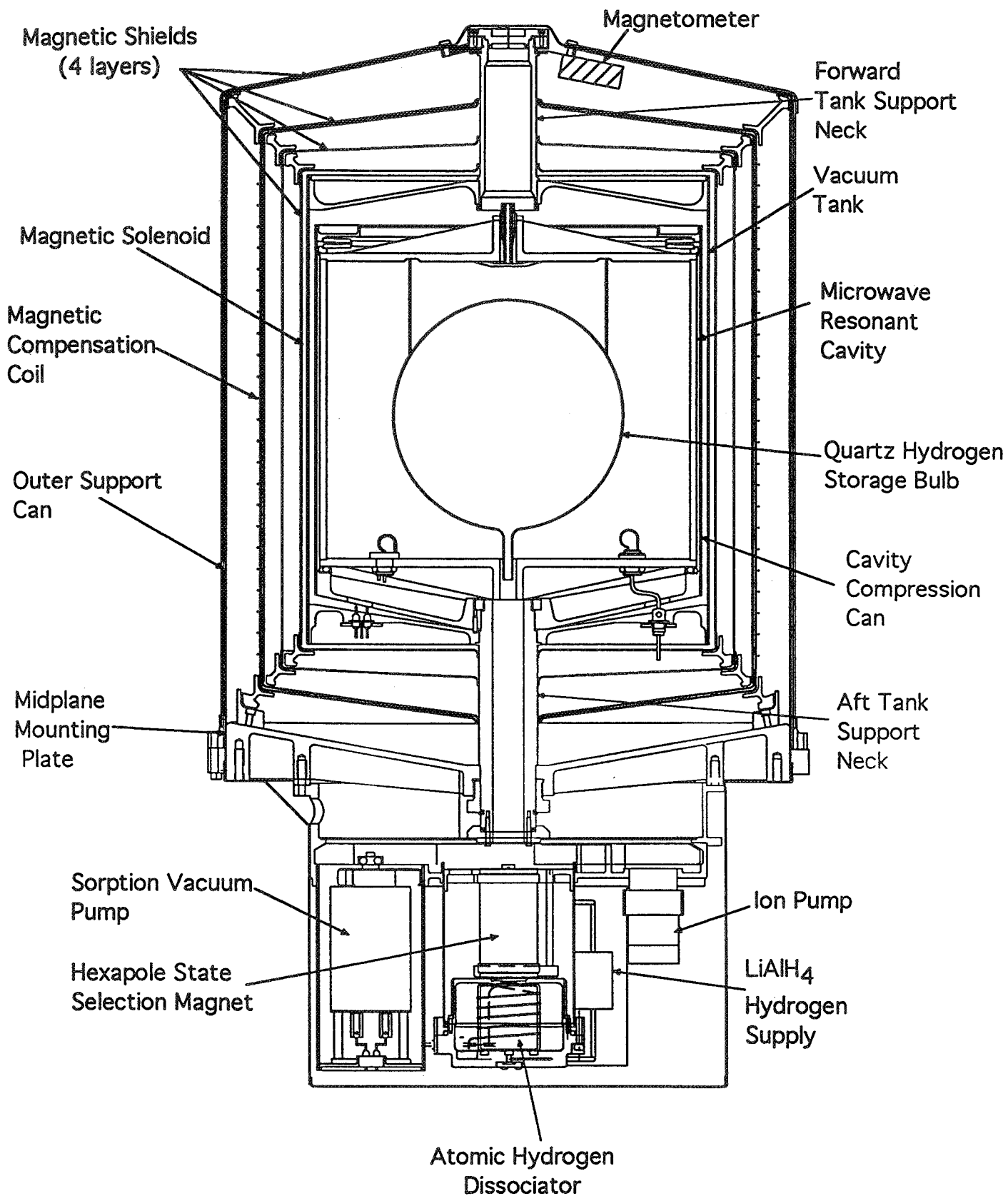


Figure 1. HMC maser - major components

40°C Zones

Forward Neck

Forward Oven

50°C Zones

Tank Forward

Oven Cylinder

Tank Cylinder

Tank Aft

Aft Oven

Aft Neck

27 °C Zone

Midplane Plate

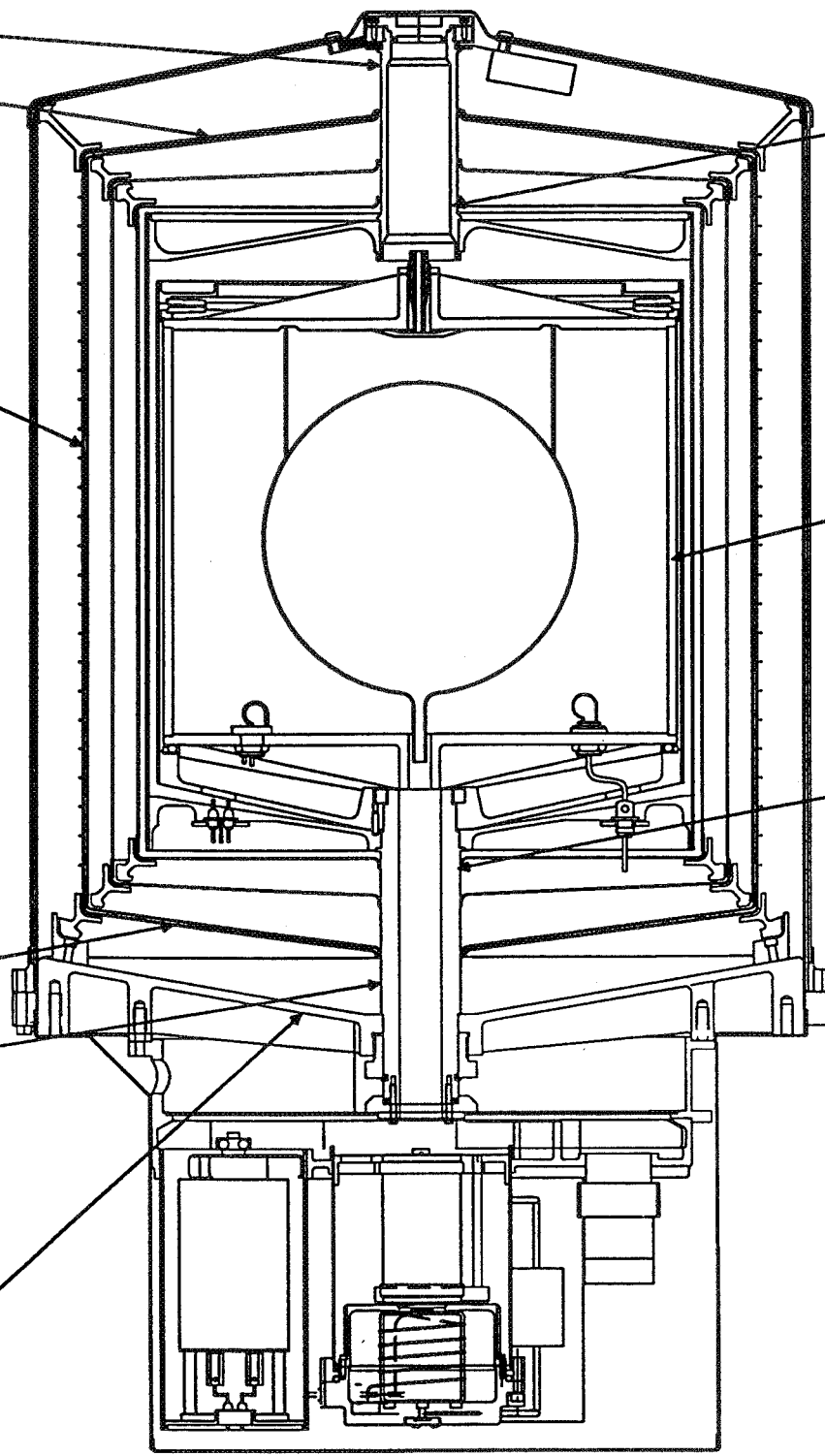


Figure 2. Thermal Control Zone Locations

Ultrastable and Ultralow Phase Noise Microwave Sapphire Oscillators

D.G. Blair, S. Chang, E.N.Ivanov, A.N. Luiten, A.G. Mann, M. Tobar, R. Woode
Department of Physics, University of Western Australia,
Nedlands, W. A. 6907, Australia.

Abstract

At the University of Western Australia we have a broad program exploiting the properties of artificial sapphire in oscillators, transducers, optics, laser stabilisation and mechanical test masses for precision experiments. Here we report progress in the development of both high stability and low phase noise microwave oscillators. We have continued to develop 12 GHz oscillators based on a whispering gallery modes of 5 cm diameter sapphire resonators operated at 5-6K. The latest resonator has been tested inside a gold-plated copper shield. It has a frequency-turning point at 5.3 K and unloaded Q of 2×10^9 . The loop oscillator frequency is locked to the resonator by active Pound stabilization and a second servo which removes amplitude modulation. The resonator temperature and incident microwave power are also servo controlled. The best oscillator stability achieved so far is characterised by an Allan standard deviation of about $2.5 \times 10^{-15} \tau^{-1/2}$ from 0.3 to 30 seconds, limited by the measurement system and servo system noise floors. At about 50 s the Allan deviation reaches a minimum of 8×10^{-16} . This represents frequency stabilization to better than 1 ppm of the resonator bandwidth. Up to 100 seconds the stability degrades as approximately 1 to $2 \times 10^{-16} \tau^{1/2}$. This medium term drift appears to be associated with mechanical instability of the resonator. Provided this problem can be solved there is scope, using high modulation index phase modulators, for achieving an Allan deviation of few times $10^{-16} \tau^{-1/2}$ in the near future.

We also report advances in low-noise microwave oscillator technology. We developed a new type of phase noise suppression technique based on the Ivanov-Tobar-Woode (ITW) phase detector. This detector is several orders of magnitude more sensitive than the conventional phase detector. At room temperature we have shown that the ITW detector can suppress the noise of a free running oscillator by at least 50 dB, whereas the conventional detector only supplies at most 25 dB suppression. A room temperature oscillator constructed using this technique exhibits a phase noise of -150 dBc/Hz @ 1 kHz offset. A liquid nitrogen temperature oscillator with a Q_e of 5×10^7 exhibits a phase noise of -165 dBc/Hz @ 1 kHz offset from a 9 GHz carrier using a conventional phase noise suppression technique. This is over 20 dB better than any other cryogenically cooled oscillator. By incorporating a liquid

nitrogen cooled ITW detector into the oscillator, we have shown that a phase noise of order -185 dBc/Hz @ 1 kHz can be achieved.

In the future we expect to achieve very high performance in an oscillator suitable for passive radiatively cooled space operation. This will use temperature compensation at 50K to achieve ultralow phase noise and ultrahigh stability comparable to the present generation of cryogenic oscillators in a small package suitable for space clock missions.

Introduction

Sapphire oscillator research at the University of Western Australia was motivated by the extreme demands of gravitational wave detection. One research program aims at ultrahigh stability oscillators based on high Q-factor cryogenically cooled sapphire dielectric resonators. Initially these were operated in superconducting cavity shields, but the latest devices should achieve comparable performance using copper shields. A second program aims at the development of ultralow phase noise oscillators based on room temperature and 77K oscillators. A third program is using cryogenically cooled sapphire Fabry-Perot cavities to create ultrahigh stability laser oscillators at 1 μ m wavelength. A fourth program combines ultralow phase noise oscillator technology with the sapphire transducer concept to create quantum limited transducers for gravitational wave detectors, and to test quantum non-demolition measurement schemes using combined microwave and mechanical resonators.

In this paper we review just the first two aspects of this work, and show how they may be combined to create space qualified clocks radiatively cooled to about 50K. In part 1 below we describe the latest developments of cryogenic ultrastable oscillators. In part 2 we describe the ultralow phase noise techniques. Finally we discuss how these may be combined to create a practical ultrahigh performance space oscillator suitable for space clock missions, local oscillators for atomic standards, and as a local oscillator for the proposed LISA laser interferometer space antenna for gravitational waves.

Part 1: Ultrastable Oscillators

Over the last four years we have been constructing high stability microwave oscillators based around large (5cm diameter) cryogenic sapphire resonators [1-13]. The resonator is used as the feedback element in a loop oscillator at 12 GHz. Locking of the oscillator frequency to the center of resonance is provided by active Pound stabilization and a second servo which removes the deleterious effects of amplitude modulation generated by the Pound stabilization phase modulator. The resonator temperature and incident microwave power are both kept under servo control to minimize fluctuations in the resonator frequency. This full set of four servos is now implemented on all oscillators under test, so that we are approaching the intrinsic stability limit of the resonator in the medium term rather than being limited, as in the past, by environmental influences acting on the oscillator components. We focus on the frequency stability results

from a comparison of the two sapphire oscillators and the noise floors of their servo systems. We report on tests on a third resonator and discuss the residual resonator drift.

The Resonator

Figure 1 shows a cross-sectional view of the cryostat insert containing the resonator. The resonator is based around a 5 cm diameter cylindrical monocrystalline sapphire element (S) supported by monolithic spindles inside an 8 cm diameter, 5 cm high metal cavity, which is nominally niobium (N). The cavity is supported on a copper post (Cu) inside a stainless steel pot (V). The pot has an indium seal (I) and is permanently evacuated through a copper crimp-off tube (C). A stainless steel support (SS) provides thermal isolation of the copper post from the liquid helium bath. Temperature (T) control to a precision of about 10^{-5} K is provided by a carbon glass thermometer and a heater mounted in good thermal contact with the copper post. The vacuum pot (V) is placed inside another cylindrical chamber (O) which can be evacuated through a vacuum pipe (P). Semirigid coaxial cables connect through the cans to the cavity probes via SMA hermetic feedthroughs (F) and isolators, circulators, couplers and detectors are mounted on a microwave electronics platform (M) attached to the copper post.

So far three nominally identical resonators have been cut from Crystal Systems "HEMEX" material; two from standard grade in 1991 (resonators 1 and 2) and one from white high purity grade in 1995 (resonator 3).

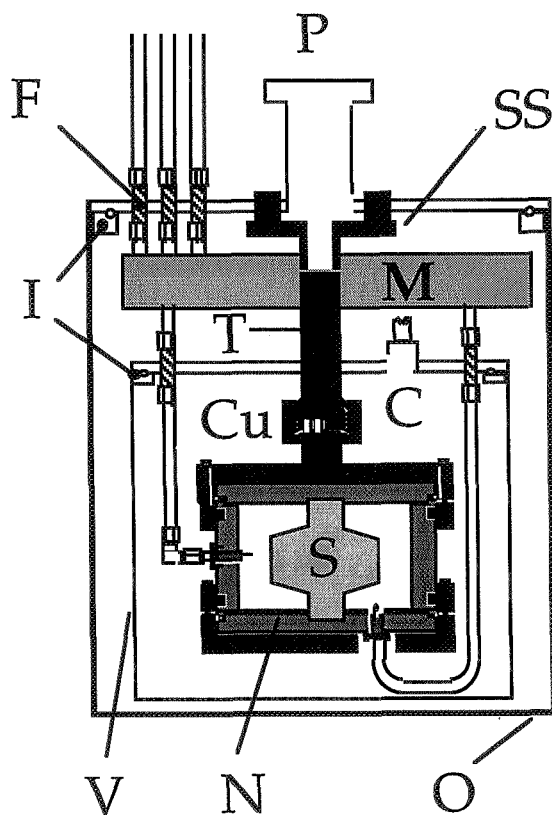


Figure 1 The sapphire resonator assembly. The letters are explained in the text.

Resonator Frequency-Temperature Dependence

Extensive details of resonators 1 and 2 have been presented elsewhere [2, 11]. The frequency-temperature behaviour of the $H_{14\ 1\ 1}$ mode, which is representative of the $H_{m\ 1\ 1}$ (quasi-TE) mode family, is shown for all three resonators in Figure 2. The high confinement of field energy to the sapphire in the $H_{14\ 1\ 1}$ mode results in the superconducting shield having a negligible influence on the mode frequency. Resonators 1 and 3 have a frequency maximum at 6K and 5.3K respectively, described by a curvature $1/f\ d^2f/dT^2 \sim 10^{-9}\ K^{-2}$. This frequency maximum considerably relaxes the temperature control requirement: with readily achievable 0.1 mK regulation, a temperature offset of 10 mK from the peak would limit the (long term) fractional frequency fluctuations to $\sim 1 \times 10^{-15}$. Unfortunately, resonator 2 has no extrema in our preferred temperature range. However, it has a minimum slope of $3 \times 10^{-10}\ K^{-1}$ at 6 K. The $E_{m\ 1\ 1}$ (quasi-TM) modes have a higher frequency-temperature turning point temperature (8-9K) which renders them less suitable for use as oscillator modes as their electrical Q-factor is lower at these higher temperatures (see below) and their curvatures are an order of magnitude higher.

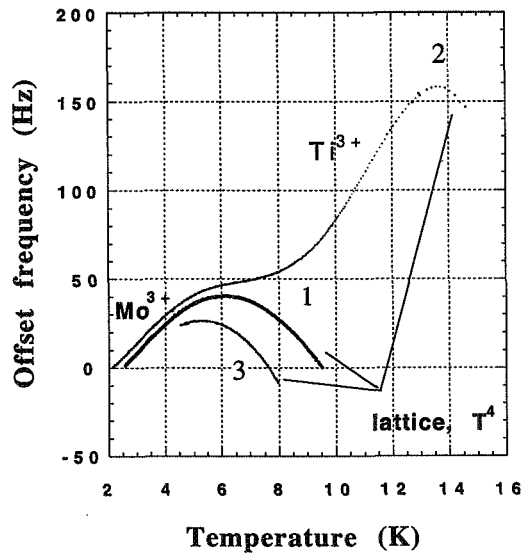


Figure 2 Mode frequency temperature dependence of $H_{14\ 1\ 1}$ mode for resonators 1, 2 and 3. The origin of the vertical scale has been adjusted for the different modes to make the diagram more clear.

The mode frequency temperature dependence of these resonators can be explained by a combination of the temperature dependence of the sapphire dielectric constant (lattice) and the ac susceptibility of

paramagnetic ions which have an electron spin resonance (ESR) above 100 GHz [11]. The temperature dependence of a given mode frequency, f , when the metallic shield has negligible influence, may be expressed as:

$$(f_0 - f) / f_0 = AT^4 + \sum C D(T)$$

where f_0 would be the frequency at absolute zero if no paramagnetic impurities were present. The first term represents the combined temperature dependence of the dielectric constant and the thermal expansion coefficient of the sapphire. A is somewhat mode dependent, being largest for $E_{m 1 1}$ modes and smallest for $H_{m 1 1}$ modes, the ratio of the two extremes being about 1.5. This mode dependence arises from the anisotropy of sapphire's thermal expansion and dielectric constant.

The second term represents the sum of the real part of the ac susceptibility, χ' , of all paramagnetic ions. The coefficient C is strongly mode dependent and proportional to the ion concentration. Below the ESR frequency of the dominant paramagnetic species mode frequency-temperature "self-compensation" can occur because the susceptibility temperature dependence has the correct sign to balance the permittivity temperature dependence. All modes in this regime feature a frequency maximum at some temperature, T_m . T_m is a very slow function of ion concentration: in the Curie law regime ($D(T) = 1/T$) it is proportional to $C^{1/5}$ while the second derivative of frequency with respect to temperature at the maxima is proportional to $C^{2/5}$ [1]. Mo^{3+} appears to be the dominant paramagnetic ion in our resonators, which is not unexpected since the sapphire is grown almost totally enclosed in a molybdenum crucible. The lowest ESR of Mo^{3+} is at 165 GHz [14], equivalent to a spin energy level spacing, $\Delta E/k$, of some 7.9 K. Since the resonator mode frequencies of interest lie well below that ESR one obtains frequency-temperature self-compensation for all microwave modes up to the limit of our test equipment (22 GHz), allowing considerable freedom of choice of operating frequency. In this situation T_m only depends on the mode type. In resonator 2 the unusual frequency-temperature dependence, which closely follows that of resonator 1 up to 6 K, but rises to a frequency maximum at 13.5 K is indicative of a second paramagnetic species in resonator 2. This ion couples well to the H modes and negligibly to the E modes and its spin resonance becomes activated only above several K. A strong candidate is Ti^{3+} , one, if not the only ion, which is highly anisotropic magnetic susceptibility in the corundum lattice and has a lowest electron spin resonance at about 1 THz [15] ($\Delta E/k \sim 54$ K). Because the period of the applied magnetic field is much less than the magnetic relaxation frequencies for these two ions the classical susceptibility should be zero. However the small Van Vleck contribution to the susceptibility is still of importance and when taken into account can explain the frequency-temperature curves very accurately. Further details of this aspect of our

work are published elsewhere [11]. Mo^{3+} and Ti^{3+} are present in all 3 resonators in varying amounts (see Table 1); resonator 2 demonstrates the effect most clearly as it has sufficient concentration to elevate T_m above 5 or 6 K.

Resonator	1	2	3
$T_m(\text{K})$	6.0	13.5	5.3
$[\text{Ti}^{3+}]$	1	1.7	2.0
$[\text{Mo}^{3+}]$	1	0.9	0.7

Table 1 T_m and concentrations [] of ions in resonators 1, 2 and 3, normalized to resonator 1, determined from the frequency-temperature dependence of the $H_{14\ 1\ 1}$ mode [11].

Spectroscopy:

In an attempt to identify the dominant paramagnetic species we have performed conventional X-band ESR spectroscopy from room temperature down to 100 K on mm size samples from a boule similar to resonator 1 and the same boule as resonator 2. A sharp resonance, whose g factor varies as the crystal is rotated, from a maximum of 4 at 90 degrees to a minimum of 2 at 0 degrees, is readily identified as Mo^{3+} [16].

Further confirmation is provided by a narrow field scan (Figure 3) which reveals its isotopic satellite peaks. The concentration, estimated by calibrating the spectrometer with a ruby sample, is about 0.3 ppm with a variation of some 50% between boules (see Table 1). Unfortunately the linewidth of Ti^{3+} is so broad that it is not easily revealed by this technique even at liquid helium temperatures. Titanium has been recently reported in HEMEX at ppm concentrations by another technique [17].

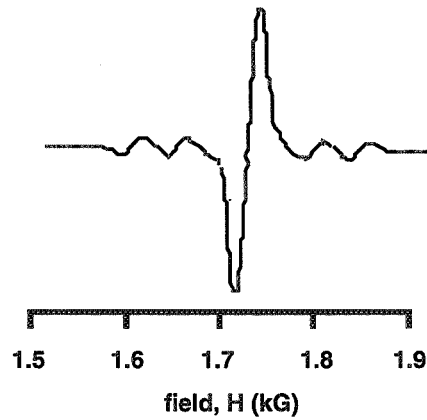


Figure 3 An ESR magnetic field scan at 90 degrees orientation and 100 K, revealing primary and two (isotopic) satellite resonances of Mo^{3+} in a Crystal Systems HEMEX sapphire sample.

Q factors

The unloaded electrical quality factor of a shielded dielectric resonator is given by:

$$Q_0^{-1} = F_c (\tan \delta + \chi'') + R_s \Gamma^{-1}$$

where F_c is the confinement factor (~ 0.95), determined by the ratio of the mode's energy stored in the dielectric to the total stored energy, $\tan \delta$ is the loss tangent of the dielectric and χ'' , the imaginary part of the ac susceptibility, represents losses due to paramagnetic impurities in the dielectric. The third term represents losses at the walls: R_s is the surface resistance and Γ is a geometry factor describing the magnetic field at the walls.

The Q as a function of temperature around 12 GHz for resonator 1 has already been reported [4] and is shown in Figure 4. The Q factor shows a steady improvement on cooling; from 2.8×10^9 at 6 K, to 4.5×10^9 at 4.2 K, to 8.3×10^9 at 1.55 K.

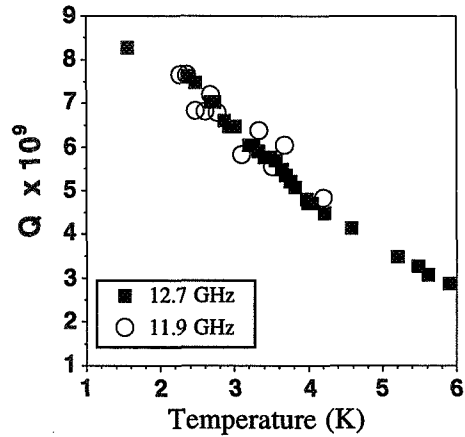


Figure 4 Unloaded Q as a function of temperature at 12.7 GHz (E18 1 1) and 11.9 GHz (H14 1 1) for resonator 1.

In Figure 5 we display the temperature dependence of Q for the H14 1 1 mode in resonator 2. The Q is again a decreasing function of temperature. Below 6 K it is somewhat lower than in resonator 1.

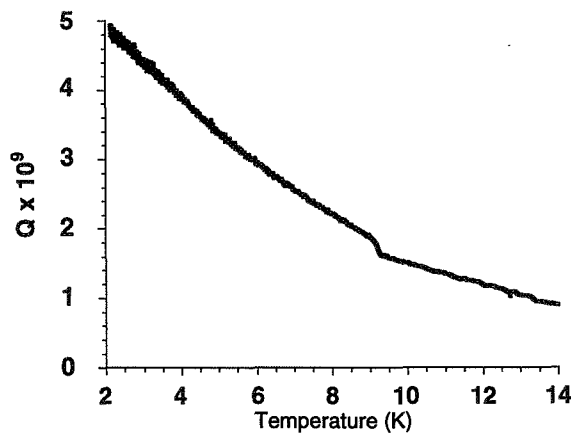


Figure 5 Unloaded Q as a function of temperature at 11.9 GHz (H14 1 1) for resonator 2.

The unloaded Q for the H14 1 1 mode in resonator 3 is about $2\text{-}2.5 \times 10^9$ at 4.3 K and 25% lower at 5.3 K. Fully coupled resonators 1 and 2 have exhibited an unloaded Q at 6K of only 1.4 to 2×10^9 , which

can be attributed to contamination of the sapphire surface. Recleaning resonators 1 in HF/nitric acid bath restored its unloaded Q to 4×10^9 at 4.2 K.

All three HEMEX resonators exhibit chromium and iron impurity levels of the order of parts per billion, as determined by measurement of the mode frequency shift (χ') as the electron spin resonances (ESRs) at 11.45 GHz (Cr^{3+}) and 12.05 GHz (Fe^{3+}) are alternately saturated [1]. Thus paramagnetic losses from the Cr^{3+} and Fe^{3+} ESRs, are expected to be negligible. The effect of the niobium walls is very small for the $H_{14} 1 1$ mode as is evident from the small change in Q across the niobium superconducting transition temperature, at 9.25 K : the geometry factor Γ is of order 10^8 [12]. Since the BCS surface resistance at X band drops by at least two orders of magnitude from 9.25 K to 6 K, we conclude that below 6 K the observed Q values are determined by the sapphire alone.

Resonator Frequency-Power Dependence

All resonators show an approximately linear dependence of mode frequency on the microwave power dissipated in the resonator, $\sim -10^{-10}$ per mW, consistent with the permittivity change due to electromagnetic radiation pressure [18] with an unloaded Q of 2×10^9 . The coefficient does not vary significantly over the $H_m 1 1$ mode family [13]. This effect would limit the long term frequency stability to the 10^{-14} level if the power level were unregulated since power fluctuations of up to 0.1 % are possible with our microwave amplifiers. To limit the influence of power instability we have implemented a power level servo.

Small multiple hysteretic effects in the power dependence of mode frequency are present in both resonators which probably don't affect the frequency stability and were not visible before the advent of extremely high resolution swept power measurements [9, 12]. In resonator 1 below 0.25 mW, one hysteresis loop and several small frequency steps are due to superconducting contamination on the surface of the sapphire, which is also seen in high resolution measurements of the temperature dependence of the electrical Q-factor [12]. In resonator 1 at 0.4 mW and resonator 2 at 1.4 mW a narrow hysteresis loop (~ 0.05 Hz high) is observed in the $H_{14} 1 1$ mode. This phenomenon, which is not related to superconductivity, may be due to saturation of an electron spin resonance and warrants further investigation.

Oscillator Configuration

The oscillator circuit is the loop oscillator configuration [9] shown in Figure 6. In transmission the sapphire dielectric resonator (SDR) is the primary frequency determining element of the free-running loop oscillator and in reflection it is the dispersive element in an active Pound-type frequency stabilisation scheme. A bandpass filter ($Q \sim 10^3$) is necessary to select the required SDR mode. The circuit losses are compensated by the gain of the GaAs FET amplifier (A) which runs in slight saturation.

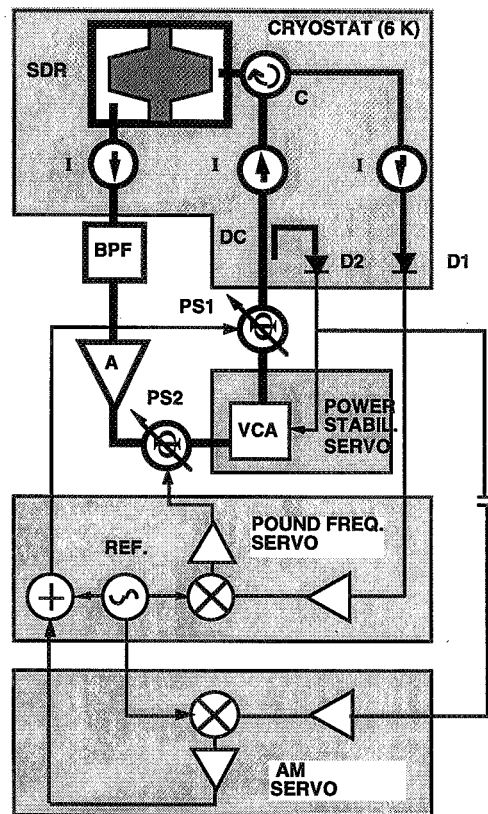


Figure 6 The loop oscillator circuit.

The loop electrical length is servo controlled by the Pound frequency stabilization scheme to lock the oscillation frequency to the center of resonance. The carrier incident on the SDR is phase modulated by a varactor diode phase shifter (PS1) driven by a crystal reference oscillator, at a rate of 80 kHz, which is much larger than the resonator bandwidth. PM-to-AM conversion upon reflection provides the discriminator signal which is recovered by synchronous detection with the reference oscillator. The SDR input coupling is set near unity for maximum carrier suppression which allows square law operation of the detector diode (D1). This maximizes the discriminator sensitivity and minimizes the sensitivity to

incidental AM generated by the phase modulator PS1 (see below). After amplification and filtering the discriminator signal is fed back to a second varactor diode phase shifter (PS2) to control the frequency of the loop oscillator. The transfer function of the Pound frequency stabilization circuit is essentially that of a single-pole integrator and has a unity gain crossover point at about 1 kHz. Power from the oscillator is extracted after the VCA and before PS1.

All of the loop oscillator components are at room temperature except for the circulator (C) and isolators (I) (typically 3 per transmission line) that are placed near the resonator to minimize frequency pulling effects. The microwave power dissipated in the resonator is typically less than 0.5 mW and is regulated by the power servo comprising detector (D2) and voltage controlled attenuator (VCA). This servo minimizes amplifier power fluctuations, the variation of insertion loss of PS2 with the error voltage from the frequency stabilization servo and the long term variation of incident power on the resonator due to the variation of transmission line attenuation with liquid helium bath level.

D1 and D2 are tunnel diode detectors placed near the resonator in the cryogenic environment. The advantage of this position is that it eliminates the room temperature dependence of detector sensitivity and improves the signal-to-noise ratio by eliminating transmission line loss (typically 5 dB) before the detectors. The power servo detector (D2) is operated at a power level corresponding to its highest sensitivity. By judicious choice of the coupling ratio of the directional coupler (DC) that provides power to D2 we can change the ratio of loop power to the fixed diode power. This allows us to trade off the noise floor of the power servo against the frequency stabilization servo noise floor in order to optimize the stability of the oscillator.

Both phase modulators have a variation of insertion loss (IL) with bias level that causes incidental amplitude modulation (AM) together with the desired phase modulation (PM). Incidental AM due to the error signal in PS2 is removed by the power servo. However the component of the AM generated by PS1 which is in phase with its PM will masquerade as a frequency offset error at the discriminator. Any variations in the level of this AM will induce frequency fluctuations. In some of our modulators we find a turning point in the variation of IL with bias. If we operate at this extremum we can eliminate the AM. This turning point has a temperature coefficient resulting in changes of the AM level (hence frequency offset) with room temperature. To reduce the variation in unwanted AM we have implemented an AM servo which keeps the phase modulator bias level at the turning point. A lock-in amplifier monitoring the power servo detector (D2) recovers the in-phase component of the AM and provides an error signal for the

bias of the phase modulator (PS1). When this fourth (AM) servo system is running the temperature sensitivity of the oscillator drops to about $1 \times 10^{-14} \text{ K}^{-1}$.

One deficiency of the loop oscillator is the feedthrough off resonance which gives a dependence of frequency on loop phase through interference of the transmitted 80 kHz sidebands with the original ones generated in PS1. The cardinal solution to this problem is locking a synthesizer chain in reflection. We locked a microwave synthesizer to resonator 3 in reflection and, without spending any time to optimize performance, beat it against oscillator 2 getting a minimum of Allan Deviation of 3×10^{-15} at 3 seconds, and medium term drift possibly because oscillator 2 was using a dc temperature bridge (Lakeshore controller, see below) instead of an ac temp. bridge.

Oscillator Stability Measurement System

To evaluate oscillator performance we constructed two nominally identical systems around resonators 1 and 2, (oscillators 1 and 2) which are mounted in separate cryostats, and performed a standard two oscillator comparison using a double heterodyne configuration. The first difference frequency of 3.75 MHz (which is due to the slight dimensional mismatch between the resonators) is mixed with a similar frequency from a HP8662A synthesizer which has less absolute instability. For time domain measurements longer than 0.4 second the synthesizer is locked to a HP5065A rubidium frequency standard and is set to generate a second difference frequency near 220 Hz which is then counted in a 300 Hz bandwidth on a HP53131A frequency counter. The noise floor of this method is inadequate to characterize our oscillators at short times (see below). Previously we had used a "zero-beat" technique to circumvent the counter noise for measurement times under a few seconds [5, 7].

Frequency Stability Measurements

The oscillator stability measured in the time domain, combining Feb 1995 frequency counter data (curves 1a and 1b) and our earlier (Aug 1993) "zero-beat" technique data (curve 3) [4] is shown in Figure 7. Also shown (point 2) is the upper bound on the stability of sapphire oscillator 1 at 1000 s obtained by beating it against a Shanghai Observatory H-maser, model H-M12A [5]. A factor of $\sqrt{2}$ has been removed from curves 1a, 1b and 3 to display the Allan deviation due to a single oscillator, assuming equal instability in each.

The noise floors of these measurements and estimates of various oscillator instabilities are discussed in the next section and shown in Figure 9. At short times ($<0.1 \text{ s}$) the Allan deviation appears to fall faster than

τ^{-1} because of the bright line structure from vibrational modes in the resonator and power line frequency modulation, as can be seen between 10 and 300 Hz in the plot of oscillator phase noise Figure 8 [10].

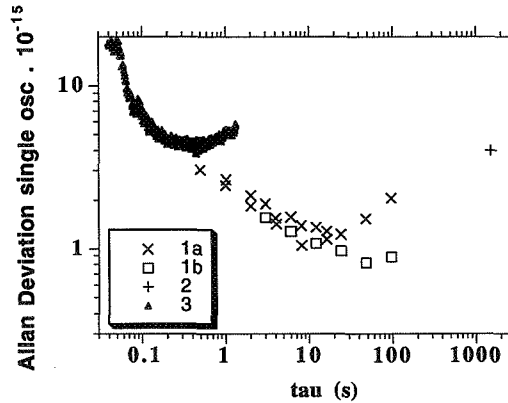


Figure 7 Allan deviation of single sapphire oscillator: 1a, 1b frequency counter data (Feb 1995); 2 sapphire osc. 1 vs H-maser (May 94) [5]; 3 "zero-beat" technique data (Aug 1993) [4].

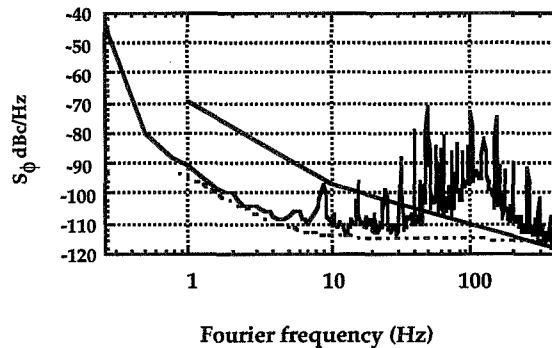


Figure 8 Single oscillator double-sided phase noise of the two oscillators. The dashed line is the measured noise floor of the frequency servo (F). The solid line shows the noise (calculated) when F is open loop. The enhancement at 100Hz is due to the small phase margin of the frequency servo.

Amplifier flicker phase noise was present in the earlier measurements [7] because at this time the oscillator output was taken from the loop immediately after the amplifier and before PS2. The measured stability below 0.1 s [7] was consistent with amplifier flicker phase noise of $S_{\phi} = 100/f$ dBc Hz⁻¹ which translates to an Allan deviation of approximately $5 \times 10^{-16}/\tau$. From 0.3 to 30 s the Allan standard deviation is about $2.5 \times 10^{-15} \tau^{-1/2}$ and limited mainly by the measurement system noise floor (see below). At about 50 s the Allan deviation reaches a minimum of 8×10^{-16} . Up to 100 seconds the stability degrades as approximately 1 to $2 \times 10^{-16} \tau^{1/2}$, which is consistent with the earlier measurement of 4×10^{-15} for oscillator 1 against a H-maser [5]. Curve 1b was obtained several days

after the initial liquid helium transfer, at an time when the after-effects of the resulting mechanical disturbance had decayed away, whilst curve 1a was obtained one to two days after the transfer.

System Noise Floors

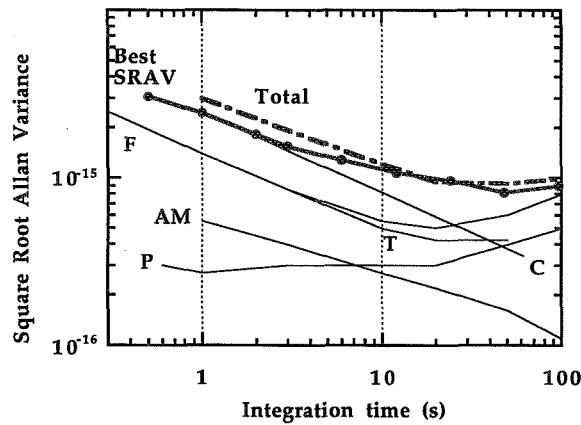


Figure 9 Frequency stability: data (Best SRAV) and noise floors; individually, of the measurement system (C) and oscillator servo systems (AM, F, P, T), and their combined total.

Before installing cryogenic detectors in oscillator 2 we measured the noise floors of the power and frequency control servo systems (for oscillator 2) by placing an identical open loop servo system in parallel with the original, including a second detector which shares half of the microwave power of the original detector. The inferred Allan deviation due to the noise floor of the frequency control servo (F) is approximately $1 \times 10^{-15} \tau^{1/2}$, as is expected for the white frequency noise of the discriminator. This is in agreement with $1.4 \times 10^{-15} \tau^{-1/2}$, calculated from the known detector sensitivity and noise floor and the -30 dB sideband to carrier power ratio of the 80 kHz modulation [10]. The Pound frequency discriminator white frequency noise floor may be described by:

$$\sigma_{y, F} = 2 \times (10^9 / Q) [0.34/J_0(m)J_1(m)] 10^{-15} \tau^{-1/2}$$

where $J_0(m)$ and $J_1(m)$ are 1st order Bessel functions and m is the 80 kHz phase modulation index. A similar calculation for the AM servo yields about $2 \times 10^{-16} \tau^{-1/2}$ while direct measurement of the noise floor yielded around $6 \times 10^{-16} \tau^{-1/2}$ [10]. The inferred Allan deviation due to the power servo (P) is essentially flat, which is consistent with operation of the detector in its $1/f$ frequency regime. By raising m

a factor of 4 (to 0.24) in both oscillators we saw no improvement in the stability of the beat note, which implies that the observed stability is limited by the measurement system noise floor (C) [10].

The requirement for temperature stability in resonator 2 is very strict as it has no turning point and only a minimum slope of 3 Hz K^{-1} . We implemented a 3 microKelvin resolution ac temperature bridge [9], initially using a room temperature reference resistor. Previously we had used a commercial dc bridge (Lake Shore DRC-91CA temperature controller) [5] which is affected by thermoelectric voltages generated in the room temperature connections to the thermometer leads. This resulted in a sensitivity to room temperature and medium term drift and was probably responsible for limiting the previously reported oscillator stability to an apparent floor near $3 \text{ to } 4 \times 10^{-15}$ [5]. The inferred Allan deviation resulting from the temperature fluctuations measured using a second (monitor) ac temperature bridge (thermometer near the resonator), when resonator 2 temperature was servoed by the ac temperature bridge is shown as “T “ in Figure 9.

Improvements to the stability limited by the electronics are possible. Abandoning resonator 2 in favor of 3, pushes the resonator temperature stability limit down to 10^{-16} to 10^{-17} . Using the optimum ($m \sim 1$ radian) index of 80 kHz modulation by using a 60 degree digital phase shifter for PS1, which would raise the modulation sidebands by about 25 dB, it would be possible to achieve a discriminator white frequency noise floor of about $10^{-16} \tau^{-1/2}$. The residual AM could be nulled via the VCA: we have achieved active nulling below 10^{-15} in bench tests. A careful design of the modulator to minimize AM may also be required, since the AM servo requires at least 25 dB more gain.

Residual Drift

The frequency drift at times longer than 20 to 50 seconds is not correlated with any of our servos, room temperature or liquid helium bath pressure. It amounts to about 10^{-13} over one day. Both oscillators are somewhat microphonic, in proportion to their measured acceleration sensitivities: $\sim 3 \times 10^{-9} \text{ g}^{-1}$ for oscillator 1 and $5 \times 10^{-10} \text{ g}^{-1}$ for oscillator 2. When a severe mechanical disturbance is applied to the dewar top-plate, oscillator 1 shifts about 10^{-10} to 10^{-9} while oscillator 2 shifts about 10^{-13} . After the disturbance a linear drift of the resonant frequency is noted. The slope of this drift decays away logarithmically to a drift rate of approximately $\sim 10^{-13}$ per day after a few days. These effects are not observed on any of the servos which implies that the offsets are changes in the resonator frequency. The

amount of offset depends on the thermal history. However we know this offset problem is soluble because in the prototype 3cm resonator, which has kept continuously at 4K for at least one year at CSIRO NML and undergone relatively few thermal cycles, the frequency offsets are only of order 10^{-13} to 10^{-14} . The best frequency stability data (curve 1b in Figure 2) we have achieved was obtained five days after the initial liquid helium transfer and the resulting mechanical after-effects had decayed away. This data also suggests that mechanical instability is responsible for the limit to the frequency stability.

Frequency pulling from nearby cavity-like modes and/or the input coupling probe have been proposed as the only viable mechanisms to account for the observed drift and acceleration sensitivity. The frequency spectrum around the $H_{14} 1 1$ operating mode is dense: in each resonator the nearest cavity-like modes are only 15 to 25 MHz away. These modes are grossly overcoupled, with loaded Q_s of 3×10^4 . We investigated the nearest one in resonator 1. One can estimate that the frequency pulling of the sapphire mode due to reactive coupling between sapphire and cavity-like modes will be attenuated by about 40 dB [19]. This is in rough agreement with the measured acceleration sensitivities: about $4 \times 10^{-7} g^{-1}$ for the cavity-like mode compared to $\sim 3 \times 10^{-9} g^{-1}$ for the $H_{14} 1 1$ mode. We are investigating the placement of absorber to reduce the influence of nearby cavity-like modes and more rigid probe structures.

Part 2. Ultralow phase noise oscillators

Recently we made a significant advancement in low-noise microwave oscillator technology. We developed a new type of phase noise suppression technique based on the Ivanov-Tobar-Woode (ITW) phase detector [20]. This detector is several orders of magnitude more sensitive than the conventional phase detector. At room temperature we have already shown that the ITW detector can suppress the noise of a free running oscillator by at least 50 dB [21], whereas the conventional detector only supplies at most 30 dB suppression [22,23]. A room temperature oscillator was constructed using this technique, and exhibited a phase noise of -150 dBc/Hz @ 1 kHz offset [21]. We are now extending this work to liquid nitrogen temperatures. So far we have built an oscillator which exhibits a phase noise of -165 dBc/Hz @ 1 kHz offset from a 9 GHz carrier using a conventional phase noise suppression technique [22]. This is over 20 dB better than any other cryogenically cooled oscillator [24,25]. The oscillator is based on a liquid nitrogen cooled sapphire dielectric resonator with a Q_e of 5×10^7 [22], and a conventional servo that suppresses the oscillators phase fluctuations [26]. Our results are summarized in figure 10. By incorporating a compact liquid nitrogen cooled ITW detector into the oscillator described in [22], we have shown that a phase noise of order -185 dBc/Hz @ 1 kHz can be achieved.

SSB Phase Noise of Room Temperature and Liquid Nitrogen Cooled Oscillators

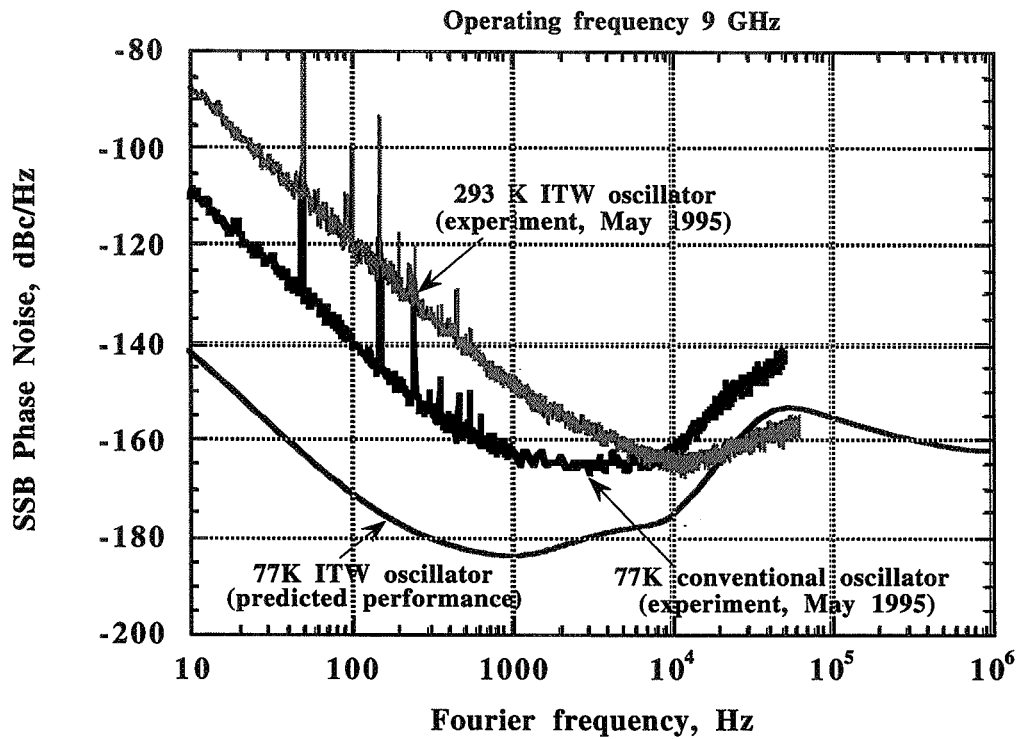


Figure 10. Measured results of a 293 K ITW microwave oscillator and a 77 K microwave oscillator experiment. From these results we can project the performance of a 77 K ITW oscillator as shown.

Principle of Operation

The general configuration of the microwave loop oscillator with phase noise suppression is shown in Figure 11.

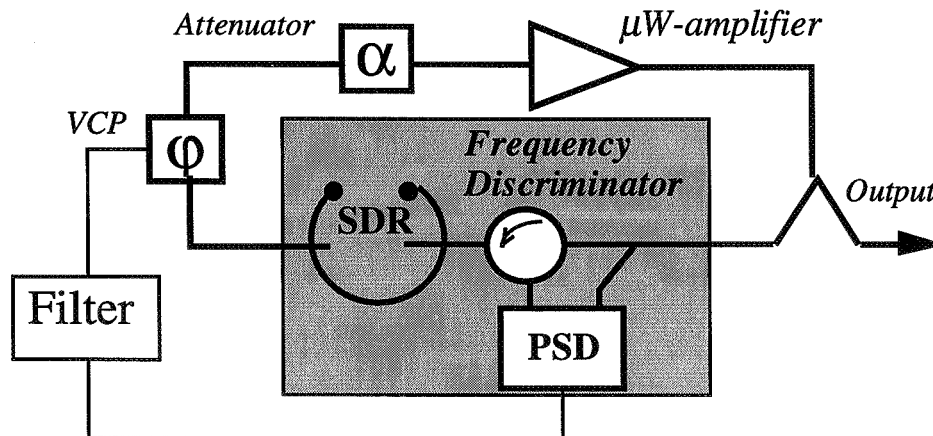


Figure 11. Microwave oscillator with phase noise suppression system

The FD comprises an SDR and a Phase Sensitive Device (PSD). The phase noise suppression is achieved by applying the filtered signal from the output of the FD to a Voltage Controlled Phase shifter (VCP) in the loop oscillator. The FD and VCP represent the sensor and actuator of the frequency control system respectively

Characterising the performance of the FD in terms of effective noise temperature allows the limit imposed on the oscillator phase noise by the finite noise temperature of the FD to be expressed as:

$$S_{\phi I}^{osc}(F) = \frac{k_B T_{FD}}{P_{inc}} \frac{(1+\beta)^4}{4\beta^2} \left\{ 1 + \left(\frac{\Delta f_{0.5}}{F} \right)^2 \right\} \quad (1)$$

where P_{inc} is the power of microwave signal incident on the SDR, k_B is the Boltzman constant, $\Delta f_{0.5}$ is the SDR loaded half bandwidth, β is the SDR equivalent coupling coefficient and T_{FD} is the FD effective noise temperature.

For a conventional FD:

$$T_{FD} = T_o + T_{PSD}, \quad (2)$$

where T_o is an ambient temperature and T_{PSD} is the PSD effective noise temperature. The latter is a function of offset frequency F and power reflected from the SDR P_{ref} . For the conventional PSD operating in X-band the T_{PSD} is of the order 10^5 K at $F = 1$ kHz and $P_{ref} \sim 0.1$ mW.

Introducing a microwave amplifier with gain $G_{AMP} \gg 1$ and low effective noise temperature into the FD allows the T_{FD} to be effectively reduced from the level determined by the PSD noise (2) to much lower limit

$$T_{FD} = T_o + T_{AMP} + T_{PSD}/G_{AMP} \approx T_o + T_{AMP}, \quad (3)$$

which is imposed by the Nyquist noise in the transmission lines and the effective noise temperature of the microwave amplifier. A minimal effective noise temperature of order $T_{FD} \sim 360$ K has been measured for an advanced FD incorporating the low-noise microwave amplifier operating in the small signal regime.

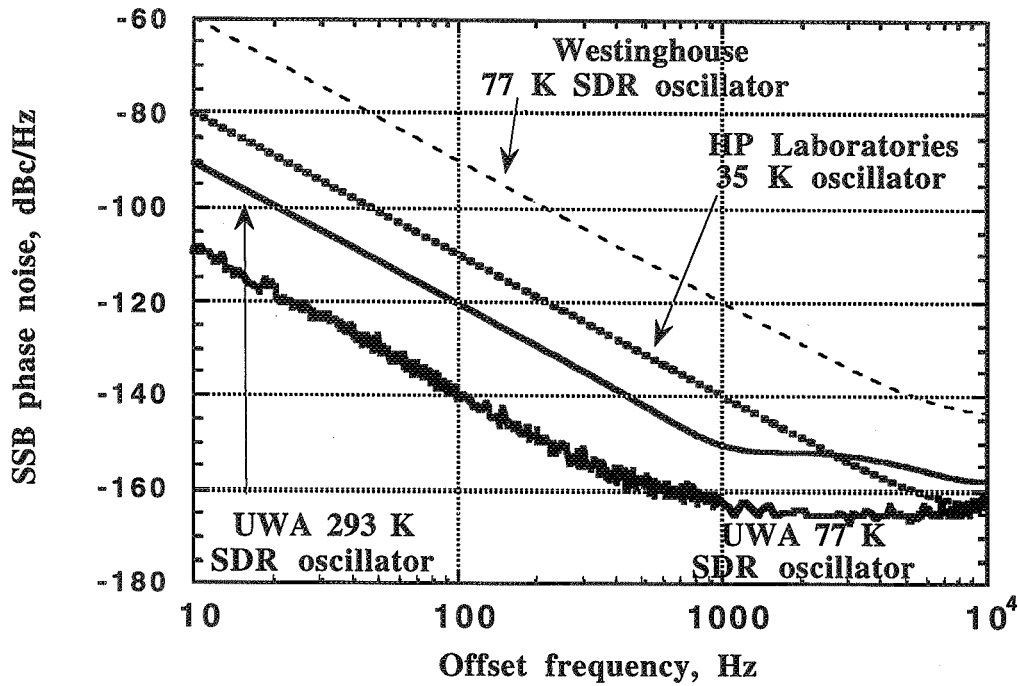


Figure 12. Comparison of phase noise spectral density of various oscillators

The phase noise of the UWA room temperature and liquid nitrogen oscillators are shown in Figure 12 in comparison with other state of the art oscillators. At low offset frequencies the UWA oscillator based on a room temperature SDR supersedes even cryogenic oscillators developed by Westinghouse and HP Laboratories.

Within the bandwidth of the high gain frequency control system (from 10 Hz to 20 kHz) the Single Side Band (SSB) phase noise of the UWA oscillator varies as

$$L_{\phi}^{osc}(F) \approx -60 - 30 \log_{10}(F), \text{ dBc/Hz} \quad (4)$$

This corresponds to $L_{\phi}^{osc}(1\text{ kHz}) \approx -150\text{ dBc/Hz}$ which is 50 dB better than a free running oscillator and represents at least 25 dB improvement in the performance of modern noncryogenic oscillators. This is also the first time when an oscillator's phase noise has been reduced below the level of its amplitude noise.

Assuming that oscillator phase noise is primarily limited by the FD finite noise temperature, phase noise as low as $S_{\phi}^{osc}(1\text{ kHz}) \sim -165\text{ dBc/Hz}$ can be expected in future room temperature oscillators operating at high power: $P_{inc} = 500\text{ mW}$.

Advanced Microwave Noise Measurement System

Accurate measurements of amplitude and phase fluctuations in passive microwave components have important implications for understanding the nature of the noise phenomena in these devices. Currently, even the best available cross-correlation noise measurement systems, developed at NIST, are not capable of measuring the extremely low level of noise exhibited by such devices as ferrite isolators (circulators), low noise voltage controlled phase shifters, attenuators etc [27,28]. Expanding on previous ideas of ultra-sensitive noise measurements [29,30], we have developed a new type of noise measurement system with a thermal noise limited sensitivity which is capable of measuring both phase and amplitude fluctuations with equal accuracy.

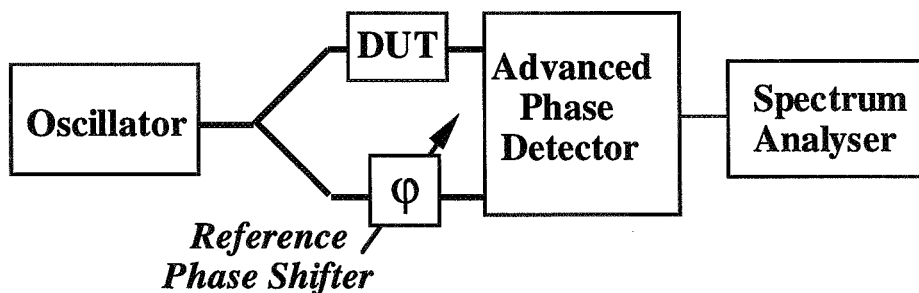


Figure 13. Simplified diagram of advanced noise measurement system

The advanced noise measurement system (NMS) is shown in Figure 13. It is similar to a conventional phase bridge which allows conversion of phase fluctuations in some arbitrary Device Under Test (DUT) into voltage noise. The distinctive feature of the NMS is an advanced phase detector (APD). The high sensitivity of the APD detector is provided by a microwave signal processing system which includes a low-noise amplifier operating in a small signal regime.

The phase noise floor of the advanced NMS due to the finite noise temperature of the APD detector is given by

$$S_{\phi}^{n/f}(F) \approx \frac{2k_B \{T_o + T_{amp}(F, P_{amp})\}}{P_{inc} L_{DUT}} \quad (5)$$

where k_B is a Boltzman constant, P_{inc} is a power incident on the DUT, L_{DUT} is an insertion loss in the DUT, T_o is an ambient temperature and T_{amp} is an effective noise temperature of the microwave amplifier. The latter is a function of the offset frequency F and a power at the amplifier input P_{amp} .

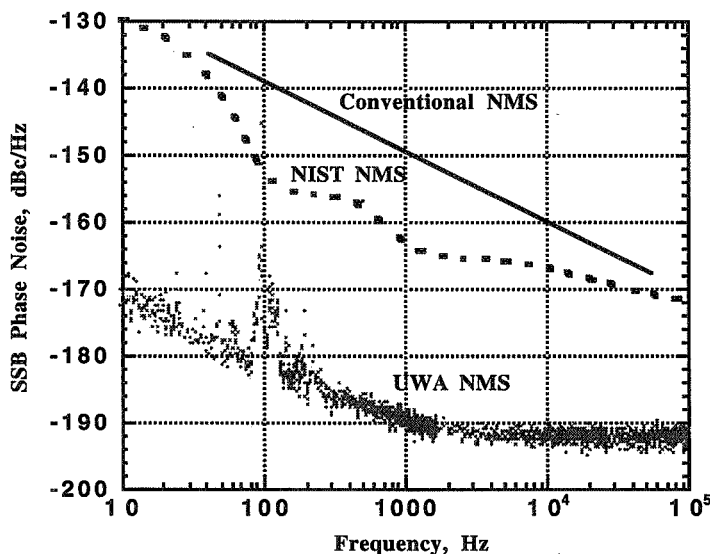


Figure 14. Phase noise floors of various measurement systems

The Single Side Band (SSB) phase noise floor of the advanced NMS, measured with input power of order 20 dBm is shown in Figure 14 in comparison with the noise floors of the standard and cross-correlation NMS.

The SSB phase noise floor of the advanced NMS is white at offset frequencies F above 1 kHz and equal to -193 dBc/Hz . At offset frequencies below 1 kHz the SSB phase noise floor follows a flicker law, reaching -173 dB/Hz at 10 Hz offset. The phase noise floor of the NMS can be further improved by increasing its input power or cooling the whole apparatus.

The advanced NMS is capable of measuring the noise in the quietest microwave components in real time. It has allowed the first experimental observations of the intrinsic phase fluctuations in the microwave isolators [20,21]. For instance, a phase noise of -186 dBc/Hz at 1 kHz offset has been measured for standard microwave isolators operating at room temperature. These results have important implications for the design of the next generation of radars and communication systems. By using these results we have already confirmed that the phase fluctuations in isolators and circulators can limit the performance of ultra-low phase noise oscillators at low offset frequencies (below 300 Hz) [20,21] .

The advanced NMS can also be used for amplitude noise measurements with sensitivity approaching the thermal noise limit [20]. This is because the APD detector is relatively immune to the pump oscillator amplitude fluctuations and enables amplitude noise measurements at a level which is much less than that of the pump oscillator.

The extremely low effective noise temperature of the APD detector allows significant improvements in the performance of many existing microwave signal processing circuits and systems. The APD detector is also ideally suitable for sensing and reducing the flicker noise in amplifiers. Using the APD detector the amplifier phase noise could be reduced to the level of the APD detector intrinsic noise which is of order -190 dB/Hz at 1 kHz offset.

Conclusions and future work

The techniques described in Part 1 and Part 2 can be combined. We have shown that a Q-factor of 10^8 may be achieved in a temperature compensated resonator at 50K . A turning point in the frequency-temperature curve, combined with a tighter locking arrangement based on the ITW technique can allow an Allan deviation $\sim 10^{-15} \tau^{-1/2}$ if the resonator temperature is controlled to $100\mu\text{K}$. We intend to develop such a clock for use in space applications. It would be compact and would avoid the need for cryogenics by being radiatively cooled. It could also be used with closed cycle refrigeration or pumped nitrogen as a local oscillator for atomic standards.

In this paper we have demonstrated that a power, phase, AM and temperature stabilized loop oscillator based on a cryogenic sapphire resonator with resonator loaded Qs of 1×10^9 can achieve an Allan standard

deviation of about $2.5 \times 10^{-15} \tau^{-1/2}$ from 0.3 to 30 s, limited by the measurement system and servo system noise floors, At about 50 s the Allan deviation reaches a minimum of 8×10^{-16} . This represents frequency stabilization to better than 1 ppm of the resonator bandwidth. However experimental results indicate that the Allen deviation is independent of the resonator Q-factor implying that the stability is not set by line splitting resolution but by perturbations to the resonator frequency. Up to 100 seconds the stability degrades as approximately 1 to $2 \times 10^{-16} \tau^{1/2}$, which is consistent with the earlier measurement of 4×10^{-15} for one oscillator against a H-maser. This medium term drift appears to be associated with mechanical instability of the resonator. Provided this problem can be solved there is scope, using high modulation index phase modulators, for achieving an Allan deviation of few times $10^{-16} \tau^{-1/2}$ in the near future.

We have also shown that sapphire resonators can be used to achieve ultralow phase noise, especially in conjunction with new phase detection techniques. Oscillator phase noise as low as -165dBc/Hz has been observed at 1kHz offset frequency. Phase noise contributions from passive components have also been measured down to almost -190dBc/Hz.

Acknowledgments

This research was supported by the Australian Research Council. The authors would like to thank the Physics Dept. Mechanical Workshop, in particular Derek Newman, for the fabrication of sapphire clock hardware.

References

- [1] A G Mann, A J Giles, D G Blair and M J Buckingham, "Ultra-stable cryogenic sapphire dielectric microwave resonators: mode frequency temperature compensation by residual paramagnetic impurities", J. Phys. D., vol 25, pp 1105-1109, 1992.
- [2] A.N. Luiten, A.G. Mann, A.J. Giles and D.G. Blair, "Ultra-Stable Sapphire Resonator-Oscillator", IEEE Trans. Instrumentation and Measurement, vol 42, 1993, pp 439-443.
- [3] A.N. Luiten, A.G. Mann and D.G. Blair, "Improved Sapphire Dielectric Resonators for Ultrastable Oscillators", Proc. 47th Annu. Freq. Control. Symp., Salt Lake City UT, 1993, pp. 757-762.
- [4] A N Luiten, A G Mann and D G Blair, "Ultra High Q Factor Cryogenic Sapphire Resonator", Electronics Letters, vol 29, 1993, 29, pp. 879-881.

- [5] A.N. Luiten, A.G. Mann, M.E. Costa and D.G. Blair, "Cryogenic Sapphire Resonator-Oscillator with Exceptional Stability: an Update", Proc. 48th Annual Frequency Control Symposium, Boston MA, 1994, pp. 441-446.
- [6] A.N. Luiten, A.G. Mann, M.E. Costa and D.G. Blair, "Power Stabilized Exceptionally High Stability Cryogenic Sapphire Resonator Oscillator", IEEE Trans. Instr. & Meas., vol. IM 44, pp , April 1995.
- [7] A.N. Luiten, A.G. Mann and D.G. Blair , "Cryogenic Sapphire Microwave Resonator-Oscillator with Exceptional Stability", Electronics Letters, vol. 30, pp. 417-419, 1994.
- [8] M.E. Costa, A.N. Luiten, M.E. Tobar and D.G. Blair "Oscillator Performance from the time evolution of relative phase", Electronics Letters, vol. 30, pp. 149-151, 1994.
- [9] AN Luiten, AG Mann, N.J. McDonald and DG Blair, "Latest results of the UWA Cryogenic Sapphire Oscillator", Proc. IEEE 49th Annual Frequency Control Symposium, San Fransisco, 1995, pp. 433-437.
- [10] A.N. Luiten, Sapphire Oscillator Secondary Frequency Standard, Ph.D. Thesis, Physics Dept., University of Western Australia, 1995, unpublished.
- [11] AN Luiten, AG Mann, and DG Blair, "Paramagnetic Susceptibility and Permittivity Measurements at Microwave Frequencies in Cryogenic Sapphire Resonators", J Phys. D., v. 29, pp. 2082-2090, 1996.
- [12] AN Luiten, AG Mann, and DG Blair, "High Resolution Measurement of the temperature dependence of the Q, Coupling and Frequency Dependence of a microwave resonator", Meas. Sci. Tech, v. 7, pp 949-953, 1996.
- [13] S Chang, A G Mann, A N Luiten and D G Blair. "Measurements of Radiation Pressure Effect in Cryogenic Sapphire Dielectric Resonators", submitted to Phys Rev Lett.
- [14] A.A. Mirzakhanyan and K.N. Kocharyan, "Temperature Dependence of the Interdoublet ESR Spectrum of Mo³⁺ Ions in Corundum at Submillimeter Wavelengths", Sov. Phys. Solid State, vol 23, 1981, pp 49-53.
- [15] R.R. Joyce and P.L. Richards, "Far-Infrared Spectra of Al₂O₃ Doped with Ti, V, and Cr", Phys. Rev., vol 179, 1969, pp 375-380.
- [16] E.G. Sharoyan, O.S. Torosyan, E.A. Markosyan and V.T. Gabrielyan, "EPR and Spin-Lattice Relaxation of Mo³⁺ Ions in Corundum", Phys. Stat. Sol. (b), vol 65, 1974, pp 773-778.

- [17] R Heidinger, "Dielectric Measurements on Sapphire for Electron Cyclotron Wave Systems", J. Nuclear Materials, 212-215, 1994, pp1101-1106.
- [18] V.B. Braginskii, V.P. Mitrafanov and V.I. Panov Systems with Small Dissipation. Chicago: University of Chicago, 1985, p 78.
- [19] M. E. Tobar, "Effects of spurious modes in cavity resonators", J. Phys. D: Appl. Phys., vol. 26, pp. 2022-2027, Nov. 1993.
- [20] Ivanov E.N., Tobar M.E., Woode R.A., 1997, An advanced noise measurement system for the study of noise phenomena in microwave components, IEEE Trans. on UFFC, 44(1).
- [21] Ivanov E.N., Tobar M.E., Woode R.A., 1996, Ultra-low noise microwave oscillator with advanced phase noise suppression system, IEEE Microwave and Guided Wave Letters, 6(9), 312-314.
- [22] Woode R.A., Tobar M.E., Ivanov E.N., Blair D.G., 1996, An ultralow noise microwave oscillator based on a High-Q liquid nitrogen cooled sapphire resonator, IEEE Trans. on UFFC, 43(5), 936-941.
- [23] Tobar M.E., Ivanov E.N., Woode R.A., Searls J.H., Mann A.G., 1995, Low noise 9 GHz sapphire resonator-oscillator with thermoelectric temperature stabilisation at 300 Kelvin, IEEE Microwave and Guided Wave Letters, 5(4), 108-110.
- [24] Tobar M.E., Blair D.G., 1994, Phase noise analysis of the sapphire loaded superconducting niobium cavity oscillator, IEEE Trans. on MTT 42(2), 344-347.
- [25] RC Taber and CA Flory, IEEE Trans. on UFFC, 1995, 42(1), pp. 111-119, (1995).
- [26] Z Galani et al, IEEE Trans. MTT 32 (1984) 1556.
- [27] F.G. Ascarrunz, E.S. Ferre and F.L. Walls, " Investigations of AM and PM noise in X-Band devices," in Proc. of 1993 IEEE Int. Freq. Control Symp., pp.303-311
- [28] W. F. Walls,"Cross-Correlation Phase Noise Measurements", in Proc. of 1992 IEEE Int. Freq. Control Symp., pp. 257-261
- [29] D. G. Santiago and G. J. Dick, "Microwave frequency discriminator with a cryogenic sapphire resonator for ultra-low phase noise", Proc. 1992 IEEE Frequency Control Symposium, pp. 176-182, June 1992.
- [30] EN Ivanov, PJ Turner and DG Blair, "Microwave signal processing system for gravitational radiation antenna", Review of Scientific Instruments, 64 (11), November 1993, p. 3191-3197

Cryo-Cooled Sapphire Oscillator for the Cassini Ka-band Experiment*

Rabi T. Wang and G. John Dick

Jet Propulsion Laboratory
California Institute of Technology
4800 Oak Grove Drive, Bldg 298
Pasadena, California 91109

ABSTRACT

We present features for an ultra-stable sapphire cryogenic oscillator which has been designed to support the Cassini Ka-band Radio Science experiment. The design of this standard is new in several respects. It is cooled by a commercial cryocooler instead of liquid cryogenics to increase operating time, and it uses a technology to adjust the temperature turn-over point to extend the upper operating temperature limit and to enable construction of multiple units with uniform operating characteristics. Objectives are 3×10^{-15} stability for measuring times $1 \text{ second} \leq \tau \leq 100 \text{ seconds}$, phase noise of -85 dBc/Hz from offset frequencies of 1 Hz to 1000 Hz at 10 GHz carrier frequency, and a one year continuous operating period.

BACKGROUND:

Cryogenic oscillators make possible the highest stability available today for short measuring times ($\tau \leq 100 \text{ seconds}$)[1,2,3]. However, they have so far proven impractical in applications outside the research environment due to their limited operating periods. Interruption of normal operation is typically required while a cryogen is replaced, the system then returning to nominal operation as temperatures settle down to a stable operating condition. It is ironic that these standards, while optimized for ultra-high stability at short operating times, must operate for periods of a year or more without interruption to be considered for many applications. This is due to the fact that frequencies generated are typically used for several purposes—e.g. radio science on one hand and scheduling on another. Cryogenic standards also represent the best promise for improved L.O. performance as required by the new generation of passive atomic standards, and continuous operation is extremely desirable in such an application.

While both superconducting and sapphire resonators can provide the very high microwave quality factors (Q's) required for ultra-stable operation, whispering-gallery sapphire resonators allow somewhat relaxed cryogenic requirements—showing Q's of 10^9 at temperatures as high as 10 K . However, the high Q makes possible high stability only if the frequency of resonator itself is stable, and for most cases this is prevented by frequency variation caused by temperature fluctuations. Compensation of the temperature-induced variation has been accomplished in sapphire resonators by paramagnetic spin[1,2] and mechanical[3] tuning effects. Such a technology can significantly relax temperature regulation requirements. For example, compensation cancels the first order temperature dependence of $3 \times 10^{-10}/\text{K}$ at 10 K , leaving a quadratic coefficient of $3.3 \times 10^{-9}/(\text{K}^2)$. Thus, for a stability of 3×10^{-15} , temperature regulation

* This work described in this paper was carried out at the Jet Propulsion Laboratory, California Institute of Technology, under a contract with the National Aeronautics and Space Administration.

must be 10 μ K for uncompensated sapphire compared to 1mK for a compensated one.

OSCILLATOR DESIGN:

Use of a cryocooler limits the achievable resonator temperatures to approximately 10K. Even though ultimate temperatures for cryocoolers are somewhat below this value, several considerations additionally limit the available cooling capability. These include thermal impedances associated with the vibration isolation system, thermal regulation stages which are required to eliminate cyclic and random temperature variations, and reduction in cryocooler performance over its operating life.

Four major aspects of the design of this compensated sapphire oscillator (CSO) include:

- *A sapphire resonator compensated for operation at a temperature of approximately 10 Kelvin.* At most temperatures from 1K to 15K, sapphire's thermal variation of frequency is partially compensated by incidental paramagnetic impurities in high-quality sapphire resonator material. This effect is strongly frequency dependent for the Cr impurities typically found, due to the 11.44 GHz zero field splitting of Cr in sapphire or ruby. Recently available sapphire resonator material without Cr but containing Mo and Ti paramagnetic impurities shows excellent Q values and no observable frequency dependence to the compensation effect at X-band frequencies due to zero field splittings that are 10 or more times higher[2]. We hope to combine these mechanisms to better control the turn-over temperature and enable the construction of multiple units with similar characteristics at a common operating temperature. The issues involved in spatially disparate compensation mechanisms were successfully dealt with in our previously reported 77K CSO[3].
- *A 2-stage commercial closed-cycle refrigerator with base temperature of 5.5 Kelvin or below.* A new cooler from Leybold/Balzers allows temperatures as low as 4.2K to be achieved for the first time without using a Joule-Thompson (J/T) expansion valve[4]. The small orifice associated with this valve can clog due to impurity condensation, and elimination of the J/T valve is expected to improve long term reliability. The new cooler, for example, can maintain 6 Kelvin at the second stage with a heat load of 1.2 watts, with 15 watts simultaneously input to the higher temperature stage.
- *A vibration isolation design sufficient to effectively eliminate cryocooler vibration.* The inherent strain sensitivity of electromagnetic resonators gives rise to an acceleration sensitivity of frequency that is typically $10^{-9}/g$ or more. Any mechanical isolation system must involve low mechanical impedances to a stable platform combined with a high mechanical impedance between the cryocooler system and the resonator system. Such a system will also have a significant thermal impedance[5].
- *A modified Pound frequency lock circuit will be used to generate the stable output frequency.* Splitting of the high-Q line by a factor of 6×10^6 was demonstrated by such a frequency-lock system in the 77K CSO[3]. Applied here, this could make possible a stability of 1×10^{-15} with a Q of only 1.7×10^8 .

CONCLUSIONS:

The first unit is currently under construction with more units scheduled to be installed in three Deep Space Network stations for the Cassini Ka-band experiment starting in the year 2000. Thermal and vibration tests of cryocooler and cryostat are presently under way. Resonator optimization and test, and first frequency stability measurements are projected by June 1997.

ACKNOWLEDGEMENTS

The authors would like to thank Lute Maleki for many valuable suggestions and discussions.

REFERENCES:

1. R. T. Wang and G. J. Dick, "Improved Performance of the Superconducting Cavity Maser At Short Measuring Times," *Proceedings of the 44th Annual Frequency Control Symposium*, pp. 89- 93, 1990.
2. A. G. Mann, A. N. Luiten, D. G. Blair, and M. J. Buckingham, "Ultra-stable Cryogenic Sapphire Dielectric Microwave Resonators," *Proceedings of the 46th Annual Frequency Control Symposium*, pp. 167-171, 1992.
3. G. J. Dick, D. G. Santiago and R. T. Wang, "Temperature-Compensated Sapphire Resonator for Ultra-Stable Oscillator capability at Temperature Above 77 K", *IEEE Transactions on Ultrasonic, Ferroelectrics and Frequency Control*, **42**, No. 5, pp. 812-819, September 1995.
4. Balzers KelCool™ 4.2GM Cryocooler from Leybold Vacuum Inc., Cryogenics Div., 8 Sagamore Park Road, Hudson, NH 03051-4914.
5. P. Boolchand, G.H. Lemon, W. J. Bresser, R. N. Enzweiler and R. Harris, "A general purpose cold finger using a vibration-free mounted He closed-cycle cryostat," *Rev. Sci. Instrum.*, **66**, No. 4, pp. 3015-3057, April 1995.

Session III

New Directions in Atomic Clocks

High-accuracy Hg^+ microwave and optical frequency standards in cryogenic linear ion traps*

D.J. Berkeland, J.D. Miller, F.C. Cruz, J.C. Bergquist, W.M. Itano, and D.J. Wineland
*National Institute of Standards and Technology, Time and Frequency Division
Boulder, CO 80303*

We discuss time and frequency standards based on laser-cooled $^{199}\text{Hg}^+$ ions confined in a cryogenic linear rf trap. In one experiment, a 40.5 GHz source, referenced to a hydrogen maser, is servoed to the ions' ground state hyperfine transition. The stability of this clock is better than 10^{-14} using 100 s Ramsey periods, and its measured accuracy is around 10^{-13} . In a second experiment under development, a strong-binding cryogenic trap will confine a single ion used for an optical frequency standard based on the narrow $S \rightarrow D$ quadrupole transition at 282 nm. The cooling laser at 194 nm and the probe laser at 282 nm are being converted to compact, efficient, solid-state systems.

Introduction

At this workshop, groups at JPL and CSIRO describe highly stable clocks that use linear rf (Paul) traps to store buffer-gas-cooled ions [1, 2]. In these traps, most of the ions lie away from the nodal line of the trap's rf electric field. For these ions, the atomic motion driven by the oscillating trap field ("micromotion") induces significant second-order Doppler (time-dilation) shifts of the average atomic transition frequency. At NIST, our goal is to develop time and frequency standards that achieve high accuracy in addition to high stability. We confine strings of laser-cooled $^{199}\text{Hg}^+$ ions in a linear rf trap such as that depicted in Fig. 1 [3, 4]. A linear trap can confine many laser-cooled ions along the rf nodal line, where Doppler shifts and AC Stark shifts are minimum [5, 6]. Furthermore, if all the ions crystallize along the rf nodal line, there is minimal heating from the trapping fields. Thus, (perturbative) cooling laser radiation can be removed during the long probe periods of the clock transition. We use $^{199}\text{Hg}^+$, which offers a microwave clock transition at 40.5 GHz and an optical clock transition at 1.06×10^{15} Hz (see Fig. 2). To first-order, both transitions are insensitive to magnetic and electric fields at zero fields. Using linear crystals of $^{199}\text{Hg}^+$ ions, we expect to reduce all systematic shifts to less than a part in 10^{16} . If the fluctuations of the atomic signal are due only to quantum statistics, then the stability of a frequency source servoed to the atomic transition is given by [7, 8]

$$\sigma_y(\tau) = \frac{1}{\omega_0 \sqrt{N} T_R} \tau^{-1/2}, \quad (1)$$

where ω_0 is the frequency of the atomic transition, N is the number of ions, T_R is the Ramsey interrogation time, and τ is the averaging time of the measurement. For the ground state hyperfine

* Supported by ONR. Work of US Government, not subject to US copyright.

transition, $\omega_0/2\pi = 40.5$ GHz. It appears feasible to use $N = 100$ ions and $T_R = 100$ s, which gives $\sigma_y(\tau) \approx 4 \times 10^{-14} \tau^{1/2}$. For the 282 nm $5d^{10}6s \ ^2S_{1/2} \rightarrow 5d^96s^2 \ ^2D_{5/2}$ electric quadrupole transition, $\omega_0/2\pi = 10^{15}$ Hz, so that using $N = 1$ and $T_R = 25$ ms gives $\sigma_y(\tau) \approx 10^{-15} \tau^{1/2}$.

We report a preliminary evaluation of a clock based on the 40.5 GHz ground state hyperfine transition in $^{199}\text{Hg}^+$. We also discuss the development of a frequency standard based on the 282 nm electric quadrupole transition. We describe the laser systems for these experiments, and the progress towards more compact solid-state systems.

Cryogenic Linear rf Trap

Figure 1 shows the linear rf trap used in the 40.5 GHz microwave clock. Two diagonally opposite rods are held at static and rf potential ground. The potential of the other two rods is $V_0 \cos(\Omega t)$, where $V_0 \approx 150$ V and $\Omega/2\pi = 8.6$ MHz. The resulting pseudopotential confines the ions radially in a well with a secular frequency $\omega/2\pi \approx 230$ kHz. To confine the ions axially, two cylindrical sections at either end of the trap are held at a potential of approximately +10 V. The resulting axial potential well has a secular frequency of $\omega/2\pi \approx 15$ kHz. The ions are laser-cooled using the 194 nm, $5d^{10}6s \ ^2S_{1/2} \rightarrow 5d^{10}6p \ ^2P_{1/2}$ electric dipole transition shown in Fig. 2. Typically, a string of approximately ten ions is confined along the axis. By minimizing the ion micromotion in all three dimensions, we assure that the laser-cooled ions lie along the rf nodal line [9].

We place the trap in a cryogenic environment to reduce problems associated with background gas. Previously, we used a linear rf trap at room-temperature with a background pressure of approximately 10^{-8} Pa [10]. At this pressure, background neutral Hg atoms cause Hg^+ loss, presumably by forming dimers with ions excited by the cooling laser. The resulting lifetime of ions in the trap was about ten minutes. At liquid helium temperatures, however, Hg and most other background gases are cryopumped onto the walls of the chamber. In this low-pressure environment, we have trapped Hg^+ ions in the presence of laser radiation without loss for periods of over ten hours. Without laser excitation, we have confined strings of approximately ten ions for several days. With this low background pressure, most pressure shifts should be negligible, although since helium is not efficiently cryopumped it may cause a pressure shift. Finally, operation at 4 K also reduces the shifts due to blackbody radiation. For the ground state hyperfine transition, at $T = 4$ K, the fractional blackbody Zeeman shift is -2×10^{-21} , and the fractional

blackbody Stark shift is -3×10^{-24} [11]. This is significantly smaller than the fractional blackbody Stark shift for neutral cesium ($1.69(4) \times 10^{-14}$ at $T = 300$ K [11]).

Laser-atom Interactions

Laser beams at 194 nm are used for both cooling and state detection. For cooling, the $^2S_{1/2}, F = 1$ to $^2P_{1/2}, F = 0$ transition is used because it is the closest to a cycling transition (see Fig. 2). The frequency of a primary laser is resonant with this transition, but can off-resonantly excite the ion into the $^2P_{1/2}, F = 1$ level, from which the ion can decay into the $^2S_{1/2}, F = 0$ level. To maintain fluorescence, a repumping laser beam, resonant with the $F = 0$ to $F = 1$ transition, is overlapped collinearly with the primary laser beam.

To determine the atomic state, the primary beam is pulsed on for a time comparable to the time necessary to pump the ions from the $^2S_{1/2}, F = 1$ to the $^2S_{1/2}, F = 0$ level (typically 10 ms). If the ion is found in the $^2S_{1/2}, F = 1$ level, it will scatter about 10^4 photons before it optically pumps into the $^2S_{1/2}, F = 0$ level. We detect and count approximately 1% of these photons. If the transition is not saturated, the number of photons scattered before the ion is optically pumped can be made nearly insensitive to laser power. Thus the signal-to-noise ratio of the state detection signal can be limited only by “quantum projection noise” [8] if the ions are monitored individually. Currently, however, the state-detection signal is simply the combined fluorescence from all the ions. As a result, we think that fluctuations in the frequency and intensity of the 194 nm radiation, and its overlap with the ions, limit our typical stability to about twice that of Eq. (1).

The $^{199}\text{Hg}^+$ ground state Zeeman structure complicates laser cooling and state detection. For any constant laser polarization and zero magnetic field, two superpositions of the $^2S_{1/2}, F = 1, m_F = 0, \pm 1$ levels are dark states. After the ion optically pumps into these states, the fluorescence vanishes. To constantly pump the ions out of the dark states, the laser field must couple each $^2S_{1/2}, F = 1, m_F = 0, \pm 1$ level to the $^2P_{1/2}, F = 0$ level. Also, each of these three couplings must have a different time dependence. We satisfy these conditions with two non-collinear laser beams. One beam passes through a photo elastic modulator whose calcite crystal axes are tilted $\pm 45^\circ$ relative to the beam polarization. The mechanical compression along one of the crystal axes is 90° out of phase with that of the other. The resulting changes in the crystal birefringence continuously cycle the laser beam’s polarization state between orthogonal circular and linear polarizations. The linear polarization of the second beam remains fixed in the plane formed by the two beams, which overlap with the ions at a 40° angle to each other.

The 40.5 GHz Microwave Clock

The measurement cycle for generating the error signal to steer the microwave frequency is as follows. First, to cool the ions, both the primary and repumping 194 nm laser beams are

pulsed on for 300 ms. Next, the repumping beam is turned off for about 90 ms, so that most of the ions are optically pumped into the $^2S_{1/2}, F = 0$ level. Both beams are then blocked during the Ramsey microwave interrogation period, which consists of two 250 ms microwave pulses separated by the free precession period T_R . Finally, the primary beam is turned on for about 10 ms while we count the number of scattered photons. This determines the ensemble average of the atomic state population. The microwave frequency is alternately stepped to either side of the central Ramsey fringe at the beginning of each measurement cycle. A digital servo using a second difference algorithm [12, 13] adjusts the average frequency to maintain a constant number of fluorescence photons during each state detection step. In this way, the microwave frequency is steered to resonance with the $F = 0$ to $F = 1, m_F = 0$ ground state hyperfine transition (a 1.5×10^{-7} T magnetic field breaks the degeneracy of the $F = 1$ states). We synthesize the microwave frequency from a low-noise crystal quartz oscillator locked to an active hydrogen maser [14].

Figure 3 shows the two-sample Allan variance $\sigma_y(\tau)$ of the average microwave frequency when it is locked to the ion resonance. For averaging times τ comparable to T_R , the calculated value of $\sigma_y(\tau)$ is erroneously small, because the digital integrator has little gain at these times. As τ increases, the integral gain grows until fluctuations in the detected ion signal dominate $\sigma_y(\tau)$. Here, $\sigma_y(\tau)$ decreases as $\tau^{1/2}$ as expected. For $T_R = 100$ s, the stability approaches the expected value of $\sigma_y(\tau) \cong 1.1 \times 10^{-13} \tau^{-1/2}$ for $\tau \gg T_R$.

For each run in which the microwave frequency is continuously servoed to the atomic transition, we average the recorded frequency. Figure 4 is a summary of the fractional deviation of the average frequencies for several runs made over nine days. The error bars are not uniform because during this time, N , T_R , the total run time τ , and other parameters were deliberately varied. The normalized value of chi-squared for this data set is 2.5, which we do not yet understand. Although the evaluation is not yet complete, the scatter in these data indicates that our fractional accuracy is probably better than 10^{-13} .

We have begun to search for systematic effects that could shift the frequency of the microwave transition. Table 1 summarizes the present status of our measurements. We measure the average ion temperature by monitoring the width of the 282 nm transition after the cooling beams have been blocked for time T_R . This determines the second-order Doppler shift and the AC Stark shift due to the trap's rf electric fields. The width also gives an upper bound on the heating rate of the ion due to background gas (presumably helium) collisions, which is approximately proportional to the helium density n_{He} . The measured shift from helium at pressure P_{He} at room

temperature is $4 \times 10^{-11} P_{He}$ (where P_{He} is in Pa) [15], or $1.6 \times 10^{-31} n_{He}$ (where n_{He} is in m^{-3}). Assuming that this shift has the same dependence on density at 4 K, the upper bound on density $n_{He} = 1.6 \times 10^{12} \text{ m}^{-3}$ implies an upper bound on the fractional frequency shift of approximately 3×10^{-19} . We do not measure the temperature after each run in the present experiments. The uncertainty in the quadratic Zeeman shift is due to fluctuations and inhomogeneities in the magnetic field. We determine the average magnetic field at the site of the ions from the frequencies of the Zeeman components of the hyperfine transition. The width of these components gives an upper bound on the field inhomogeneity since the ion positions are fixed. Currents flowing in the trap electrodes may cause an rf Zeeman shift; we have searched for this shift by varying the rf power delivered to the trap. Microwave chirp may occur as the 40.5 GHz radiation is switched on and off, and is measured by varying the Ramsey precession time. Finally, we calculate shifts due to blackbody radiation [11] for ions in a 10 K environment. (We think that the background temperature is greater than 4 K due to the quartz windows in the system and power delivered to the trap.)

Optical Frequency Standard

A frequency standard with high stability can be based on the $^{199}\text{Hg}^+$ 282 nm electric quadrupole transition, which has a natural linewidth of 1.7 Hz [16]. A laser stabilized to less than 20 Hz over one minute has been locked to this transition in a single ion confined in a room-temperature rf trap [17]. With improvements to the high-finesse cavities to which the laser is locked, we expect to reduce the laser linewidth to about 1 Hz over one minute. We are developing a second cryogenic system that will house a trap for this experiment.

All Solid-state Laser Systems

To make the 194 nm and 282 nm radiation sources more compact and reliable, we are converting them to an all-solid-state design. The system we currently use to generate 194 nm light starts with radiation from a single-frequency argon-ion (Ar^+) laser at 515 nm. About 500 mW is frequency-doubled in a cavity containing a BBO crystal to produce 257 nm radiation. About 5.5 W pumps a Ti:sapphire laser to make 500 mW of 792 nm radiation. The 792 nm and 257 nm beams are each enhanced in separate optical cavities, whose foci overlap in a second BBO crystal. This creates about 100 μW of 194 nm radiation through sum-frequency mixing. The Ti:sapphire laser can be replaced by an injection-locked diode laser that produces over 500 mW of 792 nm radiation [18, 19]. The Ar^+ laser will be replaced by a 1 W single-frequency, diode-pumped, frequency-doubled Yb:YAG laser at 1.029 μm [20]. Since the doubling efficiency in KNbO_3 can be 50% [21], we expect to generate about 500 mW of 515 nm radiation.

The present system for generating 282 nm radiation consists of an Ar^+ laser pumping a dye

laser that produces 500 mW of 563 nm radiation. The 563 nm light is frequency-doubled by single-passing it through a 90° phase-matched AD*P crystal to give up to 100 μW of 282 nm radiation. To convert this to a solid-state system, the dye laser and pump laser will be replaced by a diode-pumped Nd:FAP laser at 1.126 μm. Approximately 100 mW of single-frequency radiation from the Nd:FAP laser has been frequency-doubled in KNbO₃ to produce 7 mW of 563 nm radiation. The light at 563 nm can be frequency-doubled as before to generate about 2 μW of 282 nm radiation. When the light is focused to about 25 μm and there is no broadening, less than 1 pW of 282 nm light will saturate the quadrupole transition.

Summary

We have locked a synthesizer to the 40.5 GHz transition in laser-cooled strings of ¹⁹⁹Hg⁺ ions in a linear cryogenic rf trap. With Ramsey periods of up to 100 s, this clock has demonstrated stabilities of better than 10⁻¹⁴. Preliminary investigations of systematic frequency shifts indicate an accuracy of better than 10⁻¹³. In the future, we plan to use Ramsey times of 100 s and a smaller, more tightly confining trap that stores up to 100 ions. We will soon resume work on a cryogenic 282 nm optical frequency standard, whose potential stability is $\sigma_y(\tau) \approx 10^{-15} \tau^{1/2}$. Finally, we are converting our laser systems to an all-solid-state design, which should allow longer continuous running times.

References

- 1 R.L. Tjoelker, J.D. Prestage, and L. Maleki, in Proc. of the Fifth Symp. Freq. Standards and Metrology, ed. James C. Bergquist, 33 (World Scientific, 1996).
- 2 Peter T.H. Fisk, Mathew J. Sellars, Malcolm A. Lawn, and Colin Coles, in Proc. of the Fifth Symp. Freq. Standards and Metrology, ed. James C. Bergquist, 27 (World Scientific, 1996).
- 3 M.E. Poitzsch, J.C. Bergquist, W.M. Itano, and D. J. Wineland, *Rev. Sci. Instrum.* **67**, 129 (1996).
- 4 J.D. Miller, D.J. Berkeland, F.C. Cruz, J.C. Bergquist, W.M. Itano, and D.J. Wineland, in 1996 IEEE International Frequency Control Symposium, 1086 (1996)
- 5 H.G. Dehmelt, in Frequency Standards and Metrology, ed. A. DeMarchi. Berlin: Springer, 286 (1989).
- 6 J.D. Prestage, G.J. Dick, and L. Maleki, *J. Appl. Phys.* **66**, 1013 (1989).
- 7 D.J. Wineland, Wayne M. Itano, J.C. Bergquist, J.J. Bollinger, F. Diedrich, and S.L. Gilbert, Proc. 4th Symposium on Freq. Standards and Metrology, Ancona, Italy, Sept. 1988; ed. A. Demarchi (Springer Verlag, Heidelberg).
- 8 W.M. Itano, J.C. Bergquist, J.J. Bollinger, J.M. Gilligan, D.J. Heinzen, F.L. Moore, M.G. Raizen, and D.J. Wineland, *Phys. Rev. A* **47**, 3554 (1993).
- 9 D.J. Berkeland, J.D. Miller, J.C. Bergquist, W.M. Itano, and D.J. Wineland, (unpublished).
- 10 M.G. Raizen, J.M. Gilligan, J.C. Bergquist, W.M. Itano, and D.J. Wineland, *Phys. Rev. A* **45**, 6493 (1992).
- 11 Wayne M. Itano, L.L. Lewis, and D.J. Wineland, *Phys. Rev. A* **25**, 1233 (1982).
- 12 Leonard S. Cutler, Robing P. Giffard, and Michael D. McGuire, Proc. 13th Ann. PTTI Meeting, 563 (1981).
- 13 J.D. Prestage, G.J. Dick, and L. Maleki, Proc. 19th Ann. PTTI Meeting, 285 (1987).
- 14 C.W. Nelson, F.L. Walls, F.G. Ascarrunz, and P.A. Pond, in 1992 IEEE Frequency Control Symposium, 64 (1992)
- 15 L.S. Cutler, R.P. Giffard, and M.D. McGuire, in Proc. 37th Ann. Symp. Freq. Contr., 32 (1983).
- 16 J.C. Bergquist, F. Diedrich, Wayne M. Itano, and D.J. Wineland, in Laser Spectroscopy IX, ed. by M.S. Feld, J.E. Thomas, and A. Mooradian, 274 (Academic, San Diego, 1989).
- 17 J.C. Bergquist, W.M. Itano, and D.J. Wineland, Frontiers in Laser Spectroscopy, 357 (1994).
- 18 D.J. Berkeland, F.C. Cruz, and J.C. Bergquist, submitted to *Appl. Opt.*
- 19 F.C. Cruz, M. Rauner, J.H. Marquardt, L. Hollberg, and J.C. Bergquist, in Proc. of the Fifth Symp. Freq. Standards and Metrology, ed. James C. Bergquist, 511 (World Scientific, 1996).
- 20 P. Lacovara, H.K. Choi, C.A. Wang, R.L. Aggarwal, and T.Y. Fan, *Opt. Lett.* **16**, 1089 (1991).
- 21 Z.Y. Ou, S.F. Pereira, E.S. Polzik, and H.J. Kimble, *Opt. Lett.* **17**, 640 (1992).

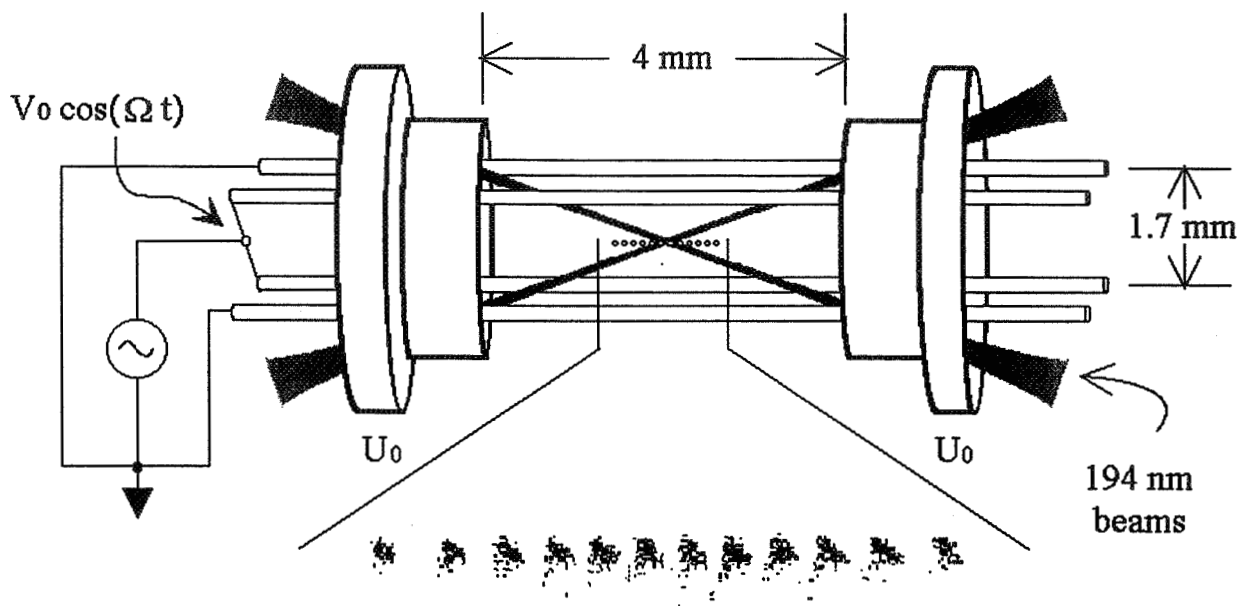


Figure 1: Linear rf trap, and an image of a string of twelve ions. The ions are spaced approximately $10 \mu\text{m}$ apart. The spatial extent of the ions is exaggerated for clarity; in reality the laser beams overlap all of the ions.

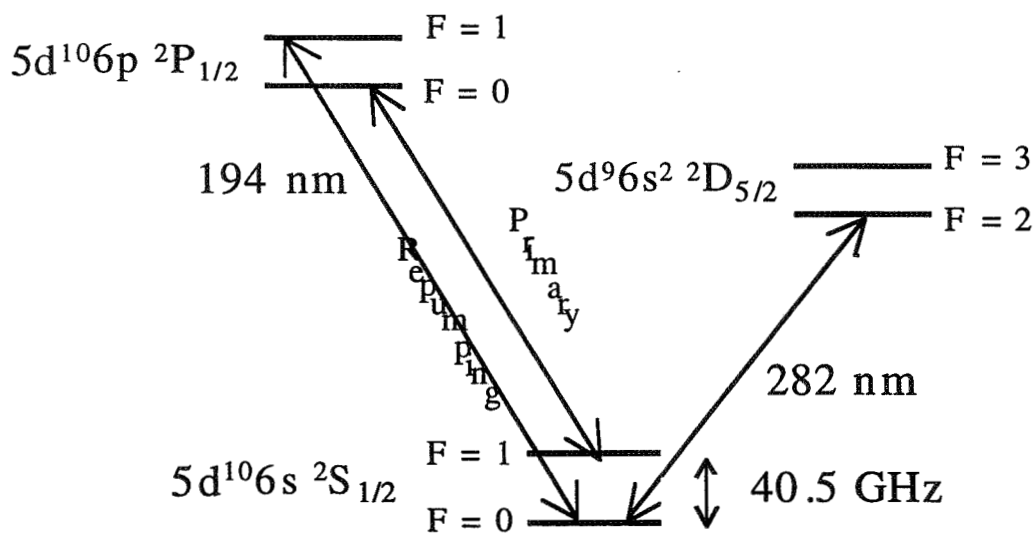


Figure 2: Partial energy diagram of $^{199}\text{Hg}^+$. The 70 MHz wide 194 nm transition is used for laser cooling and detection. The 40.5 GHz and 282 nm transitions are the clock transitions.

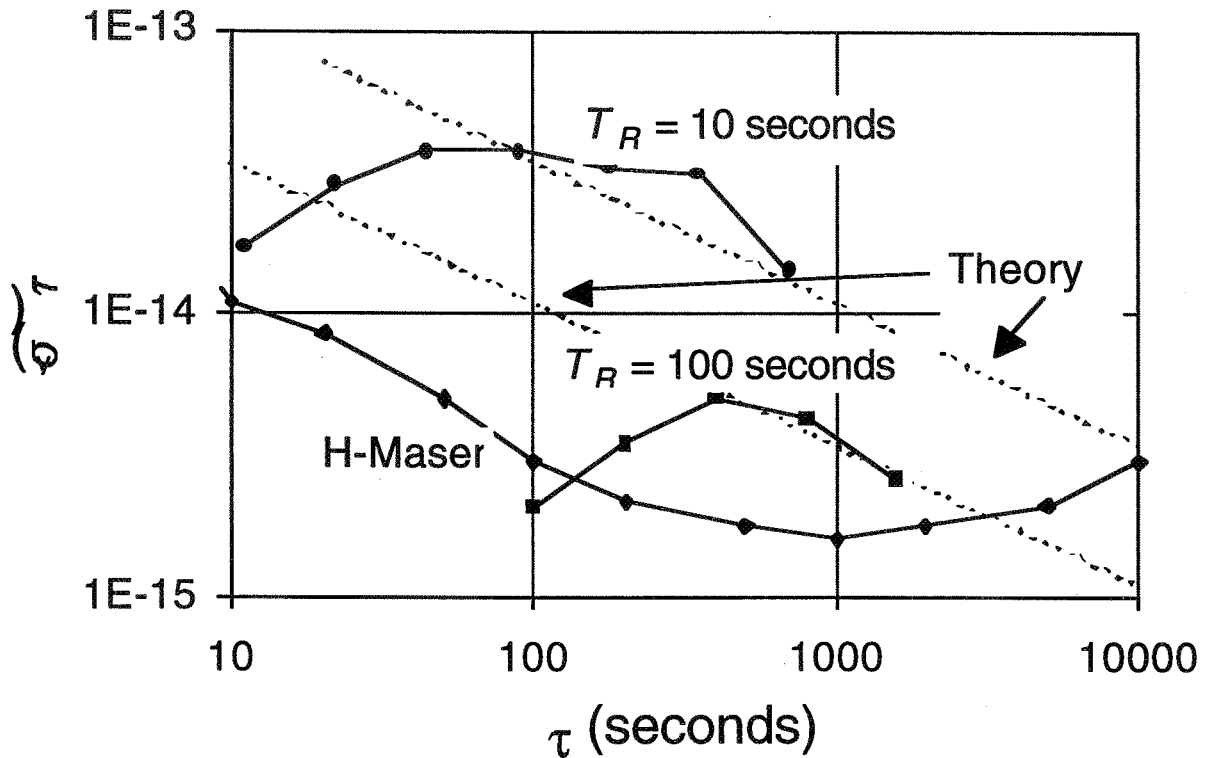


Figure 3: Stability plots for the 40.5 GHz microwave clock, using $N = 13$ ions, and both $T_R = 10$ s and $T_R = 100$ s. Also shown are the theoretically expected stabilities from Eq. (1), and the stability of the hydrogen maser reference clock.

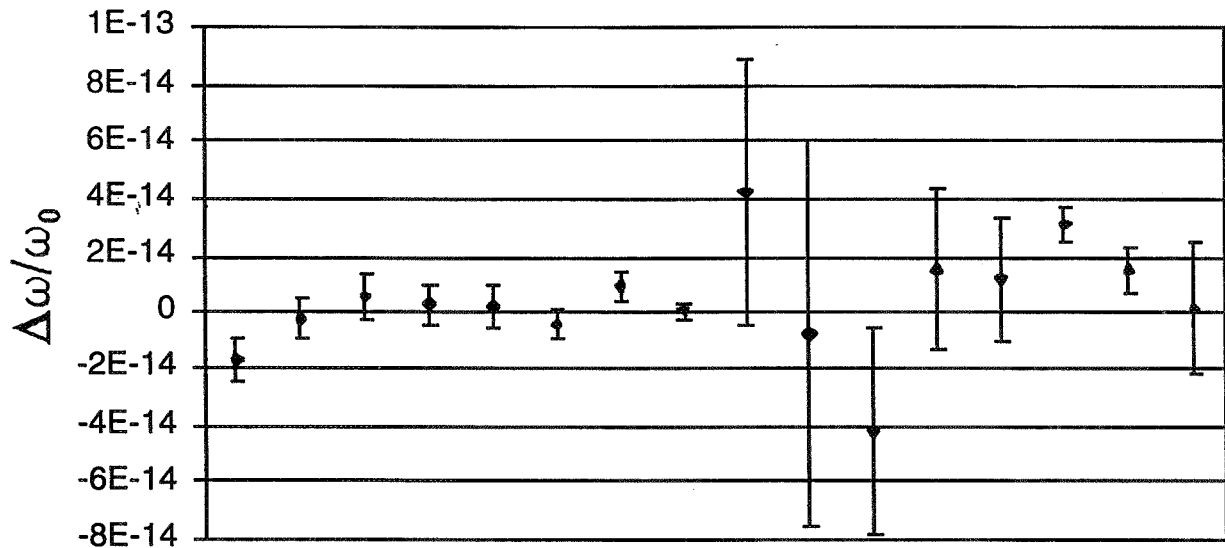


Figure 4: Summary of average frequencies over a nine-day period. The frequencies are plotted in the order in which they were measured, but the spacing of the data points does not otherwise correspond to the time in which the data were taken.

Shift	Scaling	Uncertainty
Second-order Doppler	$-\langle V^2/c^2 \rangle$	1.6×10^{-17}
Quadratic Zeeman (static)	$+\langle B^2 \rangle$	3×10^{-15}
Quadratic Zeeman (rf)	$+\langle B^2 \rangle$	3×10^{-14}
<hr style="border-top: 1px dashed black;"/>		
AC Stark (rf)	$-\langle E_{rf}^2 \rangle$	3×10^{-18}
Microwave chirp	$1/T_R$	3×10^{-15}
He pressure shift	n_{He}	3×10^{-19}
Blackbody AC Zeeman ($T = 10$ K)	$-T^2$	1.4×10^{-20}
Blackbody AC Stark ($T = 10$ K)	$-T^4$	1.2×10^{-22}

Table 1: Measured uncertainties in the microwave clock. Effects below the dashed line are expected to be negligible compared to those above the dashed line.

Progress on the CSIRO Trapped Ytterbium Ion Clocks

Peter T. H. Fisk, Malcolm A. Lawn
Colin Coles

National Measurement Laboratory
CSIRO Division of Telecommunications and Industrial Physics
PO Box 218
Sydney, 2070, Australia
email Peter.Fisk@tip.csiro.au

1 Introduction

We have previously reported [1,2] some aspects of the performance of a prototype frequency standard (IT-1) based on the 12.6 GHz ground state hyperfine 'clock' transition in $^{171}\text{Yb}^+$ ions (fig. 1) confined in a linear Paul trap.

More recently, we have constructed a second prototype standard (IT-2), similar to IT-1 but with significant improvements in magnetic shielding and optical detection efficiency. A comparison [3] of the measured clock transition frequencies of the two traps under conditions where they contain different numbers of ions, and consequently ion clouds of different sizes, provided an early test of a model which gives values for the differing second-order Doppler shifts in the two traps. In this paper we summarise some further results [4] of comparisons between the two trapped ion frequency standards.

2 Experimental

The trapped ion frequency standards discussed in this paper operate by locking [1,2] a local oscillator microwave signal generated from a sapphire-loaded superconducting dielectric resonator oscillator (DRO) [5] to the 12.6 GHz ground state hyperfine transition in $^{171}\text{Yb}^+$ ions (fig. 1) confined in a linear Paul trap. The electrode structure of the ion trap systems IT-1 and IT-2 has been described previously [1,2,3], and is shown in figure 2.

Helium at a pressure of approximately 10^{-4} Pa was introduced into both ion trap vacuum systems through heated quartz membranes to dissipate the energy absorbed by the ion clouds from the trapping RF fields, which would otherwise result in the ions ‘boiling’ out of the trap. The resulting temperature of the ion clouds in both systems was approximately 380 K.

A frequency-doubled titanium-sapphire laser generating 369.4 nm radiation was used to probe the populations of the $^{171}\text{Yb}^+$ ground state hyperfine levels following the microwave interrogation pulse sequence. The laser system was common to both ion trap systems, and the microwave signals fed to each ion trap system were independently tuneable, but generated from a common DRO [4].

The microwave interrogation sequence consisted of a pair of $\pi/2$ pulses of 400 ms duration, with pulse centres separated by 25 s, yielding Ramsey fringes with a period of 40 mHz. The cycle time of the systems was such that one comparison between the local oscillator frequency and the frequency of the central Ramsey fringe was made on both ion traps every 72 s. During each measurement cycle the Larmor frequency in each trap was obtained by measuring the frequency separation of the $M_F=0 \rightarrow 0$ and $M_F=0 \rightarrow -1$ Zeeman components of the 12.6 GHz hyperfine transition [1,2].

3. Stability performance

Typical operating parameters for the two ion traps are shown in table 1.

The frequency stability of the ion trap systems, characterised by the Allan deviation $\sigma_y(\tau)$, is shown in fig. 3.

For integrating times between 72 s and approximately 10^4 s the more recently constructed ion trap system IT-2 exhibits a white noise-limited performance $\sigma_y(\tau) = 5 \times 10^{-14} \tau^{-1/2}$. Beyond 10^4 s the stability performance is probably limited by instability of the He buffer gas pressure, which was not actively controlled.

The stability performance of IT-1 is, as expected, poorer than that of IT-2, mainly as a result of less effective magnetic shielding and larger residual magnetic inhomogeneity in the region of the ion cloud.

The expected performance of the trapped ion standards system is given by [7]

$$\sigma_y(\tau) = \frac{\delta f}{\pi f_0} \left(\frac{N}{S} \right) \sqrt{\frac{T_c}{\tau}} \quad (1)$$

where δf is the width of the central Ramsey fringe, f_0 is the frequency of the clock transition, N/S is the single-measurement cycle noise-to-signal ratio and T_c is the measurement cycle time. If we assume that the noise in the signal arises solely from the shot noise associated with the process of measuring the probability of individual ions absorbing a microwave photon, equation 1 yields the performance limit of the frequency standard. For the conditions under which the data shown in fig. 3 was obtained, we calculate a performance limit $\sigma_y(\tau) = 1.8 \times 10^{-14} \tau^{-1/2}$

For $\tau=100$ s, the in-quadrature combination of the shot noise contribution to the Allan deviation (calculated using equation 1) and the measured LO performance, $\sigma_y(100 \text{ s}) = 2.5 \times 10^{-15}$, predicts a limiting Allan deviation $\sigma_y(100 \text{ s}) = 3.3 \times 10^{-15}$ for IT-2 with respect to the LO. This is in reasonable agreement with the observed performance of IT-2, $\sigma_y(100 \text{ s}) = 5 \times 10^{-15}$. It is possible that additional frequency instability is being introduced by short-term jitter in the frequency of the 369.5 nm laser, or frequency down-conversion of phase noise in the 12.6 GHz signal occurring over the time scales of the interrogating $\pi/2$ pulses.

4. Accuracy

The measurement and calculation of the frequency offsets affecting the trapped $^{171}\text{Yb}^+$ ion frequency standards have been discussed in detail elsewhere [3,4], and are summarised in fig. 4.

We have made a number of measurements of the $^{171}\text{Yb}^+$ clock frequency over a period of more than 12 months. The results, after correction for the offsets listed in fig. 4, are shown in fig. 5. Up to the date MJD 50139, the $^{171}\text{Yb}^+$ clock frequencies are corrected for the variation (averaged over

60 days), with respect to the SI second, of the frequency of the hydrogen maser used as the local reference.

On three occasions the $^{171}\text{Yb}^+$ clock frequency was measured on IT-1 and IT-2 either simultaneously, or on the same day. In each case, the agreement between the two frequencies is much better than 1 part in 10^{13} . During the period over which the data shown in fig. 5 were obtained, both ion trap systems were dismantled and reassembled several times for various reasons, apparently without substantially affecting the corrected clock frequencies.

Much of the variation in the corrected clock frequencies since MJD 48950 can be explained by the day-to-day variation in the H maser frequency of a few parts in 10^{14} , resulting from non-optimal auto-tuning of the masers NML-Maser 2 and NML-Maser 1. We cannot find evidence of a maser frequency variation of magnitude sufficient to explain the outlying data points obtained on MJD 49826. The reason for these outlying points is not known, although the two trap systems were still in good agreement on that date.

The uncertainties in the individual clock frequency determinations represented by the error bars on fig. 5 are largely statistical. The principal systematic errors in the clock frequency determinations will result from any inaccuracies in the model of the ion cloud used to calculate the magnitude of the second-order Doppler shift.

It is evident that despite the significantly different corrections for the second order Doppler shift applied to the raw frequency from each ion trap, the two final frequency values agree to within 4 parts in 10^{14} , although the uncertainties in the two values are somewhat larger.

Discarding the MJD 49826 data, the mean of the $^{171}\text{Yb}^+$ clock frequency measurements shown in fig. 5 is 12 642 812 118.4664 Hz, with a standard deviation of 0.00055 Hz, and a calculated statistical uncertainty of ± 1.4 mHz in each determination. Consequently, we estimate our total uncertainty in Hz as $((0.0014 \text{ (stat)})^2 + (0.0015 \text{ (syst)})^2)^{1/2} = \pm 0.002$ Hz, yielding our best estimate for the $^{171}\text{Yb}^+$ clock frequency $12\,642\,812\,118.4660 \pm 0.002$ Hz.

6. Conclusion

We have measured the frequency of the $^{171}\text{Yb}^+$ 12.6 GHz $M_F=0\rightarrow 0$ ground state hyperfine 'clock' transition in buffer gas-cooled ion clouds confined in two similar, but not identical, linear Paul traps. After correction for the known differences between the two ion traps, including significantly different second-order Doppler shifts, the frequencies have agreed on each occasion on which they were measured within ± 3 parts in 10^{14} .

Measurements taken over a period of more than 12 months yield a value for the frequency of the 12.6 GHz $M_F=0\rightarrow 0$ clock transition in an isolated $^{171}\text{Yb}^+$ ion at zero temperature, velocity, electric field and magnetic field, of $12\,642\,812\,118.4660 \pm 0.002$ Hz.

7. Acknowledgment

The authors thank Dr A.G. Mann and Dr D.G. Blair of the Department of Physics, University of Western Australia, for the loan of the cryogenic sapphire resonator on which our microwave system is based.

References

- [1] P.T.H. Fisk, M.J. Sellars, M.A. Lawn, and C. Coles, "Performance of a microwave frequency standard based on laser-detected, trapped $^{171}\text{Yb}^+$ ions," *Appl. Phys. B* 60, 519-527, 1995.
- [2] P.T.H. Fisk, M.J. Sellars, M.A. Lawn, C. Coles, A.G. Mann, and D.G. Blair, "Performance of a prototype microwave frequency standard based on trapped $^{171}\text{Yb}^+$ ions.," *Proc. 48th Annual IEEE International Symposium on Frequency Control*, 731-737, 1994.
- [3] M.J. Sellars, P.T.H. Fisk, M.A. Lawn, and C. Coles, "Further investigation of a prototype microwave frequency standard based on trapped $^{171}\text{Yb}^+$ ions," *Proc. 49th Annual IEEE International Symposium on Frequency Control*, 66-73, 1995.
- [4] P.T.H. Fisk, M.J. Sellars, M.A. Lawn, C. Coles, "Accurate measurement of the 12.6 GHz 'Clock' transition in trapped $^{171}\text{Yb}^+$ ions", To appear in *IEEE Trans. Ultrasonics, Ferroelectrics and Frequency Control*, 1997.
- [5] A.J. Giles, A.G. Mann, S.K. Jones, D.G. Blair, and M.J. Buckingham, "A very high stability sapphire-loaded superconducting cavity oscillator," *Physica B*, vol. 165-166, no. 1, 145, August 1990.
- [6] A. Premoli and P. Tavella, "A revisited three-cornered hat method for estimating frequency standard instability", *IEEE Trans. Instrumentation and Measurement* 42, 7-13, 1993.
- [7] D.J. Wineland, W.M. Itano, J.C. Bergquist, J.J. Bollinger, F. Diedrich, and S.L. Gilbert, "High accuracy spectroscopy of stored ions," in *Frequency Standards and Metrology*, A.D. Marchi, 71-77. 1989.

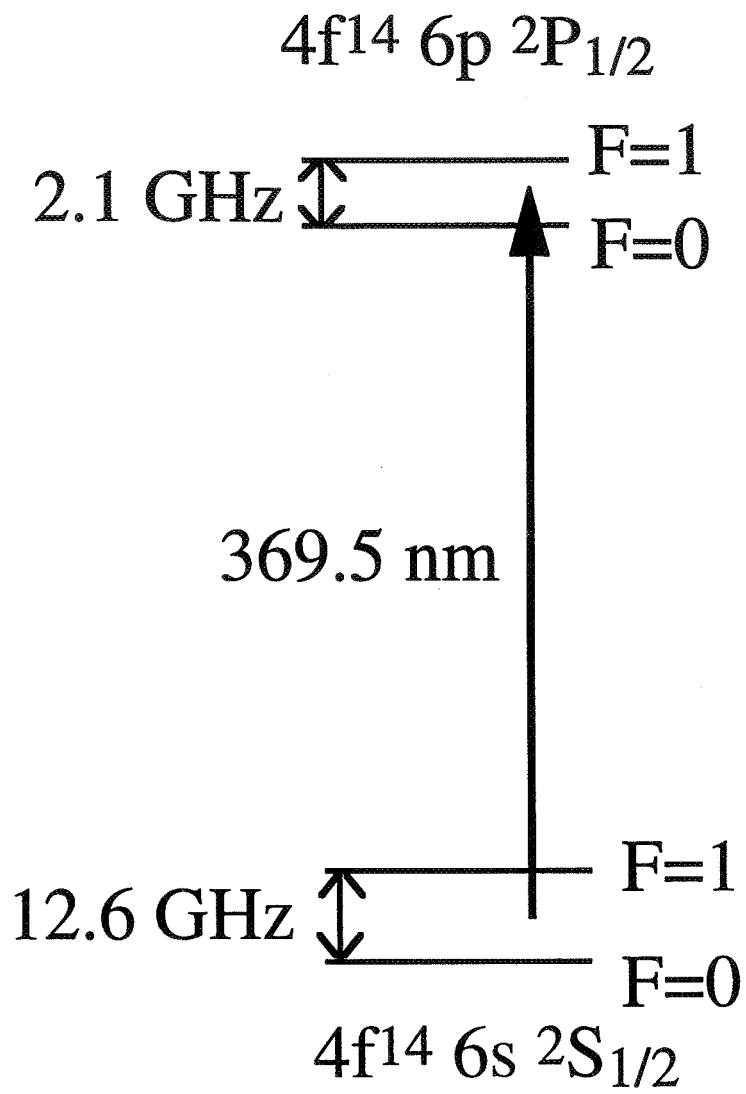


Figure 1: Partial energy level diagram for $^{171}\text{Yb}^+$.

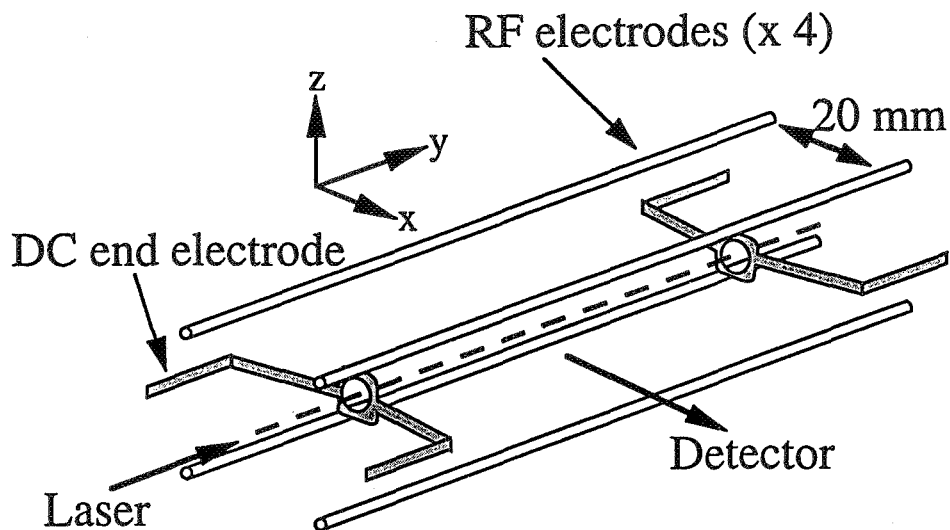


Figure 2: Electrode structure of the linear ion traps IT-1 and IT-2. The diameter of the RF electrodes is 2.3 mm.

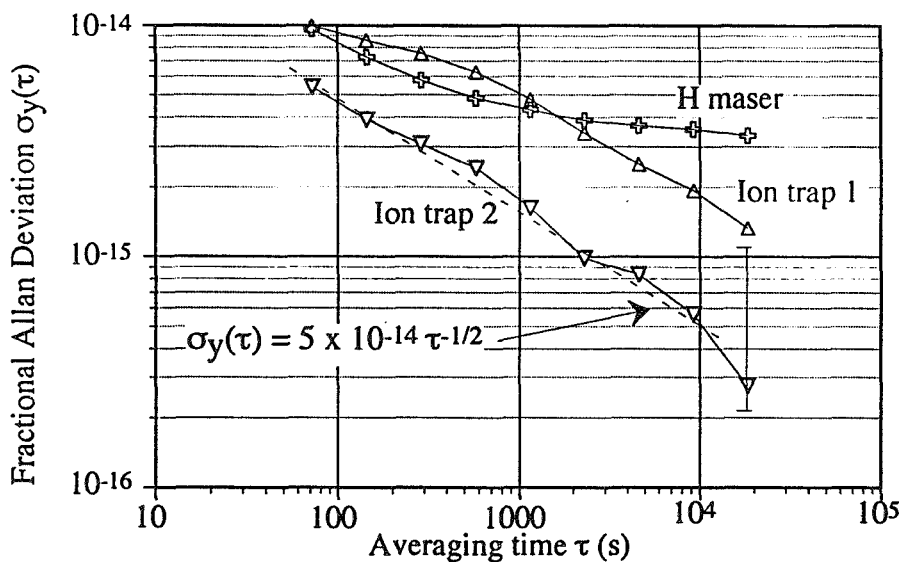


Figure 3: Frequency stability, as characterised by the fractional Allan deviation, of the trapped ion frequency standards IT-1, IT-2 and a hydrogen maser (NML-Maser 2). The result shown represents a 29 hour intercomparison between the two ion trap systems IT-1 and IT-2, and a hydrogen maser NML-M2. The performances of the individual standards were separated using a 'three-cornered hat' algorithm [6]. Longer term operation of the trapped ion standards is presently difficult due to power drift and instability in the titanium-sapphire laser system.

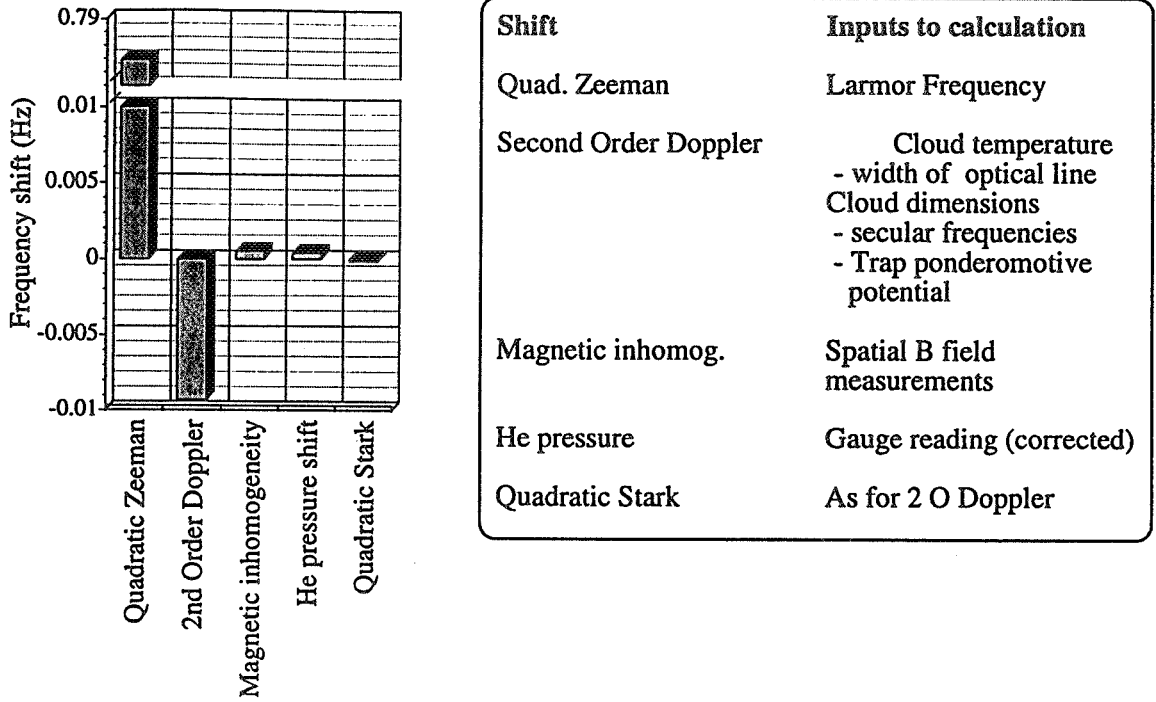


Figure 4: Typical magnitudes and sources of frequency offsets affecting the trapped ion standards IT-1 and IT-2.

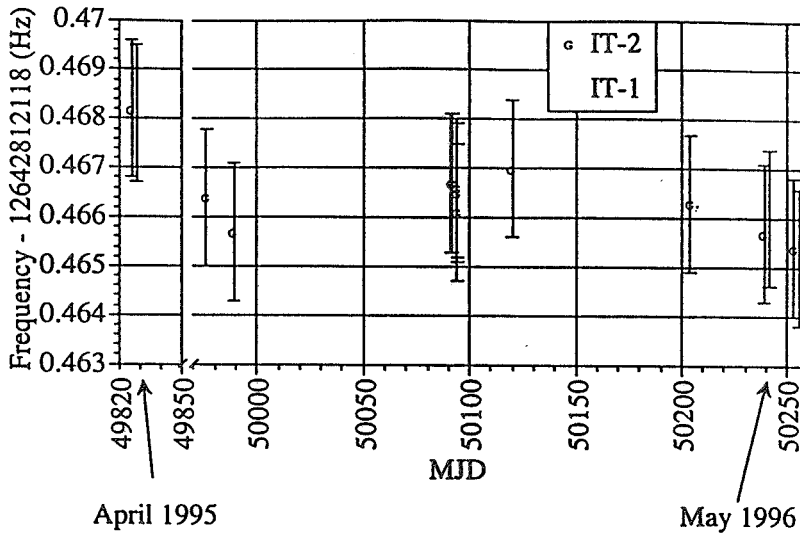


Figure 5: Corrected $^{171}\text{Yb}^+$ clock frequencies measured over a period of approximately 14 months. MJD = Modified Julian Day. On the three occasions (MJD 49826, 50239 and 50253) where determinations of the clock frequency were made using IT-1, the corresponding measurements on IT-2 were made simultaneously (on the first 2 occasions) or on the same day (third occasion). The data points are displaced horizontally on the plot for clarity. All of the data shown here were obtained with 10 V applied to the end electrodes, with the exception of the MJD 49826 data, where 20 V was used. Other trap parameters, such as He pressure, RF voltage and trap contents varied significantly between determinations.

Tables

	IT-1	IT-2
RF electrode separation	20 mm	20 mm
RF electrode diameter	2.3 mm	2.3 mm
End electrode separation	60 mm	60 mm
RF frequency	500 kHz	510 kHz
RF amplitude	287 ± 3 V _{p-p}	280 ± 3 V _{p-p}
End electrode voltage	10.0 V (stability ± 0.001 V)	10.0 V (stability ± 0.001 V)
He pressure	$1.2 \pm 0.6 \times 10^{-4}$ Pa	$1.7 \pm 0.6 \times 10^{-4}$ Pa

Table 1: Typical operational parameters applied to the ion traps for the measurements described in this paper. The uncertainty in the helium pressure is the variation observed between the readings of two independent gauge heads and gauge controllers connected to a single vacuum system. The value quoted is corrected for relative gauge sensitivity to He using the calibration factor given by the gauge manufacturer.

Ion-Atom Cold Collisions and Atomic Clocks

John D. Prestage, Lute Maleki, and Robert L. Tjoelker
Jet Propulsion Laboratory
California Institute of Technology
Pasadena, CA

Introduction

Collisions between ultracold neutral atoms have for some time been the subject of investigation, initially with hydrogen and more recently with laser cooled alkali atoms[1]. Advances in laser cooling and trapping of neutral atoms in a magneto-optic trap (MOT) have made cold atoms available as the starting point for many laser cooled atomic physics investigations. The most spectacularly successful of these, the observation of Bose-Einstein condensation (BEC) in a dilute ultra-cold spin polarized atomic vapor[2], has accelerated the study of cold collisions. Experimental and theoretical studies of BEC and the long range interaction between cold alkali atoms is at the boundary of atomic and low temperature physics. Such studies have been difficult and would not have been possible without the development and advancement of laser cooling and trapping of neutral atoms. By contrast, ion-atom interactions at low temperature, also very difficult to study prior to modern day laser cooling, have remained largely unexplored. But now, many laboratories worldwide have almost routine access to cold neutral atoms. The combined technologies of ion trapping, together with laser cooling of neutrals has made these studies experimentally feasible and several very important, novel applications might come out of such investigations.

This paper is an investigation of ion-atom interactions in the cold and ultra-cold temperature regime. Some of the collisional ion-atom interactions present at room temperature are very much reduced in the low temperature regime. Reaction rates for charge transfer between unlike atoms, $A + B^+ \Rightarrow A^+ + B$, are expected to fall rapidly with temperature, approximately as $T^{5/2}$. Thus, cold mixtures of atoms and ions are expected to coexist for very long times, unlike room temperature mixtures of the same ion-atom combination. Thus, it seems feasible to cool ions via collisions with laser cooled atoms.

Many of the conventional collisional interactions, exploited as a useful tool at room temperature and higher, are greatly enhanced at low energy. For example, collisional spin transfer from one species of polarized atoms to another has long been a useful method for polarizing a sample of atoms where no other means was available. Because optical pumping cannot be used to polarize the nuclear spin of ^{129}Xe or ^3He [3] (for use in nmr imaging of the lungs), the nuclear spins are polarized via collisions with an optically pumped Rb vapor in a cell containing both gases. In another case, a spin polarized thermal Cs beam was used [4] to polarize the hyperfine states of trapped $^3\text{He}^+$ ions in order to measure their hyperfine clock transition frequency. The absence of an x-ray light source to optically pump the ground state of the $^3\text{He}^+$ ion necessitated this alternative state preparation. Similarly, Cd^+ and Sr^+ ions were spin-oriented via collisions in a cell with optically pumped Rb vapor. Resonant RF spin changing transitions in the ground state of

the ions were detected by changes in the Rb resonance light absorption [5].

Because cold collision spin exchange rates scale with temperature as $T^{-1/2}$ this technique is expected to be a far more powerful tool than the room temperature counterpart. This factor of 100 or more enhancement in spin exchange reaction rates at low temperatures is the basis for a novel trapped ion clock where laser cooled neutrals will cool, state select and monitor the ion clock transition. The advantage over conventional direct laser cooling of trapped ions is that the very expensive and cumbersome UV laser light sources, required to excite the ionic cooling transition, are effectively replaced by simple diode lasers.

Review of Low Temperature Ion-Atom Collisions

The following sections will summarize the expected low temperature reaction rates for various processes to be investigated in the proposed work.

Long Range Ion-Atom Interactions

The cold and ultra-cold collisions to be studied in this work have not been experimentally accessible until just recently following the proliferation of laser cooled neutral vapors. Cross-sections for collision processes between ions and atoms at these energies can be estimated both classically and quantum-mechanically. One such classical cross-section is the impact collision of an ion and atom drawn together by their polarization induced attraction, written $V_{\text{pol}}(r) = -\alpha e^2/2r^4$ where α is the electric polarizability of the neutral atom. The two body classical orbit problem is reduced to an equivalent problem of a single particle of reduced mass μ ($1/\mu = 1/M_{\text{ion}} + 1/M_{\text{neutral}}$) in the attractive ion-neutral interaction $V_{\text{pol}}(r) = -\alpha e^2/2r^4 = -C_4/r^4$ and the repulsive angular momentum barrier $V_{\text{eff}}(r) = L(L+1)\hbar_{\text{bar}}^2/2\mu r^2$ where L is the angular momentum quantum number. An atom with sufficiently small impact parameter will be drawn to an ion and impact will occur. This sort of collision [6] occurs with

cross-section $\sigma \approx \pi a_0^2 \sqrt{C_4'/E(a.u.)}$ where the kinetic energy of the particles, E , is

in atomic units $e^2/a_0 = 27.2$ eV and $C_4 = C_4'(e^2/2a_0)a_0^4$. For 1K ion-atom temperatures, impact cross-sections are $\sim 10^{-12}$ cm² and increasing as $T^{-1/2}$ as the collision temperatures diminish. However, the reaction rate, $\langle \sigma v \rangle$, is independent of temperature for C_4/r^4 ion-atom potentials. Though classical, this model shows that at low collision energies the angular momentum barrier is weak and particles at large impact parameters will fall together.

Collisional Cooling of Trapped Ions

Collisional cooling between a laser cooled beam of atoms or cold atoms in a MOT should be straightforward. The energy loss per collision $\delta E/E$ for ions of mass M initially at room temperature colliding with laser cooled neutrals of mass m is $\delta E/E \sim m/M$. The cross-section for ion-atom interactions at room temperature can be estimated from the impact model at about 6×10^{-15} cm². Assuming Li as the laser cooled gas of density $10^{10}/\text{cm}^3$ [7], a collision rate of $n v \sigma \approx 60/\text{sec}$ yields an energy loss rate $1/E dE/dt \approx 2/\text{sec}$. Thus, a few seconds after the hot ion enters the cold neutral vapor it will have cooled to the cold neutral temperature.

Collisional cooling between a cold atom and an ion has never been experimentally investigated. Ion-ion “sympathetic” cooling, where one species is laser cooled and the other is thermalized via collisional energy loss has been demonstrated[8]. In this work both types of ion were confined to a Penning trap and only momentum transfer interactions can occur because the like charges repel and close approach is impossible. By contrast, ion-neutral interactions are long range attractive and close approach is likely so that spin exchange interactions can occur with high probability as we describe later. However, with close approach there is the question of charge transfer between the cold alkali atom and ion during momentum and spin transfer collisions.

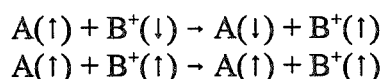
Charge Transfer in Cold Ion-Atom Collisions

Unlike impact collisions whose reaction rate is constant with falling temperature, inelastic charge transfer rates where the neutral loses its valence electron to the ion, should be drastically reduced at low temperature. The possibility of collisionally cooling a collection of trapped ions with cold neutrals would be remote should the ion be neutralized by the atom during the multiple collisions required to reach thermal equilibrium.

Charge transfer in ion-atom collisions[6] where the ion and atom are different atoms, eg., laser cooled Li atoms and trapped Hg⁺ ions, is an inelastic collision. That is, a part of the translational kinetic energy of the colliding pair, ΔE , must be converted into internal energy in transferring the electron from an energy state in the Li atom to the nearest available energy state in the resulting neutral Hg atom. For Hg⁺ colliding with the commonly used laser cooled alkali atoms, $\Delta E \approx 0.1$ eV, many orders of magnitude larger than the cold collision energies attainable in this work. Charge transfer in these asymmetric collisions (unlike ion and atom) have been successfully modelled for collision energies higher than the low temperature domain to be studied in the work proposed here. The scaling to colder collisions for the asymmetric charge transfer follows the Massey adiabatic criterion, i.e., when $a\Delta E/h_{\text{bar}}v \approx 1$ the inelastic cross-section is maximum, where a is an atomic size for the atoms in collision and v is the velocity at closest approach. The electron is able to absorb energy ΔE from the changing inter-atomic fields whose spectrum has its largest component around frequency $\omega \approx v/a \approx \Delta E/h_{\text{bar}}$. At lower velocities where $a\Delta E/h_{\text{bar}}v \gg 1$ the cross-section falls off rapidly with decreasing v [6] falling approximately as $(h_{\text{bar}}v/a\Delta E)^4$ and thus the reaction rate, $\langle\sigma v\rangle$, falls as $T^{5/2}$ with temperature. It would seem that charge transfer between unlike atoms would be very difficult at cold temperatures. We will return to this question in the next section.

Low Energy Spin Exchange Collisions

The electron spin exchange reaction between an alkali atom and an alkali-like ion, both in $^2S_{1/2}$ ground states [9] is written



The spin dependent interaction between atoms, $V(r) = V_0(r) + \mathbf{S}_A \cdot \mathbf{S}_B V_1(r)$, conserves total electron spin $\mathbf{S} = \mathbf{S}_A + \mathbf{S}_B$ without any changes in orbital state. The inter-atomic potential is very different for the $\uparrow\uparrow$ state where \mathbf{S}_A is parallel to \mathbf{S}_B than the $\downarrow\uparrow$ state where \mathbf{S}_A and \mathbf{S}_B are anti-

parallel. A typical interaction energy vs internuclear separation is shown in Figure 1. The origin of this spin dependent interaction stems from the overall symmetry requirement of the electron wavefunction. The $\uparrow\uparrow$ state has a node of the electron wavefunction between the colliding atoms and thus the two positively charged nuclei are not screened from one another as in the state $\downarrow\downarrow$ where the electron wavefunction has its maximum value between the atoms. The shielding between the nuclei in this $\downarrow\downarrow$ state results in the binding of diatomic molecules and is several orders of magnitude stronger than the dipolar magnetic interaction of the electron spin magnetic moments.

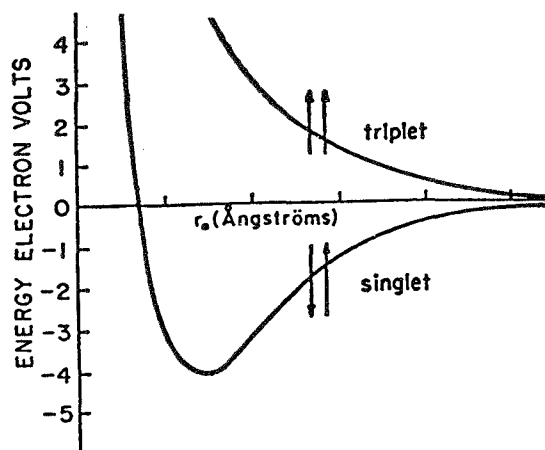


Figure 1: Interaction energy of two hydrogen atoms as a function of the internuclear separation r [ref. 9].

The quantum mechanical cross-section for spin exchange is given by

$$\sigma = \frac{\pi}{k^2} \sum_{l=0}^{l_{cutoff}} (2l+1) \sin^2(\delta_l^{\uparrow\uparrow} - \delta_l^{\downarrow\downarrow})$$

where $k = 2\pi/\lambda_{dB}$ and $\delta_l^{\uparrow\uparrow}$ and $\delta_l^{\downarrow\downarrow}$ are the phase shifts incurred in the scattering from the triplet and singlet inter-atomic potentials of Figure 1. For cold collisions where only a few partial waves contribute (see Table 1), the cross-section approaches $\pi \lambda_{dB}^2 = \pi a_0^2 82(\mu(\text{amu})E(\text{K}))^{-1}$ where μ is the reduced mass in amu of the collision partners and E is the kinetic energy in units of temperature K. Note that the rate constant, $\langle \sigma v \rangle$, for spin exchange collisions at low temperature increases as $T^{-1/2}$ with decreasing temperature. For mK collision temperatures, cross-sections can be of order 10^{-12} cm^2 , two orders of magnitude higher than room temperature values.

With regard to charge transfer in the cold collision regime, ion-atom collision partners approaching one another in the singlet state $\downarrow\downarrow$ are drawn together gaining an eV or more of energy (Figure 1), many orders of magnitude higher than their separated energy. Thus ion-atom collision speeds could satisfy the Massey criterion for these singlet state collision partners and may charge transfer. By contrast, triplet state or spin parallel collision partners experience a

repulsive exchange interaction so that $v/a \ll \Delta E/h_{\text{bar}}$ for all times preventing charge transfer. This could form the basis for state selection in the trapped ion cloud. That is, a spin polarized neutral beam will charge transfer and destroy the anti-parallel spin state ions without combining with the spin parallel ions. The remaining ion cloud would be spin aligned with the spin polarized neutral atoms. Externally driven RF spin flip transitions in the ion cloud would be followed, indeed, would be signalled by the generation of Li^+ ions, the byproduct of the charge transfer with the Hg^+ ion. Because charged particles can be detected with nearly 100% efficiency, the clock transition in the trapped ions could be monitored with very high SNR. This will be discussed more in the section on atomic clocks.

The Onset of Quantum S-wave Scattering

The long range interaction between an ion and neutral atom is via an induced electric dipole in the neutral resulting in an attractive interaction $V_{\text{pol}}(r) = -\alpha e^2/2r^4$ where α is the electric polarizability of the neutral. These measured values [10] are listed in Table 1 in units of a_0^3 , the cube of the Bohr radius. The attractive $V_{\text{pol}}(r) = -C_4/r^4$ and repulsive $V_{\text{eff}}(r) = L(L+1)h_{\text{bar}}^2/2\mu r^2$ together produce a maximum in the long range potential at $R_c(L) = (4\mu C_4/L(L+1)h_{\text{bar}}^2)^{1/2}$ of magnitude $V_c(L) = L(L+1)h_{\text{bar}}^2/4\mu R_c^2(L)$. Table 1 summarizes these values.

Table 1. Temperatures where the scattering becomes pure S-wave for different alkali atoms.

	C_4^\dagger	$R_c(L=1)/a_0$	$T_c = V_c(L=1)/k_B$	$L_{\text{cutoff}} (T=1\text{mK})$
Li + Hg^+	163	1430	6 μK	3
Na + Hg^+	158	2410	0.7 μK	5
K + Hg^+	291	4200	0.2 μK	8
Rb + Hg^+	317	5940	40 nK	12
Cs + Hg^+	400	7670	20 nK	

In the table we have listed $C_4^\dagger = \alpha/a_0^3$ where $C_4 = C_4^\dagger(e^2/2a_0)a_0^4$, $a_0 = h_{\text{bar}}^2/me^2 = 0.529 \times 10^{-8}$ cm and $e^2/2a_0 = 13.6$ eV. In addition, $a_0^3 = 0.149 \times 10^{-24}$ cm³.

For collision temperatures less than T_c , the angular momentum barrier prevents ion-atom distances closer than $R_c(L)$ except for $L = 0$, i.e., s-wave scattering. These barriers are somewhat weaker and occur at much greater inter-atom distances than the neutral-neutral $-C_6/r^6$ van der Waals induced barriers [1]. For ultracold collisions at T_c or less, only s-wave interactions are energetically allowed and the scattering is fully quantum mechanical. Even at a temperature of 1mK, only a few partial waves in the scattering process are allowed, especially for the lighter alkalis as shown in the last column of Table 1.

Applications

Atomic Clocks and Tests of Local Position Invariance

The method proposed here provides an attractive alternative to direct laser cooling and optical state preparing of trapped ions for operation as an atomic clock. There are several advantages:

- 1) The optical transition in ions, used for cooling and optical pumping, is always in the ultra-violet. Indeed, Hg^+ , one of the most attractive clock atoms with a 40.5 GHz hyperfine clock transition, requires uv light at 194 nm, nearly into the vacuum ultraviolet spectral region. Although laser light at 194 nm has been generated via optical frequency doubling and additional nonlinear optical mixing, the process is costly since multiple visible lasers with watts of output power together with delicate doubling crystals are required. This procedure is to be contrasted with the relative ease which diode laser cooling of atoms in a MOT has become. Visible light from small solid state diode lasers (as used in CD players, for example) is carried by optical fibers and split into 3 intersecting retro-reflected circularly polarized beams[11]. This technology is at the center of today's optical industry ensuring a ready supply of off-the-shelf components.
- 2) The clock transition in the Hg^+ ion is detected by the generation of Li^+ , a by-product of the spin dependent charge transfer to the laser cooled neutral. This is a natural synergy of cold collisions between heavy trapped ions and a light spin polarized neutral atom. An ion trap whose RF electric trapping field is set in frequency and amplitude to confine Hg^+ will eject the lightweight Li^+ since the amplitude of its driven motion is so much greater. This ejected Li^+ ion can be detected with nearly 100% efficiency with channeltron electron multipliers surrounding the trap. This novel detection process has enormous energy leverage since a 40.5 GHz microwave photon (2×10^{-4} eV) absorbed in the Hg^+ ion will trigger the ejection of a 100 eV or more Li^+ ion. Signal to noise in the clock resonance, with 100% detection efficiency, would allow $10^{-14} \tau^{-1/2}$ short term stabilities which enter the 10^{-17} stability regions with only a few hours averaging time.
- 3) The ions will be cooled to the temperature of the laser cooled neutrals, i.e., 1K for the LVIS/MOT earth based cold beam source and much lower for space based ultra-cold beams where gravitational deflection of a slow beam is much reduced. The second order Doppler shift of the clock transition in the ion is reduced to below 10^{-15} allowing clock stabilities into the 10^{-17} region.
- 4) This technique is non-resonant, that is, without changing the light source/cold atom source, the trapped ion species could be changed and cooling, state selection, and resonance detection would be expected to proceed as described above. The electron spin alignment between the colliding neutral and ion still mediates the close in collision dynamics and charge exchange even when the ion has more than one electron outside a closed shell. All diatomic molecules have binding and anti-binding states, determined by the relative orientation of the spins of the colliding partners[12]. Thus ions with large ground state splittings, even into the THz regime, could readily be investigated with little change in experimental apparatus. This could not be easily done with conventional uv optical pumping techniques.

5) Multiple species of ions could be trapped simultaneously (eg., Hg^+ and Cd^+) and operated as two clocks in a single apparatus. This is important for certain clock comparison tests of the Equivalence Principle where Local Position Invariance demands that all atomic clocks run at the same rate independent of location. A coupling of the atomic fine structure constant, α , to the gravitational potential would force clocks of different atomic number Z to change in relative rate [13]. Two clocks in a single apparatus passing near the sun (where gravitational potentials are the largest in the solar system) could be compared to one another onboard a small spacecraft without sending a stable clock signal downlink from the spacecraft to be compared to an earthbased clock. This eliminates the need for an ultra-stable downlink, nearly impossible over a baseline near the sun. This self contained onboard null measurement also eliminates the need to determine the s/c trajectory to sub-millimeter accuracy as required in the separated clock comparison where one clock is on earth with the other in space.

Initial Laboratory Measurements

The initial experimental apparatus will consist of a MOT source of cold atoms in the configuration recently demonstrated by Lu et. al [7]. This low velocity intense source (LVIS) of cold atoms is a simple variation of a MOT trap and will produce a beam of density 10^9 to 10^{10} / cm^3 at speeds corresponding to 1K effective temperature. This beam will be passed down the axis of a linear ion trap containing a cloud of Hg^+ ions as shown in Figure 2.

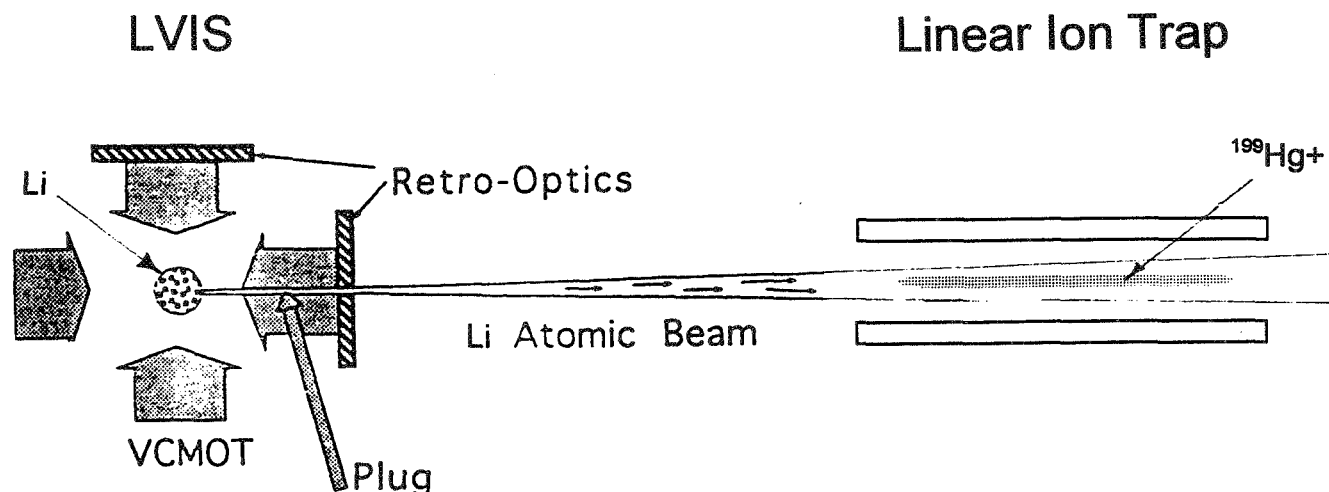


Figure 2: Schematic of the combination neutral and ion trap configuration. Neutral Lithium atoms exit a MOT in the LVIS configuration [7] and pass down the axis of a linear ion trap [16] containing $^{199}\text{Hg}^+$ ions.

The ion trap region will be surrounded by two or more channel electron multipliers to measure the Li^+ ion by-product of the charge exchange $\text{Hg}^+ + \text{Li} \rightarrow \text{Hg} + \text{Li}^+$. The lithium ion is ejected immediately after formation because of the mass selectivity of the quadrupole ion trap. In this configuration the charge transfer cross-section will be measured. Several linear ion traps have

been used as the basis of a Hg^+ frequency standard[14]. Only the LVIS source with lasers will need to be built and mated to the ion trap vacuum system.

The LVIS beam can be optically pumped before entering the ion trap region and its polarization state optically monitored just after exiting the trap. In this way spin dependent charge exchange rates and spin exchange rates could be studied as shown in Figure 3. The experimental signature of the spin dependence of the charge transfer, i.e., that spin parallel reactions $\text{Hg}^+(\uparrow) + \text{Li}(\uparrow) \rightarrow \text{Hg} + \text{Li}^+$ proceed much more slowly than the spin anti-parallel reaction $\text{Hg}^+(\uparrow) + \text{Li}(\downarrow) \rightarrow \text{Hg} + \text{Li}^+$ would be a flux of Li^+ ions from the trap following a microwave induced electron spin flip in the Hg^+ ion sample.

The spin exchange reactions would change the spin state of the transmitted alkali atom which could be optically monitored at the exit to the trap region. The ion cloud can also be optically pumped with a discharge lamp as done in the Hg^+ clock operation.

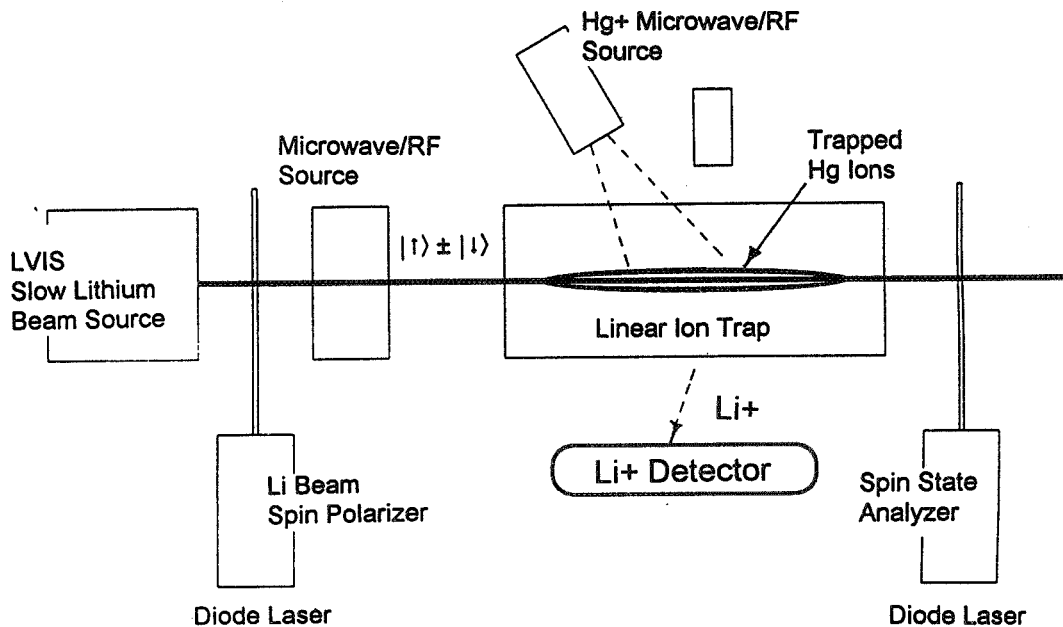


Figure 3: A low velocity intense source (LVIS) [7] generates a beam of cold lithium atoms which are spin polarized via optical pumping and pass down the axis of a linear ion trap containing Hg^+ ions. Charge transfer $\text{Hg}^+ + \text{Li} \rightarrow \text{Li}^+ + \text{Hg}$ is signalled by Li^+ ions ejected from the trap and collected in the surrounding channel electron multipliers. Spin exchange reactions with the Li or heavier slow alkali atom will result in a depolarization of the neutral beam and will be detected by optical fluorescence from the spin state analyzer as the spin states are re-aligned.

The proposed trapped ion atomic clock which uses cold atom spin exchange and collisional cooling seems well suited for the micro-gravity environment. The ion cloud is contained in a trap and is quite tolerant of departures from a perfect zero-g environment. The cold atoms are used to cool and monitor the ion internal state, a much less critical role than when the atoms serve as the reference for the actual clock. A high Q clock resonance in freely floating neutral atoms will demand a strictly low-g environment. That is, phase shifts between successive Ramsey pulses due

to a slight movement of the neutrals relative to the microwave source during the clock precession time, will make an apparent frequency shift of the clock transition. This is analogous to cavity end to end phase shifts in conventional beam tubes. Spin stabilization of the spacecraft, the cheapest means for s/c attitude control, will not be practical for such zero-g neutral atom clocks. Ions confined to an RF trap would operate quite well in such a spacecraft even with cold atoms as a source of state preparation and cooling since the ions are strictly confined relative to the microwave source.

Acknowledgment

The research described in this paper was carried out by the Jet Propulsion Laboratory, California Institute of Technology, under contract with the National Aeronautics and Space Administration.

References

- [1] P. S. Julienne and F. H. Mies, *J. Opt. Soc. Am. B* **6**, 2257 (1989). J. Wiener, *ibid*, 2270 (1989).
- [2] M. H. Anderson, J. R. Ensher, M. R. Matthews, C. E. Wieman, and E. A. Cornell, *Science* **269**, 198 (1995).
- [3] R. L. Walsworth, E. M. Mattison, E. R. Orteiza, R. E. Stoner, K. Y. N. Tan, R. F. C. Vessot, and A. I. Yu, *Proc. 5th Symposium on Frequency Standards and Metrology*, 187 (1995).
- [4] H. G. Dehmelt, *Adv. At. Mol. Phys.*, **3**, 53 (1967), and **5**, 109 (1969).
- [5] H. M. Gibbs and G. G. Churchill, *Phys. Rev. A* **3**, 1617 (1971).
- [6] D. Rapp and W. E. Francis, *J. Chem. Phys.* **37**, 2631 (1962).
- [7] Z. T. Lu, K. L. Corwin, M. J. Renn, M. H. Anderson, E. A. Cornell, and C. E. Wieman, *Phys. Rev. Lett.* **77**, 3331 (1996).
- [8] D. J. Larson, J. C. Berquist, J. J. Bollinger, W. M. Itano, and D. J. Wineland, *Phys. Rev. Lett.* **57**, 70 (1986).
- [9] R. J. Knize, Z. Wu, and W. Happer, *Adv. At. Mol. Phys.* **24**, 223 (1988).
- [10] R. W. Molof, H. L. Schwartz, T. M. Miller, and B. Bederson, *Phys. Rev. A* **10**, 1131 (1974).
- [11] E. L. Raab, M. Prentiss, A. Cable, S. Chu, and D. E. Pritchard, *Phys. Rev. Lett.* **59**, 2631 (1987).
- [12] G. Herzberg, *Molecular Spectra and Molecular Structure, I. Spectra of Diatomic Molecules*, 2nd Ed., 1989, Krieger Publishing Co., Malabar, Florida, USA.
- [13] J. D. Prestage, R. L. Tjoelker, and L. Maleki, *Phys. Rev. Lett.* **74**, 3511 (1995).
- [14] J. D. Prestage, R. L. Tjoelker, G. J. Dick, and L. Maleki, *J. Mod. Opt.* **39**, 221 (1992).

PHARAO: A SPACE CLOCK WITH COLD CESIUM ATOMS.

Ch. Salomon⁽¹⁾, P. Lemonde⁽¹⁾, Ph. Laurent⁽²⁾, E. Simon⁽²⁾, G. Santarelli⁽²⁾, A. Clairon⁽²⁾,
P. Petit⁽³⁾, N. Dimarcq⁽³⁾, C. Audoin⁽³⁾, F. Gonzalez⁽⁴⁾, F. Jamin Changeart⁽⁴⁾

(1) Laboratoire Kastler Brossel, Ecole Normale Supérieure, 24 rue Lhomond 75231 Paris, France

(2) BNM-Laboratoire Primaire du Temps et des Fréquences, 61, Av. de l'Observatoire 75014 Paris, France

(3) Laboratoire de l'Horloge Atomique, Bat.221, Université Paris-Sud, 91405 Orsay, France

(4) Centre National d'Etudes Spatiales, 18, Av. Edouard Belin, 31055 Toulouse, France.

Abstract

We describe a cold atom clock designed for operating in micro-gravity, the PHARAO project. Preliminary results have already been obtained on Earth and the prototype will be tested in the reduced gravity of aircraft parabolic flights in the beginning of 1997.

The PHARAO prototype is an extension of the work done at the BNM-LPTF on a cesium atomic fountain, which presents a resonance linewidth of 700 milliHertz, a frequency stability of $1.5 \cdot 10^{-13} \tau^{-1/2}$ where τ is the integration time in seconds. The accuracy of the fountain clock is presently $2 \cdot 10^{-15}$, more than three times better than previously achieved with uncooled conventional devices.

The expected relative stability of the PHARAO cesium clock in space is about $3 \cdot 10^{-14}$ at one second or 10^{-16} per day. Because the reduced gravity environment allows a mode of operation of the clock different from Earth fountains, the accuracy of PHARAO should surpass that of fountains and be in the 10^{-17} range.

The PHARAO frequency standard could be a key element in future space missions in fundamental physics such as SORT (Solar Orbit Relativity Test), detection of gravitational waves, or for the realization of a global time scale and a new generation of positioning system.

I Introduction

Today, the most stable frequency standards are cesium clocks, hydrogen masers and trapped ion clocks. The unit of time, the second, is defined using the hyperfine transition $F=3$ to $F=4$ of atomic cesium. In a cesium clock, the atoms pass through a microwave cavity where they undergo the hyperfine transition. The microwave frequency, generated by a local oscillator, is frequency locked on the atomic resonance. Cesium clocks have the best long term frequency stability ¹ ($\sim 10^{-14}$ from 1000 s to several years) and accuracy ($\sim 10^{-14}$), while hydrogen masers present the best short term stability ($\sim 10^{-15}$ from 1000 to 10 000 s).² A hydrogen maser has flown in space for two hours in 1976 in the NASA Gravity Probe experiment (GPA) and current plans exist to fly again hydrogen masers on board the MIR Space station before the end of this century.^{2,3} Several tens of cesium clocks (as well as less precise Rubidium clocks) are now in continuous operation in GPS satellites orbiting at 20 000 km above the Earth.

The conventional cesium clocks use a ~ 400 Kelvin thermal atomic beam of cesium atoms (beam velocity ~ 100 m/s and velocity distribution width ~ 50 m/s). Nowadays, laser cooling techniques can very easily produce a dense gas of cold cesium atoms at a temperature of $2.5 \mu\text{K}$ corresponding to atoms with an r.m.s velocity of 12 mm/s.⁴ These small velocities allow interaction times between the atoms and the electromagnetic field, approaching one second on Earth as compared to a few millisecond when using a conventional cesium clock.^{5,6,7,8} As the atomic resonance linewidth in cesium clocks is inversely proportional to the interaction time, an improvement of two orders of magnitude in the frequency stability and accuracy over conventional devices is expected. A first frequency standard using cold atoms in a fountain configuration has been constructed at the BNM-LPTF. The interaction time in this atomic fountain can reach 700 ms leading to a 0.7 Hz resonance linewidth. The frequency stability is $1.5 \cdot 10^{-13} \tau^{-1/2}$ and reaches $1.5 \cdot 10^{-15}$ at $t=10^4$ s. For longer integration times, the stability is limited by the hydrogen maser used as a reference oscillator. The accuracy of the fountain clock has been recently improved over the value reported in⁵ to $2 \cdot 10^{-15}$. These are the best results ever obtained with cesium frequency standards. We are at present constructing a second cesium fountain in order to measure the stability over one day. The expected accuracy is in the 10^{-16} range.

It is predicted that microgravity conditions should enable a further factor of ten improvement in the interaction time with a simple and compact device.⁹ The objective of the PHARAO project is to develop a space clock using cold cesium atoms. Such a frequency standard opens the way to a new generation of experiments.

II PHARAO project

In 1994, the French space agency (CNES) decided to support a preliminary research program on a space frequency standard using cold atoms. Three laboratories, the BNM-LPTF, the ENS-LKB and the LHA are now cooperating for the construction of a prototype which will be tested in aircraft parabolic flights. Simultaneously, studies on local oscillators, frequency synthesis chains, microwave cavity modeling and time-frequency transfer are being performed.

The micro-gravity clock prototype

The main progress in laser cooling were achieved in the last few years. Although well understood and quite easily reproduced in laboratories with the recent development of diode lasers, these experiments are far from being compatible with space requirements. The weight of the BNM-LPTF atomic fountain is about 2 tons, with some hundreds of optical components. The device has to operate in a quiet environment.

The main point of the PHARAO project is the construction of a much smaller, reliable and automatic prototype which will be tested in aircraft parabolic flights in the beginning of 1997. We want to record the microwave resonance fringes ($\nu \sim 9.2$ GHz) during the reduced gravity of the parabolic flights to prove the reliability of the prototype in a hostile environment. This device is also designed to be transformed later into a high performance transportable fountain frequency standard.

The experimental set-up is shown in fig 1. As in the atomic fountain,⁵ the prototype operates in a pulsed mode driven by a computer. In a vacuum tube, the cesium atoms are cooled and launched, experience a microwave interaction in a cylindrical TE_{013} cavity, and are finally optically detected. Due to the absence of gravity, only a single pass in the cavity is possible. With a low velocity of 5cm/s, the resonance linewidth can be as low as 0.1Hz, a factor of ten narrower than on earth. All the laser beams are generated on a separated optical bench and connected to the tube chamber by optical fibers. A frequency chain synthesizes the 9.19.. GHz microwave field from a 10 MHz BVA quartz oscillator.

Optical bench

The optical setup generates the laser beams ($\lambda \sim 852$ nm) for cooling and detecting the atoms. A narrow linewidth diode laser, frequency locked on the $F=4-F'=5$ transition of the cesium D_2 line, provides the two detection beams. Two different diode lasers will be tested in the aircraft: an extended cavity diode laser and a DBR diode laser spectrally narrowed with a weak optical feedback and a fast electronic servo-lock. Both have a linewidth in the 100 kHz range, a value much lower than the cesium D_2 natural linewidth (5.3 MHz). A narrow laser linewidth is required for the atom detection in order not to add noise to the fluorescence signal.¹⁰ After double-pass through an acousto optic modulator (AOM) which sets the molasses detuning, the beam of this laser is also used to inject two slave diode lasers which provide the cooling beams. The two slave lasers deliver each 200 mW of optical power. Each beam is divided in three and coupled into polarizing optical fibers after a double pass in an AOM. The laser intensity (a few mW per beam) is controlled in each fiber by means of variable retarder plates. The AOM detunes the laser to launch the atoms and allows quick turning off of the laser light. To avoid any parasitic excitation of the atoms during the microwave interaction, mechanical shutters insure a complete extinction of the laser beams. An additional DBR diode laser pumps the atoms in the upper hyperfine state ($F=4$) during the cooling process and at the detection of the atoms in $F=3$. The linewidth is 3 MHz, and the frequency is locked to the $F=3-F'=4$ of the cesium D_2 line. The whole optical bench, designed with standard optical components, has the following dimensions: 65x65x15 cm. Eight optical fibers link the optical bench to the vacuum tube: six for cooling, two for detection.

Vacuum tube

The cooling region contains a low pressure cesium vapor (10^{-6} Pa). The 10 mW output of each of the six optical fibers are expanded to a 1 cm waist and are distributed in three orthogonal pairs of counterpropagating beams. Each beam is tilted from the vertical direction. With this geometry, the cold atoms are launched in the (1,1,1) direction with the moving molasses technique.⁷ The launch velocity can be adjusted up to 8 m/s. The pressure in the interaction and detection regions is $\sim 10^{-8}$ Pa to avoid collisions and parasitic background fluorescence in the detection region. The chamber is pumped by a 20 l/s ion pump and a graphite tube cesium getter.

The microwave cavity is a 20 cm long TE_{013} cavity which has a loaded quality factor of several thousands. The duty cycle (interaction time over cycle time) is around 0.5. A highly homogeneous static magnetic field (2 mG) is produced with a long solenoid and a mu-metal magnetic shield around the cavity. Two

compensation coils and three additional magnetic shields ensure the direction homogeneity of the magnetic field along the experiment. The axial shielding factor is larger than 10^5 over the cavity lengths. In addition, an external active compensation system will improve this figure by another factor of ten.

After the atoms pass through the cavity, the populations of both hyperfine levels are independently measured by fluorescence in the detection region. The atoms in the $F=4$ level are first detected with a standing wave tuned 2 MHz below the $F=4-F'=5$ transition of the D_2 line. They are then pushed away by the radiation pressure of a traveling wave tuned at the same frequency. The remaining atoms in the $F=3$ level are optically pumped to $F=4$ by the repumping beam and detected with the same procedure. Condenser lenses collect about 3% of the fluorescence emitted by the atoms.

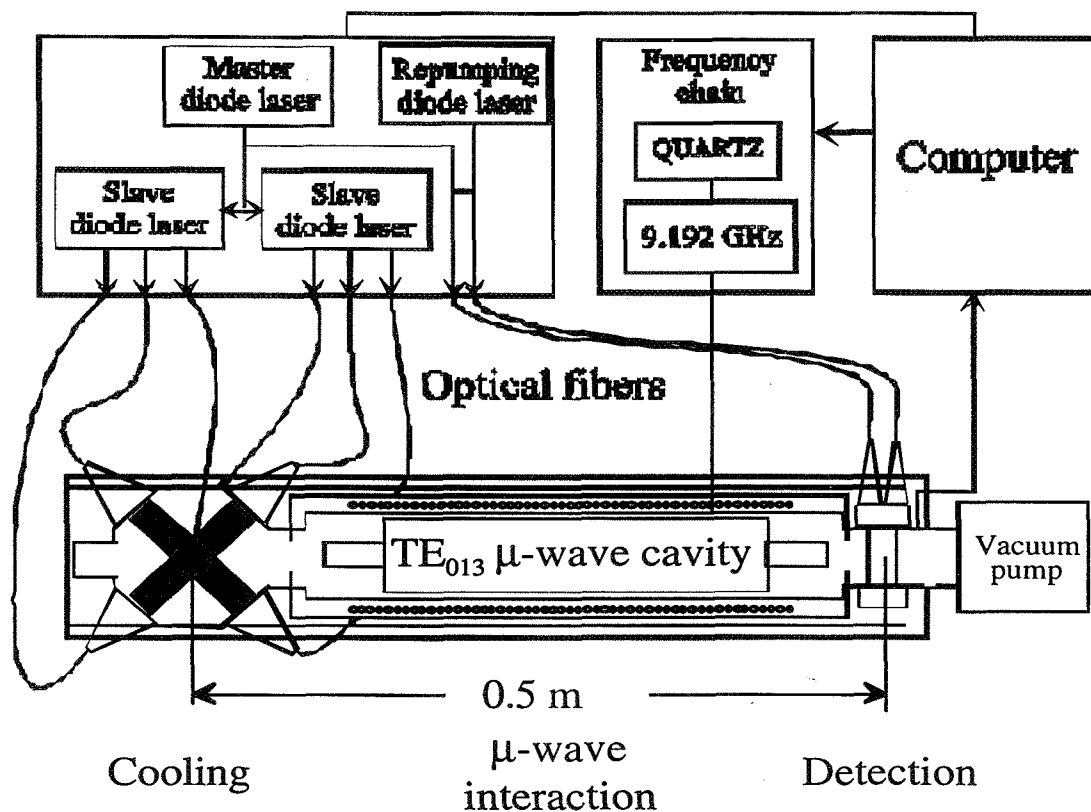


Fig. 1 Scheme of the aircraft clock prototype. The length between the cooling and the detection region is about 50 cm .

Frequency chain

The output of a 10 MHz reference oscillator is frequency multiplied to 100 MHz. The 100 MHz signal is band pass filtered and then routed to a x92 multiplier. The output power is 10 dBm. The 9.2 GHz and the 7.3 MHz of a RF synthesizer are mixed in a single sideband mixer with better than about 25 dB image and carrier rejection. The resulting signal at the interrogation frequency is then level controlled by an active microwave attenuator.

The acceleration variations in the plane are 2 g. This sets strong constraints on the accelerometric sensitivity of the reference oscillator. The projected atomic resonance linewidth is in the Hertz range. To scan this resonance without introducing errors greater than a few percent, the frequency retrace from one parabola to the other must be a few 10^{-12} . The duration of a parabola (20s) forbids long measurement averaging. The short term stability of the frequency chain must therefore be a few 10^{-13} at one second. The typical static g-sensitivity of a high performance commercial quartz is a few 10^{-11} , with a frequency stability of 3-6 10^{-13} between 1 and 10 seconds. The LCEP at Besançon has provided a quartz oscillator with an acceleration sensitivity of $\sim 4 \times 10^{-12}/g$.

The performances of the aircraft clock prototype will also be evaluated on earth and compared to the atomic fountain. The long term stability measurement of the fountain being now limited by the H-maser, this

comparison will test both the fountain and the prototype. A relative stability of 10^{-16} per day is expected. The accuracy of the prototype will also be evaluated.

III Preliminary results

The prototype is being tested on Earth in the scope of the future parabolic flights. The atoms are launched vertically with a velocity of 4 m/s in order to reach the detection region. In preliminary experiments we recently obtained a microwave resonance with a central fringe having a width of 10 Hz (Fig.2). The signal-to-noise ratio is presently 350 for a one second cycle time. We expect large improvements of the S/N in the near future.

During 1997 we will compare the PHARAO prototype to the atomic fountain. An accuracy and stability evaluation of PHARAO as a high performances compact and transportable frequency standard will then be carried out.

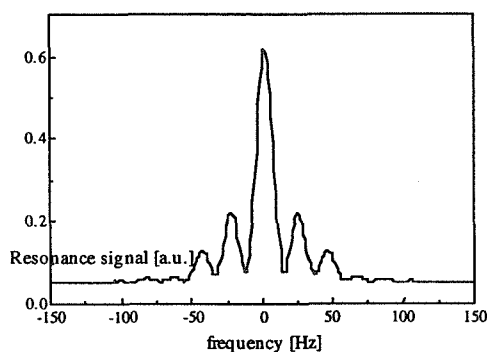


Fig. 2 Experimental microwave resonance fringes in the TE_{013} cavity. Single scan recorded with a 1 Hz frequency

IV Interest of micro-gravity environment

Operating in space with longer interaction times should lead to an improvement, in terms of accuracy and long term stability. Indeed most of the systematic effects are reduced with the atomic velocity.

The short term stability depends on both the atomic interrogation scheme and the local oscillator. If we assume a perfect local oscillator, the fractional frequency stability is given by:⁵

$$\sigma_{at}(\tau) \cong \frac{\Delta\nu}{\pi\nu} \frac{1}{\sqrt{2N_{at}}} \sqrt{\frac{T_c}{\tau}} \quad (1)$$

where ν is the frequency of the clock transition, T_c is the cycle duration, about twice the interaction time T_i and $\Delta\nu$ is the resonance linewidth varying as $1/T_i$, N_{at} is the number of detected atoms per cycle.

One way to improve the short term stability is to increase N_{at} . Yet, for an accuracy in the 10^{-16} range, the density, averaged over the flight time, cannot exceed 10^6 atom/cm³. As a matter of fact, the dominant uncertainty is that of a shift proportional to the atomic density, which is due to collisions between the cold atoms.^{8,11} In the BNM-LPTF fountain, this shift is typically 1×10^{-15} with a 0.5×10^{-15} uncertainty. It is presently a serious limitation to the performances of cold atom clocks on earth and it also dominates the design of the micro-gravity clock. In space, as the launching velocity is much smaller, several clouds of cold atoms can be prepared before the first one enters the cavity. This allows to increase the number of detected atoms with the same average density. This improves the short term stability without increasing the cold collision shift.

The radius of the cold atom cloud expands as $(V_{rms} T_i)^2 + r_0^2)^{1/2}$, where V_{rms} is the transverse velocity of the atoms and r_0 the initial cloud radius. To optimize the stability for a given initial number of cold atoms, the interaction time must be equal to r_0/V_{rms} . With the typical parameters (a rms velocity of 1 cm/s and a r_0 of

1 cm), the optimum T_i is around 1 s. Thus, in the PHARAO prototype with one cm diameter holes in the cylindrical micro-wave cavity, a transverse temperature of 1 mK, an interrogation time of 0.5 second and a cycle time T_c of 1 second, we detect $4 \cdot 10^5$ atoms in $m_F=0$ per cycle for a stability of $3 \cdot 10^{-14} \tau^{-1/2}$ or 10^{-16} per day. Using three successive clouds of cold atoms loaded in ~ 300 ms the collisional shift is $3 \cdot 10^{-16}$. Assuming 5-10% fluctuation in the average atomic density will lead to a stability floor of $1.5 \cdot 3 \cdot 10^{-17}$.

A second interesting case is to assume transverse cooling or transverse selection of the atoms to a temperature so low that all the atoms entering in the micro-wave cavity do contribute to the signal after an interaction time of ten seconds. With sub-recoil laser cooling techniques,^{12,13,14} the atomic transverse velocity can be reduced below 1 mm/s. This corresponds to an optimum T_i of 10 s, which would lead on earth to a fountain height of 100 m. In space this is realizable with a compact device. Assuming an ideal local oscillator, the Ramsey fringe width is 0.05 Hz and the short term stability is $10^{-14} \tau^{-1/2}$ with the same collisional shift of $2 \cdot 3 \cdot 10^{-16}$. The stability floor of $1 \cdot 2 \cdot 10^{-17}$ will then be reached after about three days of integration time. As pointed out by K. Gibble at this meeting, it might well turn out that Rubidium atoms would ultimately lead to still better performances if the cold collision shift is smaller than that of Cesium.

However the short term stability performances also depends on the local oscillator: for a pulsed operation, an aliasing phenomenon downconverts the local oscillator noise at all the harmonics of the sampling frequency. This can bring a strong limitation to the short term stability of the frequency standard. Over a time around T_c , if the flicker frequency noise dominates (for instance with a quartz crystal oscillator), the stability of the frequency standard is expressed by:^{15,16}

$$\sigma^2(\tau) \approx 0.25 \sigma_{LO}^2 \frac{T_c}{\tau} + \sigma_{at}^2(\tau) \quad (2)$$

where σ_{LO} is the flicker floor stability of the local oscillator. For the present BNM-LPTF atomic fountain, $\sigma_{at}(\tau) = 7 \cdot 10^{-14} \tau^{-1/2}$, $\sigma_{LO} = 2 \cdot 3 \cdot 10^{-13}$ at one second and the measured stability is $1.5 \cdot 10^{-13} \tau^{-1/2}$. Development is being carried out to improve the stability of the quartz oscillator. As long as the short term stability is limited by the flicker noise floor of the local oscillator, the degradation of the stability increases with the interaction time. With present state-of-the-art quartz oscillator technology, a local oscillator stability of $7 \cdot 10^{-14}$ at 1 s is available. Thus the PHARAO clock in space can readily reach the fractional frequency stability of $3 \cdot 10^{-14} \tau^{-1/2}$ with 1 s interaction time. For a ten second interaction time, a H-maser or a cryogenic oscillator are good candidates as local oscillator.

Depending on the requirements of each use of the clock (stability over a few hours or accuracy), a compromise between the different parameters discussed above will be determined: the choice of the local oscillator, the interaction time, the atom number and velocity.

VI Space applications

Time and frequency metrology

A space cold atom clock would be a primary frequency standard accessible from anywhere. It opens the way to frequency comparisons, to dissemination of an international time and to a next generation of navigation and positioning systems. The very low drift of the space clock would also allow frequency comparisons between clocks without the constraint of common view of the satellite.

A tool for tests of fundamental physics

With clocks having a stability of 10^{-16} over one day, it should be possible to measure with a potential 100-fold improvement over the 1976 GPA experiment² the gravitational red-shift (Einstein effect). This general relativity effect was determined at the 10^{-4} level using H masers having a stability around 10^{-15} over the 2 hour mission duration. With a measurement in the 10^{-6} level, the validity of theory could be assessed up to the second order.

A new measurement of the Shapiro effect is proposed: the SORT project.¹⁷ It intends to measure the gravitational delay on the travel time of light pulses sent from the earth and differentially detected on two satellites orbiting in the Solar system. The signature of the gravitational delay is extracted from the comparison between the arrival times of the light pulses to the satellites. This measurement will lead to a better determination of the post-Newtonian parameter γ which is equal to 1 in general relativity. Yet, a more general

class of theories predicts a slightly different value of γ .¹⁸ The best experimental evaluations so far show no deviation from 1 at the 10^{-3} level.¹⁹ With the SORT project, we could estimate γ with an accuracy of about 10^{-7} .

Various other tests and measurements can be thought of: direct detection of gravitational waves,²⁰ isotropy of light velocity²¹.

First mission

A first objective of a space experiment is the demonstration of a clock running with laser cooled atoms and the determination of its performances. In space, we expect in a first stage a stability better than $10^{-13} \tau^{-1/2}$ and an accuracy of about 10^{-16} . The evaluation of these performances would be made either on board or from the earth. On board, the comparison oscillator could be either another cold atom clock, or a frequency standard with a better short term stability (10^{-15} from 1 hour to 1 day). These include space versions of hydrogen maser, ion traps or cryogenic dielectric resonator. The international space station (ISSA) could be the platform of this first experiment (ACES proposal).

A crucial factor in the use of a space frequency standard is the quality of the frequency comparison between the onboard clock and frequency standards on earth. In order to transfer this space clock performances, a 10^{-16} accuracy is required. Today, the GPS is in the 10^{-14} - 10^{-15} range and two way links are in the 10^{-15} range.^{22,2} We need at least a one order of magnitude improvement. An optical link using pico-second laser pulses is being developed by the Observatoire de la Côte d'Azur OCA,²³ with an expected accuracy of 10^{-16} . However, by contrast to the optical link, the micro-wave link has the advantage of being independent of weather conditions and can allow a continuous link with the space clock.

The PHARAO project aims at developing a new generation of space clocks. In the beginning of 1997, a prototype will be tested in the reduced gravity of aircraft parabolic flights. It will be the first step toward the construction of a satellite cold atom clock with a stability and an accuracy in the 10^{-17} range. These performances, as well as future time and frequency transfer methods, can be validated on board the international space station. This ambitious program seems realistic with an international cooperation.

Acknowledgments.

The PHARAO project has the financial and logistic support of the French Space Agency (CNES) and of région Ile de France. Laboratoire Kastler Brossel is unité associée au C.N.R.S. et à l'université Pierre et Marie Curie. Laboratoire de l'Horloge Atomique is unité propre du C.N.R.S. We acknowledge the assistance of M.Lours, M.Dequin, L.Volodimer, P.Aynié, A.H.Gerard, D.Guitard, J.Olejnik.

References

- [1] See for instance A. Bauch et al. Proc. of the 25th Moriond conference on dark matter, cosmology, ultra-stable clocks and fundamental tests.
- [2] R. Vessot et al., Phys. Rev. Lett. **45**, 2081 (1980).
- [3] R. Vessot, Proc. of the 28^{ième} Rencontre de Moriond, (1993).
- [4] C. Salomon, J. Dalibard, W. Phillips, A. Clairon and S. Guellati, Europhys. Lett. **12**, 683 (1990).
- [5] A. Clairon, S. Ghezali, G. Santarelli, Ph. Laurent, S.N. Lea, M. Bahoura, E. Simon, S. Weyers and K. Szymaniec, Proc. Of the 5th Symposium on frequency standards and metrology, Ed. J. Bergquist, World Scientific, (1996).
- [6] M. Kasevich, E. Riis, S. Chu and R. de Voe, Phys.Rev. Lett. **63**, 612 (1989).
- [7] A. Clairon, C. Salomon, S. Guellati and W. Phillips, Europhys. Lett. **16**, 165 (1991).
- [8] K. Gibble and S. Chu, Phys.Rev. Lett, **70**, 177 (1993).
- [9] B. Lounis, J. Reichel and C. Salomon, C.R. Acad. Sci., Paris **316**, Série 2, 739 (1993).
- [10] N. Dimarcq, V. Giordano, P. Cerez and G. Theobald, IEEE Trans. Instrum. Meas., April 1993.
- [11] S. Ghezali, Ph. Laurent, S.N. Lea and A. Clairon, Europhys.lett, **36**, pp 25-30, (1996).
- [12] A. Aspect, E. Arimondo, R. Kaiser, N. Vansteenkiste and C. Cohen-Tannoudji, Phys. Rev. Lett **61**, 826 (1988).
- [13] M. Kasevich and S. Chu, Phys. Rev. Lett. **69**,1741 (1992).
- [14] J. Reichel, F. Bardou, M. Ben Dahan, E. Peik, S. Rand, C. Salomon and C. Cohen Tannoudji, Phys.Rev. Lett., **75**, 4575 (1995).
- [15] G.J. Dick, J.D. Prestage, C.A. Greenhall and L. Maleki. Proc of 22nd Ann. Precise Time and Time Interval (PTTI), 487-508, (1990).

- [16] G. Santarelli, P. Laurent, A. Clairon, G.J. Dick, C.A. Greenhall and C. Audoin, Proc. of the 10th EFTF, Brighton (1996).
- [17] C. Veillet et al., TROLL proposal to ESA for M3 mission (1993).
- [18] T. Damour and K. Nordtvedt Phys. Rev. Lett. **70**, 2217 (1993).
- [19] D. S. Robertson et al., Nature **349**, 6312 (1991).
- [20] R.F.C. Vessot, Journal de Physique, **C8**, 12, 42 (1981).
- [21] P. Wolf, Phys. Rev. A **51**, 5016 (1995)
- [22] H. Nau, J. Hahn, S. Bedrich Study on 'H-Maser in space'. Draft Final Report, German Aerospace Research Establishment, DLR Oberpfaffenhofen, Institute of Radio-frequency Technology, November 1994.
- [23] C. Veillet and P. Fridelance, Proc. of the 26th PTI, Vienna, December 1994.

Prospects for an Evaporatively Cooled Cesium Atomic Frequency Standard

William M. Klipstein, †Christopher R. Ekstrom, Steven L. Rolston,
and William D. Phillips

National Institute of Standards and Technology, Physics A167, Gaithersburg, MD 20899.

† *United States Naval Observatory, Washington, D.C., 20392.*

Abstract

Work leading to the recent achievement of Bose condensation in alkali gases has resulted in the development of a powerful set of tools for cooling atoms. A sample prepared with these techniques and ballistically expanding in a microgravity environment would remain localized for times of order 1000 seconds. Such long interrogation times would allow the construction of clocks with extremely narrow linewidths. This paper addresses parameters relevant to such a standard.

1 Introduction

The ideal system for an atomic frequency standard is an atom at rest in free space: the absence of perturbations would allow for the realization of the definition of the second, and arbitrarily long observation times would allow arbitrarily narrow linewidths. The closest realization of this ideal comes in the form of trapped ions, which have been represented by several interesting talks at this meeting. However, the definition of the second remains the province of neutral cesium, with observation times determined by the finite velocity of the atoms. This paper is aimed at addressing whether the atom-cooling techniques developed for achieving Bose-Einstein condensation (BEC) in alkalis [1] might be useful for producing a cesium clock with extremely long observation times when used in a low-gravity environment. Specifically, could a combination of laser cooling, evaporative cooling in a magnetic trap, and adiabatic expansion be used to achieve a potential accuracy of 10^{-17} with reasonable averaging times?

The goal of this paper is not to propose a better clock, which involves much more than a scheme to reduce the shot-noise limited stability, but rather to follow the trend

towards further cooling to see what might be possible with cold atoms. In order to reach the goal of 10^{-17} , we have asked the question of whether it would be possible to observe a 1 cm diameter cloud of 10^4 atoms for 1000 seconds. We imagine trapping and cooling the atoms inside of an open Fabry–Perot microwave cavity, eliminating the need to transport atoms around, but such details go beyond the scope of this paper. Such a system would give a shot–noise limited sensitivity of $5.6 \times 10^{-15}/\sqrt{T}$, beginning at 1000 seconds, or 2×10^{-17} in one day. The size of the cloud has been chosen such that collisional shifts of the cold atoms are kept to 10^{-17} .

If we are willing to let the cloud double in size during the expansion, the atoms must be cooled to a temperature of 1 pK, corresponding to an RMS velocity of $7 \mu\text{m/s}$. Such cooling would be achieved by the following sequence: laser cooling to a few μK , evaporative cooling in a magnetic trap, and finally adiabatic expansion to 1 cm. After this preparation, all traps would be turned off for the ballistic expansion used for the clock cycle. These cooling elements have been demonstrated and described elsewhere, but we review the basic concepts here.

2 Laser Cooling

The techniques for laser–cooling of atoms have been developed and extensively documented elsewhere[2]. Table 1 lists temperatures and velocities achieved with various cooling schemes. With moderate care, the atoms are left with kinetic temperatures corresponding to a few photon recoils, allowing the 10 ms interaction time of thermal beams to be extended to 1 second in an atomic fountain, limited largely by the acceleration of gravity. A space born clock such as in the PHARAO project discussed at this workshop would enjoy an interrogation time of as much as 10s in a cold beam, where even there the observation time is limited by the transverse velocity of the atoms.

Greater effort can produce samples with velocities below a single photon recoil velocity, but even the coldest 1D temperatures achieved would result in a 40 cm cloud after a 1000 second expansion time. Sub–recoil cooling will not be necessary for use with the cooling prescription described in this paper, since cooling to a few μK is a sufficient starting point for evaporative cooling in a magnetic trap.

Table 1: Temperatures and velocities achieved for cesium by various laser-cooling schemes. The current discussion requires a temperature of 1pK, or 7 $\mu\text{m/s}$ RMS velocity.

Technique	Temperature	Velocity (RMS)	Ref.
Thermal beam	300 K	10^4 cm/s	
Magneto-Optical Trap	100 μK	7 cm/s	[2]
Polarization Gradient	2 μK	1 cm/s	[3]
Optical Lattice	700 nK	6 mm/s	[4]
Raman Cooling in 3D	~ 380 nK	4 mm/s	[5]
Single Photon Recoil Limit	200 nK	3 mm/s	
Velocity Selective Coherent Population Trapping	~ 10 nK	0.65 mm/s	[6]
Raman Cooling in 1D	3 nK	0.4 mm/s	[7]

3 Evaporative Cooling

The laser-cooled atoms are cold but the cloud is too large for sufficient cooling through adiabatic expansion and not dense enough for efficient evaporative cooling, which requires a high elastic collision rate. The usual technique is to load atoms with the appropriate spin projection into a magnetic trap, then increase the strength of the trap adiabatically to produce a hot, tightly confined sample as shown in Fig. 1 and described in Ref. [8].

Application of a radio-frequency (RF) field then couples atoms at a particular trap radius to an untrapped state, with the radius determined by the RF frequency. By moving this RF “knife” in from the outer edge of the trap, the hottest atoms are removed, leaving behind the cooler atoms which rethermalize through elastic collisions. Successive application of RF of different frequencies results in a cold dense cloud.

4 Adiabatic Expansion

For the clock, we require a relatively low density and extremely low temperature. Both of these would follow from an adiabatic expansion in the magnetic trap, as represented in Fig. 2. As the trapping potential is reduced, the cloud expands and cools. In a harmonic potential, the temperature reduces as the square of the change

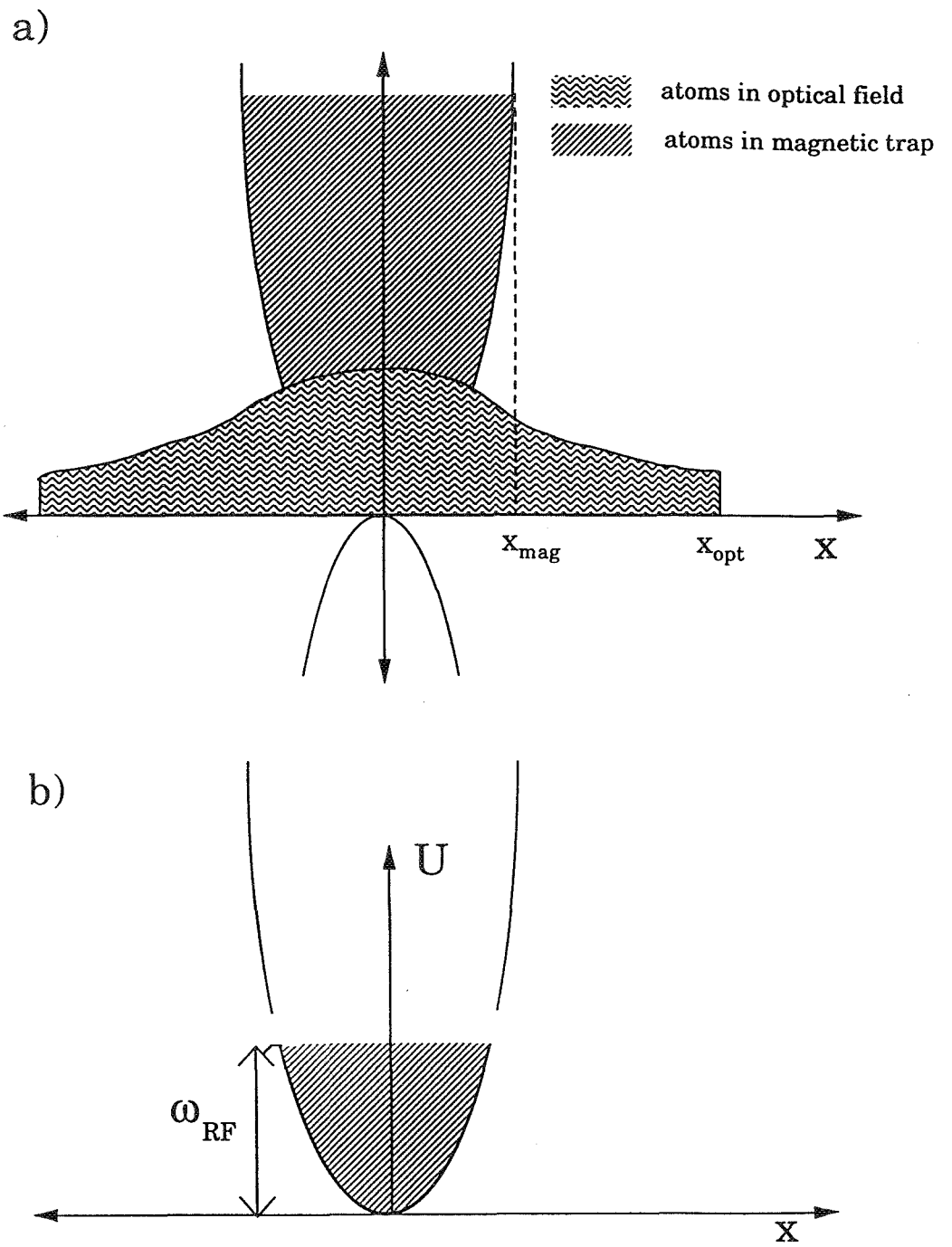


Figure 1: Magnetic trapping and evaporative cooling. In a), a low-density cloud of cold atoms gets trapped in a magnetic potential and then squeezed into a tight magnetic potential. Atoms with the wrong spin projection are ejected from the trap. In b), hotter atoms in the trap are connected to an untrapped spin state using an RF “knife.” The remaining atoms rethermalize to a cooler temperature.

in linear dimension of the cloud, or

$$\frac{T_f}{T_i} = \left(\frac{x_i}{x_f}\right)^2. \quad (1)$$

Since the atomic velocity scales as the square root of the temperature we recover the relationship

$$v_f = \frac{x_i v_i}{x_f}, \quad (2)$$

which is simply a statement of Liouville's theorem, or conservation of phase space in an adiabatic process.

For this expansion, adiabaticity requires that the change in trap depth occur slowly compared to the natural frequency of the trap. To minimize the expansion time, instead of weakening the trap adiabatically we could suddenly change to a trap which would just confine atoms with the desired final velocity of $7 \mu\text{m/s}$. This weak trap is turned off suddenly after one quarter oscillation, when the atoms are at the classical turning point of the trap. This is the reverse process of quarter-cycle magnetic focusing, leaving the atoms in the same final state as if the expansion had been adiabatic. The expansion time is then given by given by

$$t_{\text{exp}} \approx \frac{1}{4} \frac{2\pi}{\omega_f} = \frac{\pi x_f}{4 v_f}. \quad (3)$$

For our trap conditions this corresponds to an expansion time of 1100 seconds.

Notice that Eqn. 3 depends only on the final velocity, which was determined by the allowed expansion of the cloud for given averaging time, and the final size of the cloud, which was determined by our choice of atom number and density. Since the expansion process is effectively adiabatic combinations of initial velocity and position all result in equal expansion times for a desired final result, neglecting a correction proportional to $(x_i/x_f)^2$ which is only significant when very little expansion is required. For the low densities desired, it currently would be impossible to create the final state directly, so the long preparation time comes with the long observation time.

5 BEC considerations

One important consideration for such cold atoms is whether the sample will Bose condense, which would result in a sample with an undesirably high density. This

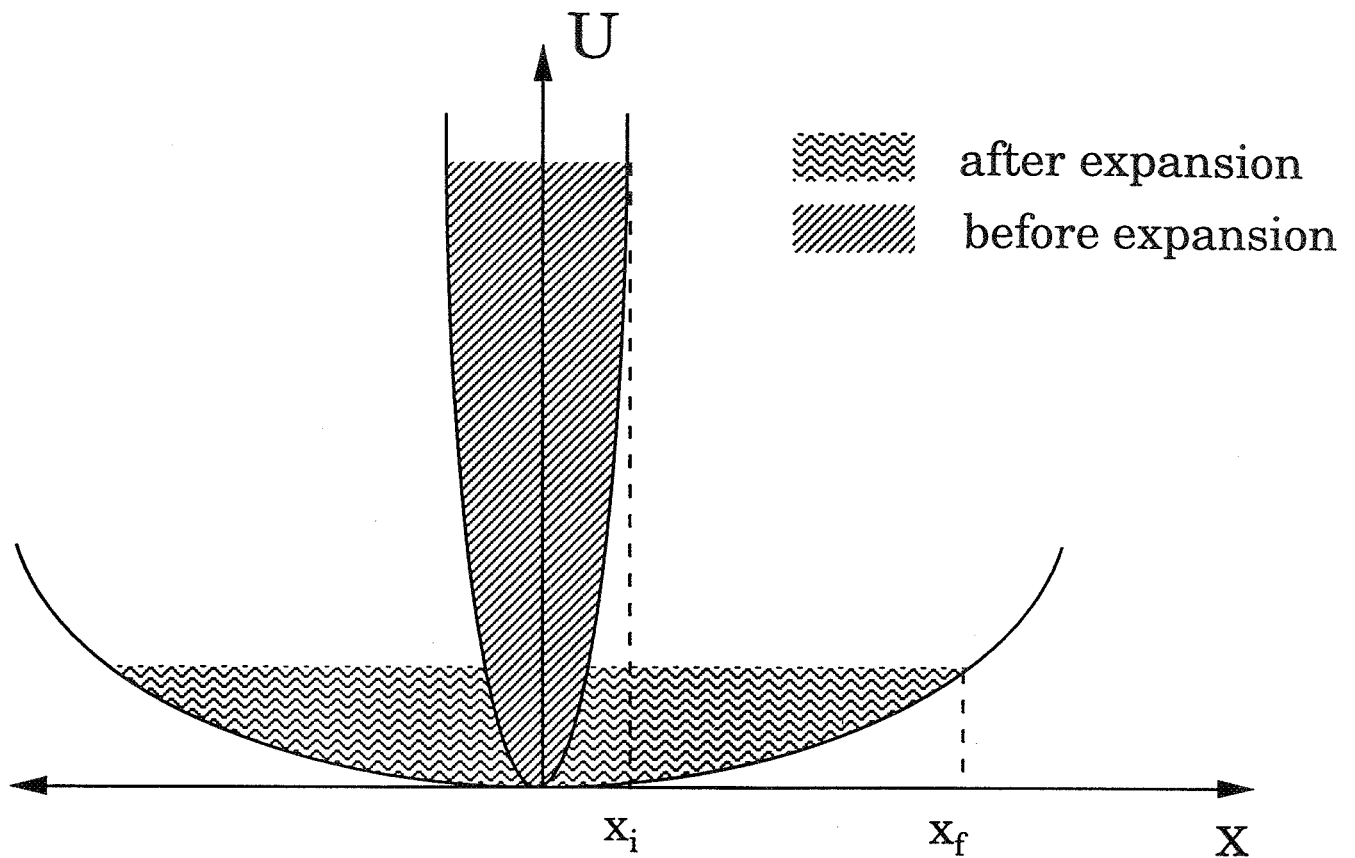


Figure 2: Adiabatic expansion in a magnetic trap. As the trap potential is reduced adiabatically, the cloud spreads out in space and cools.

issue is especially important for cesium, which appears to have a negative scattering length [9], indicating that atoms would be lost from the trapped sample. The threshold for Bose condensation occurs roughly when the thermal de Broglie wavelength of the atoms is equal to the inter-atomic spacing. More precisely, Bose condensation occurs when

$$n\lambda_{\text{dB}}^3 \geq 2.612. \quad (4)$$

Casting this relation in terms of the sample density and temperature and comparing to the threshold for BEC, a density of 10^4 cm^{-3} at a temperature of 1 pK gives

$$\frac{(nT^{-\frac{3}{2}})_{\text{clock}}}{(nT^{-\frac{3}{2}})_{\text{BEC}}} = \frac{1}{60}, \quad (5)$$

so the desired conditions are far from the BEC threshold.

6 Other Considerations

Since we have not described in any way the construction of a real clock, it would be meaningless to make any serious claims about systematic shifts, but it is interesting to note that for identical cavities, the effect of a distributed cavity phase shift, the different phase of the microwave field experienced by atoms at different locations in the microwave cavity, is reduced as the observation time is extended. Scaling the expected phase shift in a typical fountain cavity [10] to the larger size of our cloud, the phase shift increases by roughly a factor of four, but since this truly is a phase shift and not a frequency shift, the resulting shift in the observed frequency is reduced by three orders of magnitude by the longer interaction time. Such direct comparison is inappropriate since our scheme would require a dramatically different cavity design, but the reduction in importance of the phase shift would allow more flexibility in the design.

We had hoped that the long interaction time would lead to an interrogation duty cycle much greater than 50%, which is typical of atomic fountains, since this would reduce the periodic sampling noise known as the Dick effect [11]. In the proposed scheme, the expansion time always ends up being comparable to the observation time for a cloud which doubles in size, so realizing a clock of the imagined type would instead require a vastly improved local oscillator.

We have also glossed over the difficulty of magnetic trapping and evaporative cooling of the $m = 0$ state used in the clock transition. One possibility is to trap and cool atoms in a $m \neq 0$ state and then transferring them to the $m = 0$ state using RF transfer methods. A more elegant solution would be to trap and cool atoms in the $m = 0$ state directly using the second-order Zeeman shift. The field at the edge of the trap for 1 pK atoms would be $1 \mu\text{T}$, with an initial magnetic trap strength of 10 mT providing the strong confinement for evaporative cooling.

7 Summary

In the preceding pages, we have entertained an extension of current trends towards improving neutral-atom clocks through a reduction of atomic velocity. The performance potential of some future clock based on evaporative cooling and adiabatic expansion as described here would achieve a shot-noise limited sensitivity of $5.6 \times 10^{-15} / \sqrt{\tau(s)}$. However, due to the long preparation time the system would only begin reporting at 2000 seconds and would require the use of 2×10^4 atoms. Even with the increase

in number of atoms, collisional shifts will be held to $\frac{\Delta\nu}{\nu} < 10^{-17}$ since the average density of the cloud is reduced by the expansion.

This work was supported by the Office of Naval Research.

References

- [1] M.H. Anderson, *et al.*, *Science* **269**, 198 (1995); K.B. Davis, *Phys. Rev. Lett.* **75**, 3969 (1995); C.C. Bradley, *et al.*, *Phys. Rev. Lett.* **75** 1687 (1995).
- [2] For example, *Proceedings of the International School of Physics*, “Laser Manipulation of Atoms and Ions,” (North Holland Press, New York, 1992).
- [3] K. Gibble, S. Chang, and R. Legere, *Phys. Rev. Lett.* **75**, 2666 (1995).
- [4] A. Kastberg, *et al.*, *Phys. Rev. Lett.* **74**, 1542 (1995).
- [5] This number comes from scaling the results in sodium as reported in N. Davidson, H-J. Lee, M. Kasevich, and S. Chu, *Phys. Rev. Lett.* **72**, 3158 (1994).
- [6] This number comes from scaling results in metastable helium as reported by J. Lawall, *et al.*, *Phys. Rev. Lett.* **75**, 4194 (1995). Metastable helium is a much more favorable system for this cooling technique.
- [7] J. Reichel, *et al.*, *Phys. Rev. Lett.* **75**, p. 4575–9 (1995).
- [8] N. Masuhara *et al.*, *Phys. Rev. Lett.* **61**, 935 (1988).
- [9] B. Verhaar, K. Gibble, and S. Chu, *Phys. Rev. A* **48**, R3429 (1993).
- [10] A. Khursheed, G. Vecchi, and A. De Marchi, *IEEE Trans. on Ultrasonics, Ferroelectrics, and Freq. Control* **43**, p. 201–10 (1996).
- [11] J. Dick, *Proc. of Precise Time and Time Interval Workshop*, p. 133–147 (1987).

Future Laser-Cooled Microwave Clock Performance

Kurt Gibble, Sloane Physics Laboratory, Yale University, New Haven, CT 06520-8120

Limitations to the performance of laser-cooled earth and space-based Cs clocks will be critically discussed. The most significant limitation to the stability and accuracy of laser-cooled atomic clocks is the frequency shift due to cold collisions. Because of it, laser-cooled Cs clocks must be operated at low density and this implies that space based Cs clock performance will not be significantly better than earth based. To regain some of the high accuracy and stability lost to the low density, clocks can be designed to multiply launch (or *juggle*) atoms. Clocks based on other atoms, in particular ^{87}Rb or possibly ^{85}Rb , may have much smaller cold collision frequency shifts and therefore be capable of higher stability and accuracy, especially in a space environment.

The wave nature of atoms at μK temperatures implies scattering cross sections can be much larger than room temperature cross sections. In laser-cooled atomic clocks the scattering produces frequency shifts that can be large.¹ In a Cs fountain clock, the frequency shift cross section is -10^6 \AA^2 which produces a frequency shift of -1.6×10^{-12} at an atomic density of 10^9 cm^{-3} .² Of course it can be suppressed by reducing the atomic density but this compromises the stability of the clock. In this paper, we examine the potential performance of space based laser-cooled clocks and potential techniques to improve their accuracy and stability.

Microgravity Clock Designs

The atomic fountain³ is clearly an ideal technique for earth-based laser-cooled clocks.^{2,4,5} Of course, an atomic fountain will not work in μ -gravity. There are a number of possible designs and we discuss 3 of these below.

Probably the most sensible design for a μ -Gravity clock is simply a laser-cooled version of the present room-temperature atomic beam clocks.⁶ These have a "Ramsey cavity" which allows atoms to pass through 2 microwave cavities - these cavities are separated by a section of waveguide into which the microwave probe signal is injected. At one end of this microwave cavity would be a laser-trap that would launch atoms through the 2 microwave cavities. After passing through the cavities, there is a detection region where the internal state of the atom is detected by pulsing a laser beam and detecting the scattered fluorescence.

The principal advantage of μ -gravity for laser-cooled atomic clocks is a long interaction time with the atoms. We expect a μ -gravity clock will have an interaction time of $T \approx 50 \text{ s}$ giving a 10 mHz atomic transition linewidth. At first glance it seems that the

long interaction time compromises the short term stability of the clock. In a single measurement, the atoms are used to measure the frequency of the local oscillator within $\delta\nu/\nu = \Delta\nu/(\pi \nu S/N)$ where $\Delta\nu$ is the atomic linewidth, ν is the transition frequency, and S/N is the signal-to-noise ratio. If the clock is shot-noise limited, then $S/N = N$ where N is the number of detected atoms. As T increases, N scales as T^{-2} in a beam clock because the atoms spread more for longer T so that fewer pass through the opening in the second microwave cavity. Therefore S/N scales as T^{-1} and, since $\Delta\nu = 1/2T$, the instability after a single measurement is independent of T . However, because the short term stability is the product of the single measurement instability and the (measurement rate) $^{-1}$, the instability apparently increases for longer T . This is a serious problem if we expect the μ -gravity clock improvements in accuracy to be realized within the same averaging time - clock designs that simultaneously realize improvements in accuracy and stability are most attractive.

Multiply launching atoms enables a high stability while retaining the accuracy advantages of a long interaction time.⁷ Instead of launching 1 ball of atoms at a time, balls can be easily launched at a rate R as fast as 30 s^{-1} . The short term stability is then $\delta\nu/\nu = \Delta\nu/(\pi \nu S/N) R^{-1}$. For $T = 50 \text{ s}$, multiply launching at a rate $R = 5 \text{ s}^{-1}$ improves the short term stability by a factor of 16.

In most satellite clocks there is a trade-off of size and weight versus performance. Here, to achieve the high stability potential, atoms can be launched between 1 and 30 times a second even though it takes 10 to 50 s to traverse the cavity. The trade-off of size versus performance arises because the lasers used for trapping disturb the free flight of the atoms through the clock. One way to deal with this is to use a pair of rotary shutters to block the light.⁸ However, this implies that after the atoms are launched, they must clear the shutter before another ball of atoms can be launched. So, if atoms are launched at 5 s^{-1} and the shutter region occupies 1 cm, the atoms must be launched at 5 cm/s. If an interaction time of $T = 10 \text{ s}$ is used, the Ramsey cavity must be 0.5 m in length. On the other hand, at 1 launch per second, only 10 cm is required. Of course, if a 50 s interaction time is desired, then for 1 launch per second, a 50 cm length is required. From Eq. (1) we can calculate the relative performance of these 3 cases:

Interaction Time T	Launch Rate R	Cavity Length L	Short Term Stability
10 s	5 s^{-1}	0.5 m	$1 \times 10^{-15} \tau^{-}$
10 s	1 s^{-1}	0.1 m	$2 \times 10^{-15} \tau^{-}$
50 s	1 s^{-1}	0.5 m	$2 \times 10^{-15} \tau^{-}$

where τ is the averaging time in seconds.

Here, several points should be emphasized about μ -Gravity clocks:

- 1) The averaging time required to achieve a desired accuracy is simply proportional to the square root of the launch rate. The stability is independent of T and L.
- 2) The length of the microwave cavity is proportional to the launch rate, interaction time, and diameter of the ball of atoms.
- 3) There is no gain in stability for interaction times longer than ≈ 10 s but accuracy improves.
- 4) For higher launch rates, less performance is required from the reference flywheel oscillator.
- 5) For very high launch rates, some systematic errors increase. The c-field and microwave power are proportional to R but the problems these create should not be limitations for $R \approx 5 \text{ s}^{-1}$.

It is clear the exact details of the design will depend upon the particular goals and the space platform. For comparison, the latest earth-based room-temperature clock, NIST-7, has a stability of $\approx 5 \times 10^{-13} \tau^{-}$ and a Cs fountain with an ultracold shift of 10^{-15} has a demonstrated stability of $10^{-13} \tau^{-}$.⁵ Therefore, the μ -Gravity version should be 100 times more accurate and require an averaging time 10^4 times shorter to achieve a given precision.

Another μ -Gravity design traps the atoms in a single cavity. This simple design precludes the higher stability possible with multiple launches and makes efficient detection of the atoms challenging.

A more creative design is a "space fountain" where the atoms are trapped at rest and the microwave cavity moves instead. Here, the diode lasers, the microwave cavity, and cold atom source are mounted on a miniature *boom-arm* which swings the lasers, cavity, and source in a circle at 1 revolution per 10 to 50 seconds. Thus, atoms would be trapped at one spot, the cavity would swing through the ball of atoms delivering a $\pi/2$ (or $\pi/5$) pulse, the arm would rotate through the rest of the circle trapping ≈ 300 balls of atoms, and

then swing around to drive the final $\pi/2$ pulse and detect the atomic state. Again there are trade-offs. Matching the performance of 30 launches per second of an earth fountain and using $T=10$ s requires a ≈ 1 m boom-arm. For shuttle or space station missions this novel design offers phenomenal stability and accuracy while retaining all the features of an earth-based fountain at the price of significantly more complexity. However, free flying satellites are typically spun at several RPM. While a laser-cooled beam clock will most likely need to be de-spun, a space fountain may be able to take advantage of the rotation.

Rb versus Cs Clocks

Because the cold collision frequency shift is so large in a laser-cooled Cs clock, a clock based on Rb may offer much better accuracy and stability. The ratio of the maximum possible stability in a μ -Gravity Rb or Cs clock can easily be calculated. In the regime where these would be operated, the S/N is limited by the shot-noise so that $S/N = N^{-1/2}$. For measurement times longer than ≈ 10 s, $N = \pi/3 N_{\text{trap}}/(u T)^2 (\lambda_{\mu}/5)^2$ where N_{trap} is the number of trapped atoms, u is the atomic velocity, and $\lambda_{\mu}/5$ is the diameter of the hole in the microwave cavity. Substituting $u=4.8 v_{\text{rec}} = 4.8 h/(m \lambda_{\text{opt}})$ which is the minimum laser-cooled velocity achieved with 6 beam molasses,⁹ from a Fourier transform, $\Delta v = 1/2T$, we get:

$$\frac{\delta v}{v} = \frac{6h}{c} \frac{1}{\lambda_{\text{opt}} m N_{\text{trap}}^{1/2}}$$

Here we see the stability does not depend on the transition frequency in a μ -Gravity clock. This occurs simply because more atoms can get through the larger microwave cavity for a lower frequency and because, for long enough T , the clock is always shot-noise limited. Therefore, the stability of a μ -Gravity Rb clock is worse than a Cs's by the ratio of $(\lambda_{\text{opt}} \times m)$ which is 1.7. However, it may be possible to operate a Rb with no ultracold collision shift allowing a higher atom density and therefore greater stability.

The principle problem for earth-based Rb clocks is the transition Q. Here the problem is that $\Delta v = 1/2T$ and T is limited to ≈ 0.5 s due to gravity. Therefore, to achieve $\delta v/v = 10^{-16}$ in ^{137}Cs , the center of a $\Delta v=1$ Hz line must be determined to 1 μHz . For ^{85}Rb ,

which has a 3.035 GHz transition, the center must be determined to 300 nHz. While this difference is not overwhelming in light of the ultracold collision shift, the motivation for exploring μ -gravity Rb clocks is perhaps more compelling than for earth-based fountains.

Eliminating Cold Collision Frequency Shifts

Rb may be a particularly attractive atom if it is possible to completely eliminate the shift in a clock based on Rb. We have proposed¹⁰ to use population differences to cancel the shift.¹¹ For example, if in an ^{87}Rb clock the atomic population in the $F = 2$ $m_F=0$ state, n_2 , produces a frequency shift $\Delta\nu_2 = 1$ mHz for $n_2=10^9$ cm^{-3} and the population in the $F=1$ $m_F=0$ state, n_1 , produces a frequency shift $\Delta\nu_1 = -10$ mHz for $n_1=10^9$ cm^{-3} , then the frequency shift $\Delta\nu = n_1 \Delta\nu_1 + n_2 \Delta\nu_2$ can be eliminated if $n_2/n_1 = 10$. The population ratio n_2/n_1 is easily controllable by adjusting the microwave intensity in the cavity on the first (upward) pass through the cavity to drive a $\pi/5$ pulse instead of a $\pi/2$ pulse.

Exciting with less than a $\pi/2$ pulse obviously affects the clock's performance. One can easily show that the atomic frequency discrimination signal is maximal when the second pass through the cavity drives a $\pi/2$ pulse. The size of the signal, or the Ramsey fringe contrast, is $2p/(1+p)$ where p is the population ratio n_2/n_1 . This technique is viable because the contrast does not decrease rapidly for $p \neq 1$. For $p=2$ the fringe contrast is 94% and for $p=14$ the contrast is 50%. Driving less than a $\pi/2$ pulse does increase the effect of cavity pulling and the sensitivity to microwave intensity fluctuations on the second passage through the cavity (the $\pi/2$ pulse).

In the operation of such a clock, it will still be important to continuously perform an $n \rightarrow 0$ extrapolation. Here, the microwave amplitude for the upward passage will be stabilized to produce no cold-collision frequency shift. This is more attractive than the previous $n \rightarrow 0$ extrapolation because here one need only change the density to see that $\Delta\nu_{\text{Coll}} = 0$ versus needing accurate density ratios as in Ref. 2.

Unfortunately, this technique does not work for ^{133}Cs since the frequency shifts for the 2 clock states are both negative.¹² We have recently shown that the technique will work for ^{137}Cs and may work for ^{135}Cs .¹⁰ To calculate the shifts for these isotopes it was necessary to derive the Cs-Cs potential from our measured cold-collision frequency

shifts.¹² The determination of the Cs-Cs potential from the frequency shifts is also useful for other experiments - here it led to the first prediction of an alkali s-wave scattering length which is crucial for the stability of Bose condensed gases. While the determination of the potential is nearly 2 orders of magnitude better than that which can be done with RKR methods, it is still not sufficiently accurate to predict the prospects for a ¹³⁵Cs clock.¹⁰ While a ¹³⁷Cs clock can be operated with no shift, it is too radioactive to be used in a standard laser-cooled clock apparatus. We are currently pursuing a measurement of the frequency shifts in ⁸⁷Rb. The shifts must be measured because the Rb-Rb potentials are not known well enough to be able to calculate the shifts. Since the frequency shifts are cancelable over a wide range of frequency shifts as long as the 2 clock states produce opposite frequency shifts, one of the Rb isotopes is likely to allow the full stability and accuracy potential of a laser-cooled clock.

Acknowledgments

We acknowledge discussions with Boudewijn Verhaar and support from NASA, a NIST Precision Measurement Grant, and a NSF National Young Investigator award.

References

- ¹ E. Tiesinga, B. J. Verhaar, H. T. C. Stoof, and D. van Bragt, *Phys. Rev. A* **45**, 2671 (1992).
- ² K. Gibble and S. Chu, *Phys. Rev. Lett.* **70**, 1771 (1993).
- ³ M. A. Kasevich, E. Riis, S. Chu, and R. G. DeVoe, *Phys. Rev. Lett.* **63**, 612 (1989).
- ⁴ A. Clairon, C. Salomon, S. Guellati, and W. D. Phillips, *Europhys. Lett.* **16**, 165 (1991).
- ⁵ S. N. Lea, A. Clairon, C. Salomon, P. Laurent, B. Lounis, J. Reichel, A. Nadir, and G. Santarelli, *Phys. Script.* **51**, 78 (1994).
- ⁶ See C. Audoin, *Metrolog.* **29**, 113 (1992).
- ⁷ "Collisional Effects in Cold Alkalis," K. Gibble, in *Proceeding of the Fifth Symposium on Frequency Standards and Metrology*, J. C. Bergquist Ed., (World Scientific, Singapore, p. 66, 1996).
- ⁸ In Christophe Salomon's paper, another technique is suggested where a number of balls are launched and then the lasers are turned off while these travel through the clock.
- ⁹ K. Gibble, S. Chang, and R. Legere, *Phys. Rev. Lett* **75**, 2666 (1995).
- ¹⁰ K. Gibble and B. J. Verhaar, *Phys. Rev. A* **52**, 3370 (1995).
- ¹¹ Another possibility is to use a fermion such as ¹³⁴Cs or metastable ¹²⁹Xe. These have no s-wave shift and also have essentially no Rabi or Ramsey line pulling.
- ¹² B. J. Verhaar, K. Gibble, and S. Chu, *Phys. Rev. A* **48**, 3429 (1993).

Rotation Sensing with an Atom Interferometer Gyroscope

T. L. Gustavson¹, P. Bouyer², and M. A. Kasevich¹

¹*Department of Physics, Stanford University, Stanford, California, 94035*

²*Institut d'Optique, Orsay, France*

We have recently demonstrated an atom interferometer gyroscope with a short-term sensitivity of 2×10^{-8} rad/sec/ $\sqrt{\text{Hz}}$. This performance is comparable with state-of-the-art optical gyroscopes. We have used this gyroscope to measure the rotation rate of the Earth. Straight forward improvements could bring this sensitivity to better than 10^{-9} rad/sec/ $\sqrt{\text{Hz}}$ and dramatically reduce long term drift.

Matter-wave interferometry has the potential to be an extremely sensitive probe for inertial forces. For example, neutron interferometers have been used to measure the rotation of the Earth [1] and the acceleration due to gravity [2]. More recently, atom interference techniques have been used in demonstration experiments to measure rotations [3] and accelerations [4]. We have demonstrated a Sagnac effect atom interferometer gyroscope which uses stimulated Raman transitions to coherently manipulate atomic wavepackets. We have used this gyroscope to measure the Earth's rotation rate and have characterized its short-term stability.

In the Sagnac geometry [5], rotation induces a phase shift $\Delta\phi$ between two interfering propagation paths. For a Sagnac loop enclosing area \mathbf{A} , a rotation $\mathbf{\Omega}$ produces a shift

$$\Delta\phi = \frac{4\pi}{\lambda v} \mathbf{\Omega} \cdot \mathbf{A}, \quad (1)$$

where λ is the particle wavelength and v its velocity [6,7]. Thus the inherent sensitivity of a matter-wave gyroscope exceeds that of a photon-based system by a factor of $mc^2/\hbar\omega \sim 10^{11}$ (m is the particle mass, ω the photon frequency). Although optical gyroscopes have higher

particle fluxes and larger enclosed areas, atom-based systems should still out-perform optical systems by several orders of magnitude.

With the Raman method, two laser beams of frequency ω_1 and ω_2 are tuned to be nearly resonant with an allowed optical transition. Their frequency difference $\omega_1 - \omega_2$ is chosen to be resonant with a microwave transition between two atomic groundstate levels. Under appropriate conditions, the atomic population Rabi flops between the groundstate levels with a rate proportional to the product of the two single-photon Rabi frequencies and inversely proportional to the optical detuning. When the beams are aligned to counter-propagate, a momentum exchange of approximately twice the single photon momentum accompanies these transitions. This leads to a strong Doppler sensitivity of the two-photon transition frequency, and can be used to coherently divide (with a $\pi/2$ pulse) or deflect (with a π pulse) atomic wavepackets. (On the other hand, when the beams are aligned to co-propagate, these transitions have a negligible effect on the atomic momentum, and the transition frequency is Doppler insensitive.) A Mach-Zehnder type interferometer is formed using a $\pi/2$ - π - $\pi/2$ pulse sequence to coherently divide, deflect and finally recombine atomic wavepackets. The resulting interference can be directly observed by measuring the atomic groundstate populations [8].

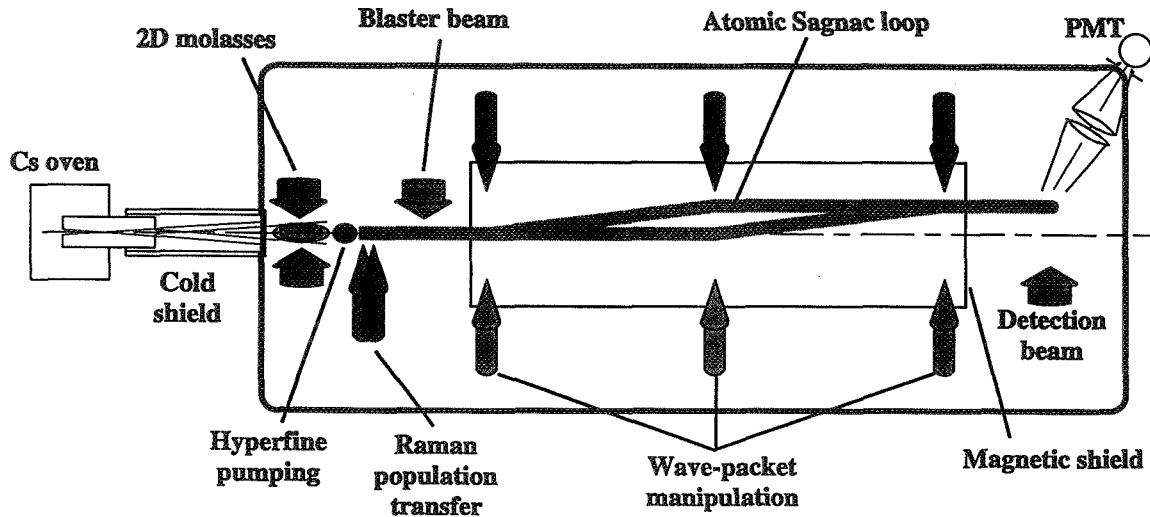


FIG. 1. Schematic illustration of the gyroscope

Our experimental apparatus is illustrated in Fig. 1. We generate a high brightness atomic beam by transversely laser cooling an effusive Cs source. Following the laser cooling, atoms are optically transferred into the Cs $F=3$, $m_f = 0$ level before entering the magnetically shielded interrogation region. Interference is manifested through the number of atoms in the $F=4$, $m_f=0$ level after the $\pi/2$ - π - $\pi/2$ pulse sequence. The resulting Sagnac loop has an area of 22 mm^2 . This corresponds to a fringe shift of ~ 8 rad for the Earth's rotation rate $\Omega_e = 7 \times 10^{-5} \text{ rad/sec}$. Our signal-to-noise was good enough to split the fringe by ~ 1 part in 500 after 1 second of data collection time. We have suppressed gravitationally induced phase shifts by aligning the Raman beams to be perpendicular to the local acceleration due

to gravity.

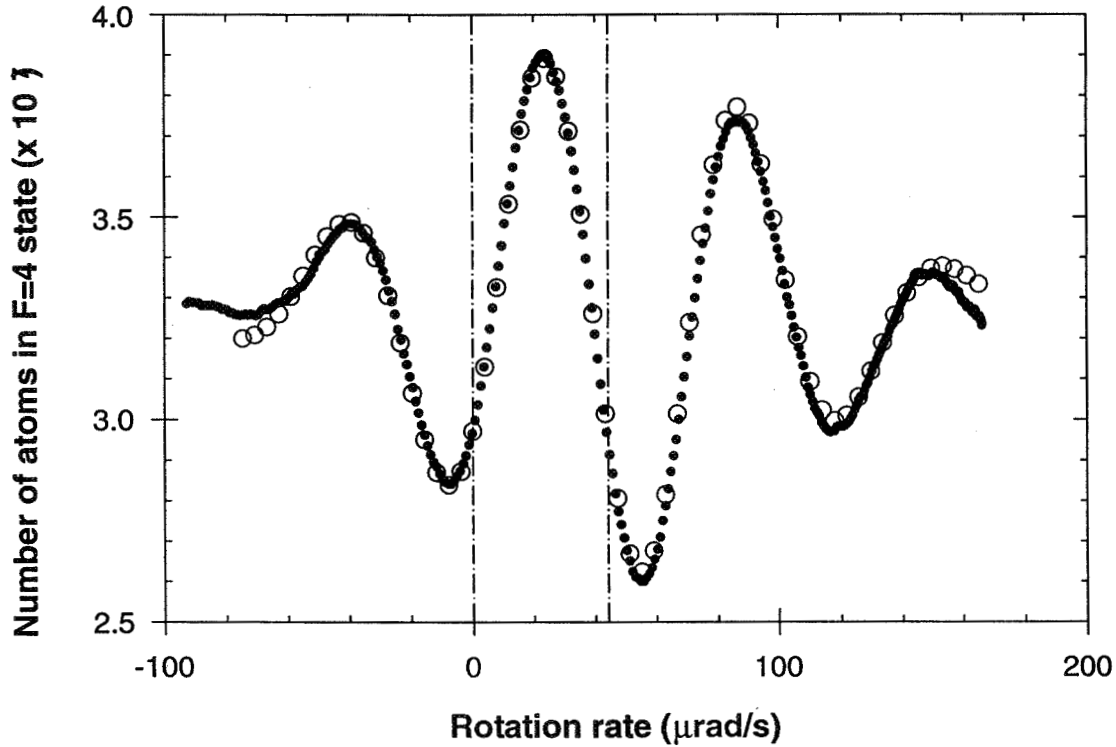


FIG. 2. Gyroscope interference signal. Dots: experiment. Open circles: theoretical model.

The ~ 2 m long UHV vacuum chamber was mounted just above a floating optical table. Care was taken to minimize vibrational coupling between the table and the chamber. The optical table contained the optics and laser system used for the wavepacket manipulation as well as for the laser cooling. In order to observe interference fringes the entire optical table was made to rotate by driving horizontal table rotational modes. This was done with a PZT which was attached at one end to the floating table, and on the other end to an independent platform just next to the optical table. The induced rotation rate was independently measured with a seismometer located on the table top. Fig. 2 shows the

number of detected atoms in an 800 msec interval vs. the induced rotation rate. Note that the center of the contrast envelope is offset from the zero rotation rate inferred from the seismometer. This offset arises because the seismometer is not sensitive to low frequency excitations such as those arising from the rotation of the Earth. The gyroscope, on the other hand, is. Accurate measurement of this offset allows for determination of the Earth's rotation rate.

The loss of contrast at high rotation rates is due to the averaging of the Sagnac phase shift over the longitudinal velocity spread of the atomic beam. We have calculated the expected signal given our measured longitudinal and transverse atomic beam velocity distribution, as shown by the open circles in Fig. 2. This calculation also accounts for an arbitrary initial optical phase offset for the Raman laser beams. This phase offset, which was not controlled in our experiment, determines the location of the interference fringes within the contrast envelope.

We developed a new laser system to drive the stimulated Raman transitions needed for wavepacket manipulation [9]. The stimulated Raman method requires two high power laser beams which differ in frequency by 9.2 GHz, the cesium clock frequency. Our approach has been to derive these two beams from a master diode laser and a high frequency acousto-optic modulator, and then to amplify these two beams using optical injection locking techniques. A key issue is whether the amplification process introduces low frequency phase noise. By driving the Cs clock transition in the classic Ramsey configuration, we characterized the phase noise in the 1 - 100 Hz band, and demonstrated that these sources can be used for precision measurements.

We are presently seeking to improve both the short term and long term stability of the apparatus. There are three directions we will pursue to improve short term stability: (i) increased atom flux, (ii) improved wavepacket manipulation techniques and (iii) a longer apparatus. The increased signal-to-noise that comes with a higher atomic flux will improve overall sensitivity simply by allowing more accurate determination of the fringe center. An improved design of our atomic beam oven should provide us with a gain of $\sim 10^4$ in atomic

flux, improving the shot-noise limit by at least a factor of 100. (We are using resonance fluorescence to detect the atoms and our signal-to-noise is currently limited by photon shot-noise due to stray light from the fluorescent probe beam.)

In making this improvement we have drawn on the experience of the Cs clock community. Our new oven design involves a combination of a recirculating "dark-wall" tube, followed by a hot "bright-wall" collimating section. This two stage design provides beam collimation sufficient to minimize contamination of the vacuum system due to background Cs atoms. Although higher brightness can be achieved using multi-channel nozzles, we feel that these gains would not significantly enhance the signal-to-noise, which will probably be limited by electronic technical noise at the $10^5:1$ level.

We are also exploring methods which increase the Sagnac phase shift $\Delta\phi$ by increasing the area A of the Sagnac loop. The most straightforward approach is simply to make the apparatus longer. Since gyroscope area scales with the length of the apparatus squared, a five-fold increase in length (from 2 m to 10 m) increases sensitivity by a factor of 25. Area can also be increased through improvements in the atom beamsplitters. We anticipate a gain of another factor of two by using higher order optical processes to manipulate the atomic wavepackets.

To summarize this discussion of short term stability, we estimate the sensitivity which might be achieved if all three of the above ideas are successfully implemented. If we improve signal-to-noise to $10^5:1$ in 1 second, run with a higher order beamsplitter, and increase the length to 10 m, the short term stability will be $\sim 10^{-9}$ deg/ $\sqrt{\text{hr}}$ or $\sim 10^{-12}$ rad/sec/ $\sqrt{\text{Hz}}$. On the other hand, a 0.5 m apparatus would have a $\sim 5 \times 10^{-7}$ deg/ $\sqrt{\text{hr}}$ sensitivity, opening the avenue to a compact portable unit.

We also need to characterize and improve the long term drift. The current limit to long term stability is phase fluctuations of the Raman field induced by air currents. Although we have enclosed the beams in tubes to minimize this effect, we will further reduce the fluctuations by (i) reducing the propagation distance along certain key optical paths and (ii) having the beams propagate through a low vacuum enclosure.

Long term drift will also be improved through installation of a second, counter-propagating, atomic beam. This beam will be aligned to interact with the same set of wavepacket manipulation beams. The basic idea is that many systematic phase shifts do not depend on the velocity of the atoms. These shifts will cancel if the interference signals from both atomic beams are measured simultaneously and then subtracted. On the other hand, the Sagnac phase shifts reverse with velocity, hence will add in the common mode rejection processing.

We can estimate the effectiveness of this procedure. Systematic phase shifts of the Raman light field which take place on a time scale comparable with the atoms transit time in the apparatus will not cancel. In our present set-up, the transit time is ~ 10 msec. Currently, air currents change the optical path length by $\lambda/10$ in 10 sec (where λ is the wavelength of the laser light used for the Raman transitions). The phase drift in the transit time, then, is roughly $\delta\phi \sim 2\pi \times 10^{-4}$ rad. This would amount to a systematic rotation error of $\sim 7 \times 10^{-9}$ rad/sec. Ultimately, we expect optical path length to be limited by the stability of the optical mounts used to steer the beams. One might expect this to approach $\lambda/10$ in a day, perhaps better if room temperature is actively controlled. This would lead to a stability of $\sim 10^{-7}$ deg/hr or $\sim 10^{-12}$ rad/sec.

-
- [1] R. Colella, A. Overhauser, and S. Werner, *Phys. Rev. Lett.* **34**, 1472 (1975).
- [2] S. A. Werner, J.-L. Staudenmann, and R. Colella, *Phys. Rev. Lett.* **42**, 1103 (1979).
- [3] F. Riehle *et al.*, *Phys. Rev. Lett.* **67**, 177 (1991).
- [4] M. Kasevich and S. Chu, *Appl. Phys. B* **54**, 321 (1992).
- [5] M. Sagnac, *Compt. Rend. Acad. Sci.* **157**, 708 (1913).
- [6] Ch. J. Bordé, in *Laser Spectroscopy X*, edited by M. Ducloy, E. Giacobino, and G. Camy (World

Scientific, Singapore, 1992), pp. 239-245.

[7] P. Storey and C. Cohen-Tannoudji, *J. Phys. II France* **4**, 1999 (1994).

[8] M. Kasevich and S. Chu, *Phys. Rev. Lett.* **67**, 181 (1991).

[9] P. Bouyer, T. Gustavson, K. Haritos, and M. Kasevich, *Opt. Lett.* **21**, 1502 (1996).

Session IV

Planetary and Space Science Applications

Trends in Performance and Characteristics of Ultra-Stable Oscillators for Deep Space Radio Science Experiments

Sami Asmar

Jet Propulsion Laboratory, California Institute of Technology

sami.asmar@jpl.nasa.gov

Introduction:

Telecommunication systems of spacecraft on deep space missions also function as instruments for Radio Science experiments. Radio scientists utilize the telecommunication links between spacecraft and Earth to examine very small changes in the phase/frequency, amplitude, and/or polarization of radio signals to investigate a host of physical phenomena in the solar system. Several missions augmented the radio communication system with an ultra-stable oscillator (USO) in order to provide a highly stable reference signal for one-way downlink. This configuration is used in order to enable better investigations of the atmospheres of the planets occulting the line-of-sight to the spacecraft; one-way communication was required and the transponders' built-in auxiliary oscillators were neither sufficiently stable nor spectrally pure for the occultation experiments. Since Radio Science instrumentation is distributed between the spacecraft and the ground stations, the Deep Space Network (DSN) is also equipped to function as a world-class instrument for Radio Science research. For a detailed account of Radio Science experiments, methodology, key discoveries, and the DSN's historical contribution to the field, see Asmar and Renzetti (1993). The tools of Radio Science can be and have also been utilized in addressing several mission engineering challenges; e.g., characterization of spacecraft nutation and anomalous motion, antenna calibrations, and communications during surface landing phases.

Since the first quartz USO was flown on Voyager, the technology has advanced significantly, affording future missions higher sensitivity in reconstructing the temperature-pressure profiles of the atmospheres under study as well as other physical phenomena of interest to Radio Science. This paper surveys the trends in stability and spectral purity performance, design characteristics including size and mass, as well as cost and history of these clocks in space.

Science Overview:

Almost every deep space mission conducted successful Radio Science experiments, which are typically divided in two classes: propagation and celestial mechanics & gravitation,

resulting in hundreds of journal publications. Examples of these experiments include: planetary atmospheric temperature-pressure profiles and ionospheric composition, structure of planetary rings, planetary gravitational fields, shapes, and masses, planetary surface characteristics, wind profiles, magnetic fields, electron content and scintillation in solar corona and solar wind, mass flux and particle distribution of comets, search for gravitational radiation, gravitational redshift, and relativistic time-delay experiments. Stable one-way downlink is essential to propagation experiments, although several aspects can be accomplished via two-way coherent links, as well as to redshift and wind profile experiments. In addition to the completed experiments to date (e.g., Mariner(s), Pioneer(s), Voyager(s), Galileo, Ulysses, Magellan, etc.), there are important planned experiments on upcoming missions (e.g., Cassini-Huygens mission to Saturn and Titan), and possible future experiments with missions in the planning stages (e.g., Pluto Express, Rosetta, Discovery missions, etc.). For a list, see Asmar et. al. (1995).

Instrumentation:

The elements of the instrumentation required for Radio Science experiments vary in complexity depending on the sophistication of the experiments (Asmar and Kursinski, 1991). They include transponders (which are available on every deep space mission although some missions have considered transceivers), an attitude control system that provides for a “quiet” spacecraft, an Ultra-Stable Oscillator, translators that are needed for coherent transmission of signals not used by the primary transponder (e.g., Ka-band for the Cassini mission), and uplink signal processing equipment for proposed uplink radio occultation experiments.

With this instrumentation, the fundamental limits on sensitivity of the end-to-end system are the frequency stability, amplitude stability, signal to noise ratio, accuracy in reconstructing navigation trajectories, and media propagation effects. The frequency stability of the one-way link is typically limited by the performance of the USO.

Ultra-Stable Oscillators:

The “ultra-stable” class of oscillators have been flown on Voyager I and II, Galileo orbiter, Galileo Probe, Mars Observer, and Mars Global Surveyor. These have been quartz crystal resonators. The Cassini spacecraft will carry another quartz USO and two Rubidium USOs for the Huygens Probe in support of the Doppler Wind Experiment. There are plans to fly USOs on several other future missions.

Needed to eliminate the time needed by the transponder to lock-up on the uplink during an occultation egress as well as the media effect on the uplink, USOs become the heart of the Radio Science instrumentation on-board the spacecraft. Quartz crystal resonators, relatively small in mass, volume, and power, have been easier to “space-qualify” than atomic clocks. The latter are also being considered for space flight.

The USO technology can be divided into these design classes:

1. Voyager Class: includes Voyager I and II and Galileo orbiter
2. Mars Class: Includes Mars Observer, Mars Global Surveyor, and Cassini
3. Pluto Class
4. Huygens Class
5. Galileo Probe Class

In the first class, five identical units were procured at the same time, two flew on the Voyagers, one on Galileo, and two were spares (Morabito et. al., 1993). In the second class, a flight unit and a spare were procured, one flew on Mars Observer and the refurbished spare flew on Mars Global Surveyor. A flight unit and a spare of a similar design were later procured for the Cassini mission. In the third class, a new "tactical BVA" design is proposed for flight on the Pluto Express mission; it shows significant reduction in mass and size without compromising the performance demonstrated by the Mars class (Norton and Cloeren, 1994).

The Huygens Rubidium USOs were chosen over quartz due to the need for a very short warm-up time and less stringent long-term stability. The Galileo Probe USOs had similar requirements but were chosen to be quartz oscillators; insufficient documentation is available on them. In the case of both probes (Huygens and Galileo Probe), one USO was on the probe as part of its transmitter chain (e.g., the Huygens TUSO) and a second identical unit was on the orbiter (Cassini and Galileo) as part of the receiving chain of the orbiter signal (e.g., Huygens RUSO).

The attached tabular summary of the Ultra-Stable Oscillator technology lists seven oscillators and several key parameters characterizing them, such as mass, size, power, performance measured by Allan deviation, phase noise, drift rates, environmental performance, etc. Cost information can be obtained from the providers.

In addition to serving as a historical summary for interested managers, scientists, and engineers, the table has two key areas to note. The first is the major improvement in the stability between the Voyager and Mars class oscillators - an order of magnitude in Allan deviation. The second area is the significant miniaturization proposed for the Pluto class oscillator.

Acknowledgments:

I thank Gordon Wood and Carole Hamilton (Jet Propulsion Laboratory) Mike Bird (University of Bonn), and David Atkinson (University of Idaho) and Mary Chiu and Jim Cloeren (JHU Applied Physics Laboratory) for the valuable information they provided. The work described here was carried out at the Jet Propulsion Laboratory, California Institute of Technology, under contract with the National Aeronautics and Space Administration.

References:

S. W. Asmar and N. A. Renzetti, "The Deep Space Network as an Instrument for Radio Science Research," JPL Publication 80-93, Rev. 1, Jet Propulsion Laboratory, Pasadena, California, April 15, 1993.

S. W. Asmar, R. G. Herrera, and T. Priest, "Radio Science Handbook," Document D-7938, vol. 6 (internal document), Jet Propulsion Laboratory, Pasadena, California, 1995.

D. D. Morabito, T. P. Krisher, and S. W. Asmar, "The Flight Performance of the Galileo Orbiter USO," IEEE Frequency Control Symposium, Salt Lake City, June 1993.

S. W. Asmar and E. R. Kursinski, "The Role of Clocks in Operating Deep Space Missions," Proceedings of the 23rd Annual Precise Time and Time Interval Applications and Planning Meeting, Pasadena, California, December 1991.

J. R. Norton and J. M. Cloeren, "Precision Quartz Oscillators and Their Use Aboard Satellites," Johns Hopkins APL Technical Digest, vol. 15, no.1, pp. 30-37, January-March 1994.

Ultra-Stable Oscillator Technology Information Summary

Sami Asmar, JPL, 1997

Deep Space Mission	<i>Voyager</i>	<i>Galileo</i>	<i>Mars Observer</i>	<i>Cassini</i>	<i>Pluto</i>	<i>Huygens</i>	<i>Galileo Probe</i>
Maker	Freq. Elect. Inc	Freq. Elect. Inc	APL	APL	APL	DASA, Germany	(Hughes contract)
Year	1975	1975	1987	1993	1994	1993	~ 1975
Type of Quartz Crystal Cut	AT	AT	SC	SC	SC	Rubidium	SC
Number of Ovens	2	2	1	1	1	2	2
Mass (kg)	1.1	1.1	1.3	2	0.32	2.1	?
Steady-State Power Consum.(W)	2.2	2.2	2.2	2.8	0.8	10.4	~ 1
Dimensions (cm LxWxH or DxL)	10.2x19.5	10.2x19.5	10.2x10.2x16.8	10.2x12.8x19.4	5.3x6.9x9.7	17x14.9x11.8	4.6x14
Resonator Frequency (MHz)	6.38	6.38	4.79	4.79	~10	6835	4.6
Nominal Output Freq. (MHz)	19.137	19.125	19.144	114.917	38.262	10.00	23.117
Assigned Deep Space Channel	18	14	20	23	16	23	n/a
USO-refer. Downlink Bands	S, X	S, X	X	S, X, Ka	X, Ka	S	1.387 GHz
Drift Rate (Hz/sec)	- 1.3 e-7	- 1.5 e-7	2.3 e-6	not avail.	not avail.	2 e-7	2 e-7
Aging/24 Hr	5 e-11	5 e-11	2 e-11	7 e-11	2 e-11	2 e-9	?
Long Term Aging /5 yrs	2 e-7	2 e-7	1 e-7	1 e-6	not avail	4 e-6	?
Temperature (/deg C)	5 e-12	5 e-12	3 e-12	2 e-12	1 e-12	4 e-12	3 e-12
Radiation (/rad)	2 e-12	2 e-12	1 e-10	1 e-10	1 e-10	2 e-14	2 e-13
Magnetic Susceptibility (/Gauss)	5 e-12	5 e-12	8 e-13	5 e-13	2 e-12	5 e-11	4 e-12
Static Acceleration (/g)	1 e-9	1 e-9	3 e-9	1 e-9	1.5 e-9	1 e-11	1 e-9
Harmonic Spur (dBc)	-40	-40	-60	-60	-50	-60	?
Phase Noise 1 Hz (dBc)	-100	-100	-110	-85	(-112)	-80	?
Phase Noise 10 Hz	-108	-108	-125	-110	(-117)	-90	?
Phase Noise 100 Hz	-118	-118	-131	-120	(-127)	-110	?
Phase Noise 1 kHz	-138	-138	-131	-125	(-132)	-120	?
Allan Deviation at 0.1 sec	(2 e-11)	(2 e-11)	2 e-12	1 e-12	1 e-12	6 e-11	?
Allan Dev. 1 sec	3 e-11	3 e-11	3 e-13	2 e-13	3 e-13	1 e-11	5 e-12
Allan Dev. 10 sec	4 e-12	4 e-12	1 e-13	1 e-13	1 e-13	5 e-12	?
Allan Dev. 100 sec	1 e-12	1 e-12	1 e-13	1 e-13	1 e-13	1 e-12	?
Allan Dev. 1000 sec	1 e-12	7 e-13	2 e-13	1 e-13	2 e-13	1 e-12	(1e-10/30 min)
Source of Allan Dev. Values	in-flight tests	in-flight tests	in-flight tests	contract specs	proposal	contract specs	(probe document)
Notes:	VGR 1& 2 identical	differ from GLL probe	MGS USO identical	RFS & RFIS	Tactical BVA	2 e-10/ 15 min	rad hard/shield

A Xylophone Detector of Gravitational Radiation

Massimo Tinto*

Jet Propulsion Laboratory, California Institute of Technology
Pasadena, California 91109

Abstract

We discuss spacecraft Doppler tracking searches for gravitational waves in which Doppler data recorded on the ground are linearly combined with Doppler measurements made on board a spacecraft. By using the four-link radio system first proposed by Vessot and Levine¹, we describe a new method for removing from the combined data the frequency fluctuations due to the Earth troposphere, ionosphere, and mechanical vibrations of the antenna on the ground. This technique provides also a way for reducing by several orders of magnitude, at selected Fourier components, the frequency fluctuations due to other noise sources, such as the clock on board the spacecraft or the antenna and buffeting of the probe by nongravitational forces². In this respect spacecraft Doppler tracking can be regarded as a xylophone detector of gravitational radiation. In the assumption of calibrating the frequency fluctuations induced by the interplanetary plasma, a strain sensitivity equal to 4.7×10^{-18} at 10^{-3} Hz is estimated.

This experimental technique could be extended to other tests of the theory of relativity, and to radio science experiments that rely on high-precision Doppler measurements.

INTRODUCTION

Searches for gravitational waves in the milliHertz frequency region, with interplanetary spacecraft Doppler tracking data, have been performed over the past twenty years^{4,5}. These Doppler observations suffer from noise sources that can be, at best, partially reduced or calibrated by implementing specialized and expensive hardware. The fundamental limitation is imposed by the frequency fluctuations inherent in the clocks referencing the microwave system. Current generation Hydrogen masers achieve their best performance at about 1000 seconds integration time with a fractional frequency stability of a few parts in 10^{-16} . This integration time is also comparable to the propagation time to spacecraft in the outer solar system.

The frequency fluctuations induced by the intervening media have severely limited the sensitivities of these experiments. Among all the propagation noise sources, the troposphere is the largest and the hardest to calibrate to a reasonably low level. Its frequency fluctuations have been estimated to be as large as 10^{-13} at 1000 seconds integration time⁶.

In order to systematically remove the frequency fluctuations due to the troposphere in the Doppler data, it was pointed out by Vessot and Levine¹ and Smarr *et al.*⁷ that by adding

* *This work was performed at the Jet Propulsion Laboratory, California Institute of Technology, under contract with the National Aeronautics and Space Administration*

to the spacecraft payload a highly stable frequency standard, a Doppler read-out system, and by utilizing a transponder at the ground antenna, one could make Doppler one-way (Earth-to-spacecraft, spacecraft-to-Earth) as well as two-way (spacecraft-Earth-spacecraft, Earth-spacecraft-Earth) measurements. This way of operation makes the Doppler link totally symmetric and allows the complete removal of the frequency fluctuations due to the Earth troposphere, ionosphere, and mechanical vibrations of the ground antenna by properly combining the Doppler data recorded on the ground with the data measured on the spacecraft. Their proposed scheme relied on the possibility of flying a Hydrogen maser on a dedicated mission. Although current designs of Hydrogen masers have demanding requirements in mass and power consumption, it seems very likely that by the beginning of the next century new space-qualified atomic clocks, with frequency stability of a few parts in 10^{-16} at 1000 seconds integration time, will be available. They would provide a sensitivity gain of almost a factor of one thousand with respect to the best performance crystal-driven oscillators. Although this clearly would imply a great improvement in the technology of space-borne clocks, it would not allow us to reach a Doppler sensitivity better than a few parts in 10^{-16} . This would be only a factor of five or ten better than the Doppler sensitivity expected to be achieved on the future Cassini project, a NASA mission to Saturn, which will take advantage of a high radio frequency link (32 GHz) in order to minimize the plasma noise, and will use a purposely built water vapor radiometer for calibrating up to eighty percent the frequency fluctuations due to the troposphere⁸.

In this paper we adopt the radio link configuration first envisioned by Vessot and Levine¹, but we combine the Doppler responses measured on board the spacecraft and on the ground in a different way, as it will be shown in the following sections. Furthermore our technique allows us to reduce by several orders of magnitude, at selected Fourier components, the noise due to the clock on board the spacecraft².

DOPPLER TRACKING AS A XYLOPHONE DETECTOR

In Doppler tracking experiments a distant interplanetary spacecraft is monitored from Earth through a radio link, and the Earth and the spacecraft act as test particles. In a *one-way* operation a radio signal of nominal frequency $\bar{\nu}_0$ referenced to an onboard clock is transmitted to Earth, where it is compared to a signal referenced to a highly stable clock. In a *two-way* operation instead a radio signal of frequency ν_0 is transmitted to the spacecraft, and coherently transponded back to Earth. In both configurations relative frequency changes $\Delta\nu/\nu_0$ as functions of time are measured, although only two-way data have been used so far in searches for gravitational waves because of relatively poor frequency stability of existing space-qualified clocks.

If a Doppler readout system is added to the spacecraft radio instrumentation, and a transponder is installed at the ground station, one-way as well as two-way Doppler data can also be recorded on board the spacecraft¹. If we assume the Earth clock and the onboard clock to be synchronized, then the one-way and two-way Doppler data measured at time t on the Earth ($E_1(t)$, $E_2(t)$ respectively), and the one-way and two-way Doppler measured at the same time t on the spacecraft ($S_1(t)$, $S_2(t)$), have the following rather

complete expressions²

$$E_1(t) = \frac{(1-\mu)}{2} [h(t - (1+\mu)L) - h(t)] + C_{sc}(t-L) - C_E(t) + T(t) + B(t-L) + A_{sc}(t-L) + EL_{E_1}(t) + P_{E_1}(t), \quad (1)$$

$$E_2(t) = -\frac{(1-\mu)}{2} h(t) - \mu h(t - (1+\mu)L) + \frac{(1+\mu)}{2} h(t - 2L) + C_E(t - 2L) - C_E(t) + 2B(t-L) + T(t - 2L) + T(t) + A_E(t - 2L) + A_{sc}(t-L) + TR_{sc}(t-L) + EL_{E_2}(t) + P_{E_2}(t), \quad (2)$$

$$S_1(t) = \frac{(1+\mu)}{2} [h(t-L) - h(t-\mu L)] + C_E(t-L) - C_{sc}(t) + T(t-L) + B(t) + A_E(t-L) + EL_{S_1}(t) + P_{S_1}(t), \quad (3)$$

$$S_2(t) = -\frac{(1+\mu)}{2} h(t-\mu L) + \mu h(t-L) + \frac{(1-\mu)}{2} h(t-2L-\mu L) + C_{sc}(t-2L) - C_{sc}(t) + 2T(t-L) + B(t-2L) + B(t) + A_{sc}(t-2L) + A_E(t-L) + TR_E(t-L) + EL_{S_2}(t) + P_{S_2}(t), \quad (4)$$

where $h(t)$ is equal to

$$h(t) = h_+(t) \cos(2\phi) + h_\times(t) \sin(2\phi),$$

and is the gravitational wave signal. In Eqs. (1-4) μ is the cosine of the angle between the direction of propagation of the wave and the line of sight to the spacecraft, $h_+(t)$, $h_\times(t)$ are the wave's two independent amplitudes referenced to a given set of axes defined in the plane of the wave, ϕ is the polar angle describing the projection of the direction to the spacecraft in the plane of the wave, and L is the distance to the spacecraft⁵ (units in which the speed of light $c = 1$)

In Eqs. (1-4) $TR_{sc}(t)$ and $TR_E(t)$ represent the noise due to the transponder on board and on the ground respectively, $EL_{E_1}(t)$, $EL_{E_2}(t)$, $EL_{S_1}(t)$, and $EL_{S_2}(t)$ the noises from the electronics at the ground station and on the spacecraft in the one-way and two-way data, and $P_{E_1}(t)$, $P_{E_2}(t)$, $P_{S_1}(t)$, and $P_{S_2}(t)$ the frequency fluctuations due to the interplanetary plasma. The plasma noise can be entirely calibrated by using dual frequencies^{8,9}. The Doppler data $S_1(t)$ and $S_2(t)$ are then time tagged, and telemetered back to Earth in real time or at a later time during the mission.

It is important to note the characteristic time signatures of the frequency fluctuations due to the Earth clock (C_E), the onboard clock (C_{sc}), the spacecraft buffeting (B), the troposphere, ionosphere, and mechanical vibrations of the ground antenna, (T), the Earth transmitter, (A_E), and the onboard amplifier (A_{sc})². It was first pointed out by Vessot and Levine¹ that by properly combining some of the four Doppler data streams it was

possible to calibrate the frequency fluctuations of the troposphere, ionosphere, and ground antenna noise, $T(t)$. Their pioneering work, however, left open the question on whether there existed some other, perhaps more complicated, linear combinations of the data that would further improve the sensitivity of Doppler tracking. In what follows we answer this question, and derive a method that allows us to uniquely identify an optimal way of combining the data.

Let $\widetilde{E}_1(f)$ be the Fourier transform of the time series $E_1(t)$

$$\widetilde{E}_1(f) \equiv \int_{-\infty}^{+\infty} E_1(t) e^{2\pi i f t} dt, \quad (5)$$

and similarly let us denote by $\widetilde{E}_2(f)$, $\widetilde{S}_1(f)$, $\widetilde{S}_2(f)$ the Fourier transforms of $E_2(t)$, $S_1(t)$, and $S_2(t)$ respectively. The most general linear combination of the four Doppler data given in Eqs. (1, 2, 3, 4), can be written in the Fourier domain as follows:

$$\widetilde{y}(f) \equiv a(f, L) \widetilde{E}_1(f) + b(f, L) \widetilde{E}_2(f) + c(f, L) \widetilde{S}_1(f) + d(f, L) \widetilde{S}_2(f), \quad (6)$$

where the coefficients a , b , c , d are for the moment arbitrary functions of f and L . If we substitute in Eq. (6) the Fourier transforms of Eqs. (1, 2, 3, 4) we deduce the following expression

$$\begin{aligned} \widetilde{y}(f) = & \left\{ a \frac{(1-\mu)}{2} \left[e^{2\pi i f(1+\mu)L} - 1 \right] + b \left[\frac{(\mu-1)}{2} - \mu e^{2\pi i f(1+\mu)L} + \frac{(1+\mu)}{2} e^{4\pi i f L} \right] \right. \\ & + c \frac{(1+\mu)}{2} \left[e^{2\pi i f L} - e^{2\pi i f \mu L} \right] + d \left[-\frac{(\mu+1)}{2} e^{2\pi i f \mu L} + \mu e^{2\pi i f L} \right. \\ & \left. \left. + \frac{(1-\mu)}{2} e^{2\pi i f(2+\mu)L} \right] \right\} \widetilde{h}(f) \\ & + \widetilde{C}_E(f) \left[-a + b(e^{4\pi i f L} - 1) + c e^{2\pi i f L} \right] \\ & + \widetilde{C}_{sc}(f) \left[a e^{2\pi i f L} - c + d(e^{4\pi i f L} - 1) \right] \\ & + \widetilde{T}(f) \left[a + b(e^{4\pi i f L} + 1) + c e^{2\pi i f L} + 2d e^{2\pi i f L} \right] \\ & + \widetilde{B}(f) \left[a e^{2\pi i f L} + 2b e^{2\pi i f L} + c + d(e^{4\pi i f L} + 1) \right] \\ & + \widetilde{A}_E(f) \left[b e^{4\pi i f L} + c e^{2\pi i f L} + d e^{2\pi i f L} \right] \\ & + \widetilde{A}_{sc}(f) \left[a e^{2\pi i f L} + b e^{2\pi i f L} + d e^{4\pi i f L} \right] \\ & + a \left[\widetilde{E}L_{E_1}(f) + \widetilde{P}_{E_1}(f) \right] + b \left[\widetilde{T}R_{sc}(f) e^{2\pi i f L} + \widetilde{E}L_{E_2}(f) + \widetilde{P}_{E_2}(f) \right] \\ & + c \left[\widetilde{E}L_{S_1}(f) + \widetilde{P}_{S_1}(f) \right] + d \left[\widetilde{T}R_E(f) e^{2\pi i f L} + \widetilde{E}L_{S_2}(f) + \widetilde{P}_{S_2}(f) \right]. \quad (7) \end{aligned}$$

The four coefficients a , b , c , d , can be determined by requiring the transfer functions of the random processes $\widetilde{C}_E(f)$, $\widetilde{C}_{sc}(f)$, $\widetilde{T}(f)$, $\widetilde{B}(f)$, $\widetilde{A}_E(f)$, $\widetilde{A}_{sc}(f)$ in Eq. (7) to be simultaneously equal to zero, and by further checking that each solution gives a non-zero gravitational wave signal in the corresponding combined data. This condition implies that

a , b , c , d must satisfy a homogeneous linear system of six equations in four unknowns. We calculated the rank of the (6×4) matrix associated with this linear system by using the algebraic computer language *Mathematica*, and we found it to be equal to two. The corresponding solution can be written in the following way

$$\begin{aligned} a(f, L) &= c(f, L) e^{-2\pi i f L} - d(f, L) [e^{2\pi i f L} - e^{-2\pi i f L}] \\ b(f, L) &= -c(f, L) e^{-2\pi i f L} - d(f, L) e^{-2\pi i f L}, \end{aligned} \quad (8)$$

where c and d can be any arbitrary complex functions not simultaneously equal to zero. If we substitute Eq. (8) into Eq. (7) however, we find that the gravitational wave signal, in the combined Doppler data, also vanishes. In other words, any linear combination of the four Doppler data that does not contain any clocks, troposphere, ionosphere, mechanical vibrations of the ground antenna, buffeting of the spacecraft, and transmitters noise, has a null response to a gravitational wave pulse. These results imply that, at any Fourier frequency f , we can remove only one of the considered noise sources. Among all the noise sources affecting spacecraft Doppler tracking, the frequency fluctuations due to the troposphere, ionosphere, and mechanical vibrations of the ground antenna, $\tilde{T}(f)$, are the largest. If we choose a , b , c , d in such a way that the transfer function of $\tilde{T}(f)$ in the combined data is equal to zero, from Eq. (7) we find that a , b , c , d , must satisfy the following condition

$$a(f, L) = -b(f, L) [e^{4\pi i f L} + 1] - c(f, L) e^{2\pi i f L} - 2d(f, L) e^{2\pi i f L}. \quad (9)$$

Since b , c , d can not be equal to zero simultaneously, we will choose c to be equal to $1/2$, and b , d to be equal to zero. In other words we will consider only linear combinations of one-way Doppler data. Note that with this choice we eliminate from the combined data $y(t)$ the frequency fluctuations due to the transponders and the interplanetary plasma that affect the two-way Doppler data. These considerations imply the following expression for $\tilde{y}(f)$

$$\tilde{y}(f) = \frac{1}{2} [\tilde{S}_1(f) - \tilde{E}_1(f) e^{2\pi i f L}]. \quad (10)$$

If we substitute the Fourier transforms of Eqs. (1,3) into Eq. (10) we get

$$\begin{aligned} \tilde{y}(f) &= \frac{e^{2\pi i f L}}{2} \left[1 - \frac{(1+\mu)}{2} e^{2\pi i f(\mu-1)L} - \frac{(1-\mu)}{2} e^{2\pi i f(\mu+1)L} \right] \tilde{h}(f) \\ &+ \tilde{C}_E(f) e^{2\pi i f L} - \frac{1}{2} \tilde{C}_{sc}(f) [e^{4\pi i f L} + 1] + \frac{1}{2} \tilde{B}(f) [1 - e^{4\pi i f L}] \\ &+ \frac{e^{2\pi i f L}}{2} [\tilde{A}_E(f) - \tilde{A}_{sc}(f) e^{2\pi i f L}] + \frac{1}{2} [\tilde{P}_{S_1}(f) - \tilde{P}_{E_1}(f) e^{2\pi i f L}] \\ &+ \frac{1}{2} [\tilde{E}L_{S_1}(f) - \tilde{E}L_{E_1}(f) e^{2\pi i f L}]. \end{aligned} \quad (11)$$

Eq. (11) shows that the transfer functions of the noise of the onboard clock, $\tilde{C}_{sc}(f)$, and of buffeting $\tilde{B}(f)$, can in principle be set to zero (not simultaneously) at specific

Fourier frequencies. Let δ be the time interval over which a Doppler tracking search for gravitational waves is performed. The corresponding frequency resolution Δf of the data is equal to $1/\delta$. This implies that the fluctuations of the clock on board can be minimized at the following frequencies

$$f_k = \frac{(2k-1)}{4L} \pm \frac{\Delta f}{2} ; \quad k = 1, 2, 3, \dots \quad (12)$$

We should point out, however, that these resonant frequencies in general will not be constant, since the distance to the spacecraft will change over a time interval of forty days. As an example, however, let us assume again $L = 1$ AU, $\delta = 40$ days, and $f = 5 \times 10^{-4}$ Hz. The variation in spacecraft distance corresponding to a frequency change equal to the width of the resolution bin (3×10^{-7} Hz) is equal to 1.0×10^5 km. Trajectory configurations fulfilling a requirement compatible to the one just derived have been observed during past spacecraft missions¹⁰, and therefore we do not expect this to be a limiting factor.

At these frequencies, and to first order in $\Delta f L$, the Doppler response $\tilde{y}(f_k)$ is equal to

$$\begin{aligned} \tilde{y}(f_k) \approx & \frac{i}{2} (-1)^k \left[-1 + i \mu e^{\frac{\pi}{2} i \mu (2k-1)} (-1)^k \right] \tilde{h}(f) \pm (\pi i \Delta f L) \widetilde{C}_{sc}(f_k) \\ & + i (-1)^{k+1} \widetilde{C}_E(f_k) + \widetilde{B}(f_k) + \frac{1}{2} \left[\widetilde{E}L_{S_1}(f_k) - i \widetilde{E}L_{E_1}(f_k) (-1)^{k+1} \right] \\ & + \frac{1}{2} \left[\widetilde{P}_{S_1}(f_k) - i \widetilde{P}_{E_1}(f_k) (-1)^{k+1} \right] + \frac{1}{2} \left[\widetilde{A}_{sc}(f_k) + i (-1)^{k+1} \widetilde{A}_E(f_k) \right] . \end{aligned} \quad (13)$$

For a typical gravitational wave experiment, $\delta = 40$ days, and $\Delta f = 3.0 \times 10^{-7}$. Therefore the frequency fluctuations of a clock on board a spacecraft that is out to 1 AU are reduced at the xylophone frequencies by the following amount:

$$\frac{\pi \Delta f L}{c} = 4.7 \times 10^{-4} .$$

EXPECTED XYLOPHONE SENSITIVITIES

From Eq. (13) we can estimate the expected root-mean-squared (r.m.s.) noise level $\sigma(f_k)$ of the frequency fluctuations in the bins of width Δf , around the frequencies f_k ($k = 1, 2, 3, \dots$). This is given by the following expression

$$\sigma(f_k) = [S_y(f_k) \Delta f]^{1/2} , \quad k = 1, 2, 3, \dots , \quad (14)$$

where $S_y(f_k)$ is the one-sided power spectral density of the noise sources in the Doppler response $y(t)$ at the frequency f_k . We will assume that the random processes representing the noise sources affecting the combined response (Eq. (13)) are uncorrelated with each other, and their one-sided power spectral densities are as given in Tinto². In that reference a frequency stability of 1.0×10^{-16} at 1000 seconds integration time for the clock at the ground station was assumed. Although this is a factor of four better than what has

been measured so far⁸, it seems very likely that by the beginning of next century such a sensitivity can be achieved. As far as the remaining sensitivity figures used in our estimate are concerned, they were obtained from the Riley *et al.* report⁸. This document is a summary of a detailed study, performed jointly by scientists and engineers of NASA's Jet Propulsion Laboratory and the Italian Space Agency (ASI) Alenia Spazio, for assessing the magnitude and spectral characteristics of the noise sources that will determine the Doppler sensitivity of the future gravitational wave experiment on the Cassini mission.

If dual radio frequencies in the uplink and downlink are used, then the frequency fluctuations due to the interplanetary plasma can be entirely removed^{8,9}. We will refer to this configuration as MODE I. If only one frequency is adopted instead, which we will assume to be Ka-Band (32 GHz), we will refer to this configuration as MODE II. Ka-Band is planned to be used on most of the forthcoming NASA missions, and will be implemented on the ground antennas of the Deep Space Network (DSN) by the year 1999 for the Cassini mission.

The r.m.s. $\sigma(f_k)$ of the noise as a function of the frequencies f_k ($k = 1, 2, 3, \dots$), assuming that an interplanetary spacecraft is out to a distance $L = 1.0$ AU, has been estimated by Tinto². For this configuration the fundamental frequency of the xylophone (Eq. (12)) is equal to 5.0×10^{-4} Hz. A complete analysis covering configurations with spacecraft at several other distances is also given in reference [2].

The MODE I configuration is represented in reference [2] by two curves, depending on whether an atomic clock or an Ultra Stable Oscillator (USO) is operated on board the spacecraft. Sensitivity curves for the MODE II configuration are also included in that reference, again with an atomic clock on board or a USO. The best sensitivity is achieved in the MODE I configuration, regardless of whether an atomic clock or a USO is operated on board the spacecraft. This is because the amplitude of the noise of the clock onboard is reduced by a factor $\pi\Delta fL/c = 4.7 \times 10^{-4}$ at the xylophone frequencies. At $f = 10^{-3}$ Hz the corresponding r.m.s. noise level is equal to 4.7×10^{-18} , and it increases to a value of 5.7×10^{-18} at $f = 10^{-2}$ Hz. As far as the MODE II configuration is concerned, the r.m.s. noise level is equal to 7.9×10^{-18} at $f = 10^{-3}$ Hz, while it decreases to 6.3×10^{-18} at $f = 10^{-2}$ Hz. This is due to the fact that the one-sided power spectral density of the fractional frequency fluctuations due to the interplanetary plasma¹¹ decays as $f^{-2/3}$.

CONCLUSIONS

We have discussed a method for significantly increasing the sensitivity of Doppler tracking experiments aimed at the detection of gravitational waves. The main result of our analysis, deduced in Eq. (13), shows that by flying a frequency reference and by adding a Doppler extractor on board the spacecraft and a transponder at the DSN antenna, we can achieve at selected Fourier components a strain sensitivity of 4.7×10^{-18} . This sensitivity figure is obtained by completely removing the frequency fluctuations due to the interplanetary plasma, at a Fourier frequency equal to 10^{-3} Hz. Our method relies on a properly chosen linear combination of the one-way Doppler data recorded on board with those measured on the ground. It allows us to remove entirely the frequency fluctuations due to the troposphere, ionosphere, and antenna mechanical, and for a spacecraft that is

tracked for forty days out to 1 AU it reduces by almost four orders of magnitude the noise due to the onboard clock.

The experimental technique presented in this paper can be extended to a configuration with two spacecraft tracking each other through a microwave or a laser link³. Future space-based laser interferometric detectors of gravitational waves¹², for instance, could implement this technique as a backup option, if failure of some of their components would make the normal interferometric operation impossible.

As a final note, a method similar to the one presented can be used in all those radio science experiments in which one-way and two-way spacecraft Doppler measurements are used as primary data set. We will analyze the implications of the sensitivity improvements that this technique will provide for direct measurements of quantities such as the gravitational red shift, possible anisotropy in the velocity of light, the Parameterized Post-Newtonian parameters, the deflection and time delay by the sun in radio signals, and occultation experiments.

REFERENCES

- ¹ Vessot, R.F.C. and Levine, M.W., *Gen. Relativ. Gravit.* **10**, 181 (1979).
- ² Tinto, M., *Phys. Rev. D*, **53**, 5354, (1996).
- ³ Tinto, M., *Phys. Rev. D*. In preparation.
- ⁴ Estabrook, F.B.: *Proposal for Participation on Radio Science/Celestial Mechanics Team for an Investigation of Gravitational Radiation*. Internal document, Galileo Project, Jet Propulsion Laboratory (1976). See also Estabrook, F.B., Hellings, R.W., Wahlquist, H.D., Anderson, J.D. and Wolff, R.S.. In: *Sources of Gravitational Radiation*, ed. Smarr, L. (Cambridge University Press, Cambridge, 1979).
- ⁵ Estabrook F.B. and Wahlquist H.D., *Gen. Rel. Grav.* **6** 439, (1975).
- ⁶ Armstrong, J.W. In: *Gravitational Wave Data Analysis*, Editor B.F. Schutz, *Dordrecht, Kluwer*, p.153 (1989).
- ⁷ Smarr, L.L., Vessot, R.F.C., Lundquist, C.A., Decher, R., and Piran, T., *Gen. Relativ. Gravit.* **15**, 2 (1983).
- ⁸ Riley, A.L., Antsos, D., Armstrong, J.W., Kinman, P., Wahlquist, H.D., Bertotti, B., Comoretto, G., Pernice, B., Carnicella, G., and Giordani, R.: *Cassini Ka-Band Precision Doppler and Enhanced Telecommunications System Study*. Internal document, Jet Propulsion Laboratory (1990).
- ⁹ Bertotti, B., Comoretto, G., and Iess, L., *Astron. Astrophys.*, **269**, 608 (1993).
- ¹⁰ Armstrong, J.W.. Private communication.
- ¹¹ Armstrong, J.W., Woo, R., and Estabrook, F.B., *Ap. J.* **30** 574, (1979).
- ¹² LISA: (Laser Interferometer Space Antenna) *A Cornerstone Project in ESA's long term space science programme "Horizon 2000 Plus"*. Pre-Phase A Report MPQ 208, (Max-Planck-Institute für Quantenoptic, Garching bei München, 1996)

Clock Requirements for Gamma-Ray Burst Localization Experiments

Dave Van Buren, California Institute of Technology

Abstract. Precise localization of gamma-ray bursts requires accurate timing information. A feasible space experiment places a number of detectors in the inner solar system with AU separations. To attain arcsecond positions, clock accuracy must be held to 1 millisecond. Mission costs are significantly reduced if the clock drift can be held to 1 millisecond over the entire mission, *i.e.* for several years.

Gamma-ray Bursts

Gamma-ray bursts are intense impulsive radiative events taking place outside our solar system with a rate of once per day at the detection limit of current experiments. If located at cosmological distances, a distinct possibility, then they are the most energetic events known in the Universe. Their properties have been the subject of study and debate for nearly three decades, since their discovery by satellites monitoring the nuclear test ban treaty. For an early discussion, see Ruderman (1975). A set of good recent reviews are available on the Web by Fishman (1995), Paczynski (1995), and Lamb (1995) which lay out the open issues.

There is strong consensus that the most important question to be answered is what are the objects responsible for gamma ray bursts. Attempts to associate various classes of objects using the rather large error regions currently available have all met with failure. These error regions are so large that even the smallest have thousands of objects contained within their boundaries in the deepest images. Progress requires narrowing the error regions to the arcsecond scale, a scale so small that only a single astrophysical object is likely to be present.

Localization via Timing

Arrival directions for gamma ray events are most accurately determined via time of arrival analysis of the wavefront at widely dispersed detectors. Aperture masking techniques can also give modest directional information over limited fields of view. In a timing experiment, the delays in arrival time between different detectors at different positions constrain the location on the sky. A single time of arrival of course contains no position information. A pair, yielding a single delay gives as allowed positions all points on the circle marking the intersection of a cone with the celestial sphere. The axis of the cone is oriented along the displacement vector between the two spacecraft. The circle becomes a band of some width when timing uncertainties are taken into account. Two pairs, from three detectors give a pair of intersecting bands, which yield a 2-fold ambiguity for the source position. Four non-coplanar detectors are needed to give a single simply-connected error region on the sky.

Clock Requirements

The fastest time scales t observed in gamma ray bursts are about 1 millisecond. To attain an angular accuracy $d\theta$ over a detector array with linear extent L needs clocks good to

$$\frac{dt}{1 \text{ ms}} = 0.4 \frac{d\theta}{1 \text{ arcsec}} \frac{L}{1 \text{ AU}}$$

Detectability considerations require that sufficient gamma rays are counted to accurately determine the event timing, leading to very large detectors for L corresponding to earth-orbiting arrays, and small "pop-can" detectors for a mission to the edge of the solar system. For 1 millisecond timing resolution, one requires detector areas of several hundred cm^2 and $L \approx 1 \text{ AU}$, which can be packaged into a 20 kg spacecraft, *i.e.* a very attractive experiment cost-wise. This mass is chosen so that to first order the spacecraft serves the needs of the detector, rather than the clock.

An experiment of this kind would yield arcsecond positions of one to a few bursts per month once the array is deployed to $L = 1$ AU. It takes some time to get to this size though, depending on the velocity imparted by each spacecraft's final stage. To remain in earth-like orbits around the sun for thermal and telecommunications reasons requires a relatively small kick, giving deployment times of about 1 year. This puts a stability requirement on the clock of drifts less than 10^{-11} over a course of a several year mission life.

Another requirement comes from the small spacecraft size. A 20 kg spacecraft will have a limited area available for solar panels to generate power unless costly panel deployment schemes are employed. Much of the power budget will be required for the telecommunications system to get the data to the ground, detectors and CPU, leaving little left over for the clock. Out of perhaps 10 W of power, only 1 W will be available for the clock.

Also flowing down from the need for a small spacecraft is the requirement of small clock mass. The clock must be less than 1 kg.

Exceeding these performance numbers will yield the following benefits: increased stability will help achieve more precise positions, the solid angle goes as dt^2 ; reducing the power requirement will allow slightly longer baselines to be achieved via larger orbits which carry the spacecraft to regions of lower solar illumination; lower mass clocks marginally improve the experiment by either achieving slightly larger L , or by slightly increasing the detector sensitivity by making them a bit larger. In the latter regard, note that the next generation of detectors themselves will provide a performance per unit mass improvement of a factor of 2-5, making a small savings in clock mass potentially translate to a large gain in detector area for the same total package mass.

Once the quoted requirements are met, improvements in clock stability will give the most benefit since the clocks are already minor components of the mass and power budgets. One can anticipate the availability of space qualifiable clocks with these properties in the near term, enabling a gamma-ray burst localization experiment of unprecedented accuracy to be undertaken for low cost.

Acknowledgements

This work was funded by the National Aeronautics and Space Administration via a contract to the Jet Propulsion Laboratory of the California Institute of Technology. I thank the conference organizers for the opportunity to present these thoughts.

References

- Fishman, G. J., 1995, http://antwarp.gsfc.nasa.gov/diamond_jubilee/papers/fishman.html.
- Lamb, D. Q., 1995, http://antwarp.gsfc.nasa.gov/diamond_jubilee/papers/lamb/lamb.html.
- Paczynski, B. A., 1995, http://antwarp.gsfc.nasa.gov/diamond_jubilee/pac/lamb/debate.html.
- Ruderman, M., 1975, Ann. N.Y. Acad. Sci., 262, 164.

RUBIDIUM ULTRA-STABLE OSCILLATORS AT TITAN: THE HUYGENS DOPPLER WIND EXPERIMENT

M.K. Bird¹, M. Allison², S.W. Asmar³, D.H. Atkinson⁴, R. Dutta-Roy¹,
P. Edenhofer⁵, W.M. Folkner³, M. Heyl¹, L. Iess⁶, D. Plettmeier⁵,
R.A. Preston³, G.L. Tyler⁷ and R. Wohlmuth⁴

¹Radioastronomisches Inst., Universität Bonn, Auf dem Hügel 71, 53121 Bonn, Germany

²NASA-Goddard Institute for Space Studies, New York, NY 10025, USA

³Jet Propulsion Laboratory, California Institute of Technology, Pasadena, CA 91109, USA

⁴Department of Electrical Engineering, University of Idaho, Moscow, ID 83843, USA

⁵Institut für Hochfrequenztechnik, Universität Bochum, 44801 Bochum, Germany

⁶Dipartimento Aerospaziale, Università di Roma 'La Sapienza', 00184 Roma, Italy

⁷Center for Radar Astronomy, Stanford University, Stanford, CA 94305, USA

Abstract. The Doppler Wind Experiment (DWE) is one of six investigations to be performed during the Titan atmospheric descent of the ESA Huygens Probe. The primary scientific objective is to measure the direction and strength of Titan's zonal winds with an accuracy better than 1 m s^{-1} . The Probe's wind-induced horizontal motion will be derived from the residual Doppler shift of its S-band radio link to the Cassini Orbiter, corrected for all known orbit and propagation effects, from the beginning of the mission (altitude: $\sim 160 \text{ km}$) down to impact on the surface. The DWE Instrumentation consists of Rb-based Ultra-Stable Oscillators used to (a) generate the transmitted signal from the Probe and (b) extract the frequency of the received signal on the Orbiter. The capabilities of these USOs under the rugged experimental conditions on Titan and some results from the DWE pre-launch test program are described.

1 Introduction

The Doppler Wind Experiment (DWE) of the Huygens Mission is a radio tracking investigation designed to measure wind velocities in the atmosphere of Saturn's moon Titan (Atkinson *et al.*, 1990; Bird *et al.*, 1997). A similar experiment under considerably more severe environmental conditions was performed with the Galileo Probe at Jupiter (Pollack *et al.*, 1992; Atkinson *et al.*, 1996). The primary scientific objective of DWE is a height profile of the zonal (east-west) wind speeds as deduced from the Doppler shift of the Probe's radio signal to the Cassini Orbiter. As with the Galileo Probe descent at Jupiter (Folkner *et al.*, 1996), prospects are good that additional measurements to obtain an additional wind component can be recorded at a large ground-based radio telescope. Upon applying

corrections for the motion of the Orbiter and the Probe descent velocity, it is estimated that the horizontal drift due to winds can be measured to a precision better than 1 m/s. Radio propagation effects on the received frequency can be shown to be negligible for the Huygens DWE geometry (Bird, 1997). Measurements commence upon establishment of the link shortly after parachute deployment at a nominal altitude (~ 160 km) and continue for at least 135 ± 15 minutes until touchdown on Titan. Although post-impact survival of the Probe is not guaranteed, the special Huygens receivers on the Orbiter will continue to monitor a possible Probe broadcast from Titan's surface for a minimum of 30 minutes.

Specific secondary science objectives of DWE include measurements of: (a) Doppler fluctuations to determine the turbulence spectrum and possible wave activity in the Titan atmosphere; (b) Doppler and signal level modulation to monitor Probe descent dynamics (e.g., spin rate, spin phase, parachute swing); (c) Probe coordinates and orientation during descent and after impact on Titan. DWE will complement remote-sensing observations of temperatures and winds from the Cassini Orbiter, providing "ground truth" for the zonal wind retrievals from the Composite Infrared Spectrometer (CIRS) experiment.

A potentially severe constraint on the accuracy of the DWE wind measurement is the stability of the oscillators used to generate the radio signal on the Probe and receive it on the Orbiter. The required long-term frequency drift stability ($\delta f/f \lesssim 2 \cdot 10^{-10} \Rightarrow \delta f \lesssim 0.4$ Hz at S-band) is expected to be met by using rubidium-based ultrastable oscillators in both the transmitter (TUSO) and receiver (RUSO).

The present paper summarizes the science objectives and the planning/execution of the DWE investigation. This is followed by a short description of the DWE-instrumentation and its development within the context of the Huygens pre-launch test program. More information about DWE may be found in Bird *et al.* (1997).

2 Titan winds: A brief overview

Our only previous close look at Titan's atmosphere was during the Voyager 1 flyby on November 12, 1980. Doppler tracking data collected during Earth occultation were used to derive Titan's vertical temperature-pressure curve (Lindal *et al.*, 1983) that indicated a surface temperature of 97 ± 7 K. The temperature was seen to decrease with altitude to a minimum of ~ 70 K at the tropopause near 40 km (weak greenhouse effect).

The featureless orange-brown haze of the upper atmosphere prevented surface observations at optical wavelengths. Motions of purported methane clouds in the lower atmosphere were thus not available for inferring atmospheric circulation. Indirect evidence for strong zonal winds, however, was the temperature difference from pole to equator derived from infrared observations (Flasar *et al.* 1981). Requiring conservation of angular momentum, any gradient in latitudinal temperature must be accompanied by bulk motion in the zonal direction. Flasar *et al.* (1981) suggested that the zonal wind would increase monotonically with height, approaching values ~ 100 m/s in the upper stratosphere at mid-latitudes near 200 km. Ironically, the simple theory can be satisfied by winds blowing either west-to-east

(prograde: in the direction of Titan's rotation) or east-to-west (retrograde). Even stronger winds would be attained at lower latitudes. A recent review of evidence supporting the existence of Titan's zonal winds has been published by Flasar *et al.* (1997).

The hypothesized zonal flow on Titan, however, is still a fundamental enigma in the theory of atmospheric dynamics. The meridional and vertical winds, although thought to be much weaker, are also unknown. Only recently have general circulation models (GCMs) been adapted to studies of atmospheric superrotation on Titan (Del Genio *et al.*, 1993; Hourdin *et al.*, 1995). The picture becomes even less clear at heights within the planetary boundary layer (~ 5 km), where surface effects can rotate and shear the mean flow.

Some independent evidence for winds on Titan has emerged from recent Earth-based observations. Hubbard *et al.* (1993) reported photometric measurements of optical limb extinction during Titan's occultation by a relatively bright star. The observations could be explained in terms of a nonspherical atmosphere, implying zonal winds ranging from 80 m/s to 170 m/s at an altitude near 250 km. Infrared heterodyne observations of Titan's 12 μm ethane emission, originating from heights near 200 km, indicate that the winds are *prograde* and have speeds of the order of 80 m/s (Kostiuk *et al.* 1997). Finally, near-infrared images of Titan obtained with the refurbished planetary camera (WF/PC2) of the Hubble Space Telescope (Lorenz *et al.*, 1995; Smith *et al.*, 1996) have been closely examined for cloud motions. Unfortunately, the quest has been thus far unsuccessful.

3 DWE Planning and Execution

Geometry was an essential element in designing the DWE. The Huygens descent mission on Titan is presently scheduled to occur on 27 November 2004, about five months after Cassini arrives at Saturn and seven years after launch. Approximately 22 days prior to its mission, the Probe is separated from the Orbiter and targeted for entry into Titan's atmosphere. The Orbiter then performs a deflection maneuver into a trajectory that delays its arrival by about four hours and misses the Titan surface by 1500 km.

The Probe is decelerated at atmospheric entry up to a maximum of 16.1 *g* at an altitude near 250 km. Parachute deployment at a speed near Mach 1.5 marks the start of the descent phase (time = t_0). A smaller drogue parachute is deployed at $t_0 + 15$ minutes in order to decrease the descent time. The radio link to the Orbiter is established by $t_0 + 150$ s.

It was originally planned to target the Probe to a location near Titan's central meridian as viewed from the approaching Orbiter. This resulted in an unfavorable DWE geometry because of the extremely small east/west projection on the line-of-sight to the Orbiter. The effective Doppler shift from the zonal drift would thus be too small to be measured. After considerable negotiation, it was decided to move the target about 700 km to the east while retaining the same atmospheric entry angle. The present nominal target position is latitude 18°N, longitude 152°W, for which the mean angle between the line-of-sight and the zonal direction during the Huygens mission will be 64°. The targeting errors about this nominal position are ± 452 km in longitude and ± 59 km in latitude. The new entry site also

improves the experimental geometry for coordinated Doppler measurements along the two lines-of-sight from Probe-to-Orbiter and Probe-to-Earth, respectively. The horizontal wind projections for these two viewing directions are now separated by $\sim 20^\circ$. A prograde zonal wind would shift the Probe's final touchdown site to the east of its atmospheric injection point, thereby improving the Doppler projection.

4 DWE Instrumentation

4.1 End-to-end design

Of the six Huygens investigations, DWE is the only one with instrumentation on both the Probe and Orbiter (in the Probe Support Equipment-PSE). The DWE experimental configuration is shown in Fig. 1.

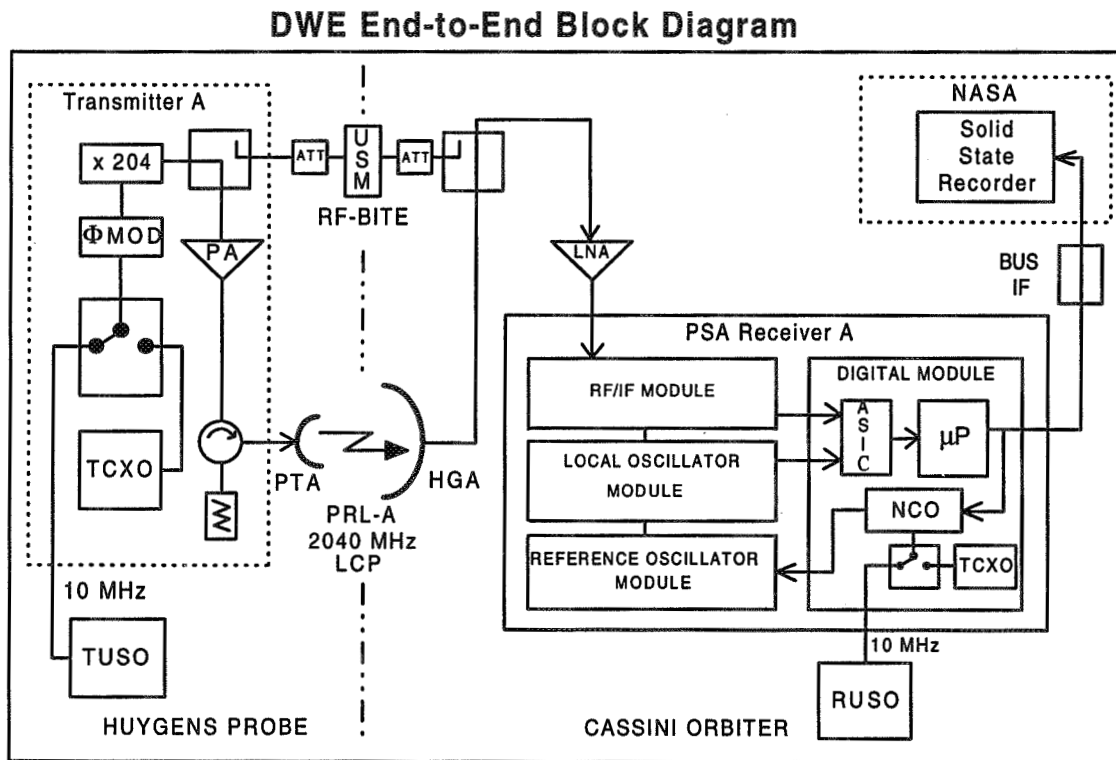


Figure 1: DWE experiment configuration [reprinted from Bird *et al.*, 1997].

The DWE-TUSO is used to generate the radio signal of chain A (Tx A). An internal TCXO oscillator serves as back-up in the event of a TUSO failure. The eventual decision to use the TUSO or its backup will be taken a few days prior to Probe-Orbiter separation. The TUSO output frequency at 10 MHz is multiplied by 204 to S-band and transmitted to the dedicated Probe receiver (Rx A) in the PSE on the Orbiter. The semiannual cruise checkouts can be conducted with the radio frequency built-in-test equipment (RF-BITE)

across the Umbilical Separation Mechanism (USM). At Titan the signal is amplified for free-space transmission via the Probe Antenna (PTA) to the Orbiter's HGA.

Timing and signal generation for Rx A are controlled by the DWE-RUSO. In order to maintain interchangeability, the RUSO was fabricated as an exact clone of the TUSO. Consistent with the Probe strategy, an integrated TCXO can be substituted for the RUSO if needed. The phase-locked loop control in Rx A is monitored by a numerically controlled oscillator (NCO), the output of which is recorded to provide the DWE frequency measurement at a sample rate of 8 Hz. The signal level (AGC) is monitored in parallel at the same sample rate. In addition to these DWE "science data", temperatures and internal lock status of TUSO and RUSO are recorded as housekeeping data.

The TUSO will be powered well in advance of the start of transmission from the Probe (~30 minute head start), in order to warm up and achieve the required frequency stability. The RUSO will be switched on even earlier, together with the rest of the PSE on the Orbiter.

4.2 Transmitter and Receiver USO programs

The DWE ultrastable oscillators, the first rubidium oscillators used in a deep space mission, were developed and constructed by Daimler-Benz Aerospace (DASA), Satellite Systems Division, Ottobrunn, Germany. The key ingredient of the DASA design concept is the Rb-resonator in a "physics package" supplied by Efratom Elektronik GmbH. The final flight model (FM) units, a TUSO, a RUSO and a spare, were delivered to the Huygens Probe FM test program in early 1996.

The DWE USOs must survive the Cassini/Huygens launch, cruise phase, and atmospheric entry/descent on Titan. In addition to the required fast warm-up time, another major driver in the selection of a rubidium USO was the high level of mechanical loads during the Huygens entry phase. The frequency stability required in the DWE instrument specification ($\delta f_0/f_0 < 2 \cdot 10^{-10}$, $f_0 =$ nominal output frequency) could not be guaranteed with a state-of-the-art quartz oscillator. It was feared that the continuously changing mechanical stresses at entry and the following variation in pressure from one millibar to the surface pressure of 1.5 bar could cause deformation of the internal quartz fastening system and produce nonreproducible frequency offsets and relaxation curves. A rubidium oscillator is much less susceptible to these effects because the nominal output frequency is locked to the very stable frequency of the rubidium ground-state hyperfine transition.

A block diagram of the USO unit is shown in Fig. 2. The USO consists of the Physics Package (rubidium resonance cell and lamp) and printed circuit boards integrated into an aluminium box (Faraday cage). Starting at upper left and moving clockwise in Fig. 2, the separate elements are: (i) Lamp Board: controls power and heating for the Rb lamp. (ii) Physics Package: consists of the Rb lamp, Rb resonance cell and sc-cut quartz crystal, the temperatures of which are monitored by three analogue sensors. (iii) Oscillator Board: provides the 10 MHz output via VCXO quartz through a buffer amplifier. (iv) Servo Board: generates the error signal for the VCXO from the photocurrent of the Physics Package and

provides a telemetry lock indicator when the output is phase-locked to the Rb resonance frequency. (v) Synthesizer Board: upconverts the output signal from the VCXO to the Rb resonance frequency. (vi) DC/DC converter: converts external supply voltages of 28/30 V (TUSO/RUSO) to 5 V and 17 V.

DWE-USO Block Diagram

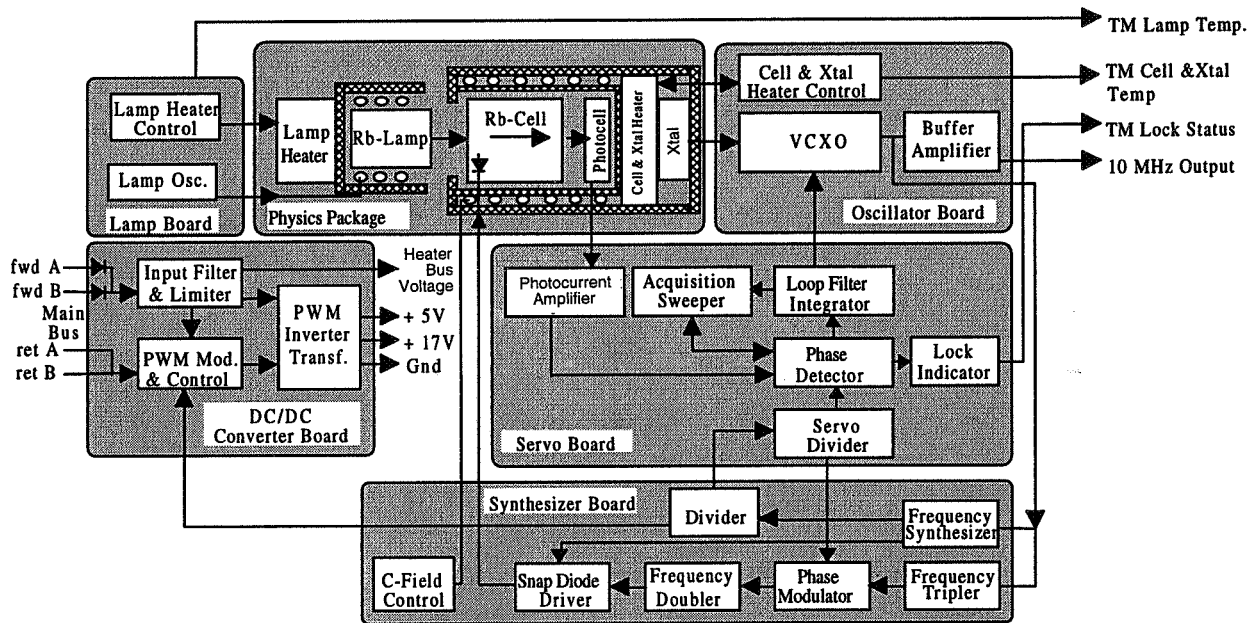


Figure 2: DWE-USO block diagram [reprinted from Bird *et al.*, 1997].

The actual physical and electrical characteristics of the DWE-USO, as determined during the extensive qualification test program at unit level, are presented in Table 1. The expected decreases in USO steady-state power consumption and warm-up time (until Rb-lock) with increasing ambient temperature are illustrated in Fig. 3.

The USO long-term frequency drift stability requirement of $\delta f_0/f_0 \leq 1.4 \cdot 10^{-9}$ (i.e., the specified frequency deviation over the longest possible mission time of 3 hours) is critical for a successful wind measurement. This figure of stability was determined during the qualification test program over an expanded range of temperatures ($-30^\circ < T < 60^\circ$) in vacuum (0.1 mbar) and ambient pressure. The original USO specification of $\delta f_0/f_0 \leq 2 \cdot 10^{-10}$ could be met only over a more restricted range of temperature ($-20^\circ < T < 40^\circ$). Even for the somewhat degraded USO performance, however, the maximum measurement error of the line-of-sight velocity due to intrinsic USO stability will still be only about ± 40 cm/s over the entire Huygens mission. This error is of the order of the errors expected from uncertainties in the reconstructed trajectories.

Table 1: DWE-USO physical and electrical characteristics

Physical parameters		
Mass [g]	1898±2	radiation shielding: 150 g
Dimensions [mm]	170×117×119	(L×W×H)
Frequency parameters		
Output Frequency [MHz]	10	±0.1 Hz
Frequency long-term drift	1.4·10 ⁻⁹	$\delta f_0/f_0$ over 3 hours
Allan variation	3·10 ⁻¹¹	$\tau = 1$ s
	6·10 ⁻¹²	$\tau = 10$ s
Phase Noise [dBc/Hz]	< -75	$df = 1$ Hz
	< -110	$df = 10$ Hz
	< -130	$df = 100$ Hz
Signal level/Waveform		
Output Signal Level [dBm]	0±2	into 50 Ω impedance
harmonics [dBc]	< -45,-36	2 nd , 3 rd , respectively
Spurious signals [dBc]	< -60	up to 50 MHz
Return loss [dB]	< -30	50 Ω impedance
DC Power		
Supply Voltage [V]	28 ^{+0.35} / _{-0.63} /30 ^{+1.5} / _{-3.38}	TUSO / RUSO
Warm-up Power [W]	< 18.4	< 40 min (Fig. 3)
DC current [mA]	< 675	System limit: 0.7 A
Energy [Wh]	< 32.5	worst case (min temp)

4.3 USO Performance during System Flight Model Tests

A discussion of the unit level and engineering model test programs was given in Bird *et al.* (1997). An example from the Huygens flight model program is presented here.

The Huygens radio signal frequency recorded by the NCO in Rx A during the first FM Integrated System Test is shown as a function of time from start of test in the upper panel of Fig. 4. The first part of the test was performed using the internal TCXOs in the transmitter/receiver chain A. The TUSO/RUSO combination was switched from standby to operation at the time $t \simeq 104$ min. The characteristics of the received frequency change at this point from a series of discontinuous jumps and unpredictable drifts to a stable value near the zero line (nominal for check-out mode with no Doppler shift). The lower panel of Fig. 4 shows a 30-minute interval of the upper trace on an expanded scale. The individual points are single measurements recorded at the sample rate of 8 Hz. The digitization of these measurements ($\Delta f \simeq 0.15$ Hz, corresponding to ~ 2 cm/s) is apparent in the discrete levels of this point cluster. The solid line is a running average over 80 continuous points (10 sec). The standard deviations of the two traces are 2.8 Hz and 0.29 Hz, respectively, consistent with the 80-fold increase in integration time.

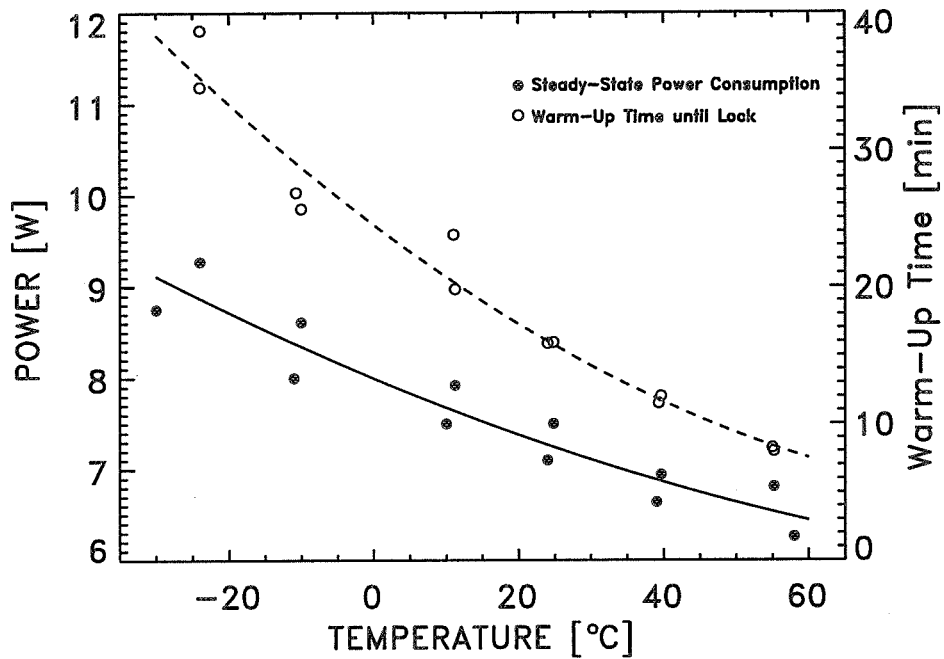


Figure 3: DWE-USO steady-state power consumption (solid circles) and warm-up time to internal lock (open circles) as a function of ambient temperature. The solid and dashed lines are quadratic least-squares fits to the solid and open circles, respectively.

5 Conclusions

The main scientific goal of the Huygens Doppler Wind Experiment is to determine the velocity of Titan's horizontal winds at heights 0–160 km from frequency measurements of the Probe's radio signal recorded on the Orbiter. Similar Earth-based observations will be recorded in order to separate meridional from zonal drift motion. Adequate frequency stability is attained by using rubidium ultrastable oscillators to generate the transmitted signal and drive the electronics of the monitoring receiver. Final trajectory reconstruction and analysis of Probe dynamics using DWE data will provide valuable ancillary information that should enhance the overall scientific yield of the Huygens Mission.

Acknowledgements

This paper presents results of a research project partially funded by the Deutsche Agentur für Raumfahrtangelegenheiten (DARA) GmbH under contract 50 OH 9207. We thank R. Kohl and K.-P. Wagner (DASA, Ottobrunn) for their continued efforts throughout the DWE-USO Program. Portions of this work were performed at the Jet Propulsion Laboratory, California Institute of Technology, under contract with the National Aeronautics and Space Administration.

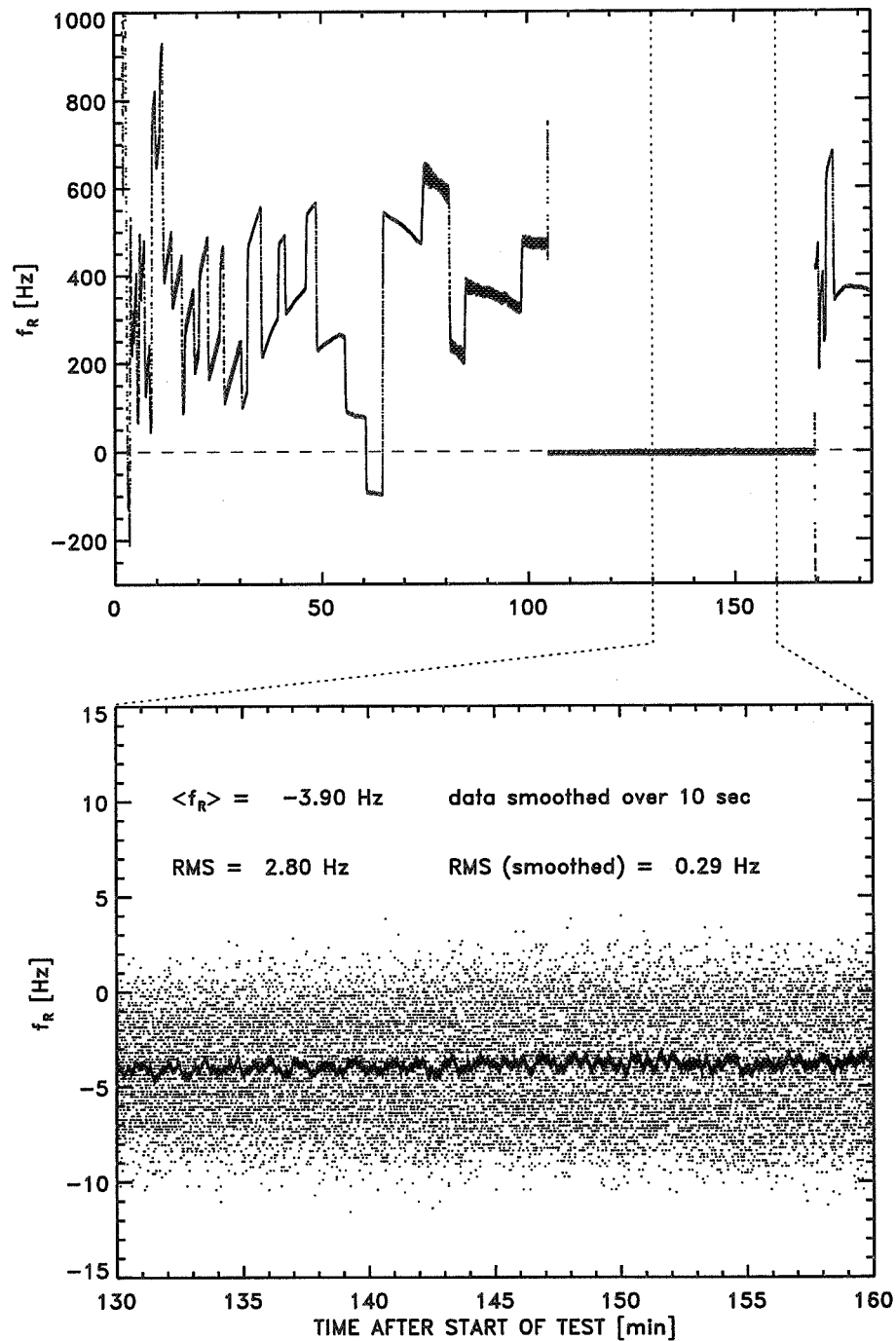


Figure 4: Frequency measurements of Huygens radio signal during first Integrated System Test. Upper panel: Comparison TCXO vs. TUSO/RUSO. The radio subsystem was driven by ordinary oscillators (TCXOs) except for the interval from approximately 104 to 169 min. after start, during which time the driver function was switched to the TUSO/RUSO combination. Lower panel: High-resolution plot showing DWE frequency measurement accuracy at integration times of 0.125 s (point cluster) and 10 s (solid line).

References

- Atkinson, D.H., Pollack, J.B. and Seiff, A., Measurement of a zonal wind profile on Titan by Doppler tracking of the Cassini entry probe, *Radio Sci.* **25**, 865-882, 1990.
- Atkinson, D.H., Pollack, J.B. and Seiff, A., Galileo Doppler measurements of the deep zonal winds at Jupiter, *Science* **272**, 842-843, 1996.
- Bird, M.K., Atmospheric attenuation of the Huygens S-Band Radio Signal during the Titan Descent, in *Huygens: Science Payload and Mission*, ESA-SP 1177, ESTEC, Noordwijk, Netherlands, in press, 1997.
- Bird, M.K., Heyl, M., Allison, M., Asmar, S.W., Atkinson, D.H., Edenhofer, P., Plettemeier, D., Wohlmuth, R., Iess, L., and Tyler, G.L., The Huygens Doppler wind experiment, in *Huygens: Science Payload and Mission*, ESA-SP 1177, ESTEC, Noordwijk, Netherlands, in press, 1997.
- Del Genio, A.D., Zhou, W. and Eichler, T.P., Equatorial superrotation in a slowly rotating GCM: Implications for Titan and Venus, *Icarus* **101**, 1-17, 1993.
- Flasar, F.M., Allison, M. and Lunine, J.I., Huygens Probe wind drift: science issues and recommendations, in *Huygens: Science Payload and Mission*, ESA-SP 1177, ESTEC, Noordwijk, Netherlands, in press, 1997.
- Flasar, F.M., Samuelson, R.E. and Conrath, B.J., Titan's atmosphere: temperature and dynamics, *Nature* **292**, 693-698, 1981.
- Folkner, W.M., Preston, R.A., Border, J.S., Navarro, J., Wilson, W.E., and Oestreich, M., Earth-based radio-tracking of the Galileo Probe for Jupiter wind estimation, *Science* **275**, 644-646, 1997.
- Hourdin, F., Talagrand, O., Sadourny, R., Courtin, R., Gautier, D. and McKay, C.P., Numerical simulation of the general circulation of the atmosphere of Titan, *Icarus* **117**, 358-374, 1995.
- Hubbard, W.B. et al., The occultation of 28 Sgr by Titan, *Astron. Astrophys.* **269**, 541-563, 1993.
- Kostiuk, T., Fast, K., Livengood, T.A., Espenak, F., Buhl, D., Goldstein, J., Hewagama, T., Ho Ro, K., Stratospheric circulation on Titan: a direct measurement, in *Physics and Chemistry of the Earth*, Pergamon-Elsevier, Oxford, UK, in press, 1997.
- Lindal, G.F., Wood, G.E., Holtz, H.B., Sweetnam, D.N., Eshleman, V.R. and Tyler, G.L., The atmosphere of Titan: An analysis of the Voyager 1 radio occultation measurements, *Icarus* **53**, 348-363, 1983.
- Lorenz, R.D., Smith, P.H. and Lemmon, M.T., The search for clouds on Titan using HST imaging, *BAAS* **27**, 1107, 1995.
- Pollack, J.B., Atkinson, D.H., Seiff, A. and Anderson, J.D., Retrieval of a wind profile from the Galileo Probe telemetry signal, *Space Sci. Rev.* **60**, 143-178, 1992.
- Smith, P.H., Lemmon, M.T., Lorenz, R.D., Sromovsky, L.R., Caldwell, J.J. and Allison, M.D., Titan's surface, revealed by HST imaging, *Icarus* **119**, 336-349, 1996.

Limits to the Stability of Phase Transfer from Ground to Space

by

Roger P. Linfield

Jet Propulsion Laboratory, California Institute of Technology

ABSTRACT

An alternative to having a primary frequency standard on board a spacecraft is to phase lock a simple oscillator on the spacecraft to a microwave tone transmitted from the ground. The received tone is transponded and rebroadcast to the ground. The round trip phase is measured, and used to correct for effects on time scales longer than the round trip light travel time. This method is used with the TDRSS relay satellites, and will be used for the Japanese space VLBI mission VSOP. There are several sources of error introduced by this process.

The most important error source is a loss of the on board standard for all times that the satellite is out of contact with a ground tracking station. The fractional loss will be $> 10\%$ for almost any orbit, even with a network of several ground tracking stations, and it will be considerably worse for a low earth orbit. Only a geostationary orbit can eliminate this problem.

Another error source is connected to the previous one. Round trip phase tracking can remove, after the fact, link effects during a tracking pass on time scales greater than the round trip light travel time. However, there will be a jump in the spacecraft clock when multiple passes are connected (*e.g.* when the spacecraft is reacquired after passing out of sight). These jumps will be equal in magnitude (except for a geometrical factor) to the accuracy with which the spacecraft orbit is known. With a GPS receiver and GPS-like beacon on a spacecraft, the orbit can be known to a few cm, giving timing jumps on the order of 100 picoseconds. Even with a geostationary orbit, these jumps would occur any time the link was interrupted due to mechanical or electrical problems.

I. BACKGROUND

Flying an on board, high precision clock will introduce cost, mass, and power penalties to a mission. Therefore, it is useful to consider the option of phase transfer from a primary clock on the ground. Such a process is used for space VLBI, in which a radio telescope in earth orbit observes simultaneously with a network of ground radio telescopes. Space VLBI observations were successfully conducted using an antenna on a TDRSS satellite in 1986–1988 (Levy *et al.*, 1986), and they are planned for the VSOP mission, scheduled for launch in Feb. 1997 (Hirabayashi, 1991). VLBI observations (Burke, 1969) require excellent

(Hydrogen maser quality) frequency stability on time scales up to ~ 500 s, but are relatively insensitive to variations on longer time scales.

II. PHASE TRANSFER FOR SPACE VLBI

For the TDRSS space VLBI observations, an existing (non-optimized) system was used (Levy *et al.*, 1989). For VSOP, a customized phase transfer system has been designed, with link frequencies in the 15 GHz band (Springett, 1992). A predicted spacecraft orbit (based on tracking measurements over the previous week) is used to generate an uplink signal. If the predicted orbit were perfect, the received on board signal would be monochromatic (ignoring media effects) at the nominal frequency. The 6 hour elliptical orbit of VSOP involves spacecraft velocities, relative to a ground tracking station, of up to ± 9 km/s. The predicted orbit will be accurate to ~ 1 m/s (Estefan, Christensen, and Ellis, 1991).

The uplink signal is used to phase lock an on board oscillator that has good stability on time scales < 1 s. This oscillator is then used 1) to mix the amplified signal from a radio source to baseband before it is sampled and digitized, 2) to generate a clock to time tag these samples before they are transmitted to the ground, and 3) to generate a downlink signal coherent with the uplink.

The phase of this downlink signal is measured, and compared against the value expected from the predicted orbit. The residual phase (Measured–Predicted) is used during VLBI data correlation to correct the on board oscillator ‘after the fact.’ Any non-dispersive error source on time scales significantly greater than the round trip light travel time (≤ 0.19 s for VSOP) will be corrected. Orbit prediction errors and static troposphere delays fall into this category. Analysis has been done on the effect of the earth’s ionosphere (Linfield, 1996b) and on fluctuations in the earth’s troposphere (Linfield, 1996a). The conclusion is that the coherence of the phase transfer, after correction with round trip measurements, will be $> 99.5\%$ at 22 GHz (the highest observing frequency of VSOP) over time scales < 1000 s (see Thompson, Moran, and Swenson, 1986 for a definition of coherence as applied to VLBI). This is much better than the coherence of a hydrogen maser, so that the overall coherence of the orbiting telescope will be limited by the ground frequency standard.

III. ADVANTAGES AND DRAWBACKS

Using a phase transfer system instead of a precise on board clock on any earth orbiting spacecraft would save significant mass, power, complexity, and cost on the spacecraft. The on board mass and power requirements for phase transfer are likely to be in the 10 kg and 10 W range. However, there are some serious drawbacks for most applications.

The most serious drawback is that the on board clock can only operate intermittently, because it requires two-way communication with a ground tracking station. For the elliptical orbit of VSOP (1000 km perigee; 20,000 km apogee), a global network of 5 ground tracking stations will allow tracking $\approx 80\%$ of the time. For a geostationary orbit, one ground station could provide 100% coverage; for a low earth orbit, the fractional coverage would be quite small with any plausible ground network. In addition, the cost of tracking station time may be a significant issue for phase transfer.

For space VLBI, these two issues are not a concern. The data rate generated during VLBI observations is so large (128 Mbit/s for VSOP) that on board storage is not feasible. Therefore, a real time downlink to a sizable (≥ 10 m diameter) ground tracking station is required for observations, even with an on board clock.

When the round trip link is reestablished after a break (such as that due to the spacecraft dropping below the horizon at a tracking station), there will be a clock jump, due to the uncertainty in the one way light travel time along the spacecraft-tracking station direction. With on board GPS receivers and GPS-like beacons, the reconstructed (after the fact) orbit error can be as small as ~ 5 cm for a VSOP-like orbit (Wu and Malla, 1994), giving a clock jump of ~ 170 picosec.

A final limitation is that some effects of science interest (*e.g.*, gravitational redshift) require a primary frequency standard on board as well as one on the ground, and cannot be measured using round trip phase.

ACKNOWLEDGEMENT

The research described in this paper was carried out by the Jet Propulsion Laboratory, California Institute of Technology, under contract with the National Aeronautics and Space Administration.

REFERENCES

- B. F. Burke, "Long Baseline Interferometry," *Physics Today*, vol. 22, No. 7, pp. 54–63, 1969.
- J. Estefan, C. Christensen, and J. Ellis, "Japanese and DSN Orbit Prediction Capability for the VSOP Mission," July 1, 1991, *JPL Interoffice Memorandum*, 314.5–1551, available electronically at http://sgra.jpl.nasa.gov/mosaic_v0.0/JPL_Project_dir/Library_dir/memo/y91/91_72.txt
- H. Hirabayashi, "Introduction to the VSOP Mission and Its Scientific Goals," *COSPAR: Adv. Space Res.*, vol. 11, No. 2, p. 173, 1991.

- G. S. Levy *et al.*, "Very Long Baseline Interferometric Observations Made With an Orbiting Radio Telescope," *Science*, vol. 234, pp. 187–189, 1986.
- G. S. Levy *et al.*, "VLBI Using a Telescope in Earth Orbit. I. The Observations," *The Astrophysical Journal*, vol. 336, pp. 1098–1104, 1989.
- R. Linfield, "Tropospheric Coherence in the Space VLBI Phase Transfer Process. II. Inclusion of a Nonzero Phase Averaging Interval," April 2, 1996, available electronically at http://sgra.jpl.nasa.gov/mosaic_v0.0/JPL_Project_dir/Library_dir/memo/y96 (1996a).
- R. Linfield, "Ionospheric Coherence Loss in the Space VLBI Phase Transfer Process," April 29, 1996, JPL Space VLBI Memo #288, available electronically at http://sgra.jpl.nasa.gov/mosaic_v0.0/JPL_Project_dir/Library_dir/memo/y96 (1996b).
- J. C. Springett, "Phase Stable Frequency Transfer for Orbiting VLBI Radio Telescopes", NeoComm Systems, Inc., La Canada-Flintridge, California, October 15, 1992.
- A. R. Thompson, J. M. Moran, and G. W. Swenson, Jr. "Interferometry and Synthesis in Radio Astronomy," pp. 277–278, John Wiley & Sons, New York, 1986.
- S.-C. Wu and R. P. Malla, "GPS-Based Precision Determination of Highly Elliptical Orbits for Orbiting VLBI Applications" *JPL Interoffice Memorandum*, **335.8–94–004**, March 29, 1994.

DLR's research for space-maser monitoring with two-way microwave links

J. Hahn
DLR Oberpfaffenhofen, Germany
Institut f. Hochfrequenztechnik



BIBLIOGRAPHY

JÖRG HAHN

Jörg Hahn received the M.Sc. degree of Physics and Mathematics from the Belorussian State University in Minsk city, department of Radiophysics and Electronics, in 1993. In the same year he joined DLR in Oberpfaffenhofen, Institute of Radio Frequency Technology working as a young scientist in the navigation group. Since 1996 he works as a scientific collaborator. In his activities he is mainly involved with investigations into methods of ultra-precise clock synchronization, and research into synchronization tasks for future navigation systems.

contact:

phone: +49-8153-282335
fax: +49-8153-281135
e-mail: joerg.hahn@dlr.de

SUMMARY

This workshop handout presents DLR's research activities for ultra-precise clock monitoring. We will mainly refer to the so called „H-maser in space“ study as part of the ExTRAS project funded by ESA in which we investigated the modification of a two-way microwave ranging instrument for time transfer purposes. This leads to the introduction of the PRARETIME instrument. The expected accuracies for ground to space clock synchronization are presented assuming a H-maser clock onboard the Russian Meteor 3-M satellite.

Because ExTRAS was not continued due to financial constraints, an experimental effort has been made to show the PRARE(TIME) capabilities for ultra-precise clock synchronization. The outcome of a joint DLR-GFZ measurement campaign using PRARE on ERS-2 and GPS is presented here.

We also want to preview the next planned time experiments, i.e. H-maser on MIR, PHARAO and ACES on ISS ALPHA. To monitor future generation clocks in space more study work has to be done into ultra-precise time links. A proposal is made using the SATRE system to design a time link of the next generation. These results can be included in the concept for a future GNSS II.

**DLR's research for space-maser monitoring
with two-way microwave link**

J. Hahn

J. Hahn



Outline

- 1 Review on "H-maser in space" study
- 2 Experiments with two-way micro wave systems
- 3 Future work

J. Hahn



Review on "H-maser in space" study

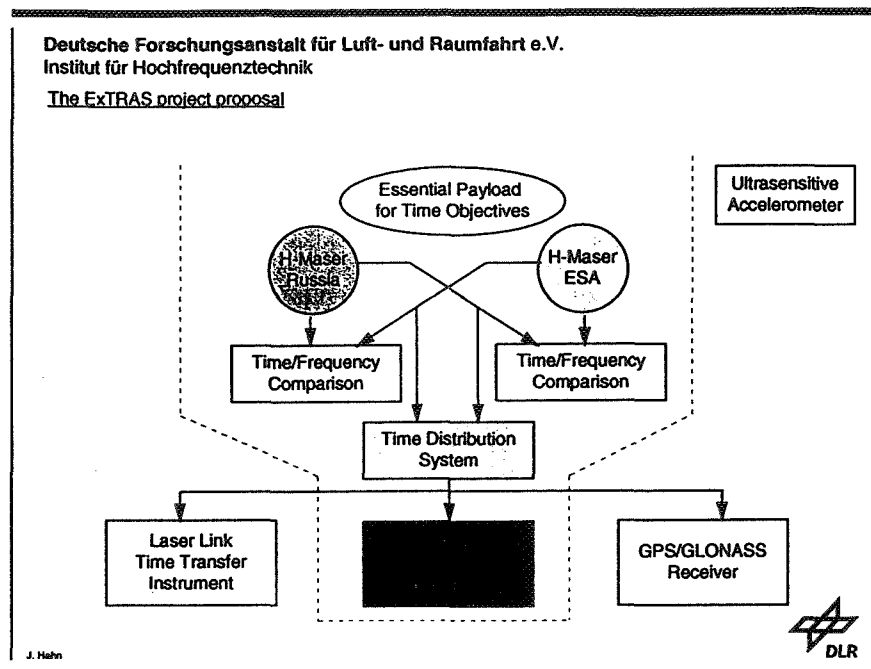
J. Hahn



In recent years, significant progress has been made in development of H-maser atomic clocks, which are the up to now most stable type of oscillators in the time interval range between 10^2 and 10^5 sec. Since several years, these clocks are off the laboratory and commercially available, and they are more and more used round the world for very precise timing applications, such as contributing to the time scales of TAI and UTC and time keeping in navigation and ranging systems (we refer mainly to [HAHN, J. et al, 1995]).

To make these ultra-stable clocks usable in space as well, there is a development of a space-qualified H-maser funded since several years by the European Space Agency ESA for application on a satellite. In consequence, the European and Russian Space Agencies ESA and RSA had planned to orbit in a joint technology demonstration experiment two space-qualified, active and auto-tuned H-maser oscillator clocks.

A Russian meteorological satellite, the first of the advanced Meteor-3M series, had been selected as a candidate mission. The H-maser clocks plus assistant equipment payload had been called ExTRAS for *Experiment on Time Ranging and Atmospheric Sounding*.



The satellite should circle the Earth in a near-polar sun-synchronous orbit at an altitude of about 1020 Km and would thus be observable from any point on Earth on the basis of a regular schedule.

Such an experiment would have the potential to serve as a global reference time station enabling world-wide time transfer with an accuracy that might be one order of magnitude better than the best alternative satellite timing technique currently in use.

The main objectives of the mission were:

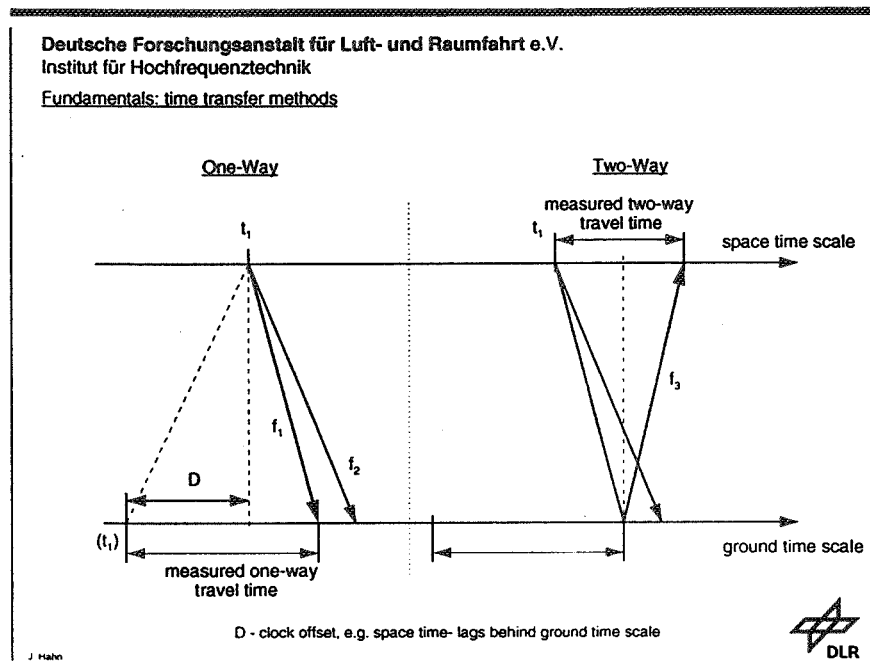
- in-orbit demonstration and performance verification of space-qualified H-masers;
- time transfer and time dissemination applicable in ultra-precise time metrology, satellite communication and navigation, and fundamental physics experiments;
- applications in geodetic and geophysical research activities, mainly precise point positioning on ground and orbit determination.

To make this orbiting ultra-stable time scale available at any station either on ground or in space, electromagnetic links have to be established, either in optical (laser) or in microwave (radio frequency) range.

ExTRAS should be cover both options, provided presumably with the French T²L² equipment (*Time Transfer by Laser Link*) on the one hand, and the German PRARETIME system (*Precise Range and Range-rate Equipment modified for TIME transfer*) on the other hand, both instruments linked coherently to the H-maser oscillators (a European and Russian one).

In the study, the time transfer possibilities and the achievable time comparison accuracy with the microwave signal transmission system PRARETIME, provided with the ultra-stable H-maser oscillator, had been detailed.

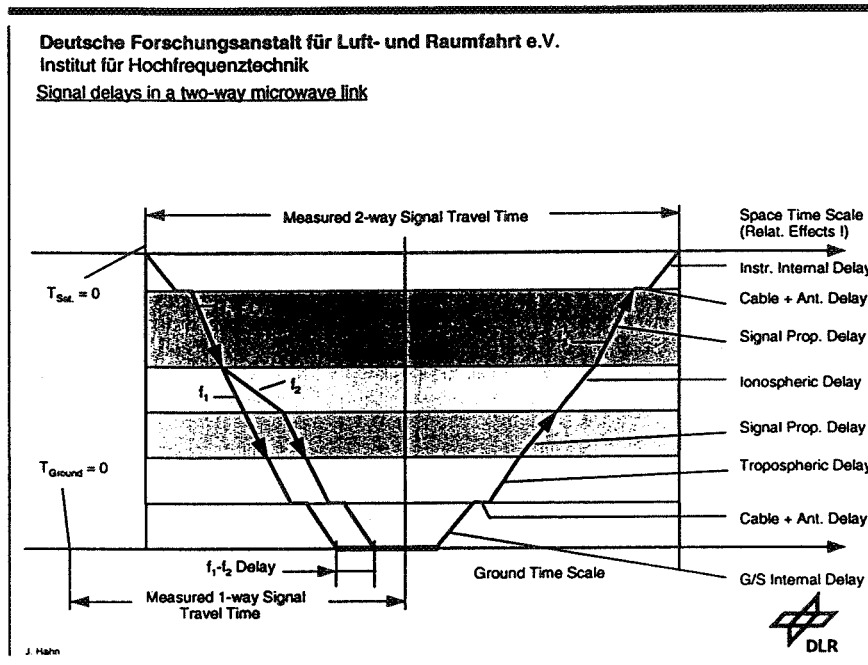
Two time transfer methods can be applied to synchronize a space and ground based clock: the one- and two-way method.



A time signal is started at a dedicated time t_1 from the satellite. The signal is received on ground where the one-way travel time is recorded. After accounting for the signal delays on the propagation path the clock offset D between the two clocks can be computed. For this the accurate knowledge of the satellite and ground station position is necessary.

In the case of a two-way link the signal after reception on the ground station is retransmitted to the satellite, and after arrival the measured two-way travel time can be recorded. Combining one- and two-way travel time the clock offset D can be computed. The advantage of the two-way over the one-way link is that NO accurate position coordinates of the satellite and ground station are needed to compute the signal propagation delays of the mainly reciprocal paths and the clock offset D respectively. Also the signal delays have to be evaluated in a differential matter only.

Below the signal delays which will be met in a two-way microwave link are presented. For evaluation of the ionospheric delay a second frequency is usual applied in the down link.



PRARE / PRARETIME

Simultaneous the figure outlines the principal operation of the PRARE (*Precise Range and Range-rate Equipment*) instrument. Note: the one-way signal travel time is not included presently, and represents a modification for timing purposes as identified in the study.

PRARE is a space-borne two-way three-frequency microwave tracking system which performs - in its present design - highly precise range and range-rate measurements at sub-decimeter level of accuracy with the assistance of transportable, dedicated ground-station transponders more detailed in [HARTL, Ph., 1984].

In its present status, it is operational onboard the ERS-2 satellite launched in April 1995, where it is used as main navigation payload for various applications in the field of orbit determination, geodesy, and modelling of the atmosphere.

With its design derived from the time transfer and synchronization equipment MITREX, the instrument offers already in its present status all necessary features for highly precise time transfer purposes.

The main technical features of PRARE can be obtained from the next figure.

X-band downlink	8489 MHz 10 Mbits/sec BPSK (bandwidth 10 MHz) 1 watt transmit power
S-band downlink	2248 MHz 1 Mbits/sec BPSK (bandwidth 1 MHz) 1 watt transmit power
ground transponder	coherent, 60 cm parabolic dish
X-band uplink	7225.296 MHz 10 Mbits/sec BPSK (bandwidth 10 MHz) 5 watts transmit power
satellite antennas	crossed dipoles at X- and S-band



J. Mann

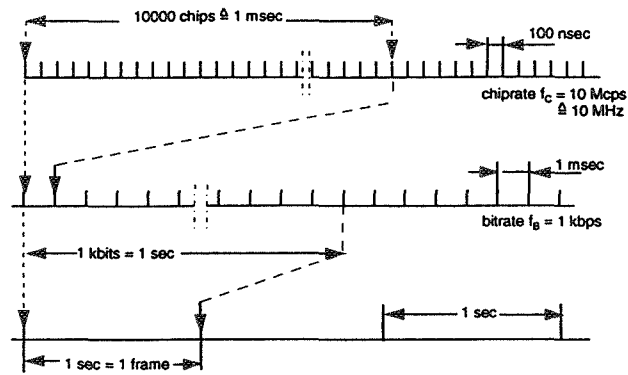
The instrument's measurement principle is based on two-way group delay and carrier phase measurements of spread-spectrum modulated, PN-coded microwave signals in X- and S-band. In X-band, the code length is 10.000 chips, in S-band 2.000 chips. The codes are repeated 998 times per second in X-band and 499 times in S-band, followed by 2 respectively 1 specifically modulated PN-sequences forming a 1 pps time mark. The measurement rate is, therefore, 1ms in X- and 2 ms in S-band, whereas the chip length is 100 ns in X- and 1 μ s in S-band. Data storage is carried out once per second, because the instrument is autonomously averaging and integrating over this period to reduce noise jitter and to improve system stability.

Below the X- and S-band ranging code structures are presented.

By taking advantage of the code-multiplexing technique realizable with PN-codes, up to four ground stations can be tracked simultaneously by the onboard equipment's four parallel receiver channels. As a result of the two-way technique, all measurements are referenced to one single reference frequency, the onboard instrument's main clock oscillation. This is the main reason for the very good overall measurement precision and accuracy of this system.

The instrument collects autonomously all data provided by the ground-station uplinks and processes it together with the measurement results centrally in the main processor. Measurement, telecommand, and telemetry data transmission in both directions (space - ground and ground - space) is performed by mod(2)-addition of the appropriately coded information onto the PN-code sequence. PRARE data rates are 2, 4, 5, 8, or 10 kbits per second. In present design, only the data rates 2 and 4 kbits/s are used; this is sufficient for real-time transmission of the measurement results of all four channels, for continuous transmission of about 120 telemetry values (temperatures, voltages, power amplitudes, ...), and for reception of ground commands.

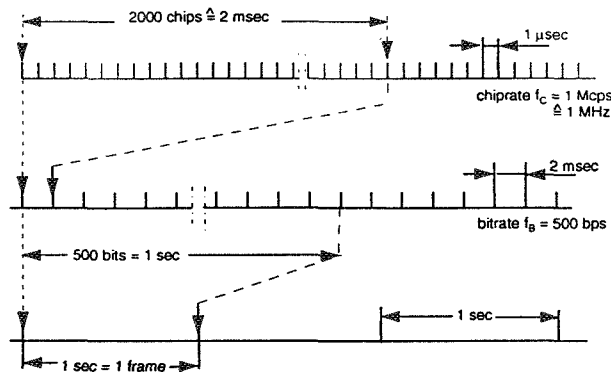
PRARE X-band ranging code structure



J. Hahn



PRARE S-band ranging code structure

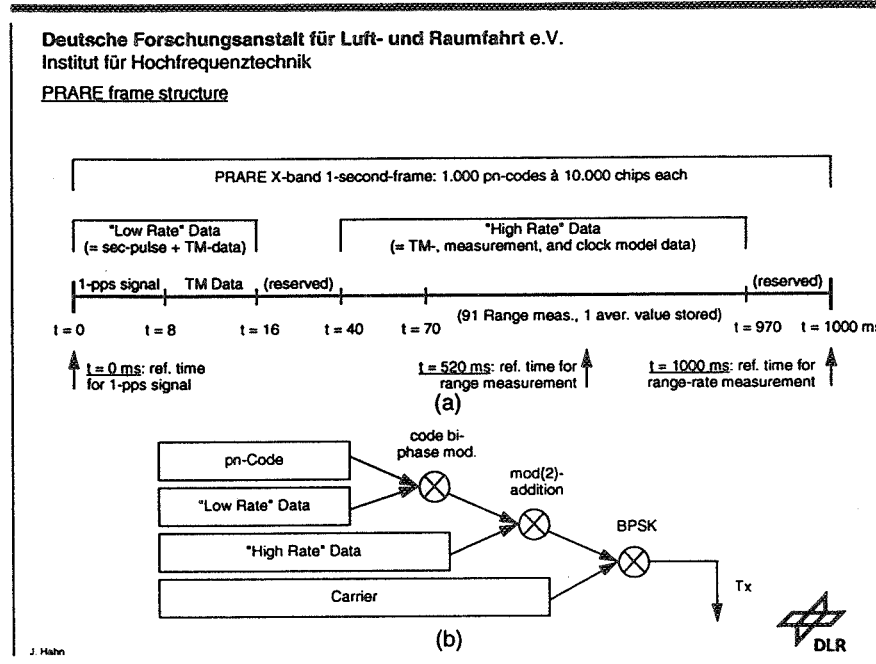


J. Hahn



In the modified PRARE design projected for EXTRAS, the remaining data transmission reserve will be used for transmission of additional data. Two-way clock comparison is entirely reliant on exchange of the measurement results obtained onboard with the ground station, and vice versa. The fact that, even in highest data transmission mode of 10 kbits/s, the resulting data/chip ratio is 1:1000 (X-band), guarantees easy code correlation and data decoding. Thus no changing of the

existing code and carrier schemes will become necessary; this enables compatibility of a modified PRARE with the existing ground-station network. The next figure shows the structure of a PRARE second-frame including the data modulation sections, and it summarizes the overall data modulation scheme.



The onboard equipment (mass 19 kg, power consumption 32 watts in present design) performs the two-way measurements in X-Band (signal flow: space - ground - space). Additionally, it transmits coherent signals in S-Band for ionospheric error correcting purposes and for data transfer redundancy (signal flow: space - ground). The dedicated ground-stations are small, mobile units. At X-Band, they work as regenerative and coherent transponders, at S-band, they are receivers for the transmitted signals performing measurement of the difference of the time-of-arrival of both signals which is the direct measure of the total electron content of the transmission path.

The procedure to perform two-way measurements is as follows: Transmission of X-band signals starts aboard, time-tagged by the onboard oscillator, as soon as the satellite is within the line-of-sight of a ground-station (above 10 deg elevation angle). After completion of the acquisition phase, the precise tracking begins above 30 deg elevation angle.

The PN-coded signals are received by the ground-station which generates itself, time-tagged by its clock, coherent PN-codes. The received PN-codes are locked to the on ground generated codes, demodulated, and the PN-sequence remodulates the X-Band uplink transmitter (regenerative transponder). The cleaned signal is then sent up back to the space-segment.

The transponders being at the same time coherent, the carrier frequency of the uplink is in the fixed phase relationship of 749/880 to the down-link carrier frequency.

On-board, the instrument is therefore able to measure both the two-way travel time and the received twice Doppler-shifted signal very precisely by comparing the phase of the received signal to the phase of the on-board instrument clock (DLL and PLL techniques). The overall accuracy results mainly from this two-way configuration of the measurement system which eliminates most clock error terms.

It should be denoted again: what the PRARE instrument really measures, is the time delay of the returning code signal with respect to the transmitted signal. Multiplied by the velocity of light, this delay represents the two-way range, whereas, in combination with the one-way delay time measurement on ground and with the respective clock time readings of the two measurements, it gives immediately the clock offset D of the two clocks.

For registration of signal delay within the instrument transmitter and receiver channels, there is a built-in test transponder which measures the internal delay time prior and after ground-station contacts. Together with the scientific measurement data, they are stored inside the instrument. Used for total delay measurement correction, they allow additionally to monitor long term stability and performance dependencies.

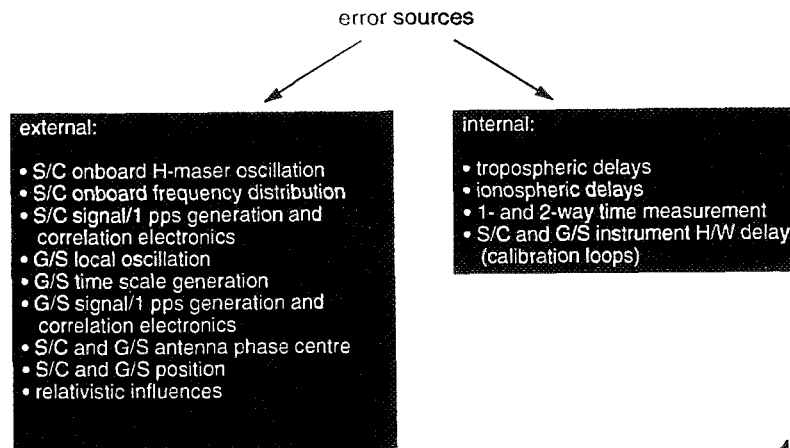
For ionospheric error correction, the coherently downlinked PN-sequences of the X- and the S-band are demodulated in the ground-station. The 10 MHz PN-code of the X-band down-link is compared to the corresponding 1 MHz PN-code of the S-Band. The time difference is a measure for the total electron content of the ionospheric path. The delay value is sent up to the satellite together with the meteorological data and the housekeeping values of the ground-station including its internal signal delay time.

Together with the other correction terms, which are all stored centrally in the onboard instrument memory, immediate evaluation of the true geometric range respectively the current clock desynchronization are calculated.

The overall measurement precision of the existing PRARE system is as follows (i.e. PRARE onboard ERS-2):

noise values	2.5 cm RMS for X-band ranging (1 measurement/sec.) 0.05 mm/sec RMS for X-band Doppler (30 sec integration time, 90° elevation)
hardware bias	< 1 cm for X-band
total ranging accuracy	3 ... 7 cm RMS (1 sec integration time)
total range-rate accuracy	0.05 mm/sec RMS (30 sec integration time)

During the study an attempt has been made to identify and quantify all error sources influencing the clock synchronization.



TIME TRANSFER WITH PRARETIME

The crucial parameter for the accuracy of two-way microwave time transfer is the precise determination of the asymmetries of the down- and of the uplink signal transmission paths. The existing PRARE instrument does only round-trip, i.e. two-way measurements, which do not allow to distinguish between the two directions. This must be fulfilled by additional one-way signal delay measurement of one of the paths which can only be provided by a second atomic clock standard on ground.

In the current PRARE system layout, only the GFZ Master Ground Station (GFZ - *GeoForschungsZentrum* Potsdam with its branch in Oberpfaffenhofen), which is responsible for final data collection and processing, is equipped with an atomic clock and with the necessary one-way delay time measurement facilities. This way, the station is able to time-tag the measurements collected by the PRARE instrument to UTC and to make them utilizable for the geodetic user community. The overall time system is, however, currently designed to provide a conformity to UTC of only 1 ms, which is sufficient for the long-term averaged orbit determination and point positioning purposes the geodetic users require.

It should be emphasized here again: although its design is in principle adequate for two-way time transfer, the PRARE system is - in its present form - not usable for the wished immediate, ultra-precise time dissemination and clock comparison. Besides the fact that the potential user has to be equipped with a modified PRARE ground station, which must be able to provide a one-way (downlink) clock signal received from the onboard segment to be compared to the user's clock signal by TIC measurement, the software routines and the code data signals for continuous, ultra-precise, two-way space-clock monitoring and correction are presently not implemented.

As a second fact, it must be repeated here that the present PRARE instrument is not in all its elements of the signal transmission chain as accurately designed as it is necessary to achieve the desired figures. Careful analyses of data available from PRARE on Meteor-3 showed a clock comparison accuracy of better than 2.5 ns which is indeed a very good value compared to other time transfer techniques in use, but it does not meet the required accuracies and the precision potential the PRARE system offers.

The points for instrument respectively system improvement are summarized here:

- The modified PRARE instrument PRARETIME must have access to the H-maser's very stable oscillation output. This includes delay time variation control of the elements connecting H-maser output with PRARETIME instrument input.
- The instrument's internal signal transmitter and receiver chains (signal generation and modulation, amplification, plugs, cables) have to be calibrated separately prior to launch, and they have to be monitored independently in-flight by a modified internal test-transponder.
- Transmitter carrier and signal generation inside the instrument have to be stabilized by including output amplification and filter within the control loop.

- Asymmetry of the down- and the uplink paths has to be determined by appropriate one-way travel time measurement on ground: atomic oscillator + high-quality time interval counter + routine data evaluation software.
- Additional data, which is to be transmitted in near real-time in both directions, must be appropriately coded and included in the existing data transmission structure to ensure compatibility of PRARETIME with the existing ground-station network.

As a last point, some comments on the instrument's range-rate measurements, i.e. the onboard carrier phase correlation, should be made. In present design, carrier phase measurement of the returning signal is not realized to full extent. The twice Doppler-shifted signal is phase-locked to the onboard receiver frequency, which is shifted itself due to the a-priori knowledge of the expected Doppler. Pre-calculated by onboard ephemeris software, and phase-locked to the incoming signal, the receiver carrier phase is finally registered by means of a Doppler counter.

Residual noise is much less on carrier than on code phase because of the much higher frequency. For utmost precision, instrument design could, therefore, be changed with respect to an improved Doppler phase measurement resolution, or even by introduction of real carrier phase measurement. By these means, full access to the important carrier phase information could be gained which would result in an even better overall performance utilising cross-correlation techniques.

It must be noticed, however, that this modification would only come into effect, if all other proposed points of improvement are realized first, i.e. mainly improved signal stability and hardware calibration. With respect to diverse practical experiences gained so far concerning this problem, it seems that here the crucial point for ultra-precise time transfer has been identified. Only when hardware calibration efforts come into the accuracy range of residual carrier phase noise, measurement and evaluation of this parameter becomes useful.

Some estimated accuracies of PRARETIME + H-maser, the study results and their applications can be found below.

total accuracy = method accuracy + external uncertainties

time-ranging			time comparison		
G/C-S/C	CV	Ext. CV	G/C-S/C	CV	Ext. CV
133	169	188	82	90	117

(figures in [ps])

conditions:

- observations around culmination point
- number of measurements n = 10

J. Hahn



In the study work also a possible one-way mode has been quantified.

total accuracy = method accuracy + external uncertainties

G/C-S/C	CV	Ext. CV
1024	539	1452

(figures in [ps])

conditions:

- neighborhood around culmination point
- number of measurements n = 10
- Meteor 3M-orbit

J. Hahn



Additional Data needed for PRARETIME One-Way Mode

- orbit parameters
(ephemerides)
- clock correction parameters
(clock model)
- UTC(k) parameters
- ionospheric corrections
(ionospheric model)

J. Hehn



Accuracy comparison between GPS and PRARETIME + H-Maser one-way modes

	G/C-S/C	CV	Ext. CV
PRARETIME	1	0.5	1.5
*GPS (SA-off)	16	8	-
*GPS (SA-on)	49	22	-

all figures in [ns], * measurement over 780 seconds, measured ionosphere

J. Hehn



Navigation:

- Independent orbit determination and synchronization calculation due to two-way principle of PRARETIME;
- Highly accurate synchronization of all ground and space clocks of a navigation satellite system;
- Due to full maintenance of ranging features, PRARETIME provides by itself all necessary features of a satellite navigation system;
- Predecessor of a European navigation system, technology and orbital use demonstration of an H-maser clock.

Science:

Various fields of application, e.g. geoscience, fundamental physics, etc., have been identified during previous ESA science and experiment planning meetings.



Summary and Conclusion

- PRARETIME equipment is adequate to monitor a "H-maser clock in space";
- total synchronization accuracy (two-way) is about one order of magnitude better than all other time receiver methods in use today;
- measurements around culmination point provide best results;
- one-way signal travel time measurement equipment on ground (atomic oscillator + high-quality TIC + data evaluation SW) is inevitably necessary;
- active (two-way) civil user gets access to UTC(k) with an accuracy of about 300 ps, passive (one-way) user with about 1500 ps;
- precise instrument ranging and range-rate capabilities are fully maintained.

"H-maser clock in space"
offers to connect the most precise clocks around the world to an ensemble
provides simultaneous, highly precise orbit determination and point positioning
is the first step to an European navigation satellite system



Experiments with two-way systems

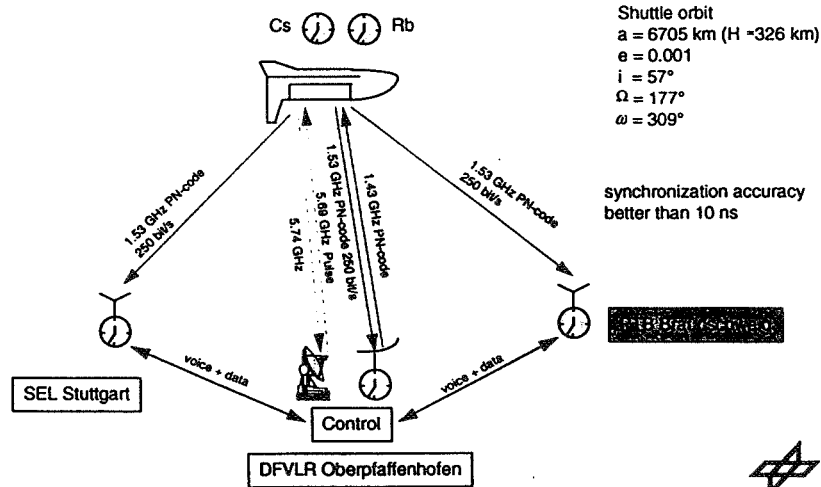


J. Maeh

NAVEX

In April 1981 DLR's NAVEX proposal was accepted by NASA as an experiment of mission D1, and project work began. The general objective of NAVEX was to gain experience with new techniques and problems of the new generation of satellite navigation systems coming up. This seemed the more desirable since in western Europe no experience with satellite navigation systems existed at that time. Spacelab offered a unique opportunity to change this situation quickly and at a comparatively low expenditure. Beyond this the chance for a relativity experiment was given, provided that all technical tests proceeded well [STARKER, S. et al, 1990].

NAVEX experiment setup (1985)



J. Maeh

PRARE on ERS-2

Unfortunately the EXTRAS project was not funded by ESA. To test the above described two-way clock comparison method, an experiment has been planned between DLR and GFZ in 1995 performing a "Common View" (CV) ground clock synchronization scenario by means of PRARE onboard ERS-2 and GPS time receivers [HAHN, J., BEDRICH, S., 1996]. For DLR it was the first experiment with PRARE equipment data. The main goal of this experiment was clock comparison via two-way microwave time links. Existing systems like MITREX use geostationary satellites (GEO) for this purpose. But a GEO only covers a certain area of the Earth. For global time comparison operation or time dissemination a polar orbiting reference has to be used. Two-way clock synchronization using an orbiting time reference has been studied

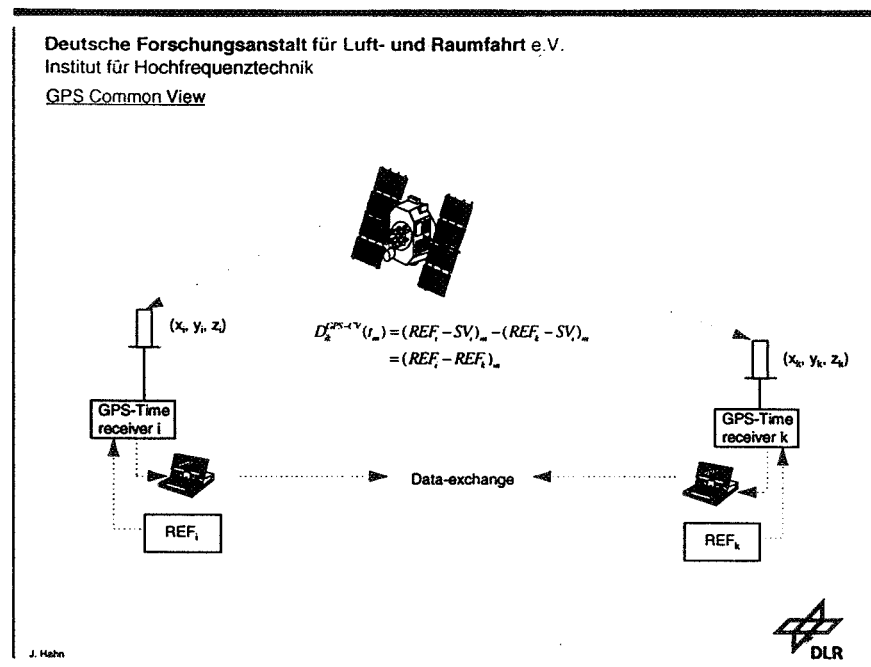
During the measurement campaign two different clock comparison techniques have been used simultaneously: clock comparison via

- GPS CV and
- PRARE instrument onboard ERS-2.

These methods are outlined here briefly.

GPS-"Common View"

The GPS CV is a well proved time comparison method of remote clocks using the BIPM GPS tracking schedule. Following this schedule, all participating time receivers monitor a dedicated GPS satellite clock simultaneously.



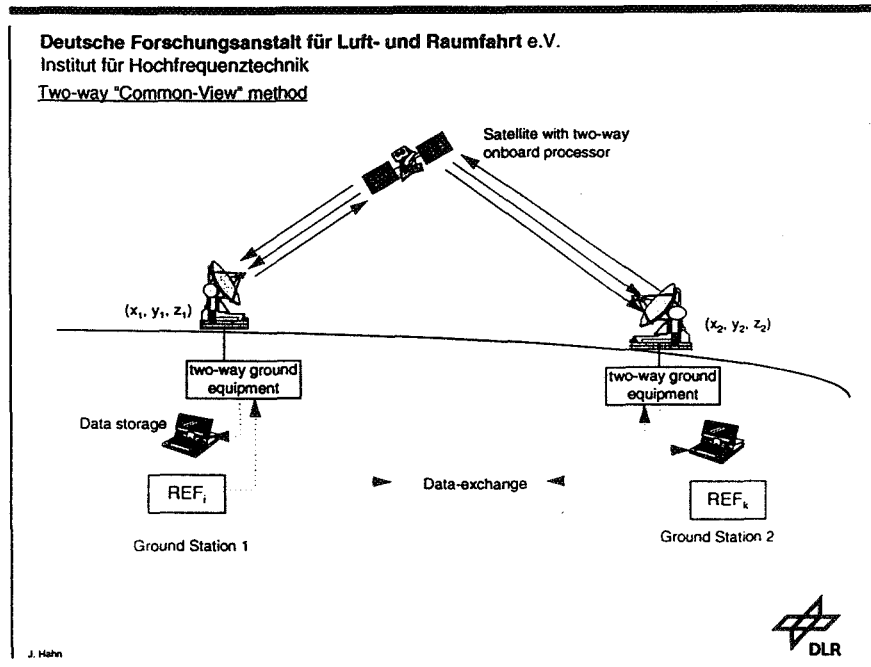
Each GPS time receiver with its reference clock REF_i records the time difference $(REF_i - SV)_m$ averaged over a certain interval (780 sec) at time t_m , where j is the

pseudo range number of GPS satellite SV . Data correction accounting for ionospheric, tropospheric, relativistic and range delays are implemented in the receiver with different effort.

By exchange and subtracting the recorded files the clocks REF_i and REF_k can be synchronized respectively. Repeating this procedure for any available time $t_m, t_{m+1}, t_{m+2}, \dots$ the rate R between the clocks can be computed over a certain time interval. The accuracy for this comparison method is around 3.6 ns following [Lewandowski, W., THOMAS, C., 1991].

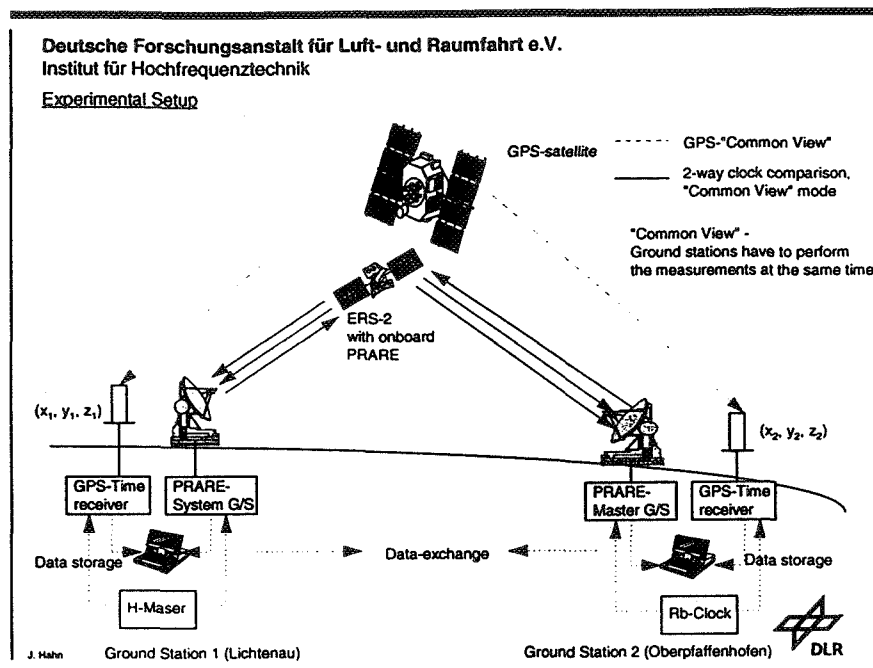
PRARE Clock Comparison

The two-way clock comparison principle with PRARE / PRARETIME has been given above. Now, synchronization of remote G/C's mutually is possible by CV observation of the S/C. When subtracting the computed clock offsets at two distant sites the clock offset between the ground clocks can be calculated.



Experimental Setup

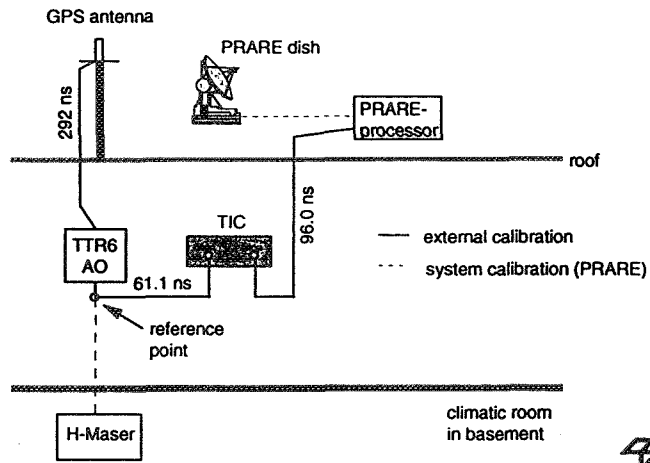
The figure presents an overview of the experimental setup with ground station sites in DLR's branch in Lichtenau near Weilheim and GFZ's branch in Oberpfaffenhofen near Munich. Each station was equipped with an appropriate PRARE station and GPS time receiver.



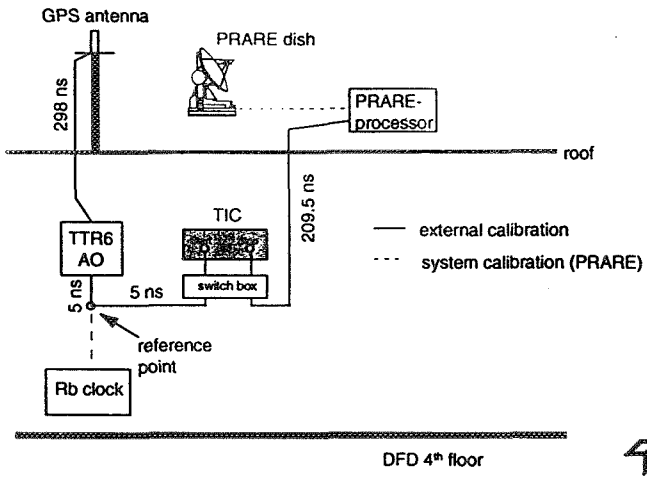
Next the principal structure of the experimental setup in DLR's branch in Lichtenau can be obtained. The reference clock, a H-maser CH1-75 of Russian company "KVARZ" is located in a climatic room in the basement. The GPS time receiver AO TTR6 operates in the time lab where the TIC for the one-way measurement is placed too. The PRARE processor with antenna dish at roof is connected via cable to the TIC in the time lab.

The setup in GFZ's branch in Oberpfaffenhofen corresponds particularly to the PRARE Master Station configuration. The reference clock is represented by a Rb-clock in phase locked redundancy by EFRATOM which is DCF-77 disciplined to follow the UTC(PTB) time scale, cf. [BEDRICH, S., FLECHTNER, F. 1996]. Also a GPS time receiver AO TTR6 with a TIC for registration of one-way measurements is located in the operation room. The PRARE processor with antenna dish at roof is connected via cable to the TIC in the operation room.

Deutsche Forschungsanstalt für Luft- und Raumfahrt e.V.
 Institut für Hochfrequenztechnik
 Hardware calibration - experimental setup at DLR's branch in Lichtenau

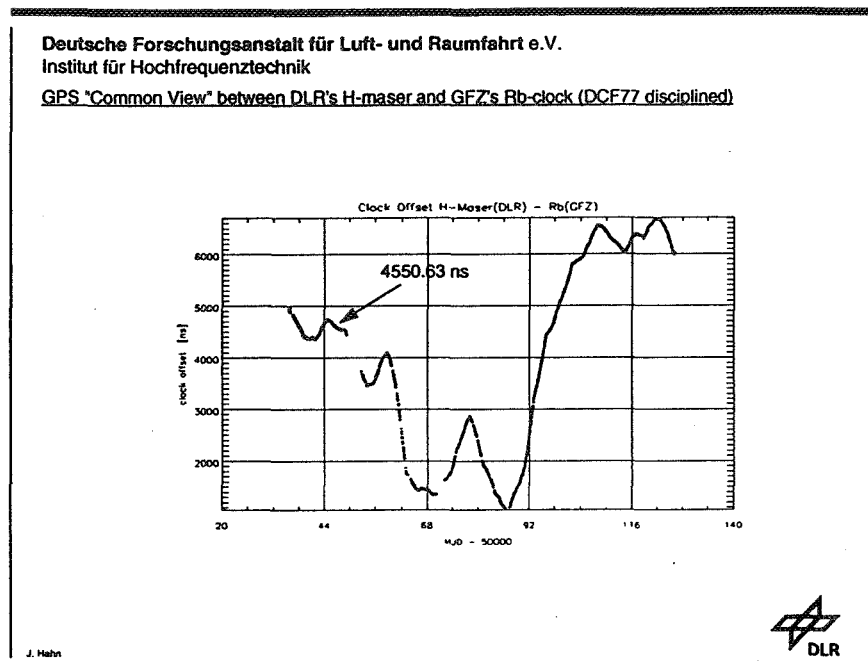


Deutsche Forschungsanstalt für Luft- und Raumfahrt e.V.
 Institut für Hochfrequenztechnik
 Hardware calibration - experimental setup at GFZ's branch in Oberpfaffenhofen

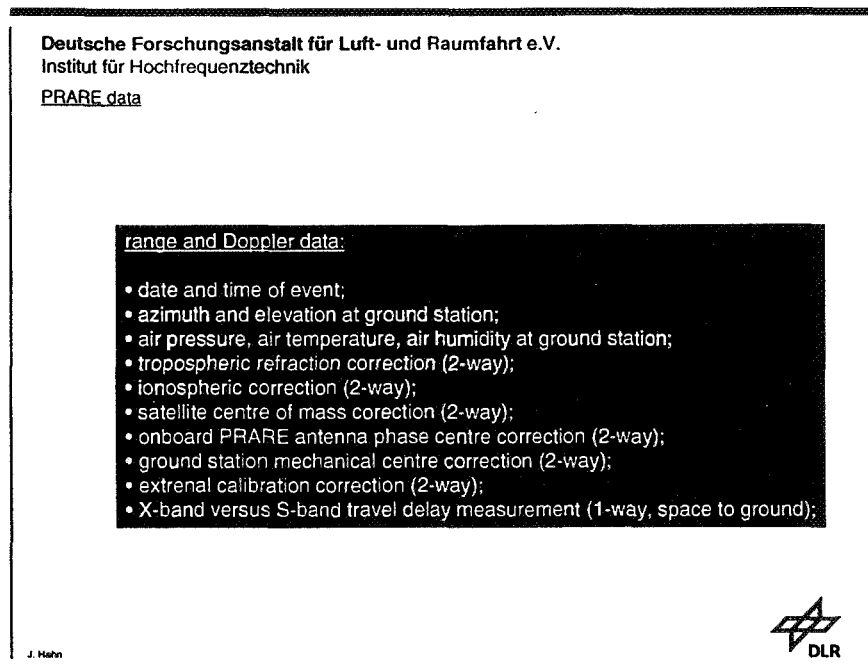


Data Evaluation:

GPS-CV



PRARE data



PRARE data

in only range data:

- two-way travel time including internal calibration of the space segment and ground station and 91 value range correction;

in only Doppler data:

- measured Doppler cycles (2-way) including internal calibration of the space segment and ground station;
- frequency offset relative to nominal satellite frequency 8.489 GHz

at ground station site:

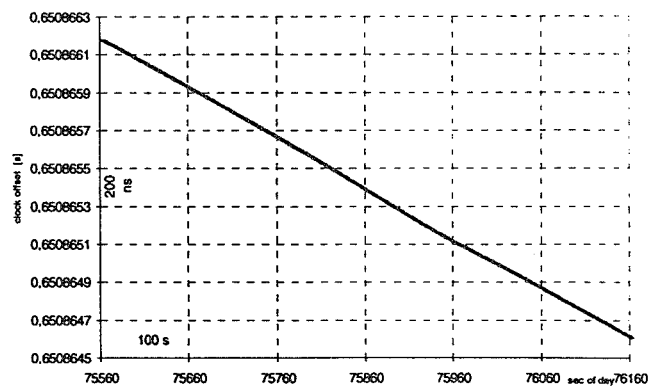
- date and time of event;
- one-way travel time measurement.

J. Hahn



An example of two-way clock comparison between the H-maser reference in Lichtenau and PRARE onboard clock (ERS-2) during a 600 sec pass on 25 November 1995 is presented. Here the rate of the PRARE oscillator can be identified; it includes relativistic effects which have not been accounted for yet.

PRARE Two-Way Clock Comparison, 25.11.95 (DLR's H-maser - PRARE ERS-2)



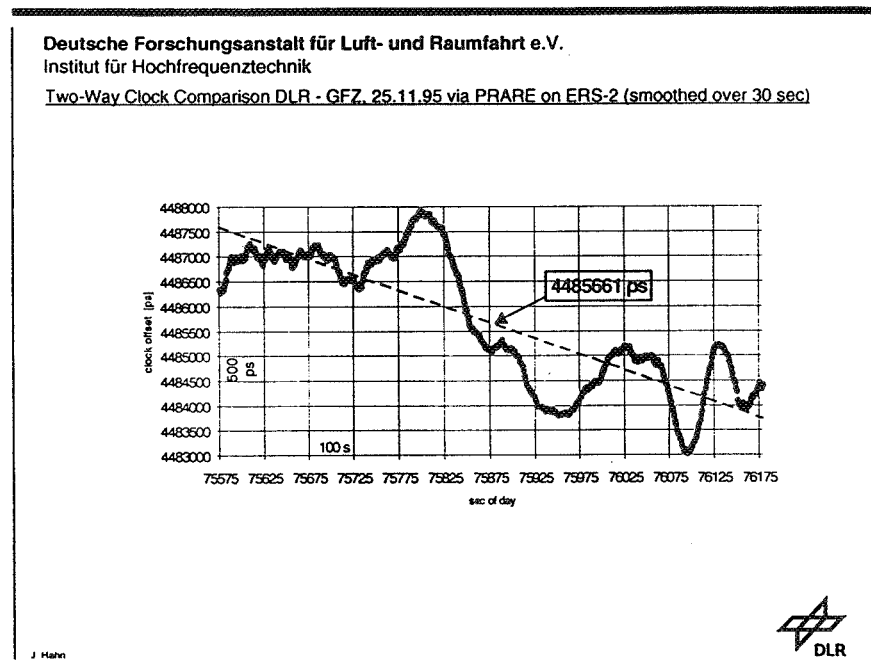
J. Hahn



In the following, the results of the differential data processing of the PRARE pass from 25 November 1995 are presented. The pass had a duration of about 650 sec. Data points calculated are smoothed over 30 sec. The standard deviation from the linear regression line is given by a figure of 770 ps (1σ). To compare the processed time offset with the GPS CV results, the midpoint of the regression line has been determined to be $D_{12}^{TW}(t_m = 75878 \text{ sec of 25 Nov 1995}) = 4485.66 \text{ ns}$.

For the time corresponding to the above evaluated midpoint GPS CV clock data have been processed in the following manner: For the 25 November 1995 a linear regression line has been computed. The clock offset corresponding to the midpoint of PRARE pass has been evaluated by interpolation to be $D_{12}^{GPS-CV}(t_m = 75878 \text{ sec of 25 Nov 1995}) = 4550.63 \text{ ns}$. Here the standard deviation from the linear regression line is given by a figure of 8.91 ns (1σ).

With a great number of other PRARE CV data processings the fact could be verified that the precision of PRARE two-way clock comparison in present design is always around 1 ns.



Results

25.11.95, sec 75878

PRARE differential clock comparison (DLR - GFZ):

D = 4485.66 ns, standard deviation: 770 ps (1σ)

GPS CV (DLR - GFZ):

D = 4550.63 ns, standard deviation: 8.91 ns (1σ)

J. Hahn



Reasons of bias discrepancy

- uncertainty of time offset between the GPS time receivers;
- the calibration measurement was not sufficient for accurate GPS calibration;
- missing one-way travel time calibration of the PRARE ground stations.

J. Hahn



Conclusion

- differential two-way clock comparison by means of PRARE onboard ERS-2 is presently possible with a precision of around 1 ns;
- a similar figure is expected for space to ground clock comparison;
- achievable accuracy is supposed to be of the same order;

experiment output:

- possibility of highly accurate global clock comparison and time transfer if a two-way time and ranging system of PRARE like type is carried onboard a polar orbiting satellite;
- application for synchronization purposes within future navigation satellite systems.

J. Hahn



Differential two-way clock comparison (ground to ground) by means of PRARE onboard ERS-2 is presently possible with a precision of around 1 ns. A similar figure is expected for space to ground clock comparison causing from the two-way principle. The achievable accuracy which is supposed to be of the same order must be further investigated. Due to time constraints this matter could not be discussed finally (calibration problems with GPS).

The experiment emphasizes the possibility of highly accurate global clock comparison and time transfer if a two-way time and ranging system of PRARE like type is carried onboard a polar orbiting satellite. The results point out that in conjunction with an ultrastable onboard reference this configuration could be applied for clock synchronization within future satellite navigation systems (GNSS I and II) and for benefit of the whole time community.

Future work

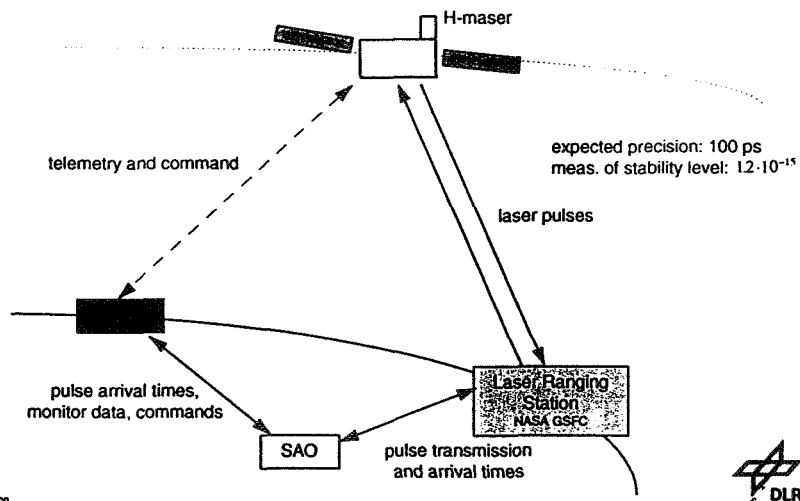
J. Hahn



H-maser on MIR

An atomic hydrogen maser clock system designed for long term operation in space will be installed on the Russian space station, MIR, in late 1997 [MATTISON, E.M., VESSOT, R.F.C., 1996].

H-maser on MIR (planned for late 1997)



J. Hahn



The H-maser's frequency stability will be measured using pulsed laser time transfer techniques. Daily time comparisons made with a precision of better than 100 ps will allow an assessment of the long-term stability of the space maser at a level on the order of 1 part in 10^{15} or better. Laser pulse arrival times at the spacecraft will be recorded with a resolution of 10 ps relative to the space clock's time scale. Cube reflectors will reflect the pulses back to the Earth laser station to determine the propagation delay and enable comparison with the Earth-based time scale. Data for relativistic and gravitational frequency corrections will be obtained from a GPS receiver.

Unfortunately no microwave link has been included in the experimental setup what would offer much more possibilities for research on this matter.

PHARAO

In 1994, the French space agency (CNES) decided to support a preliminary research program on a space frequency standard using cold atoms, cf. [CHANGEART, F.J., 1996]. Three laboratories are cooperating for the construction of a prototype which will be tested in aircraft parabolic flights. Simultaneously, studies on local oscillator, frequency synthesis chains, microwave cavity modeling and time-frequency transfer are being performed.

Deutsche Forschungsanstalt für Luft- und Raumfahrt e.V.
Institut für Hochfrequenztechnik

PHARAO (Projet d'Horloge Atomique par Refroidissement d'Atomes en Orbite)

development under CNES

ENS (Ecole Normale Supérieure) / LKB (Laboratoire Kastler-Brossel),
BNM (Bureau National de Metrologie / LPTF (Laboratoire Primaire du Temps et des Frequences),
LHA (Laboratoire de l'Horloge Atomique)

supported by French Space Agency (CNES)


DLR

J. Hahn

objectives:

- demonstration of a clock running with laser cooled atoms in micro-gravity conditions and determination of its performances. ($10^{-13} \tau^{-2}$; one day: $3 \cdot 10^{-16}$, 30 ps);

open a new era of space missions using ultra-stable clocks as space VLBI, high precision measurement of the sun gravitational potential to second order (quadrupole term) or of the Shapiro delay as proposed in the SORT mission;

for realization either fly two identical systems to make frequency comparisons or use high performance two-way time and frequency transfer systems with Earth based clocks of similar performances;

- measurement of the gravitational red-shift with a potential 100-fold improvement over the GPA experiment (1976);
- global time and frequency dissemination.

J. Hahn



A crucial factor in the use of a space frequency standard is the quality of the frequency comparison between the onboard clock and frequency standards on Earth. In order to transfer this space clock performance, a 10^{-16} accuracy is required. Today, GPS is in the 10^{-14} - 10^{-15} range and two-way links are in the 10^{-15} range. At least a one order of magnitude improvement is needed. An optical link using ps-laser pulses is being developed by the Observatoire de la Côte d'Azur, with an expected accuracy of 10^{-16}

However, by contrast to the optical link, the micro-wave links has the advantage of being independent of weather conditions and can allow a continuous link with the space clock.

ACES

For the *International Space Station ALPHA* (ISSA) an atomic clock ensemble in space has been discussed [VEILLET, Ch., 1995]. ACES (*Atomic Clock Ensemble in Space*) is both a test of technology using ISSA for an operational use on other spacecrafts and an experiment by itself on ISSA. For ISSA a H-maser, cooled atom clock and trapped ion clock monitored by an optical and microwave link respectively have been proposed.

Clearly it is outlined in the report:

ML, the microwave link has been studied by Vessot in its parabolic flight of a H-maser in 1976. On ISSA however, the method has to be modified, as it is impossible to observe ACES continuously from the ground. The phase is lost from an ISSA pass to the next one some time later. A microwave link able to transfer time, and not just the frequency, has to be used. Various possibilities are under study, but none has been tested yet. And: ML is not ready. Studies and investments will

have to be made, and some of them are already undertaken. In Europe, the microwave link should be studied also in cooperation with Germany.

Deutsche Forschungsanstalt für Luft- und Raumfahrt e.V.
 Institut für Hochfrequenztechnik
ACES on ISSA

ACES - Atomic Clock Ensemble in Space FCDP - frequency comparison and distribution package

goals:

1. characterize and intercompare 3 different clocks :
 H-Maser (HM), cooled atom clock (CA), trapped ion clock (TI)
 in a microgravity environment
2. provide, through radio (ML) and optic links (OL), an unique flying time scale based on an ensemble of very stable clocks, on a worldwide basis. Possibility of time transfer between remote ground laboratories all over the Earth

J. Hahn 

Deutsche Forschungsanstalt für Luft- und Raumfahrt e.V.
 Institut für Hochfrequenztechnik
ACES / ISSA

T/F measurements

- applications in: navigation, time scale realization and maintenance, large-scale synchronization, fundamental physics experiment, ultra-stable clock studies
- new era in time scale monitoring: unique very stable flying atomic clock time scale
- possible experiments:
 - gravitational redshift
 - isotropy of light
 - gravitational delay of the light passing close to the sun (determination of the post Newtonian parameter γ four orders of magnitude better than presently achieved)
 - investigation of gravitational field of the Sun
- qualify some of the best clocks available for future missions

available by the end of 1999

J. Hahn 

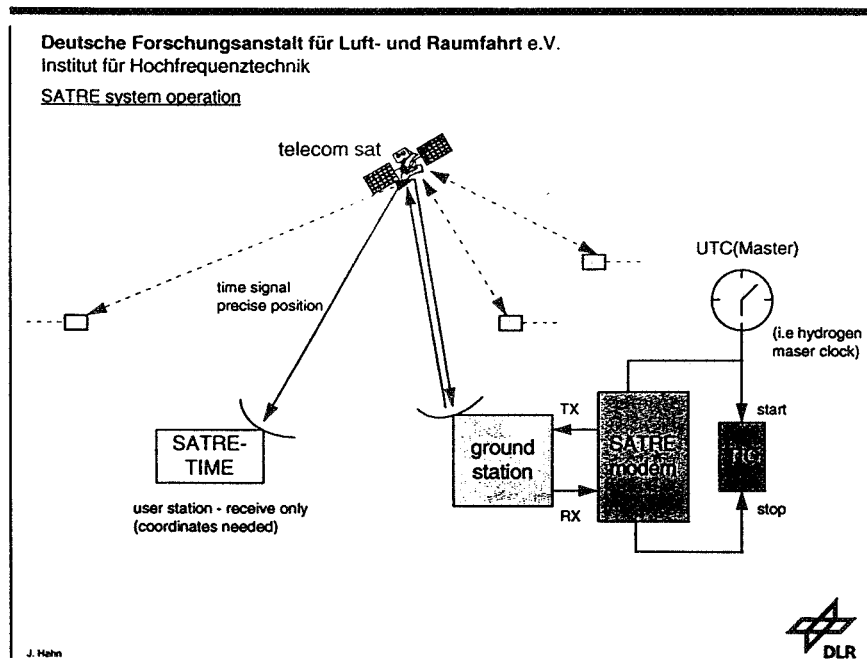
SATRE system

In 1983 the University of Berlin developed and manufactured a time transfer-modem using the spread spectrum technique. The *Microwave Time and Range Experiment* MITREX was designed to operate with Telecom-satellites and ground stations using a carrier frequency of 70 MHz [MITREX 2500A, 1989].

The new developed *SATellite Time and Range Equipment* SATRE introduces great improvements in accuracy and usage [DIENERT, M., 1992]. The SATRE modem allows very precise synchronization of remote clocks. Accuracies of 0.7 ns are well within the capabilities of the system with a precision as high as 30 ps [SATRE, 1995]. These values are obtainable within the first minutes of operation. Intercontinental links are possible using geosynchronous communication satellites.

For the instrument no special communication channel is needed. It is possible to transmit the time synchronization signals of the modem over a busy transponder, in this manner, the telecommunication signal performance is not degraded. The equipment is not susceptible to ionospheric errors and military secrecy. SATRE-modems deal with two-way time comparison measurements for synchronizing two remote ground clocks via a geosynchronous direct TV-broadcasting satellite.

Aside from the time transfer the pseudo-noise signal of SATRE can be used for ranging. In both cases, it is not necessary to have special instrumentation aboard the satellite or any modification of its transponders.



Two-way measurements of a ground station by means of SATRE-modem via satellite with its own signal lead to the slant range measurement between ground station and satellite. This transmitted pseudo-noise signal can also be used to disseminate time synchronization signals to be received and processed by the new developed SATRE-TIME instrument. This equipment represents a receiver only

modem generating an ultra-stable time scale for the one-way user. SATRE-TIME generates an ultra-stable time scale using time synchronization signals, and precise position from a dedicated direct TV-broadcasting satellite.

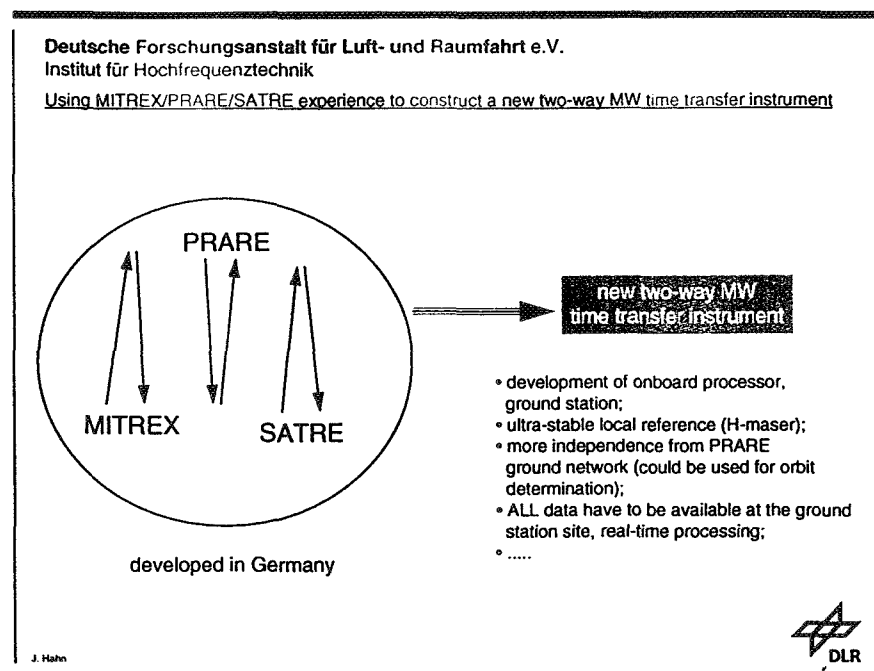
The out- and input carrier frequency of the SATRE-modem are equal to the IF of TV-Station, the ranging signals are transferred via the RF-carrier frequency of the TV-signal. The chip rate of SATRE is 20 Mchips corresponding to 30 MHz transmitter bandwidth.

The SATRE modem can be expanded to contain up to four receiver channels which operate independently and simultaneously. The system can be freely configured. For example, one channel can be assigned to receive the own re-transmitted signal and the remaining three channels can receive signals from remote sites. The unique combination of time and data (500 bit/sec) transmission in one instrument allows efficient time synchronisation and maintenance of large network [SATRE, 1995].

Using SATRE for the future

SATRE is a ground based equipment. It was induced from the MITREX and PRARE system architecture. This modem represents the state of the art in ultra-precise remote clock comparison using PN-codes and spread spectrum technology.

It should be possible to use the technical advantage of the SATRE system to create a new space based two-way microwave equipment.



All lessons learned with PRARE(TIME) have to be included in such a process. This concerns the technical aspects to develop either the onboard processor and the

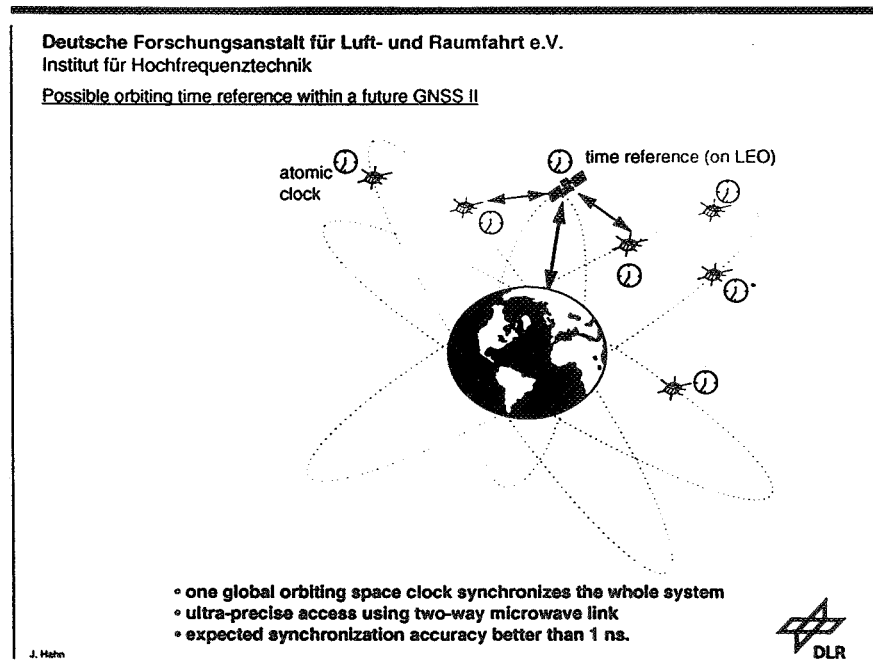
ground station. The instrument must be designed to operate with an ultra-stable onboard oscillator, at least a H-maser clock.

Also to meet the requirements of the timing community the new system should be more independent from the current PRARE ground station network. This network is worldwide established and operates in order to solve problems in the field of orbit determination, geodesy, and modelling of the atmosphere. It should be applied to calculate the orbit of the satellite carrying the new system.

The generation of the system's time scale to be disseminated or investigated should be a concern of the timing community. Here accurate two-way space clock monitoring is necessary. It is essential, that all data needed for time transfer operations must be available at the ground station site and thus have to be processed there in real-time.

In the development of such a new system concept and equipment DLR would commit all of its experience in this field and generally offers its readiness to cooperate with other institutions and companies.

Such a new system proposed here could be implemented in a future GNSS II. Installed onboard a suitable satellite platform (for example polar orbit) it could satisfy the needs either of the navigation users and of the timing community, i.e. ultra-precise access to an ultra-stable, global available time reference.



References

- HAHN, J., Bedrich S., Nau, H., *Study on 'H-Maser in Space' as Ultra-Stable Clock for Time Transfer and Time Dissemination*, DLR Oberpfaffenhofen, January 1995
- HAHN, J., BEDRICH, S., *Ultra-Precise Clock Synchronization of Remote Atomic Clocks with PRARE onboard ERS-2*, Proc. 4th IEEE ISSSTA, Mainz, 22.-25.09.96
- STARKER, S. et al, *NAVEX Final Report*, DLR Oberpfaffenhofen, October 1990
- LEWANDOWSKI, W., THOMAS, C., *GPS Time Transfer*, Proc. IEEE 79 (7), Special Issue on Time and Frequency, 1991
- BEDRICH, S., FLECHTNER, F., *PRARE One rep. Two Yeras in Orbit - Performance Analysis of the Instruments' Oscillator onboard ERS-2 and Meteor-3/7*, Proc. 10th EFTF, Brighton, 1996
- HARTL, Ph., *The Precise Range and Range-rate Equipment (PRARE)*, Proc. Workshop on ERS-1 Radar Altimeter Data Products, Frascati, 1984
- MATTISON, E.M., VESSOT, R. F.C., *High Precision Time Transfer in Space with a Hydrogen Maser on MIR*, personal communication, 1996
- VEILLET, Ch., *ACES, Atomic Clock Ensemble in Space*, Time and Frequency Utilization Study, Final Report, ESA contract: 11287/94/NL/VK, October 1995
- CHANGEART, J.C., *The PHARAO project*, personal communication, 1996
- DIENERT, M., *A new Modem for Microwave Time Synchronisation via Geosynchronous Telecommunication Satellites*, Proc. 6th EFTF, June 1992
- MITREX 2500A, *A Modem for Microwave Time and Ranging Experiments via Telecommunication Satellites*, INS, Stuttgart 1989
- SATRE, technical documentation, TimeTech GmbH, Stuttgart, 6.03.95